Carnegie Mellon University

Ultrafine Particles in the Atmosphere: Formation, Emissions and Growth

A Dissertation

Submitted to the Graduate School

In Partial Fulfillment of the Requirements

For the degree of

Doctor of Philosophy

in

Chemical Engineering

by

Charles Oliver Stanier

Pittsburgh, Pennsylvania

June 2003

Abstract

Despite progress in controlling air pollution in the United States over the past thirty years, airborne particulate matter remains an important focus area for the public health, engineering, and scientific communities. The reason for this concern is the continuing influence of particulate matter (PM) in human health, visibility, and climate. While many aspects of particulate matter are well understood, several important areas are not. This work addresses: (1) in-situ nucleation as an important source of ultrafine (<100 nm) aerosol in the Eastern United States; (2) the formation of secondary organic aerosol; and (3) the role of relative humidity in determining aerosol size and mass. The field-based investigations were performed as part of the Pittsburgh Air Quality Study, a multi-investigator, two-year sampling study focused on characterizing particulate matter, quantifying sources, and developing and evaluating advanced aerosol monitoring techniques.

New particle formation from homogeneous nucleation is an important process in shaping the ambient aerosol size distribution. Prior research on new particle formation mainly focused on its occurrence in clean (non-urban) atmospheres. However, during the Pittsburgh Air Quality Study, new particle formation was observed on over 30% of the study days using Scanning Mobility Particle Sizers (SMPS). The field observations lead to (1) demonstration of the role of photochemical sulfuric acid in nucleation; (2) demonstration of the wide geographic scope of new particle formation; and (3) quantification of the impact of new particle formation on the regional aerosol size distribution.

An automated system to measure the amount of aerosol water at given atmospheric conditions was developed and deployed during the Pittsburgh Air Quality Study. Algorithms for data reduction were developed, including an algorithm for merging aerodynamic diameter number distributions from the Aerosol Particle Sizer with mobility number distributions from Scanning Mobility Particle Sizers. Results from this system showed observations of the water content of ambient aerosols not predicted by thermodynamic partitioning models. Specifically, during the Pittsburgh Air Quality Study, summer aerosols were almost always hydrated, even at relative humidities below 40%, while winter aerosols were not hydrated (up to relative humidities of 60%). The field results were compared with detailed equilibrium thermodynamic calculations based on measured aerosol chemistry.

Currently, our ability to accurately model the formation of secondary organic aerosol and its impact on air quality is limited by our understanding of its chemistry, gas-aerosol partitioning, and hygroscopic properties. Historically, secondary organic aerosol yields (the fraction of reacting organic precursor gas that forms aerosol) have been measured in chamber studies with temperatures from 30-35 ºC and reactant concentrations from 20-500 ppb. In many locations and regions of the atmosphere, lower temperatures and reactant concentrations prevail, and parameters for these conditions are calculated by extrapolation, leading to inaccurate model calculations. Novel techniques were developed to extend the temperature range of chamber experiments beyond the typical range of 30 – 35 ºC to a broader range from 15 – 40 ºC. The methods rely on perturbing

laboratory generated aerosol by heating, and then measuring the rate and equilibrium extent of growth or shrinkage of the particles. Methods were demonstrated using ozone oxidation of monoterpenes such as α-pinene, β-pinene and Δ-carene.

Acknowledgements

I would like to thank my advisor Spyros N. Pandis for all his efforts in guiding this research and furthering my career.

I am deeply grateful for the support, patience and encouragement of my wife Heather. She gracefully endured the long and irregular hours, the late night experiments and filter changes, and the overlong explanations of aerosol phenomena. I also am thankful for and inspired by our baby Caleigh, born during the final year of my doctoral studies.

I also appreciate the support of my family, especially from my father Bill and my father-in-law Ray Widmayer. I thank my mother Samantha for fostering my education for so many years and know that she is pushing me on in spirit, if not in person.

I thank those that funded my graduate studies, including the National Science Foundation Graduate Fellowship Program, the Teresa Heinz Environmental Scholars Program, the Air and Waste Graduate Scholarship Program, the Environmental Protection Agency, and the Department of Energy.

I appreciate the work of my thesis committee, which included Spyros Pandis, John Anderson, Cliff Davidson, Neil Donahue, and Lee White.

Kudos and thanks to my many coworkers and collaborators both at Carnegie Mellon and elsewhere. Special thanks to Tim Raymond, Ray Dagastine, Mirete Bilde, Juan Cabada, Eric Lipsky, Andrey Khlystov, and Allen Robinson.

Table of Contents

List of Tables

List of Figures

Chapter 2

Chapter 3

Chapter 4

Chapter 5

Chapter 6

Chapter 7

Chapter 1 Introduction

Airborne particles, from a few nanometers to tens of microns in size, are key components of our atmosphere. They influence our health, our climate, our lakes and oceans, and the color of the sky. It is widely known that mankind's activities change aerosol concentrations in the atmosphere, both on the local and global scale. For example, in the United States, urban aerosol pollution rose as a consequence of industrialization and then decreased due to technological improvements and stricter regulations. Despite the progress to date in reducing air pollution levels, recent studies find robust correlations between atmospheric pollution levels and adverse health effects in sensitive subgroups of the population, such as those with cardiac and respiratory conditions (EPA 1996; Samet et al., 2000). Furthermore, there has been a steadily growing appreciation of the links between air pollution and climate over the past two decades (Penner et al., 2001). For example, the haze over populated areas of North America limits visibility at ground level and cools the region by reflecting radiation back to space; however, the magnitude of this effect is highly uncertain. In fact, over parts of the planet aerosols may have a net warming effect due to the absorption of radiation by soot aerosols (Ramaswamy et al., 2001). Because of these and other radiative and health effects, a good understanding of sources, chemistry, and physics of air pollution is critical to the design of effective policies to manage air quality, visibility, and climate.

While the societal importance of air pollution provides one impetus for its study, the complexity and challenge of the problem provides another. The

atmosphere can be thought of as an enormous chemical reactor, with thousands of chemical components, multiple phases, complex mass and energy transport, and intricate catalytic, radical, and surface reactions. Length scales of importance range from the sub-nanometer to millimeter size and larger. Aerosols typically contain a variety of inorganic ions, metals, water, soot, oxides, and hundreds of organic compounds. They are found as solids, dilute solutions, highly concentrated solutions, and multiphase particles. Atmospheric aerosols are emitted from a variety of manmade and natural sources and are formed in the atmosphere from gas-to-particle partitioning. These complexities require an interdisciplinary approach for solution and a combination of laboratory, field, and theoretical investigations.

Perhaps because a measure of aerosol mass in air is straightforward (particles caught in a filter are then weighed), the bulk of prior research in airborne aerosols focused on particle *mass* concentrations. Recently, research has begun to focus more on the *number* concentration of airborne aerosols, the formation and emission of fresh aerosol particles, and the health and climate roles of particles of very small particles, which by their nature can be found in high concentrations without significantly increasing aerosol mass concentration.

This focus on particles that can be found in high number concentrations but relatively low mass concentrations is supported by recent health studies that show that for a given mass concentration, health effects are larger for smaller particle sizes (Oberdörster et al., 1992; Oberdörster et al., 1995; Donaldson et al., 1998; Wichmann and Peters, 2000). It is further motivated by recent work on the

cloud seeding properties of small particles and the link between aerosols, clouds, and climate.

1.1 Background

Airborne particles include both organic and inorganic components and are formed from a variety of sources, including combustion, dust, and particle formation from oxidation of precursor gases. Major components include sulfate, nitrate, ammonium, trace elements, organic material, soot, water, and crustal components. The dynamics of atmospheric aerosols are complex because of their wide variation in size, composition, and spatial distribution.

Airborne particulate matter (PM) is classified into *primary* PM, which is emitted directly from sources, and *secondary* PM, which is formed *in situ* from gas-to-particle conversion in the atmosphere. A further classification is by particle size: *Fine* particulate matter has a diameter less than 2.5 μm. Additional distinctions of fine PM are *ultrafine* PM (less than 100 nm) and *nuclei mode* particles (less than 10 nm). Three size distributions are typically considered, the *number* size distribution, *surface area* size distribution, and *volume* (or mass) size distribution. Sizes are often indicated in the literature as a subscript. For example, $PM_{2.5}$ refers to the mass of particulate matter (aerosols) with sizes smaller than 2.5 μm while PM_{10} refers to the mass of particulate matter with sizes less than 10 μm.

The three largest contributors to urban fine PM in the Northeast United States are sulfate, carbonaceous material, and water (Seinfeld and Pandis, 1998). Sulfate is mainly formed as secondary PM from the oxidation of SO_2 emitted

from combustion sources such as power plants and engines. The carbonaceous fraction of ambient PM consists of both elemental carbon and a variety of organic compounds (organic carbon). Elemental carbon (EC), also called black carbon or soot, is directly emitted from combustion sources. Organic carbon (OC) is emitted as primary aerosol from a variety of sources. Alternatively, organic compounds can partition from the gas phase to the aerosol phase, creating secondary organic aerosol. Secondary organic aerosol (SOA) is an important component of urban smog, comprising up to 70% of organic aerosols during episodes in Los Angeles (Turpin 1991).

Recently, there has been increased interest in organic aerosols derived from biogenic volatile organic compounds, which are emitted from vegetation. This interest is due to the reactivity of biogenic compounds, their large flux to the atmosphere (7 to 10 times man-made emissions on a global scale), and their potentially large impact on global and regional air pollution and aerosols (Müller et al., 1992; Guenther et al., 1995; Griffin et al., 1999a). Monoterpenes ($C_{10}H_{16}$), a class of biogenic hydrocarbons emitted from trees, have been shown to create significant quantities of secondary organic aerosols in smog chamber experiments (Hoffmann et al., 1997).

Ambient aerosols take up water depending on their chemical composition and the surrounding relative humidity. Particles consisting of inorganic salts (e.g. ammonium sulfate, ammonium nitrate, sodium sulfate) can exist either as solids or in solution with water. If starting from a dry, solid state, salt particles will not take up water until their *deliquescence relative humidity* (DRH) is exceeded. For

ammonium sulfate at 25 °C, the DRH is 80%. As relative humidity is increased above the DRH, even more water is absorbed. Pure ammonium sulfate aerosols will double in size due to water uptake if taken from a dry state to about 93% RH (Seinfeld and Pandis, 1998). On the other hand, as RH is decreased below the DRH, the particle will not immediately crystallize and return to zero water content. Rather, it will remain in the metastable supersaturated solution phase until the RH reaches critical supersaturation and induces crystallization. Some aerosol components, such as sulfuric acid, do not exhibit deliquescence behavior, but respond smoothly to relative humidity changes (Seinfeld and Pandis, 1998).

Through changes in aerosol water content, relative humidity influences visibility, aerosol aerodynamic behavior, and climatic effects of aerosols. Aerosol water also influences gas-to-particle partitioning, chemical reaction rates, and particle shape.

Given the wide variety of sources, one can expect a rich variety of primary particles in the air, including micron sized fragment from road dust, tire wear, and machining; ultrafine combustion soot agglomerates; metal oxide fume from coal combustion; and condensed unburnt engine oil. Sources of exclusively ultrafine particles have a strong influence on particle number but little effect on overall particle mass. Conversely, sources emitting only larger particles will directly impact ambient aerosol mass concentration without significantly changing the ambient number concentration. Many combustion sources emit both ultrafine and larger particles, contributing to both the number and mass concentrations.

Epidemiological studies have shown adverse health effects of PM including respiratory irritation and changes in pulmonary function as well as associations between PM mass concentrations and mortality (Oberdorster et al., 1992; Schwartz et al., 1996; Donaldson and MacKnee, 1998; Samet et al., 2000; EPA, 1996). Some studies have also shown that ultrafine particles are likely to cause adverse health effects (Seaton et al., 1995; Peters et al., 1997; Daily et al., 2001). Recent works by Laden et al. (2000) and Hoek et al. (2002) have indicated that fine PM from mobile and coal combustion sources are highly correlated with increased mortality. In addition to affecting human health, fine particulate matter impacts climate change and visibility. Because of these impacts, sources of fine PM and secondary PM precursors are increasingly controlled by regulation. A good understanding of emission sources and atmospheric processes that govern fine PM concentrations is critical to the design of an effective control policy.

Fine particles impact visibility and climate because of their ability to scatter and absorb sunlight. Anthropogenic emissions of primary PM and secondary PM precursors create a haze in many industrialized parts of the world, increasing the planetary albedo and decreasing the amount of radiation reaching the surface. Finally, fine particles serve as seeds for cloud droplets, influencing the formation and optical properties of clouds.

1.2 Current Knowledge of Ultrafine Particles

1.2.1 Ultrafine Particle Sources: Nucleation and Emissions

Instruments for counting and sizing particles have been commercially available for at least 30 years (Whitby, 1978; Went, 1960). Accordingly,

measurements of number concentrations and size distributions have been performed at urban, rural, and remote sites around the world, focusing on particle sizes from 15 – 500 nm. However, until recently, nuclei mode particles could not be detected because the lower limit of the sizing equipment was about 10 nm. Within the past 10 years, advances in instrumentation have made possible the monitoring of particles as small as 2 nm (Stolzenburg and McMurry, 1991).

The combination of potential health effects of ultrafine particles, growing appreciation of the climate-aerosol interaction, and instrumentation advances spurred a growing body of research into the sources of ultrafine (<100 nm) and new (<10 nm) aerosol particles.[1] While the sources of these are known (in situ nucleation from gas-to-particle conversion, and emission from combustion processes) their relative strengths in different parts of the atmosphere, the chemistry involved, and impact on the atmosphere are not known.

Until recently, nucleation was assumed to be limited to (1) clean areas of the atmosphere such as the free troposphere and (2) concentrated plumes such as SO_2 rich stack emissions from coal combustion (Whitby, 1978). It was not considered important in urban areas. However, a number of recent studies at both rural and urban sites have examined the time evolution of particle number distribution in both urban and rural continental settings (Birmili and Wiedensohler, 1998; Allen et al., 1999; Harrison et al., 1999,2000,2001; Kim et al., 2001; Shi et al., 2001; Woo et al., 2001; Ruuskannen et al., 2001). Studies of

[1] Because of their small size, nuclei mode aerosol particles have considerable Brownian motion and will collide with other particles, leading to a relatively short (minutes to hours, depending on available area for collisions). On the other hand, larger aerosols (50 nm – 1 μm) have lifetimes of hours to days.

ultrafine particle concentrations share the following important findings: (1) aerosol number and mass are largely independent, and in some locations they are anti-correlated; (2) evidence of two main sources of ultrafine particles (primary emissions and *in situ* nucleation); and (3) in some sites, periodic nucleation bursts, where the number of nuclei mode particles increases by an order of magnitude or more in a short period of time.

It is recognized that there are two important steps to the production of new particles that can grow to detectable size (Zhang and Wexler, 2002; Kerminen, 1999). The first step is the formation of an initial nucleus, and the second step is the growth of the particles to larger sizes. A number of mechanisms have been proposed as candidates for the initial nucleus formation step based on observations and theoretical considerations, including (a) homogeneous binary nucleation of sulfuric acid and water (Weber et al., 1999); (b) homogeneous ternary nucleation of ammonia-water-sulfuric acid (Eisele and McMurry, 1997; Kulmala et al., 2001a; O'Dowd et al., 1999); (c) homogenous nucleation of low vapor pressure organic compounds (O'Dowd et al., 2002); (d) and ion-induced nucleation (Kim et al., 2002). The second step in forming detectable new particles, growth, is also uncertain. These particles can grow by condensation of sulfuric acid or by self-coagulation. Both of these processes are relatively inefficient, and additional growth mechanisms have been proposed (Kerminen 1999). The limited experimental evidence indicates a potential role for organic compounds (Novakov and Penner 1993; Rivera-Carpio et al., 1996). Recent work considers the potential for heterogenous reactions of SO_2 (Kerminen, 1999)

and organic compounds (Kerminen, 1999; Jang and Kamens, 2001; Zhang and Wexler, 2002) to significantly contribute to growth.

Steps toward a better understanding of tropospheric nucleation include: (a) elucidation of the mechanism responsible for the initial nuclei formation in different environments; (b) identification of the chemical compounds responsible for growth; and (c) determination of the geographic scope, frequency, strength and impact of tropospheric nucleation.

1.2.2 Aerosol Water Content

Understanding of water uptake of aerosols composed of single and multiple inorganic salts (e.g. NaCl, $(NH_4)_2SO_4$) is well advanced. Many computational and laboratory studies have been completed in this area. Water uptake and deliquescence relative humidities are routinely computed by thermodynamic equilibrium models (see Ansari and Pandis (1999) and Nenes et al. (1998) and references therein). However, water uptake by the organic fraction of aerosols is currently not well understood.

Measurements of water uptake by aerosols have been performed in the laboratory with inorganic (Tang, 1980; Tang and Munkelwitz ,1993) and mixed organic-inorganic particles (Cruz and Pandis, 1999). Water uptake in aerosols is typically measured by Hygroscopic Tandem Differential Mobility Analysis (H-TDMA)[2], which quantifies the growth of dry particles of a specific size under

[2] The Differential Mobility Analyzer (DMA) is a device which separates particles according electrical mobility, which can be related to particle size. The DMA is widely used in aerosol studies and is mentioned throughout this work in several contexts. DMAs have two operational modes. They can either be used to select particles of a specific size (classification) or they can be used in conjunction with a particle detector to measure the size distribution of an aerosol sample

humidification (typically to 90%). This has been done in a number of locations for ambient aerosols (see Cocker et al. (2001) for a review of field studies). Many of these studies have classified the aerosol into more hygroscopic and less hygroscopic fractions, although recent results from Pasadena, California indicate that this may be an oversimplification (Cocker et al., 2001). Another typical finding from H-TDMA studies of polluted air masses is that the less hygroscopic mode consists of smaller particles (around 50 nm) and the more hygroscopic mode occurs at larger particle sizes (around 500 nm).

H-TDMA studies have some important limitations. First, H-TDMA experiments do not measure the water content of ambient aerosols. Instead, the hygroscopicity of the aerosol is measured, defined as the water uptake upon humidification from an initially dry state. Second, unless specially configured, H-TDMA instruments do not measure the crystallization and deliquescence relative humidities of ambient aerosols.

Recent developments in H-TDMA include computer controls in conjunction with high-flow particle sizing instruments to rapidly scan hygroscopic growth in several size channels (Kriesberg et al., 2001), operation of H-TDMA in subzero temperatures (Weingartner et al., 2001), and measurement of hygroscopic growth of ultrafine diesel exhaust aerosol (Sakurai et al., 2001). An alternate technique for measuring hygroscopic growth has been used where

---

(e.g. Scanning Mobility Particle Sizing, SMPS). When two DMAs are operated in series to first select a particle size and then measure the particle size after some process, the configuration is called Tandem DMA (TDMA).

the light scattering of aerosols is measured as a function of relative humidity (Day et al., 2001).

Knowledge gaps regarding aerosol water content include (1) the hydration state of "real" particles in the atmosphere at relative humidities below 60%; (2) the role of organic compounds in water uptake; (3) the accuracy of existing thermodynamic models for predicting water content of particles in continental, polluted atmospheres; and (4) the amount of water retained in "dry" filter-based aerosol samples.

1.2.3 Secondary Organic Aerosols (SOA)

Volatile organic compounds (VOC) are ubiquitous in the lower atmosphere. They are removed primarily by oxidation and conversion to CO_2, water soluble compounds, and semivolatile compounds that are incorporated into aerosol particles. Oxidation of VOCs typically leads to a large number of products.

$$\mathrm{VOC} \rightarrow a_1\mathrm{P}_1 + a_2\mathrm{P}_2 + \ldots + a_n\mathrm{P}_n \qquad (1.1)$$

where VOC is a reactive volatile organic compound (e.g. toluene), a_1 through a_n are molar yields, and P_1 through P_n represent the products of the reaction. Often, at least some of the products of the reaction are more polar and less volatile than the reactant gas. Accordingly, some of the products partition between the gas and aerosol phases. Measuring and predicting the partitioning of the products is a key problem in understanding secondary organic aerosol formation. Typically, the *aerosol yield* Y is defined as the fraction:

$$Y = \frac{\Delta M_o}{\Delta ROG} \tag{1.2}$$

where ΔM_o is the amount of aerosol formed and ΔROG is the amount of reactive organic gas consumed in the formation reaction. A number of approaches to predicting secondary organic aerosol (SOA) yield have been published in the literature. The earliest assumed that each precursor VOC had an almost constant yield of SOA (Hatakeyama et al., 1989; Grosjean et al., 1989; Pandis et al., 1991); for example, experiments in 1989 indicated that oxidation of α-pinene led to an 18% mass yield of SOA (Hatakeyama et al., 1989). This approach was used to calculate saturation vapor concentrations of condensable species which were then used to predict atmospheric SOA concentrations (Pandis et al., 1992). Subsequent theoretical (Pankow, 1994a,b) and experimental studies (Odum et al., 1996) suggested that the SOA thermodynamics were consistent with an organic solution of multiple semivolatile reaction products.

Organic solution models were successful at reproducing smog chamber data. Odum et al. (1996) showed that a wide variety of oxidation experiments could be fitted with a two product model containing four adjustable parameters. Following his work, the parameters were estimated for a variety of systems based on smog chamber data (Griffin et al., 1999b). These parameters have been applied to atmospheric prediction of SOA concentrations by modelers as well (Strader et al., 1999; Sheehan and Bowman, 2001).

As gas chromatography techniques were successfully adapted to these systems, quantification of the molar yields of actual products became more

feasible (Hallquist et al., 1999; Kavouras et al., 1999; Glasius et al., 2000). For example, over 13 products were identified in the α-pinene plus ozone reaction (Yu et al., 1999). Using group contribution methods to estimate vapor pressures and activity coefficients, investigators have solved for the vapor-liquid equilibrium for systems (such as α-pinene plus ozone) yielding reasonable agreement to smog chamber results (Pankow et al., 2001).

Areas where secondary organic aerosol formation is not as well understood include the effects of temperature, relative humidity, and oxidant chemistry. Water vapor has been shown to be absorbed by polar organic aerosols and involved as a reactant in the aerosol formation stage. Oxidant chemistry is also important to aerosol yields, with ozone reactions typically forming greater aerosol concentrations than OH reactions (Hoffmann et al., 1997).

This work is concerned primarily with the effect of temperature on semivolatile gas-particle equilibrium, which has been investigated theoretically (Strader et al., 1999; Sheehan and Bowman, 2001) but not experimentally.

1.3 Pittsburgh Air Quality Study

The field portions of this work were conducted as part of the Pittsburgh Air Quality Study (PAQS). The Pittsburgh Air Quality Study is a comprehensive multidisciplinary set of projects in the Pittsburgh region collecting data on air pollution, aerosols, and health indicators. The study, summarized by Wittig et al. (2003) involved over 25 collaborators and at least 4 dozen simultaneous measurements of gas- and aerosol-phase chemical and physical characteristics.

The study was hypothesis driven, and the work of this thesis is directly connected to several of the project hypotheses:

- Aerosol nucleation can be a major source of aerosol number in both urban and rural areas in the study region.
- Most particles in the region are liquid throughout the day in both winter and summer.
- The measured aerosol mass can be fully explained if the water retained by organics and inorganics, the full organic aerosol contribution, and the full crustal contribution are accounted for.

1.4 Overview of Thesis

Chapter 2 describes the design, validation and first results of an automated system to measure the aerosol number distribution from 3 nm to 20 μm in size, at both dried and ambient relative humidities. A number of data reduction procedures are presented and demonstrated to calculate the aerosol water content of ambient aerosols. The system ran at the Schenley Park site of the Pittsburgh Air Quality Study from July 1, 2001 – September 2002, and data from July 2001 is used to demonstrate the capabilities of the system.

Chapter 3 is an overview of results from the Dry-Ambient Aerosol Size Spectrometer (described in Chapter 2) for the period July 1, 2001 – June 30, 2002. Results such as the average and variation of the particle concentration at the Pittsburgh Air Quality Study are presented. The results from the main sampling

site (Schenley Park) are compared to an upwind rural site, and the results from the Pittsburgh region are compared to results from other studies around the globe.

New particle formation in the Pittsburgh region, as measured by the Dry-Ambient Aerosol Size Spectrometer, is presented in Chapter 4. The frequency, spatial scale, and meteorology of new particle formation are discussed, and the involvement of photochemically produced sulfuric acid is investigated.

Aerosol size distributions are routinely monitored by Scanning Mobility Particle Sizers to sizes from 0.003 - 0.8 μm, and by Aerosol Particle Sizers from 0.5 – 20 μm. However, due to the different physical principles of these instruments (electrical mobility sizing versus aerodynamic sizing), there are difficulties in combining the results into a single aerosol size distribution. An algorithm for combining the results is presented in Chapter 5.

Aerosol water content as measured during the Pittsburgh Air Quality Study is discussed in detail in Chapter 6. Predictions of an advanced thermodynamic equilibrium model, previously developed by Ansari and Pandis (1999) are compared to the measurements. Crystallization behavior of ambient aerosols and the role of organics in water uptake are discussed.

Laboratory experiments aimed at improving our understanding of secondary organic aerosol formation are presented in Chapter 7. With a focus on the thermodynamics of secondary organic aerosols, several smog chamber experiments performed in Carnegie Mellon's newly constructed Air Quality Laboratory are discussed. Two new experimental techniques and their

implications for air quality modeling are also discussed. Ozone oxidation of monoterpenes, particularly α-pinene is used as a model reaction.

Chapter 8 summarizes the thesis and discusses future work that could be accomplished using this research as a starting point.

1.5 References

Allen, A.G.; Grenfell, J.L.; Harrision, R.M.; James, J.; Evans, M.J. Nanoparticle formation in marine airmasses: contrasting behaviour of the open ocean and coastal environments. Atmos. Res. 1999, 51, 1-14.

Ansari, A.S.; Pandis, S.N. Prediction of multicompnent inorganic atmospheric aerosol behavior. Atmos. Environ. 1999, 33, 745-757.

Birmili, W. and Wiedensohler, A. (1998) The influence of meteorological parameters on ultrafine particle production at a continental site. J. Aerosol Sci. 29, S1015-S1016.

Cocker, D.R.; Whitlock, N.E.; Flagan, R.C.; Seinfeld, J.H. Hygroscopic Properties of Pasadena, California Aerosol. Aerosol Sci. and Technol., 2001, 35, 637-647.

Cruz, C.N.; Panids, S.N. Deliquescence and Hygroscopic Growth of Mixed Inorganic-Organic Atmospheric Aerosol. Environ. Sci. Tech. 2000, 34, 4313-4319.

Daily, L.A.; Kim, S.; Sioutas, C.; Devlin, R.B.; The response of human airway epithelial cells to ultrafine, fine and coarse PM; Manuscript submitted to Inhal. Toxicol. 2001.

Day, D.E. and Malm, W.C. (2001) Aerosol light scattering measurements as a function of relative humidity: a comparison between measurements made at three different sites. Atmos. Environ. 35, 5169-5176.

Donaldson, K.; MacNee, W. The mechanism of lung injury casued by PM10 in Issues in environmental science and technology, Ed. R.E. Hester & R.M. Harrison. 1998. The Royal Society of Chemisty.

Environmental Protection Agency (US). Air Quality Criteria for Particulate Matter, Vol. III. EPA/600/P-95/001CF. 1996, National Center for Environmental Assessment, Research Triangle Park NC.

Ferin, J.; Oberdorster, G.; Soderholm, S.C.; Gelein, R. Pulmonary tissue access of ultrafine particles. J. Aerosol Medicine. 1991, 4, 57-68

Griffin, R.J.; Cocker, D.R. III; Seinfeld, J.H. Geophysical Research Letters. 1999, 26, 2721-2724.

Griffin, R.J.; Cocker, D.R.; Flagan, R.C.; Seinfeld, J.H. Organic aerosol formation from the oxidation of biogenic hydrocarbons. J. Geophys. Res. 1999, 104, 2555-2567.

Grosjean, D.; Seinfeld, J.H. Parameterization of the formation potential of secondary organic aerosols. Atmos. Environ. 1989, 23, 1733-1747.

Guenther, A.; Hewitt, C.; Erickson, D.; Fall, R.; Geron, C.; Graedel, T.; Harley, P.; Klinger, L.; Lerdau, M.; McKay, W.; Piersce, T.; Scholes, B.; Steinbrecher, R.; Tallamraju, R.; Taylor, J.; Zimmerman, P. A Global Model of Natural Volatile Organic Compound Emissions. J. Geophys. Res. 1995, 100, 8873-8892.

Harrison, R.M.; Shi, J.P; Jones, M.R. Continuous Measurement of aerosol physical properties in the urban atmosphere. Atmos. Environ. 1999, 33, 1037-1047.

Harrison, R.M.; Grenfell, J.L,; Allen, A.G.; Clemitshaw, K.C.; Penkett, S.A.; Davison, B. Observations of new particle production in the atmosphere of a moderately polluted site in eastern England. J. Geophys. Res. 2000, 105, 17819-17832.

Hatakeyama, S.; Izumi, K.; Fukuyama, T.; Akimoto, H. Reactions of ozone with a-pinene and b-pinene in air: yields of gaseous and particulate products. J. of Geophys. Res. 1989, 94, 13,013-13,024.

Hoek, G., Brunekreef, B., Goldbohm, S., Fischer, P., van den Brandt, P.A. (2002) Association between mortality and indicators of traffic-related air pollution in the Netherlands: a cohort study. Lancet 360: 1203-1209.

Hoffmann, T.; Odum, J.R.; Bowman, F.; Collins, D.; Klockow, D.; Flagan, R.C.; Seinfeld, J.H. Formation of Organic Aerosols from the Oxidation of Biogenic Hydrocarbons. J. Atmos. Chem. 1997, 26, 189-222.

Kim, S.; Shen, S.; Zhu, Y.; Hinds, W.C.; Sioutas, C. Size Distribution and Seasonal Trends of Ultrafine Particles in Source and Receptor Sites of the Los Angeles Basin. Manuscript submitted to J. of Air & Waste Management, 2001.

Kreisberg, N.M.; Stolzenburg, M.R.; Hering, Susanne V. A new method for measuring the dependence of particle size distributions on relative humidity, with application to the Southeastern Aerosol and Visibility Study. J. Geophys. Res. 2001, 106, 14,935-14,949.

Laden, F.; Neas, L.M.; Dockery, D.W.; Schwartz, J. Association of Fine Particulate Matter from Different Sources with Daily Mortality in Six U.S. Cities. Environ. Health Perspect. 2000, 108, 941-947.

Müller, J. F. Geographical Distribution and Seasonal Variation of Surface Emissions and Deposition Velocities of Atmospheric Trace Gases. J. Geophys. Res. 1992, 97, 3787-3804.

Nenes, A.; Pandis, S.N.; Pilinis, C. A New Thermodynamic Equilibrium Model for Multiphase Multicomponent Inorganic Aerosols. Aquat. Geochem. 1998, 4, 123-152.

Oberdorster, G.; Ferin, J.; Gelein, R.; Soderholdm, S.C.; Finkelstein, J. Role of alveolar macrophage in lung injury; studies with ultrafine particles; Environ. Health Perspect. 1992, 102, 173-179.

Oberdorster, G.; Gelein, R.M.; Ferin, J.; Weiss, B. Association of particulate air pollution and acute mortality: involvement of ultrafine particles. Inhal. Toxicol. 1995, 7, 111-124.

Odum, J.R.; Hoffmann, T.; Bowman, F.; Collins, D.; Flagan, R.C.; Seinfeld, J.H. Gas/particle partitioning and secondary organic aerosol yield. Environ. Sci. Technol. 1996, 30, 2580-2585.

Pandis, S. N.; Paulson, S. E.; Seinfeld, J. H.; Flagan, R. C.; Aerosol Formation in the Photooxidation of Isoprene and β-pinene. Atmos. Environ. 1991, 25A, 997-1008.

Pandis, S.N.; Harley, R.A.; Cass, G.R.; Seinfeld, J.H. Secondary Organic Aerosol Formation and Transport. Atmos. Environ. 1992, 26A, 2269-2282.

Pankow, J.F. An absorption model of gas/particle partitioning of organic compounds in the atmosphere. Atmos. Environ. 1994, 28, 185-188.

Pankow, J.F. An absorption model of the gas/particle partitioning involved in the formation of organic aerosols. Atmos. Environ. 1994, 28, 189-193.

Pankow, J.F.; Seinfeld, J.H.; Asher, W.E.; Erdakos, G.E. Modeling the Formation of Secondary Organic Aerosol. 1. Application of Theoretical Principles to Measurements Obtained in the α-Pinene/, β-Pinene/, Sabinene/, Δ3-Carene/, and Cyclohexene/Ozone Systems. Pending Publication in Environ. Sci. Technol. 2001.

Penner, J.E. Aerosols, their Direct and Indirect Effects. In Climate Change 2001, The Scientific Basis: Contribution of the Working Group 1 to the Third Assessment Report of the IPCC. 2001, Ed. Houghton, J.T.; Ding, Y.; Griggs, D.J.; Noguer, M.; van der Linden, D.J.; Dai, X.; Maskell, K.; and Johnson, C.A. Cambridge University Press, Cambridge.

Peters, A.; Wichmann, E.; Tuch, T.; Heinrich, J.; Heyder, J. Respiratory Effects are Associated with the Number of Ultrafine Particles, Am. J. Respir. Crit. Care Med. 1997, 155, 1276-1383.

Ramaswamy, V. Radiative Forcing of Climate Change. In Climate Change 2001, The Scientific Basis: Contribution of the Working Group 1 to the Third Assessment Report of the IPCC. 2001, Ed. Houghton, J.T.; Ding, Y.; Griggs, D.J.; Noguer, M.; van der Linden, D.J.; Dai, X.; Maskell, K.; and Johnson, C.A. Cambridge University Press, Cambridge.

Ruuskannen, J.; Tuch, T.; Bring, H,; Peters, A.; Khlystov, A.; Mirme, A.; Kos, G.P.A.; Brunekreef, B.; Wichmann, H.E.; Buzorius, G.; Vallius, M.; Kreyling, W.G.; Pekkanen, J. Concentrations of ultrafine, fine and PM2.5 particles in three European cities. Atmos. Environ. 2001, 35, 3729-3738.

Sakurai, H., Tobias, H.J., Park, K., Zarling, D., Docherty, S., Kittelson, D.B., McMurry P.,H., and Ziemann, P.J. (2003) On-line measurements of diesel nanoparticle composition and volatility. *Atmos. Environ*. 39, 1199-1210.

Samet, J.M.; Dominici, F.; Curriero, F.C.; Coursac, I.; Zeger, S.L. Fine particulate air pollution and mortality in 20 U.S. cities, 1987-1994. N. Engl. J. Med. 2000, 343, 1742-1749.

Seaton, A.; MacNee, W.; Conaldson, D.; Goddon, G. Particulate air pollution and acute health effects. Lancet. 1995, 345, 176-178.

Seinfeld, J.H.; Pandis, S.N. Atmospheric Chemistry and Physics; Wiley and Sons: New York, 1998.

Schwartz, J.; Dockery, D.W.; Neas, L.M. J. of the Air & Waste Management Association. 1996, 46, 927-939.

Sheehan, P.E.; Bowman, F.M. (2001). Estimated Effects of Temperature on Secondary Organic Aerosol Concentrations. *Environ. Sci. & Technol. 35*, 2129-2135.

Shi, J.P.; Evans, D.E.; Khan, A.A.; Harrison, R.M. Source and Concentration of Nanoparticles (<10 nm diameter) in the Urban Atmosphere; Atmos. Environ. 2001, 35, 1193-1202.

Stolzenburg, M.R.; McMurry, P.H. An Ultrafine Aerosol Condensation Nucleus Counter. Aerosol Sci. Technol. 1991, 14, 48-65.

Strader, R.; Lurmann, F.; Pandis, S.N. Evaluation of secondary organic aerosol formation in winter. Atmos. Environ. 1999, 33, 4849-4863.

Tang, I.N. On the equilibrium partial pressures of nitric acid and ammonia in the atmosphere. Atmos. Environ., 1980, 14, 819-828.

Tang, I.N.; Munkelwitz, H.R. Composition and temperature dependence of the deliquescence properties of hygroscopic aerosols. 1993, Atmos. Environ., 27A, 467-473.

Turpin, B.J.; Huntziker, J.J.; Larson, S.M.; Cass, G.R. Environ. Sci. Technol. 1991, 25, 1788-1793.

Weingartner, E.; Gysel, M.; Baltensperger, U. (200) Hygroscopicity of Aerosol Particle at Low Temperatures. 1. New Low-Temperature H-TDMA Instrument: Setup and First Applications. *Environ. Sci. Technol.* 36, 55-62.

Went, F.W. (1960) Blue hazes in the atmosphere. *Nature* 187, 641-643.

Whitby, K.T., Cantrell, B.K. Husar, R.B., Gillani, N.V., Anderson, J.A., Blumenthal, D.L., and Wilson, W.E. (1978) Aerosol formation in a coal-fired power plant plume. *Atmos. Environ.*

Wittig, B., Anderson, N., Khlystov, A.Y., Pandis, S.N., Davidson C. and Robinson A.L. (2003) Pittsburgh Air Quality Study overview and preliminary scientific findings, Submitted to Atmos. Environ.

Woo, K.S.; Chen, D.R.; Pui, D.Y.H.; McMurry, P.H. Measurement of Atlanta Aerosol Size Distributions: Observations of Ultrafine Particle Events. Aerosol Sci. & Technol., 2001, 34, 75-87.

Yu, J.; Cocker D.R.; Griffin, R.J.; Flagan, R.C.; Seinfeld, J.J.; Blanchard, P. J. Atmos. Chem. 1999, 34, 207-258.

Chapter 2 A Method for the In-situ Measurement of Fine Aerosol Water Content of Ambient Aerosols: The Dry-Ambient Aerosol Size Spectrometer[†]

2.1 Introduction

The absorption of water by atmospheric aerosols with increasing relative humidity influences their size, composition, lifetime, chemical reactivity, and light scattering. Water is the most prevalent aerosol component at relative humidities above 80% and is often a significant component at lower relative humidities (Hanel 1976). Accordingly, hygroscopic growth is important in a number of air pollution problems, including visibility impairment, climate effects of aerosols, acid deposition, long range transport, and the ability of particles to penetrate into the human respiratory system.

A number of laboratory investigations of water uptake by laboratory-generated or smog chamber aerosols have been conducted. Laboratory studies have used single-particle levitation (Tang and Munkelwitz 1993; Chan 1992; Wagner et al. 1996) and Hygroscopic Tandem DMA (H-TDMA) (Rader 1986) to investigate water uptake, deliquescence, and crystallization of a number of inorganic compounds. More recently, these techniques have been used to investigate hygroscopicity in organic compounds and organic-inorganic mixtures (Xiong et al. 1998; Virkulla et al. 1999; Cruz and Pandis 2000; Peng et al. 2001; Cocker et al. 2001a,b; Brooks et al. 2002).

[†] Published as "A Method for the In-situ Measurement of Fine Aerosol Water Content of Ambient Aerosols: The Dry-Ambient Aerosol Size Spectrometer" by Charles Stanier, Andrey Khlystov, Wan-Yu R. Chan, Mulia Mandiro, and Spyros Pandis. *Aerosol Science and Technology*, 2003 (in press).

Most field studies of water uptake in ambient aerosols have used a H-TDMA (McMurry and Stolzenberg 1989; Berg et al. 1997; Dick 2000). Results of H-TDMA studies are reviewed by Cocker et al. (2001c) and typically classify particles into more hygroscopic and less hygroscopic fractions, with the number of fractions, relative size of fractions, and growth factors varying at different sites. Other techniques devised to measure water uptake include RH-conditioned nephelometry (Rood 1987; ten Brink et al. 2000; Day et al. 2000), filter analysis by gravimetry (Vartiainen et al. 1994), filter analysis by chemical analysis (Ohta et al. 1998), filter analysis by beta attenuation (Speer et al. 1997), observation by Fourier transform infrared spectroscopy (Han and Martin 1999; Onasch et al. 1999; Martin et al. 2001; Han et al. 2002), and in situ measurement of evaporated water (Lee and Hsu 1998). Kreisberg et al. (2001) used an optical particle counter for in-situ automated measurement of dried, humidified, and ambient size distributions.

Several thermodynamic models have been developed that calculate the water uptake of pure and mixed salts (see Ansari and Pandis 1999 and references therein). Recently, these methods have been extended to particles containing organic compounds (Saxena and Hildemann 1997; Ansari and Pandis 2000; Clegg et al. 2001; Ming and Russell 2002).

While this body of experimental, theoretical, and field research has significantly advanced understanding of water uptake by aerosols, significant uncertainties remain. First, there is a limited amount of information about the liquid water content of "real" particles in the atmosphere. Second, many aerosol

compositions exhibit hysteresis in aerosol water content, potentially existing at more than one thermodynamically stable state. Third, field data are required to validate and improve models for mixed organic-inorganic-water models. Finally, a method is needed for direct in-situ measurement of this important particulate matter component. Therefore, there is a need for additional field measurements that focus on the in-situ aerosol water content, crystallization behavior, comparison with mass-based measurements, and the influence of organic compounds.

This work describes a new field instrument, the Dry-Ambient Aerosol Size Spectrometer (DAASS) for the in situ measurement of the atmospheric fine aerosol liquid water content. The DAASS was designed and deployed during the Pittsburgh Air Quality Study (PAQS) and its design, calibration, data reduction procedure, and first results are reported in this work.

2.2 Experimental

The DAASS is an automated combination of aerosol sizing instruments that measures the dried (<30%) and ambient relative humidity aerosol number distribution. The aerosol water content is calculated from the difference of the dried and ambient volume distributions.

The design goals for the DAASS included:

- Measurement of the dried (< 30 % RH) aerosol size distribution from 3 nm to 10 microns for several months with a frequency of at least 4 times per hour.

- Measurement of the ambient aerosol water content, up to ambient RH levels of 90%, and on a frequency of at least once per hour.
- Automatic operation and data-acquisition with minimal maintenance for field deployment.
- Operation from -15 °C to 35 °C temperatures, and dewpoints up to 25 °C.

The Dry-Ambient Aerosol Size Spectrometer (DAASS) includes three particle sizing instruments with associated supporting equipment as shown in Figure 2.1. The particle sizing instruments include two Scanning Mobility Particle Sizers (SMPS) and one Aerosol Particle Sizer (APS). The SMPS instruments size particles from 3 – 80 nm (TSI 3936N25) and 13 – 680 nm (TSI 3936L10), while the APS (TSI 3320) covers 0.5 – 10 μm. These systems are referred to as the Nano-SMPS, SMPS, and APS systems in the rest of this paper. Two separate relative humidity controlled inlets served the aerosol sizing instruments. One inlet conditioned aerosols for the SMPS systems while a separate inlet conditioned aerosols for the APS. Supporting these components are a dry air supply system, and humidity conditioning systems for the sheath air flows of both SMPS systems and the APS.

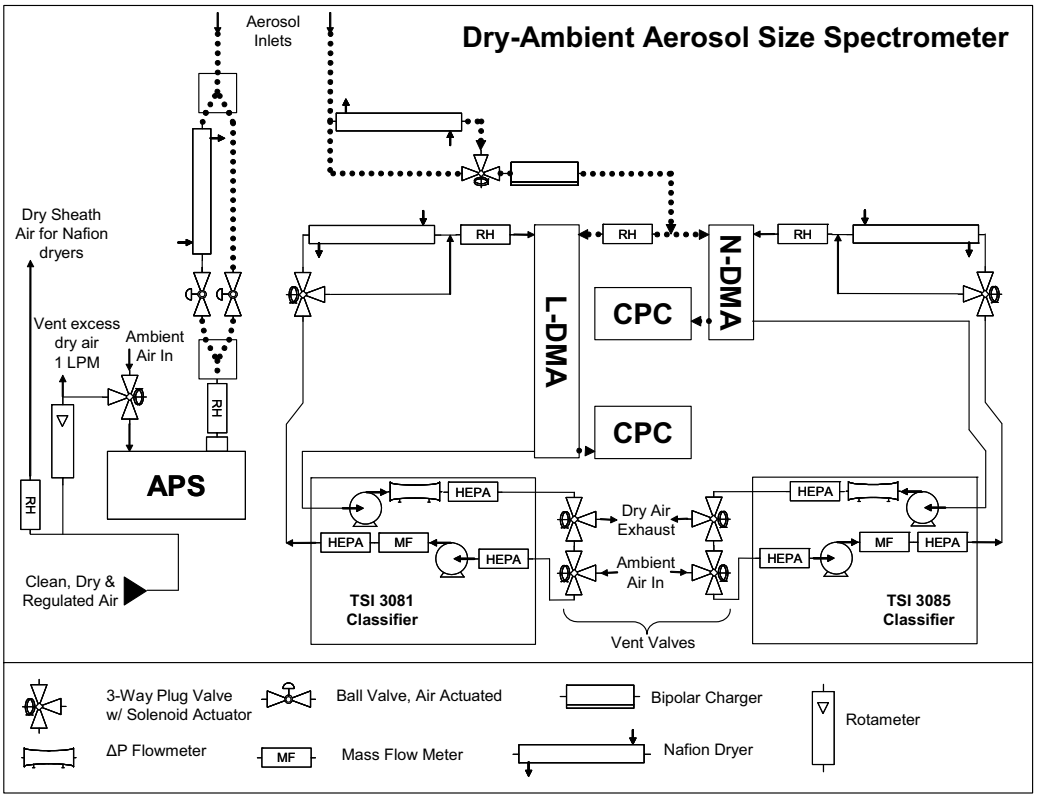

Figure 2.1 Flow diagram of Dry-Ambient Aerosol Size Spectrometer (DAASS). Aerosol streams are shown by dotted lines and other flows are indicated by solid lines.

All components were housed in a weather-proof plywood enclosure with a volume of 3.6 m^3. To meet the goal of measuring the ambient aerosol size distribution at ambient temperature and relative humidity without active temperature and relative humidity control, the instruments, particularly the Differential Mobility Analyzer (DMA) columns needed be kept at ambient temperature. In the first set of tests, all equipment, including the DMA columns was placed inside the enclosure, and temperatures were kept near ambient using a large exhaust fan (~35 $m^3 min^{-1}$). In spite of the large flow of outside air, the DMA column temperatures were elevated about 4 ºC relative to ambient and were therefore drying the ambient samples. The ambient scans reached only approximately 80% of the ambient relative humidity (e.g. outdoor relative

humidity of 95% yielded an ambient channel RH of around 76%). To keep the DMA column temperatures closer to ambient, the columns were moved to a protected ledge just outside the enclosure while fans pulled ambient air over them. This improved performance, and the DMAs then achieved greater than 90% of ambient relative humidity (e.g. outdoor relative humidity of 95% yielded an ambient channel RH of greater than 86%). The effects of this mismatch are discussed in the data reduction section below.

During winter, the enclosure was maintained at a minimum temperature of 9 ºC which was required for the maintenance of condenser and saturator temperature setpoints in the CPCs. This did not significantly affect the final sheath and aerosol relative humidities because the DMA columns were outside the enclosure at (or close to) the outdoor temperature. However, the aerosol flow did pass through this heated enclosure, and the charger was located in the enclosed section of the inlet. This caused the minimum relative humidity encountered by the aerosol flow and the relative humidity (and therefore size) during charging to be different from the final relative humidity at the Differential Mobility Analyzer column. In future deployments of the DAASS, it is recommended that the entire inlet be placed outside of the enclosure in a shaded, ventilated area. The effects of this relative humidity minimum are considered below in the data reduction section.

Drying of aerosol streams was accomplished using Nafion™ membrane dryers (Permapure MD-110, Toms River, NJ). Single tube dryers with stainless steel housings were selected for drying aerosols rather than multi-tube dryers to

limit losses (Woo et al., 2001). For ambient relative humidity measurements, the dryer could be bypassed using automated valves. For the SMPS system, three-way solenoid valves (Alcon U33-43-21-12, Itasca, IL) were used. For the APS inlet, flow selection between the dried and ambient inlet was achieved using full-bore ball valves (Swagelock SS-41S2-31DDM) with orifice diameters that matched tubing inner diameters. Copper and stainless steel tubing was used throughout to minimize particle losses.

The APS was modified slightly to allow for drying. With factory settings, the APS samples five liters per minute (LPM) and then separates the flow into a 1 LPM aerosol flow and a 4 LPM sheath flow. The sheath flow is filtered and returned in the time-of-flight section of the instrument. In the DAASS system, the dry-ambient inlet sampled 1 LPM and was connected directly to the APS inner nozzle. Particle free air was supplied at atmospheric pressure directly to the APS sheath air inlet (Figure 2.1). Depending on the sampling mode, this air was at ambient relative humidity or dried. The standard APS pump and flow control was used for both the aerosol and sheath flows.

In the SMPS systems, the aerosol is assumed to equilibrate with the sheath flow relative humidity because of the 0.3-6 s exposure time of aerosols to the sheath flow (this assumption is considered in the data reduction section). In the data analysis, it is the SMPS sheath flow relative humidity that is used to analyze particle size as a function of relative humidity. However, in the APS, the aerosol has a much shorter exposure time to the sheath air ($< 10^{-4}$ s). In that case, the

aerosol is assumed to be equilibrated at the aerosol stream relative humidity and unaffected by the sheath relative humidity.

Operation of the dry-ambient SMPS systems required three flow configurations of DMA sheath air: dried, ambient, and vent. The flow configurations for these modes are shown in Figure 2.2. In dried and ambient modes, the sheath air ran in a closed loop and passed through dryers or bypassed them, depending on the mode. After the dried scans, the system was put in "vent" mode and the sheath flow was switched to a once-through flow configuration. Dry air was exhausted from the system and ambient relative humidity air was drawn into the system.

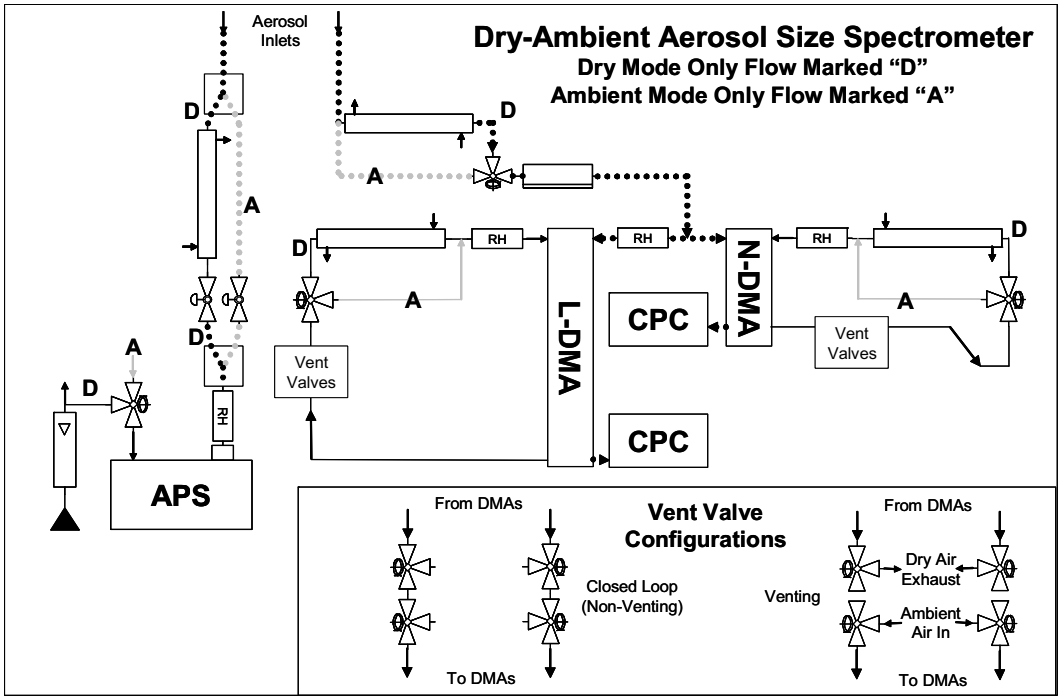

Figure 2.2 Dry, ambient and vent configurations of the DAASS System. Dark flow paths labeled with "D" are only active during the dried mode. Light colored flow paths labeled with "A" are only active in the ambient sampling mode. The third flow configuration is the venting of air from the sheath loops, shown in the lower right-hand inset.

Drying of sheath air flows for the SMPS systems was accomplished using Nafion™ membrane dryers (Permapure PD-50T and PD-200T). Multitube dryers were selected to accommodate the flowrates, which were 3.2 and 7.0 LPM. These dryers were rated to achieve dewpoints of -15 ºC for incoming air at a 20 ºC dewpoint using shell-side utility air supplied at a -40 ºC dewpoint. This system achieved relative humidities in sheath air of less than 15% during the initial summer tests. However, during the winter tests, silica gel desiccant was added to assist in the drying. The winter drop in performance of the membrane dryers was partly due to problems in supplying -40 ºC dew point utility air during winter, and partly due to the need to reach lower dewpoints in winter than in summer to achieve relative humidities below 30% at ambient temperatures. During the coldest periods of the study (-10 ºC), DMA sheath air dewpoints of less than -32 ºC were required. Figures 2.3 and 2.4 show examples of the relative humidity cycling achieved in the field for the SMPS systems and the APS, respectively. Two ambient cycles and two dry cycles are shown. The SMPS sheath air responded quickly when the drying cycle started. The venting took longer, and the relative humidity decreased somewhat during the ambient RH scans.

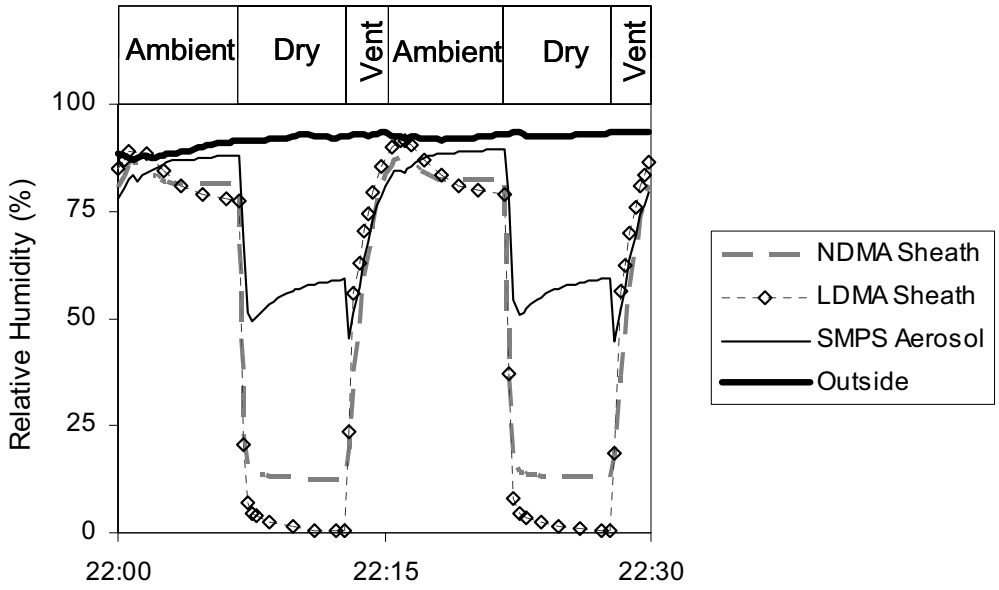

Figure 2.3 Example of relative humidity time series in the SMPS instruments in DAASS. The SMPS Aerosol RH is the air sample RH before it enters the SMPS and is exposed to the sheath RH and further dried.

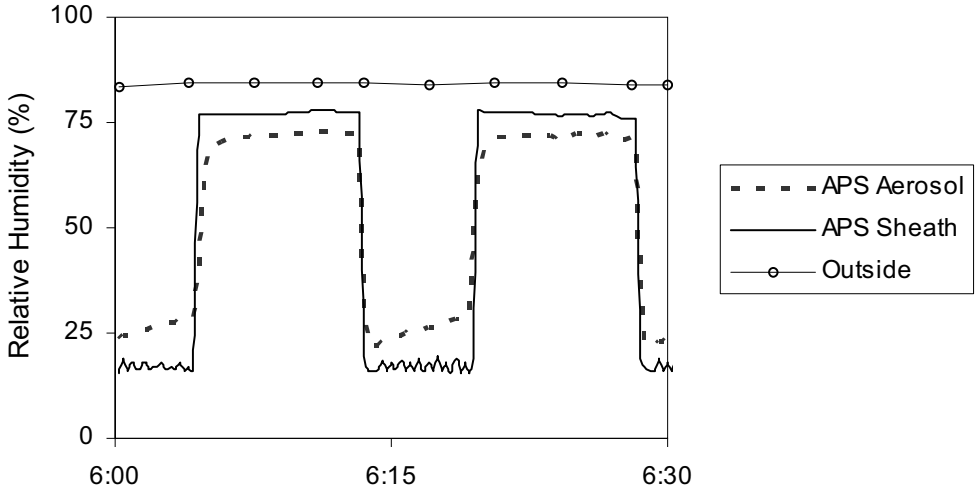

Figure 2.4 Example of relative humidity time series for APS portion of DAASS.

This slight mismatch in outdoor and SMPS ambient channel sheath flow relative humidities (evident in Figure 2.3) occurred during the duration of the Pittsburgh Air Quality Study. The mismatch was caused by insufficient purging of dry air from the system during the vent mode, which was limited by the strength of the standard sheath and bypass blowers in the TSI 3080 Differential

Mobility Analyzers. In future DAASS deployments, it is recommended that supplemental vacuum be used to assist in purging the system during the vent stage. Other explanations, such as a leak at the 3-way solenoid for the dryer bypass, and a positive pressure leak from the sheath- to the tube-side of the dryers were ruled out. When the vent time was increased from 5 minutes to 8 minutes for a test in August 2001, the outdoor-ambient water content mismatch decreased.

Raw particle count data from SMPS systems, temperatures and relative humidities were acquired using a PC, which also controlled solenoid valves responsible for selecting the operation mode (ambient, dried, or vent). Figure 2.5 shows an example of dried and wet size distributions measured during one hour. During that hour, the DAASS measured four dried size distributions at around 14% RH and 4 size distributions at 64% RH.

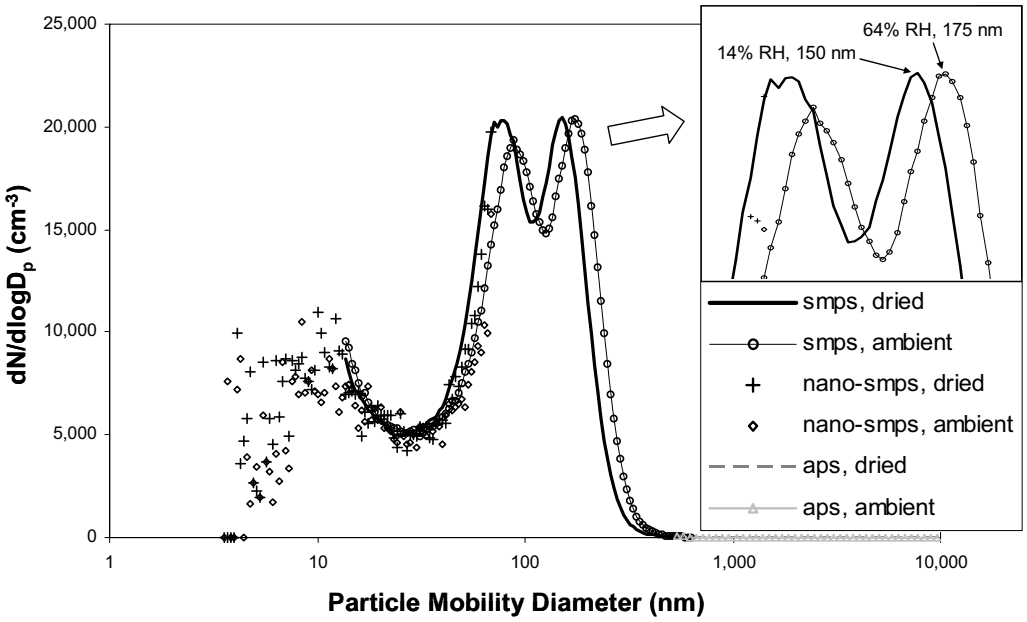

Figure 2.5 Dried and ambient number size distributions measured during the Pittsburgh Air Quality Study. Shown are one hour averages for 22:00 – 23:00 EST on July 3, 2001. The distribution labeled 64% RH is the average of 4 ambient distributions while the distribution labeled 14% RH is the average of 4 dried distributions.

2.3 Calibration and Testing

A number of characterization tests were performed in the laboratory. Goals during the calibration and characterization stage included inlet loss characterization, determining absolute sizing accuracy, measuring the sizing precision for ambient and dried inlet paths, and measuring the sizing precision when two instruments measured particles of the same size.

The APS time of flight response was calibrated using monodisperse aerosols prior to deployment in the field. This was done using polystryrene latex (PSL) spheres (Duke Scientific, Palo Alto, CA) at diameters equal to 600 nm and 2.1 μm and with monodisperse ammonium sulfate aerosols[3] with aerodynamic diameters from 0.5 to 1.6 μm. Above 2.1 μm, the factory time of flight calibration curve was used.

After the APS calibration, all three instruments of the DAASS system were checked for sizing accuracy simultaneously with monodisperse aerosols fed through a common inlet. PSL spheres (Duke Scientific, Palo Alto, CA) at diameters equal to 150 nm, 500 nm, 600 nm, and 2.1 μm were used.

The nano-SMPS system and SMPS system measurements overlapped in the diameter range from 13 to 80 nm. The SMPS and APS systems overlapped from 542 to 680 nm (mobility equivalent size). Sizing precision between dried and ambient inlets, and sizing from instrument-to-instrument in overlapping size ranges, were checked by sizing monodisperse ammonium sulfate through a

[3] Generated using a solution of ammonium sulfate in water, atomized using a TSI 3076 Constant Output Atomizer, dried in a silica gel diffusion dryer, and size classified using a TSI 3071 DMA.

common inlet to the DAASS in 14 different size ranges from 20 nm to 900 nm. Differences in particle sizing between instruments, and between ambient and drying inlet channels were less than 3% across the entire size range. Size-dependent inlet losses for the SMPS inlet were determined by measuring the difference in total particle counts across the DAASS inlet (including the aerosol dryer, dryer bypass line, neutralizers, and aerosol RH probe). Particle losses below 20 nm were estimated using empirical particle loss correlations from Willeke and Baron (1993). Default manufacture counting efficiencies were used for the CPC 3010 and CPC 3025.

The APS RH-conditioning inlet was designed for maximum possible particle transmission by minimization of tubing restrictions and bends. An inlet transmission efficiency was calculated accounting for turbulent inertial impaction to the inlet tubing walls with enhanced depositions at restrictions and bends (Willeke and Baron, 1993). The calculated transmission was nearly 100% for 0.5 μm particles and greater than 90% through 2.5 μm, but fell off to 85% transmission at 5 μm.

APS counting efficiencies from Leinert and Weidensohler (2000) were used in data reduction, and ranged from 58% for 512 nm, reaching 90% at 1 μm, and 100% at 1.33 μm. The APS 3320 is known to suffer from false counts, or "ghost particles" in sizing channels greater than 2.5 μm due to recirculation of small particles (Armendariz and Leith 2002). This behavior can clearly be seen in the APS 3320 data, and the reported size distributions, especially the surface area

and volume distributions, are elevated, sometimes significantly, above 2.5 microns.

After all these basic system characterizations were performed, the DAASS was used to measure diameters of hydrated and dried ammonium sulfate particles. This test was performed at the Pittsburgh Air Quality Study central sampling site by filling a 2 m^3 teflon bag with polydisperse ammonium sulfate particles. The ammonium sulfate was drawn from the Teflon bag, through a humidifier, and into the DAASS system which sampled alternately at the elevated (hydrated) relative humidity and a lower relative humidity (< 10% sheath RH). The results of the test are shown in Figure 2.6 and show reasonable agreement with calculated ammonium sulfate growth data (Ansari and Pandis 1999).

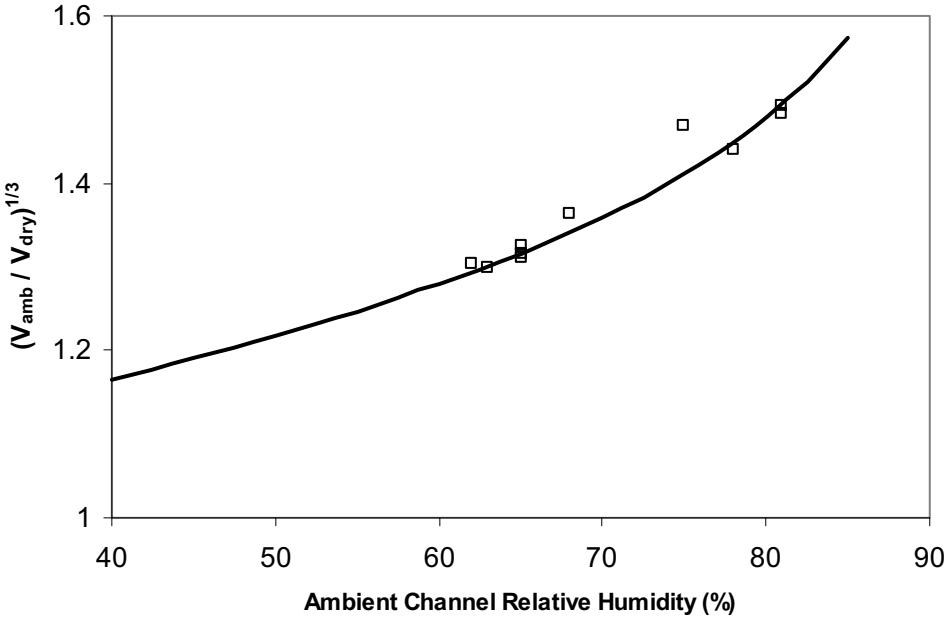

Figure 2.6 Theoretical (line) and measured (squares) growth factors for ammonium sulfate aerosol. Data for diameter growth factors calculated from Ansari and Pandis (1999). V_{amb} and V_{dry} are the aerosol volumes measured by the DAASS system in the ambient and dried configurations.

2.4 Data Reduction

2.4.1 Merging of separate size distributions into one size distribution

The raw SMPS size distributions were inverted by the TSI SMPS program (Version 3.2) and the APS distributions were inverted by the TSI Aerosol Instrument Manager program (Version 4.3). These inverted size distributions were then further corrected for counting efficiencies and inlet losses using the approach outlined in the previous section. The three different instrument distributions (nano-SMPS, SMPS, and APS) were merged to form a single size distribution for each 7.5 minute sampling interval. Merging size distributions between the nano-SMPS and SMPS instruments in the overlapping region of 13-80 nm was accomplished by using nano-SMPS data up to 30 nm, and then SMPS data above 30 nm. This creates a potential discontinuity in the merged size distribution at 30 nm. During most periods of operation, the agreement between the nano-SMPS and SMPS in the overlap region was within 10%.[4] However, when the strength of local sources varied rapidly relative to the 5 minute scan time, the agreement between the two instruments was not good on a distribution-by-distribution comparison. During periods of highly variable particle size distributions, one-hour averaging reduced, but did not always eliminate, the discontinuity in size distribution at 30 nm. This limits the use of the data taken during these periods for applications that depend on the shape of the number distribution between 20 and 40 nm. However, for applications using the aerosol volume distribution, the discontinuity is not a serious issue.

[4] See the DAASS Data Quality Statement in the appendix for additional information on the accuracy and precision of the DAASS instrument during the Pittsburgh Air Quality Study.

Merging the SMPS and APS data was more involved, due to the inherent difference between the electrical mobility measured by the SMPS and the aerodynamic diameter measured by the APS. The procedure used is explained in detail in Khylstov et al. (2002). Briefly an apparent density was selected to minimize the difference between the SMPS and APS number distributions in the overlap region. Thus, the shape of the APS distribution was preserved, while the x-axis of the APS-measured size distribution was shifted to achieve a good fit with the SMPS-measured size distribution.

2.4.2 Calculation of aerosol water content

A number of related calculations can be performed with the size distributions measured by the DAASS. The selection among the data reduction methods depends on the application. Described below are calculations for (a) volume growth factors; (b) $PM_{2.5}$ water content; (c) efflorescence branch humidigrams; and (d) mass growth factors. The first two calculations focus on measuring aerosol water at ambient relative humidity. The third examines water content as a function of relative humidity, and the last is necessary for comparison of DAASS data to mass-based aerosol water correlations and models. The first three calculations are performed with data solely from the DAASS, while the fourth calculation requires aerosol composition data.

As discussed in the experimental section, the ambient channel relative humidity was slightly lower than the outdoor relative humidity. Therefore, for the calculations presented below, it should be recognized that they are calculated and

reported as a function of the ambient channel relative humidity, rather than the outdoor relative humidity.[5]

2.4.2.1 Calculation of volume growth factor

Once the size distributions are merged, hygroscopic growth factors are calculated for pairs of ambient and dried size distributions using the volume distributions and assuming a single, size independent growth factor GF_{VOL}:

$$GF_{VOL} = \frac{V_{RH2}}{V_{RH1}} = \frac{\int_0^{D_{RH2}} D^3 n^o_{N,RH2}(\log D) d\log D}{\int_0^{D_{RH1}} D^3 n^o_{N,RH1}(\log D) d\log D} \quad (2.1)$$

where D is the particle diameter, V_{RH2} and V_{RH1} are the aerosol volume concentrations measured using the ambient (RH2) and dried (RH1) inlets, $n°_{N,RH2}$ and $n°_{N,RH1}$ are the ambient and dried aerosol size distributions, and D_{RH2} and D_{RH1} are appropriately selected limits of integration. Figure 2.7 shows an example of the relationship between hypothetical dried and ambient size distributions (assuming a single size-independent growth factor), and the limits of integration. For this study, focusing on the water content of the fine aerosol, an upper integration limit D_{RH2} of 2.5 μm was used. This limit is analogous to the size selection performed by the $PM_{2.5}$ cyclone often employed in aerosol sampling. Using larger diameters was not possible due to the ghost particle artifact in the APS 3320 volume distributions (Armendariz and Leith 2002). The

[5] This means that the reported absolute value of the aerosol water concentration of hydrated aerosols is biased low, especially when ambient RH > 80%. However, the growth factor as a function of relative humidity is a property of the aerosol, and is measured without bias. For 10 μg m^{-3} pure ammonium sulfate aerosol, an outdoor RH of 60% and an instrument RH of 48%, the reported vs. actual water concentration would be 4.0 vs. 6.0 μg m^{-3}. For an outdoor RH of 90% and an instrument RH of 72%, the reported vs. actual concentration is 9.2 vs. 24.5 μg m^{-3}.

lower limit of integration is theoretically zero, but any value where there is minimal aerosol volume smaller than that size is acceptable. The integration limits for the dried and ambient size distributions are related by the volume (or diameter) growth factor, again assuming a single, size independent growth factor:

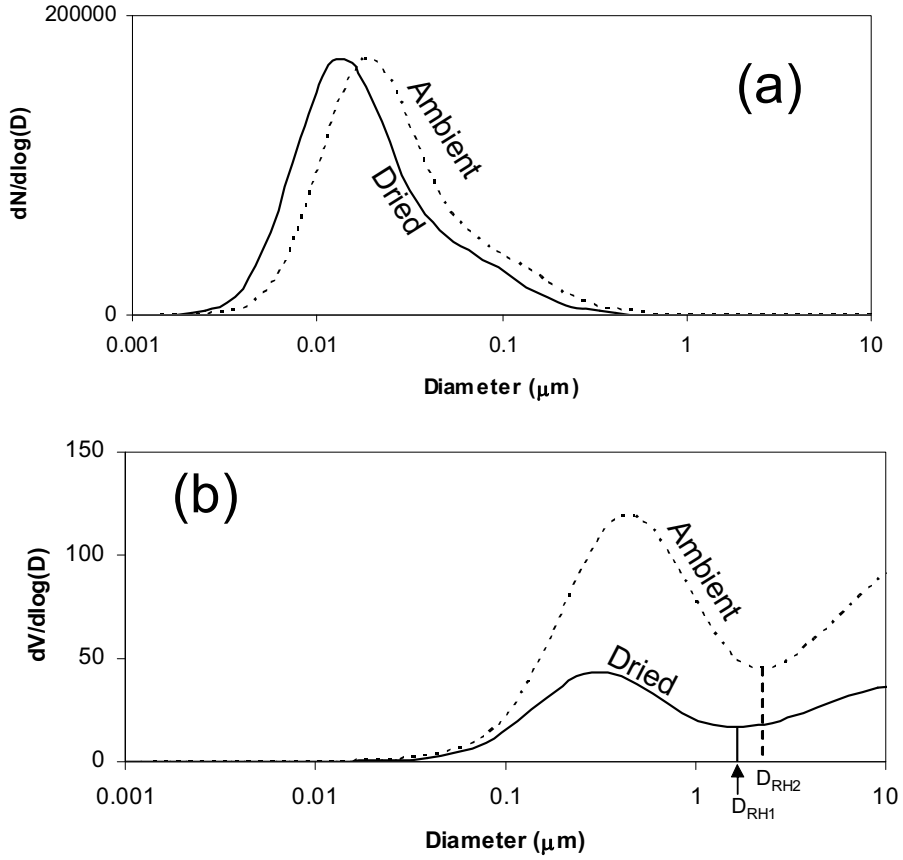

Figure 2.7 Illustration of the difference between dried and hydrated number and volume distributions. The figure shows a hypothetical tri-modal log-normal distribution being shifted by a size-independent growth factor. The volume growth factor calculated in this study is the ratio of the volume integrals. The shifting of the upper volume integration limit with hygroscopic growth (equation 2.2) is shown by the difference between D_{RH2} and D_{RH1}.

$$D_{RH2} = D_{RH1}\sqrt[3]{GF_{VOL}} \tag{2.2}$$

Equations (2.1) and (2.2) can be solved iteratively[6], given any pair of size distributions to find a volume growth factor GF_{VOL} that accounts for the differences between the ambient and dried volume distributions.

A brief discussion of the assumption of a single growth factor is instructive, as several H-TDMA investigations (Cocker et al. 2001b and sources therein) have shown that urban aerosols are usually externally mixed, with two or more populations of aerosols with different hygroscopicities. What is calculated by equations (2.1) and (2.2) is approximately the volume-weighted average growth factor of the various externally mixed aerosol subpopulations. Interpretation of this growth factor (as a volume-weighted average) is relatively straight forward unless the limit of integration D_{RH2} is inappropriately selected and a significant fraction of the particle volume lies above the limit. Simulations with log-normal externally-mixed aerosol modes of different hygroscopicities show that the growth factor calculated by equations (2.1) and (2.2) may be biased low under this circumstance. This error is expected to be small for the Pittsburgh Air Quality Study when an upper integration limit of 2.5 μm is used, as most aerosol volume is less than 2.5 μm and coarse aerosols are expected to be less hygroscopic than the accumulation mode.

As the dried and ambient aerosol distributions are not measured at the same time, but are separated by some sampling interval Δt, steady increases or

[6] The unknowns in the iterative solution of equations 2.1 and 2.2 are GF_{VOL} and $D_{2,RH1}$. For the Pittsburgh Air Quality Study, the value of $D_{2,RH2}$ was set at 2.5 μm or 0.56 μm depending on data availability in the size range 0.56-2.5 μm. The lower limits of integration were 3 nm. The size distribution functions $n^{o}_{N,RH1}(\log D)$ and $n^{o}_{N,RH2}(\log D)$ were measured by the DAASS.

decreases in the aerosol volume will lead to biases in the growth factor calculated by equation (2.1). This can be corrected for with the following correction factor β:

$$GF'_{VOL} = GF_{VOL}\beta = GF_{VOL}\frac{1}{1+\frac{V'_{dry}}{V_{dry}}\Delta t} \tag{2.3}$$

where Δt is the amount of time by which the dried measurements precede the ambient measurements and V'_{dry} is the rate of change of the background dry aerosol volume with respect to time. In the limits where the dried and ambient measurements are performed simultaneously or the background aerosol volume is stable with respect to time, the correction factor β goes to unity. This factor was usually between 0.97 and 1.03 for the Pittsburgh Air Quality Study.

As the DAASS method relies on the difference between two aerosol size distributions measured at different times (about 7 minutes from the start of the ambient scan to the dried scan), variability in the underlying aerosol size distribution on a timescale of shorter than a few minutes can lead to random error in water content calculations. Variability in the mean and average rate of change of the dried volume for each hour is calculated and propagated through the water content calculations as uncertainty in the parameters GF_{VOL} calculated in equation (2.1) and β calculated in equation (2.2). Calculated growth factors for four days of sampling are shown in Figure 2.8. The time series shows that growth factors are not a simple function of relative humidity and that they can change rapidly with changing meteorology and composition.

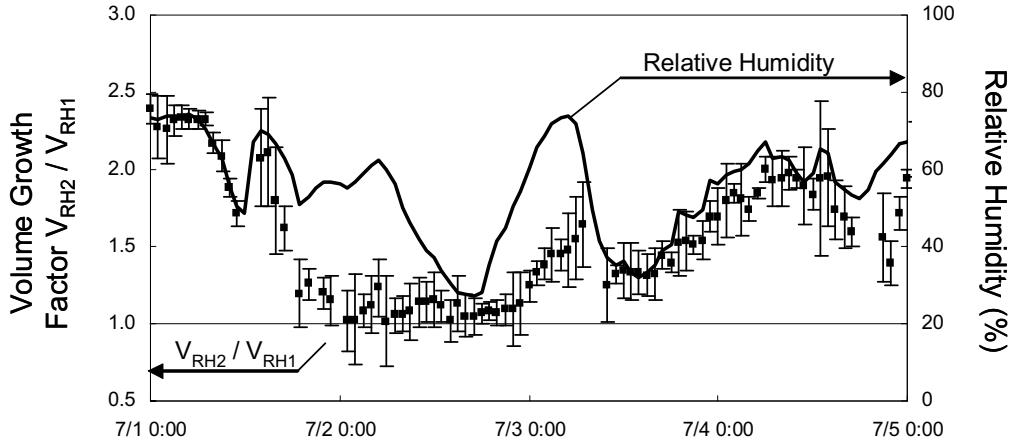

Figure 2.8 Sample results of volume growth factors as measured by the DAASS for July 1 – July 4, 2001. The relative humidity trace is the relative humidity of the ambient channel. The relative humidity of the dried samples was 18 ± 6%.

2.4.2.2 Calculation of PM2.5 water content at ambient channel relative humidity

Using the growth factor calculated above in equation (2.1), the aerosol water content can be estimated. The method uses only data from the DAASS and relies on two assumptions: (1) water is the only semivolative species causing a volume change; and (2) volume is additive between aerosol water and non-volatile aerosol components. Applying these assumptions, we can write equation (2.4)

$$V_{H2O,RH2-RH1} \cong V_{RH2} - V_{RH1} \tag{2.4}$$

where $V_{H2O,RH2-RH1}$ is the volume of evaporated water from the ambient (RH2) channel to the dried (RH1) channel. Combining equations (2.4) and (2.1)

$$V_{H2O,RH2-RH1} = (GF_{VOL} - 1)V_{RH1} \tag{2.5}$$

where the upper limit for integration of aerosol volume is 2.5 μm for the ambient channel (D_{RH2}) and the upper limit for integration of the dried distribution is given by equation (2.2). If we further assume minimal residual water content at the

dried relative humidity, then $V_{H2O,RH2-RH1}$ is equal to $V_{H2O,RH2}$, or the amount of aerosol water at ambient relative humidity. Aerosol water contents for July 1 – July 7, 2001 calculated using this method are shown by the filled squares in Figure 2.9b and as a fraction of total dried aerosol mass in Figure 2.9d. These time series correspond to ambient channel relative humidities shown in Figure 2.9a. Figure 2.9 shows that that the DAASS system has good dynamic range in the aerosol water content measurements, ranging from less than 1 $\mu g/m^3$ of water up to 20-30 $\mu g/m^3$ of water and from less than 5% of the dried aerosol mass to around 100% of the dried aerosol mass. Furthermore, the time response is excellent, with experimental system and data reduction methods following rapid changes in aerosol volume, aerosol water content, and hygroscopicity.

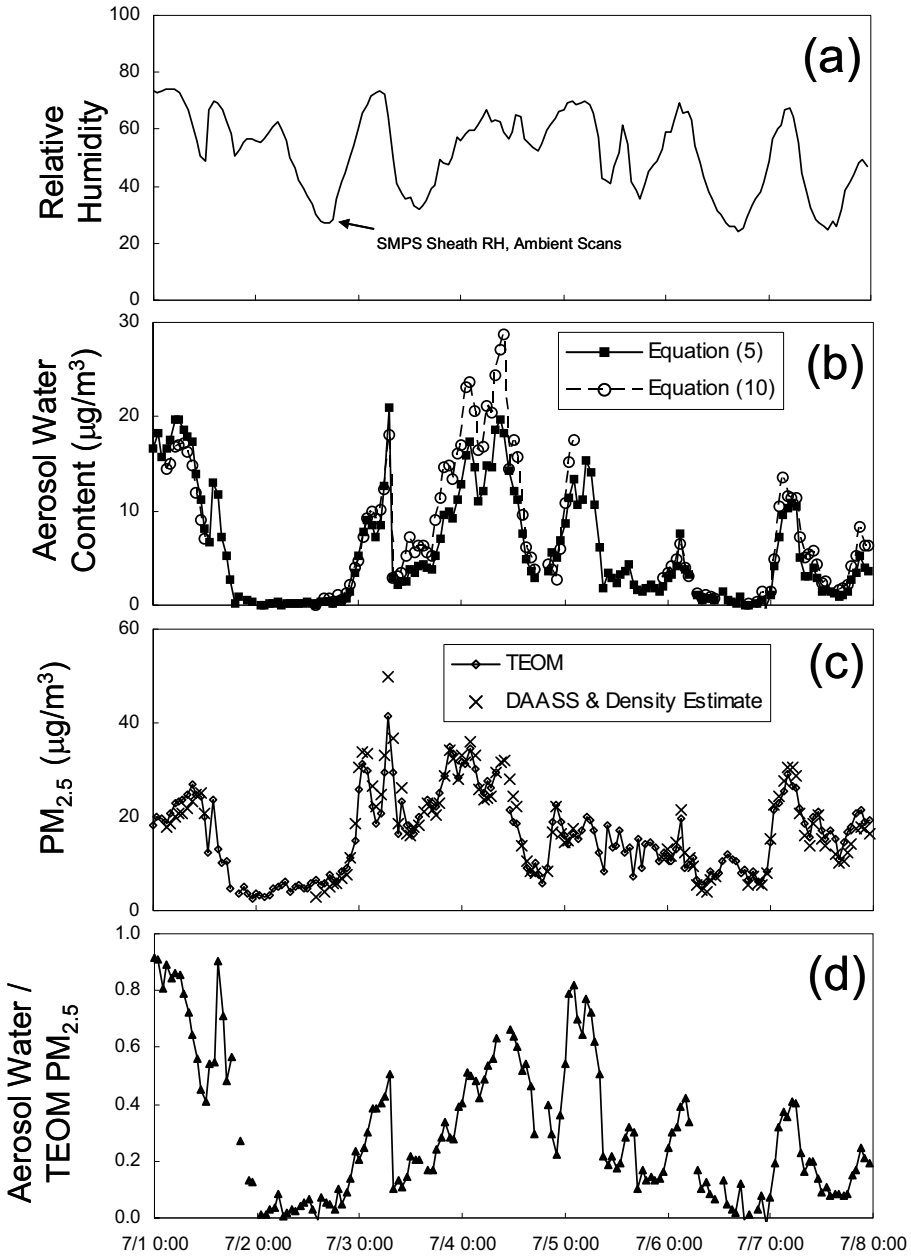

Figure 2.9 Example of aerosol water content measurement for a 7 day period. (a) ambient channel relative humidity; (b) calculated mass of aerosol water by the difference of ambient and dried volume (equation 2.5) and using an estimated mass growth factor (equation 2.10); (c) PM2.5 measured by TEOM (circles and solid line) and using the DAASS measured volume and composition-based density estimate (x symbols); and (d) ratio of measured water to the TEOM. As noted in the experimental section, these samples are from the time period when the DMA columns were inside the enclosure and the outdoor RH may be up to 20% higher than the ambient channel value in the figure.

2.4.2.3 Calculation of efflorescence branch humidigrams

Aerosol water content is a function of relative humidity, chemical composition, and state of hydration (deliquescence branch or efflorescence branch). When aerosol water content is a smooth function of relative humidity (e.g. moving on the efflorescence branch without crystallization) growth factors as a function of relative humidity can be fit to simple empirical functions. For significant periods of the Pittsburgh Air Quality Study, growth factors were a smooth function of relative humidity, with no apparent deliquescence or crystallization behavior (Khlystov et al. 2003). Therefore, groups of growth factors representing relatively constant aerosol composition, but with different relative humidities, could be fit to an empirical function such as that used by Dick et al. (2000):

$$\frac{V(RH)}{V_{dry}} = 1 + (a + bRH + cRH^2)\frac{RH}{1 - RH} \tag{2.6}$$

where a, b, and c are adjustable parameters. In conjunction with DAASS determined volume growth factors GF_{VOL}, the parameters a, b, and c could be determined by regression:

$$GF_{VOL} = \frac{1 + (a + bRH_2 + cRH_2{}^2)\dfrac{RH_2}{1 - RH_2}}{1 + (a + bRH_1 + cRH_1{}^2)\dfrac{RH_1}{1 - RH_1}} \tag{2.7}$$

Examples of the humidigrams calculated using groups of measured growth factors are shown in Figure 2.10. The difference in the humidigrams between these two time periods is probably related to the aerosol chemistry, which contained more organic matter (52 wt%) on July 7 than on July 5 (38 wt%).

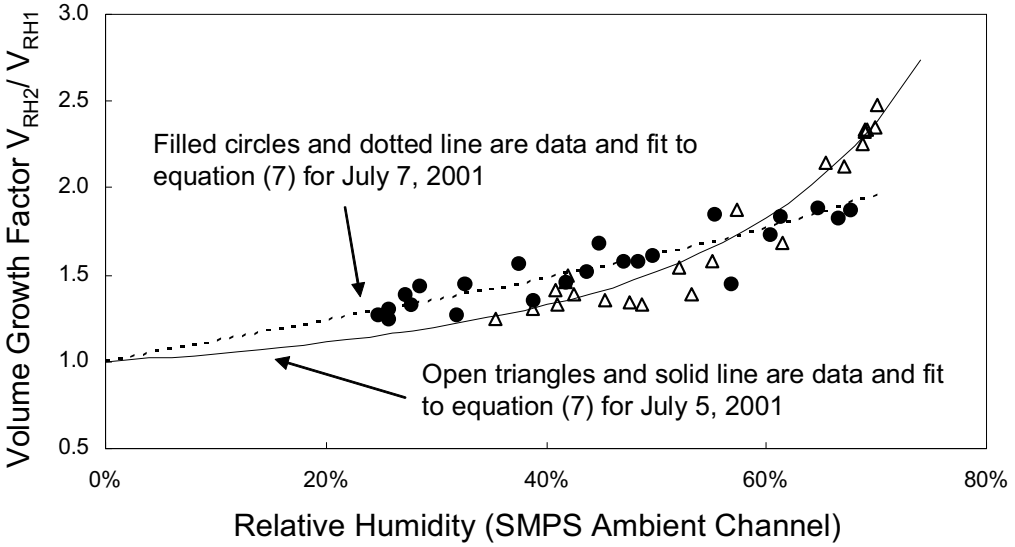

Figure 2.10 Example of humidigrams for two different days (July 5 and 7, 2001). Points are measured hourly volume growth factors, and lines are fits of the hourly data to equation (2.7).

In certain applications, it is necessary to calculate aerosol water content at a specific relative humidity. For example, DAASS data has been used to help estimate residual aerosol water in filter-based samples equilibrated at relative humidities from 15-35% (Rees et al. 2003). The calculation of residual water is performed using equation (2.6), subject to the assumptions discussed above.

2.4.2.4 Calculation of the mass growth factor

For comparison of volume growth factors to models and correlations involving mass growth factors, it can be useful to convert the DAASS measured volume growth factors to mass growth factors. To do this we need to estimate the density of the aerosols as a function of relative humidity using aerosol composition information from sources other than the DAASS instrument. The equations involved in the conversion from the volume to mass growth factor, and

a simple method for density estimation during the Pittsburgh Air Quality Study, are developed below.

The volume and mass growth factors are related by equation (2.8)

$$GF_{MASS} = GF_{VOL} \frac{\rho_{RH2}}{\rho_{RH1}} \tag{2.8}$$

where ρ_{RH2} and ρ_{RH1} are the hydrated (RH2) and dried (RH1) densities.

With this mass-based growth factor in hand, a mass-based estimate of aerosol water content can be made and compared to the volume-based calculation in equation (2.5). The remainder of this section first covers the aerosol water mass balance, and then methods for aerosol density estimation for the Pittsburgh Air Quality Study are developed.

This definition of the mass growth factor can be used to write the aerosol mass balance (assuming water is the only semivolatile species that partitions as relative humidity changes). If M_{dry} is the completely dehydrated aerosol mass, $M_{H2O,RH2\text{-}RH1}$ is the water released from the aerosol as it dries from ambient relative humidity (RH2) to the dried channel relative humidity (RH1), and $M_{H2O,RH1}$ is the residual aerosol water at the dried relative humidity (RH1) then

$$M_{RH2} = M_{dry} + M_{H2O,RH2-RH1} + M_{H2O,RH1} = \left(M_{dry} + M_{H2O,RH1}\right) GF_{MASS} \tag{2.9}$$

where ρ_{RH2} and ρ_{RH1} are the hydrated (RH2) and dried (RH1) densities. $M_{H2O,RH2\text{-}RH1}$ is the water released from the aerosol as it dries from ambient relative humidity (RH2) to the dried channel relative humidity (RH1). Conceptually, there are three possibilities for the behavior of the aerosol water content as the aerosol is dehydrated. At the low RH all particles are dry, or they all have some

water, or some of them lose water and some do not. The first case corresponds to $M_{H2O,RH1}$ equal to zero. The other two cases correspond to non-zero values for $M_{H2O,RH1}$. The DAASS instrument gives the a measurement of $M_{H2O,RH2\text{-}RH1}$. Since the relative humidity RH1 is kept as low as possible, $M_{H2O,RH1}$ is expected to be small compared to $M_{H2O,RH2\text{-}RH1}$. Assuming $M_{H2O,RH1}$ is negligible, $M_{H2O,RH2}$ is then given by equation (2.10).

$$M_{H2O,RH2} \approx M_{dry}\left(GF_{MASS} - 1\right) = M_{dry}\left(GF_{VOL} - 1\right)\frac{\rho_{RH2}}{\rho_{RH1}} \tag{2.10}$$

The density calculations assume that the aerosol is an internal mixture consisting of inorganic matter, organic matter, and elemental carbon fractions, each with a fixed characteristic density. The dry density is calculated assuming volume additivity and that $M_{H2O,RH1}$ is negligible:

$$\rho_{RH1} = \left(\sum \frac{f_{OM}}{\rho_{OM}} + \frac{f_{EC}}{\rho_{EC}} + \frac{f_{inorg,dry}}{\rho_{inorg,dry}}\right)^{-1} \tag{2.11}$$

where f refers to mass fraction, ρ to density, and the subscripts OM, EC, and inorg,dry refer to organic matter, elemental carbon, and dry inorganic mass. The ambient humidity density is estimated assuming the aerosol consists of three fractions, a hydrated inorganic fraction, an elemental carbon fraction (assumed not to take up any water), and an organic fraction (assumed not to take up any aerosol water).

$$\rho_{RH2} = \left(\sum \frac{f_{OM}}{\rho_{OM}} + \frac{f_{EC}}{\rho_{EC}} + \frac{f_{inorg,dry} + f_{H2O,RH2}}{\rho_{inorg,wet}}\right)^{-1} \tag{2.12}$$

where $\rho_{inorg,wet}$ refers to the density of the hydrated inorganics.

For this work the $PM_{2.5}$ measured by a TEOM (Rupprecht & Patashnick, Albany, NY) at 30 °C with a sample equilibration system (Meyer et al. 2002) was used for M_{dry}. The mass measured by the instrument was in good agreement with the Federal Reference Method for particulate mass during these tests (Rees et al. 2003). The sample equilibration system is a semipermeable membrane drying inlet for the TEOM that conditions the aerosol sample at 30°C and ~15% relative humidity. The organic matter mass used for calculations in this study was 1.8 times the organic carbon (OC). EC (elemental carbon) and OC were measured by the thermal optical method (Cabada et al. 2002). The 1.8 multiplier for carbonaceous mass is based on estimates of Turpin and Lim (2001). Densities of 1.2, 1.6, and 1.77 g/cm^{-3} were assumed for organic matter, elemental carbon aerosol, and dry inorganic aerosol, respectively. The organic matter density is based on Turpin and Lim (2001) and the dry inorganic mass corresponds to that of ammonium sulfate, the dominant inorganic component in the Pittsburgh area (Anderson et al. 2002). The elemental carbon density is most uncertain as recent measurements show great variability in the effective density (0.2 – 1.6 g/cm^3) of soot agglomerates depending on formation conditions (Park et al. 2003 and references therein). However, because of the small contribution of elemental carbon to the total aerosol concentration in Pittsburgh, the specific value chosen has little effect on the volume to mass growth factor conversion in this study. The 1.6 g/cm^3 value used in this work is at the upper end of effective densities measured by Park (2003) and at the lower end of the range for the physical density of graphite (Perry et al. 1984). The carbonaceous fraction is assumed to

not take up any water in this work, and the hydrated density for ammonium sulfate, calculated using empirical values from Tang (1997), is used for the ambient relative humidity inorganic density.

The main use of the equations (2.8) – (2.12) is for comparison of experimental (volume-based) growth factors with mass-based growth factors from other sources (i.e. thermodynamic models). The comparison can be made on the basis of predicted versus measured aerosol water content, or on the basis of predicted versus measured growth factors. In both cases, equations (2.8) – (2.12) will be required to make the comparison. While this work does not contain any mass-based water content measurements or model predictions (see Khlystov et al. (2003) for model-measurement comparisons), this type of calculation is demonstrated by the open circles in Figure 2.9b, which are an estimate of aerosol water content from equation (2.10) based on the DAASS-measured volume growth factors, estimates of aerosol density using equations (2.11) and (2.12), and the time series of M_{dry} measured independently of the DAASS system. The difference between the water content calculation by equations (2.5) and (2.10) can be attributed to (a) uncertainty in the density calculations, composition, and organic mass multiplier; (b) violations of assumptions such as non-hygroscopic organics and negligible water content in the dried channel; and (c) drifts in the absolute accuracies of the various independent instruments that are involved in making the volume-based aerosol calculations (SMPS & APS) and the mass-based calculations (TEOM, OC/EC sampler, and inorganic ions sampler). The mismatch is particularly evident during July 3 and 4. In light of these possible

errors and uncertainties, equation (2.5) is recommended as a more robust estimate of aerosol water content than equation (2.10). A further demonstration of the connection between aerosol mass, aerosol volume, and composition-based density estimates (all measured independently) is shown by the comparison in Figure 2.9c of M_{dry} measured by two independent techniques. The TEOM mass measurement is compared to the DAASS estimated aerosol mass calculated using the density formula in equation (2.11).

2.5 Discussion of some sources of error

Differences in relative humidity between the bipolar aerosol charger, aerosol flow entering the DMA, and DMA sheath flow can cause changes in the physical state of the particles and errors in particle sizing and/or counting. First, the aerosol may be charged in the bipolar charger while at a different relative humidity (and therefore size) than in the DMA. Second, heated zones of the inlet prior to the classifier (which is at ambient temperature) may induce crystallization of the aerosol. Finally, the difference in the aerosol and sheath flows may cause a size change during size classification. The implications of these errors are discussed below.

Parts of the aerosol inlet (including the bipolar charger) were inside the enclosure, which was usually a few degrees warmer than the DMA column, located outside the enclosure. This caused the relative humidity of the aerosol flow during ambient scans to go through a minimum inside the enclosure, at the time of aerosol charging. In winter, the enclosure (and bipolar charger) was maintained at 9 °C, while outdoor temperatures dropped to approximately -5 °C.

As a result of these two effects, in general, the aerosol charging was not at the same relative humidity as the size classification in the DMA. For hydrated particles, this means that aerosols may be charged at one size and then classified at another, creating an error in the equilibrium charge distribution assumed during the inversion of the raw SMPS data. This generally leads to an underestimation in the particle number at sizes smaller than about 200 nm, and an overestimation at sizes greater than about 200 nm. The magnitude of this error was estimated using the study average size distribution and an assumed composition of 50% ammonium sulfate and 50% organics and other nonhygroscopic material. Volume growth factors are biased high by a factor of 1.00 to 1.14, with the greatest effects at low temperatures and humid conditions. Our error estimates are shown in Table 2.1.

Table 2.1 Estimates in growth factor bias due to charging under dryer conditions than classification

	Outside Temperature		
Outside Relative Humidity	5 °C	0 °C	-5 °C
50%	+ 3%	+ 3%	+ 3%
70%	+ 2%	+ 6%	+ 6%
85%	+ 4%	+ 6%	+ 10%
92%	+ 7%	+ 10%	+ 14%

The higher inlet temperatures compared to ambient caused temporary drying of the ambient channel aerosol before it was returned to ambient temperature for size classification. During the coldest periods of the study, this drying effect could be important. Therefore, the minimum relative humidity experienced by the aerosol en route to classification is calculated and reported with the PAQS data to allow more complete interpretation of the results.

Sheath-aerosol stream mismatch should not pose a problem as the thermodynamic equilibration time is expected to be short compared to the transit times in the DMAs (0.3 s and 6 s for the N-SMPS and SMPS, respectively). Characteristic times for equilibration of pure water droplets up to 1 micron in size under the conditions in the SMPS should be of order 10^{-3} s. There is evidence from laboratory studies that coatings of hydrophobic organics over salts (5-60% wt% organics) may hinder mass transfer (Wagner et al. 1996; Xiong et al. 1998), although the extension of these laboratory studies to atmospheric particles has not been established. To test the assumption that the sheath-aerosol relative humidity mismatch did not significantly affect the results, an experiment was performed in 2002 during the Pittsburgh Air Quality Study where the SMPS aerosol was dried more thoroughly (~20% RH) than usual (~50% RH) while the sheath relative humidity was held at around 5%. The organic fraction of the aerosol was between 30 and 50% on the day of the experiment and the outdoor relative humidity was between 85 and 95%. No shift in the dried aerosol size distribution could be detected due to the lower relative humidity and increased time for mass transfer at low relative humidity.

2.6 Summary and Conclusion

A system has been constructed for the in-situ measurement of aerosol water content at atmospheric conditions. The system relies on a combination of aerosol sizing instruments and samples the atmospheric aerosol at ambient temperature and at two relative humidities. The DAASS measures the aerosol volume growth factor (ratio of the ambient and dried aerosol volume

concentrations) and aerosol water content every 15 minutes. A variety of data reduction procedures were presented to convert the raw data to growth factors and aerosol water content, and (when combined with aerosol composition measurements) to facilitate comparison with mass-based growth factors from other sources. DAASS operated for a year during the Pittsburgh Air Quality Study.

The system was tested with ammonium sulfate particles equilibrated at different relative humidities and its results were in good agreement with the known hygroscopic properties of the particles. The preliminary field results show good response to relative humidity and dry particle mass with the water concentration varying from almost zero to more than 20 $\mu g/m^3$ (0-50% of the hydrated particle mass). The detailed measurements of water during PAQS and the comparison of these measurements with predictions of theoretical models are discussed in detail in a companion paper (Khlystov et al. 2003).

2.7 Acknowledgements

This research was conducted as part of the Pittsburgh Air Quality Study which was supported by US Environmental Protection Agency under contract R82806101 and the US Department of Energy National Energy Technology Laboratory under contract DE-FC26-01NT41017.

2.8 References

Anderson, R.R., Martello, D.V., Rohar, P.C., Stazisar, B.R., Tamilia, J.P., Waldner, K., and White, C.M. (2002). Sources and Composition of PM2.5 at

the National Energy Technology Laboratory in Pittsburgh During July and August 2000, Energy and Fuels 16:261-269.

Ansari, A.S., and Pandis, S.N. (1999). Prediction of Multicomponent Inorganic Atmospheric Aerosol Behavior, *Atmos. Environ*. 33:745-757.

Ansari, A.S., and Pandis, S.N. (2000). Water Absorption by Secondary Organic Aerosol and Its Effect on Inorganic Aerosol Behavior, *Environ. Sci. Technol*. 34:71-77.

Armendariz, A.J., and Leith, D. (2002). Concentration Measurement and Counting Efficiency for the Aerosol Particle Sizer 3320, *J. Aerosol Sci.* 33:133-148.

Berg, O.H., Swietlick, E., and Krejci, R. (1998). Hygroscopic Growth of Aerosol Particles in the Marine Boundary Layer Over the Pacific and Southern Oceans During the First Aerosol Characterization Experiment, *J. Geophys. Res*. 103(D13):16,535-16,545.

Brooks, S.D., Wise, S.E., Cushing, M., and Tolbert, M.A. (2002). Deliquescence Behavior of Organic/Ammonium Sulfate Aerosol, *Geophys. Res. Let.* 29(19):1917.

Cabada, J.C., Pandis, S.N., and Robinson, A.L. (2002). Sources of Atmospheric Carbonaceous Particulate Matter in Pittsburgh, Pennsylvania, *J. Air Waste Manage*. 52(6):732-741.

Chan, C.K., Flagan, R.C., and Seinfeld, J.H. (1992). Water Activities of Ammonium Nitrate/Ammonium Sulfate Solutions, *Atmos. Environ*. 26A(9):1661-1673.

Clegg, S. L., Seinfeld, J. H., and Brimblecombe, P. (2001). Thermodynamic Modeling of Aqueous Aerosols Containing Electrolytes and Dissolved Organic Compounds, *J. Aerosol Sci*. 32(6):713-738.

Cocker, D.R. III, Clegg, S.L., Flagan, R.C., and Seinfeld, J.H. (2001). The Effect of Water on Gas-Particle Partitioning of Secondary Organic Aerosol. Part I: α-Pinene/Ozone System, *Atmos. Environ.* 35:6049-6072.

Cocker, D.R., III, Mader, B.T., Kalberer, M., Flagan, R.C., and Seinfeld, J.H. (2001). The Effect of Water on Gas-Particle Partitioning of Secondary

Organic Aerosol: II. m-Xylene and 1,3,5-Trimethylbenzene Photooxidation Systems, *Atmos. Environ.* 35:6073-6085.

Cocker, D.R., III, Whitlock, N.E., Flagan, R.C., and Seinfeld, J.H. (2001). Hygroscopic Properties of Pasadena, California Aerosol, *Aerosol Sci. Technol.* 35:637-647.

Cruz, C.N. and Pandis, S.N. (2000). Deliquescence and Hygroscopic Growth of Mixed Inorganic-Organic Atmospheric Aerosol, *Environ. Sci. Technol*. 34:4313-4319.

Day, D.E., Malm, W.C., and Kreidenweis, S.M. (2000). Aerosol Light Scattering Measurements as a Function of Relative Humidity, *J. Air Waste Manage.* 50:710-716.

Dick, W.D., Saxena, P., and McMurry, P.H. (2000). Estimation of Water Uptake by Organic Compounds in Submicron Aerosols Measured During the Southeastern Aerosol and Visibility Study, *J. Geophys. Res*. 105(D1):1471-1479.

Han, J. and Martin, S.T. (1999). Heterogeneous Nucleation of the Efflorescence of $(NH_4)_2SO_4$ Particles Internally Mixed with Al_2O_3, TiO_2, and ZrO_2, *J. Geophys. Res.* 104:3543.

Han, J.H., Hung, H.M., and Martin, S.T. (2002). The Size Effect of Hematite and Corundum Inclusions on the Efflorescence Relative Humidities of Aqueous Ammonium Nitrate Particles, *J. Geophys. Res.* 107(D10):4086.

Hanel, G. (1976). The Properties of Atmospheric Aerosol Particles as Functions of Relative Humidity at Thermodynamic Equilibrium with Surrounding Moist Air in *Advances in Geophysics, Vol. 19*. Academic Press. New York, pp. 73 - 188.

Khlystov, A., Stanier, C., Vayenas, D., and Pandis, S.N. (2003). Water Content of Ambient Aerosols During the Pittsburgh Air Quality Study: Experimental Measurements and Thermodynamic Modeling Results. Submitted to *Atmos. Environ*.

Kreisberg, N.M., Stolzenburg, M.R., and Hering, S.V. (2001). A New Method for Measuring the Dependence of Particle Size Distributions on Relative

Humidity, with Application to the Southeastern Aerosol and Visibility Study, *J. Geophys. Res*. 106:14,935-14,949.

Lee, C.T., and Hsu, W.C. (1998). A Novel Method to Measure Aerosol Water Mass. *J. of Aerosol Sci.* 29(7):827-837.

Leinert, S. and Wiedensohler, A. (2000). APS Counting Efficiency Calibration for Submicrometer Particles. *J. Aerosol Sci*. 31:S404-S405.

Martin, S.T., Han, J., and Hung, H.M. (2001). The Size Effect of Hematite and Corundum Inclusions on the Efflorescence Relative Humidities of Aqueous Ammonium Sulfate Particles, *Geophys. Res. Let.* 28:2601.

Meyer, M.B., Patashnick, H., Ambs, J.L., and Repprecht, E. (2000). Development of a Sample Equilibration System for the TEOM Continuous PM Monitor, *J. Air Waste Manage. 5*0(8):1345-1349.

McMurry, P.H., and Stolzenberg, M. (1989). On the Sensitivity of Particle Size to Relative Humidity for Los Angeles Aerosols, *Atmos. Environ*. 23(2):497-507.

Ohta, S., Hori, M., Yamagata, S., and Murao, N. (1998). Chemical Characterization of Atmospheric Fine Particles in Sapporo With Determination of Water Content, *Atmos. Environ*. 32(6):1021-1025.

Onasch, T.B., Siefert, R.L., Brooks, S.D., Prenni, A.J., Murray, B., Wilson, M.A., and Tolbert, M.A. (1999). Infrared Spectroscopic Study of the Deliquescence and Efflorescence of Ammonium Sulfate Aerosol as a Function of Temperature, *J. of Geophys. Res*. 104 (D17): 21,317-21,326.

Park, K., Cao, F., Kittelson, D., and McMurry, P.H. (2003). Relationship Between Particle Mass and Mobility for Diesel Exhaust, *Environ. Sci. and Technol*. 37: 577-583.

Peng, C., Chan, M.N., and Chan, C.K. (2001). The Hygroscopic Properties of Dicarboxylic and Multifunctional Acids: Measurements and UNIFAC Predictions, *Environ. Sci. Technol.*, 35(22):4495-4501.

Perry, R.H., Green, D.W., and Maloney, J.O. (1984). *Perry's Chemical Engineering Handbook*, *6th Ed*., McGraw Hill: New York, NY. pp. 3-96.

Rader, D.J. and McMurry, P.H. (1986). Application of the Tandem Differential Mobility Analyzer to Studies of Droplet Growth or Evaporation, *J. Aerosol Sci*. 17(5):771-787.

Rees, S.L., Robinson A.L, Khlystov, A., Stanier, C.O., Pandis, S.N. (2003). Mass Balance Closure and the Federal Reference Method for $PM_{2.5}$ in Pittsburgh, Pennsylvania, submitted to Atmospheric Environment.

Rood, M.J., Covert, D.S., and Larson, T.V. (1987). Temperature and Humidity Controlled Nephelometry: Improvements and Calibration, *Aerosol Sci. Technol*. 7: 57-65.

Saxena, P. and Hildemann, L.M. (1997). Water Absorption by Organics: Survey of Laboratory Evidence and Evaluation of UNIFAC for Estimating Water Activity, *Environ. Sci. Technol*. 31:3318-3324.

Speer, R. E., Barnes, H. M., and Brown, R. (1997). An Instrument for Measuring the Liquid Water Content of Aerosols, *Aerosol Sci. Technol*. 27(1):50-61.

Tang, I.N., and Munkelwitz, H.R. (1993). Composition and Temperature Dependence of the Deliquescence Properties of Hygroscopic Aerosols, *Atmos. Environ*. 27A:467-473.

Tang, I.N. (1997). Thermodynamic and Optical Properties of Mixed-Salt Aerosols of Atmospheric Importance, *J. Geophys. Res*. 102:1883-1893.

ten Brink, H.M., Khlystov, A., Kos, G.P.A., Tuch, T., Roth, C., and Kreyling, W. (2000). High-Flow Humidograph for Testing the Water Uptake by Ambient Aerosol, *Atmos. Environ*. 34:4291-4300.

Turpin, B. and Lim, H. (2001). Species Contributions to $PM_{2.5}$ Mass Concentrations: Revisiting Common Assumptions for Estimating Organic Mass, *Aerosol Sci. Technol*. 35:602-610.

Vartiainen, M., McDow, S.R., and Kamens, R.M. (1994). Water Uptake by Aerosol Particles from Automobile Exhaust and Wood Smoke, *Chemosphere* 29:1661-1669.

Virkkula, A., Van Dingenen, R., Raes, F., and Hjorth, J. (1999). Hygroscopic Properties of Aerosol Formed by Oxidation of Limonene, α-Pinene, and β-Pinene, *J. Geophys. Res.* 104(D3):3569-3579.

Wagner, J., Andrews, E., and Larson, S.M. (1996). Sorption of Vapor Phase Octanoic Acid Onto Deliquescent Salt Particles. *J. Geophys. Res.* 101(D14):19,533-19,540.

Willeke, K., and Baron, P.A. (1993) *Aerosol Measurement Principles, Techniques, and Applications*. Van Nostrand Reinhold: New York.

Woo, K.S., Shi, Q., Sakurai, H., and McMurry, P.H. (2001). A Relative Humidity Conditioner for Atmospheric Sampling. Presented at the American Association of Aerosol Research. Portland, Oregon, Oct 2001.

Xiong, J.Q., Zhong, C.F., Chen, L.C., and Lippmann, M. (1998). Influence of Organic Films on the Hygroscopicity of Ultrafine Sulfuric Acid Aerosol, *Environ. Sci. Technol*. 32:3536-3541.

Yi, M., and Russell, L.M. (2002). Thermodynamic Equilibrium of Organic-Electrolyte Mixtures in Aerosol Particles. *AIChE Journal*, 48(6):1331-1348.

Chapter 3 Ambient Aerosol Size Distributions and Number Concentrations Measured During the Pittsburgh Air Quality Study (PAQS)[†]

3.1 Introduction

The size distribution of atmospheric aerosols, together with composition, sources, and sinks, is a key element in understanding and managing aerosol effects on health, visibility, and climate. Numerous epidemiological studies have shown adverse health effects of particulate matter (PM) including respiratory irritation and changes in pulmonary function as well as associations between particulate mass concentrations and mortality (Samet et al., 2000; Wichmann et al., 2000; Lippmann et al., 2000). Recently, there has been an increased interest in the relative health effects of particles of smaller sizes (Oberdörster et al., 1992; Oberdörster et al., 1995; Donaldson et al., 1998). Some laboratory studies have also shown that for a given mass concentration, health effects are larger for smaller particle sizes (Wichmann and Peters, 2000). In addition, for the estimation of the magnitude of direct and indirect aerosol-climate effects, the particle size distribution is an important parameter.

Accordingly, there have been many sampling efforts to measure aerosol size distributions in urban, rural, and remote sites around the globe, and nearly all field campaigns now include some measurements of aerosol size distributions. Some recent continental sampling campaigns that measured size distributions include the Atlanta PM Supersite program (Woo et al., 2002), and sampling

[†] Submitted for publication as "Ambient Aerosol Size Distributions and Number Concentrations Meaured During the Pittsburgh Air Quality Study (PAQS)" by Charles Stanier, Andrey Khlystov, and Spyros Pandis. *Atmospheric Environment,* 2003.

campaigns in Los Angeles (Kim et al., 2002), Northern Europe (Ruuskanen et al., 2001), Tennessee (Cheng and Tanner, 2002), Brisbane, Australia (Morawska et al., 2002), England (Harrison et al., 1999), Estonia and Finland (Kikas et al., 1996) and Central Europe (Birmili et al., 2001).

Most of these studies find 24-hr average number concentrations (10-500 nm) at continental sites in a range from around 5,000 to 25,000 cm^{-3} (Ruuskanen et al., 2001; Kim et al., 2002; Woo et al., 2000; Morawska et al., 2002). Sites that have monitored 3-10 nm particles find comparable numbers of particles in that size range relative to the 10-500 nm size range (Woo et al., 2000). Diurnal patterns vary between two extremes: (a) influenced predominantly by mixing height changes and meteorology for sites without local particle sources or nucleation; and (b) strongly influenced by local sources such as traffic and nucleation (Kim et al., 2002; Morawska et al. 2002). Little has been reported regarding seasonal patterns in aerosol concentrations due to the lack of long term monitoring.

Some parameterizations for model size distributions are available for urban and continental aerosols (Whitby, 1978; Jaenicke, 1993). Even if these parameterizations are widely used, their applicability to areas other than the ones for which they were developed has not been investigated.

This paper presents a statistical summary of size distributions measured during one year of continuous monitoring at the Pittsburgh Supersite during the Pittsburgh Air Quality Study (PAQS), forming one of the first long-term datasets for aerosol size distributions in the Northeastern United States. Aerosol size

distributions from 3 nm to 2.5 μm were monitored for over 15 months at the central sampling site of the study. Aerosol number size distributions were measured at low relative humidity, and at ambient relative humidity to assess the impact of aerosol water on the particulate matter size distribution. Additional aerosol size distributions were collected at an upwind location for approximately two months to assess the difference between rural and urban particulate matter size distributions in the airshed. The wide size range, long-term (more than a year) deployment, rural/urban comparison, and dual relative humidity sampling provide advantages in using the size distribution dataset to understand and quantify atmospheric aerosol formation, processes, and exposure.

Statistical averages, diurnal and seasonal trends for the urban location, and local sources of particles are discussed. These results are compared to size distributions measured continuously for 6 weeks at a rural site upwind of Pittsburgh to assess the spatial variability and impact of the urban sources on the particulate matter number distribution. Finally, the measurement results are compared to other similar investigations and to model size distributions.

3.2 Experimental

The main sampling location was in a park 5 km east (downwind) of downtown Pittsburgh[7]. Two SMPS systems (TSI 3936L10 and TSI 3936N25) were operated at the main location continuously from July 2001 – July 2002.

[7] A brief site description of the PAQS sampling site is included in the experimental sections of Chapters 3-6. The distances to sources such as roads are approximate and there are discrepancies between the values in the different chapters, which were each published separately. For a complete description of the central and satellite sites, see Wittig et al. (2003). The central site was at 40.4395 ºN / -79.9405 ºE. Nearest major road (Forbes Ave.): 0.33 km N. Nearest major stationary source: Bellafield Boiler: 0.6 km NW. Nearest highway (376): 1.1 km S.

These instruments measured the size distribution of particles from 3 nm to 600 nm. These were augmented by a TSI APS 3320 measuring from 0.5 μm to 20 μm for the first 3 months of the sampling period and a TSI APS 3321 measuring in the same size range for the final 2 months of the sampling period. Aerosol measurements at the main size were made at both low relative humidity and ambient relative humidities to assess the importance of relative humidity to the size distribution. This combination of 3 sizing instruments with RH control, called the Dry-Ambient Aerosol Size Spectrometer (DAASS) is described in Stanier et al. (2003a). Another SMPS system (TSI 3071/3010) was located at a rural site in Florence, Pennsylvania, 38 km west (mostly upwind) of the city during 2002. At the Florence site, the aerosol size distribution was measured at slightly sub-ambient relative humidity.

The urban sampling site was relatively far from local sources of primary particles. The nearest major city street was 0.5 km away, and the nearest highway was 1.1 km away. Small local sources included the nearby Carnegie Mellon University campus and a local coal-fired steam plant that was approximately 1 km away from the site.

Each of the 3 sizing instruments acquired an aerosol size distribution 8 times per hour, with 4 of these using the low relative humidity channel, and 4 of them using the ambient relative humidity inlet. The raw data, and associated temperature and relative humidity information, were acquired using a PC and then processed afterward. Data processing consisted of inversion of the raw size distributions using the TSI SMPS program (Version 3.2) and the TSI Aerosol

Instrument Manager Program (Version 4.3) and corrections for inlet losses and counting efficiencies (see Stanier et al., 2003a for additional discussion). The size distributions from the individual instruments were then merged into a single size distribution by using the nano-SMPS data through 30 nm, the SMPS data from 30-600 nm, and the APS data above 600 nm (together with an algorithm (Khlystov et al., 2003a) to account for the inherent difference between the mobility size measured by the SMPS instruments and the aerodynamic mobility measured by the APS). The size distributions reported here are a function of mobility diameter for sizes below 600 nm and as a function of estimated mobility diameter for sizes above 600 nm.

Extensive quality assurance checks were performed prior to instrument deployment and during the field study. Pre-study tests are described in Stanier et al. (2003a) and include various counting and sizing precision and accuracy checks using monodisperse aerosols. During the study, a schedule of maintenance activities was adhered to, including daily, weekly, and monthly equipment inspections focusing on maintenance of dry butanol in Condensation Particle Counters, leak checks, and flow calibration.

After initial data reduction, two levels of data validation were performed. The first level of data validation focused on internal consistency of the size distribution data between the three instruments that made up the DAASS system, while the second looked for consistency between the DAASS system and other instruments, particularly those that provided continuous measurements of aerosol mass or aerosol chemical components (e.g. Tapered Element Oscillating

Microbalance). During validation, a small portion of the data was flagged as invalid. Calibration factors and flowrates used for data reduction were occasionally modified to maintain instrument-to-instrument precision, typically by ±20% or less. Modifications in data reduction parameters were supported by field data (e.g. documented drift in a flowrate) and were typically associated with the replacement of major system components necessary for maintenance (e.g. particle counters, pumps & blowers, and dryers). The cycling between low and ambient relative humidity caused a slightly higher frequency of failures in sizing equipment than is typical in long term sampling using SMPS, APS, and Optical Particle Counters.

3.3 Results and Discussion

The results are divided into several sections, including (a) summary statistics; (b) temporal (seasonal and diurnal) trends; (c) rural versus urban distributions; (d) sources of particles; and (e) comparison to other distribution measurements.

3.3.1 Summary Statistics

The grand average number distribution measured during the Pittsburgh Air Quality Study (Figure 3.1) has a number mode at 40 nm and a particle count of 22,000 cm^{-3}. The corresponding surface area and volume distributions, calculated from the number distribution assuming spherical particles, are also shown in Figure 3.1. The small discontinuity in the surface area and volume distributions are at the point where the SMPS and APS distributions are merged together. These are merged using a procedure described by Khlystov et al. (2003a). The

merging procedure removes discontinuities almost completely in the number distribution, but not necessarily in the surface and volume distributions.

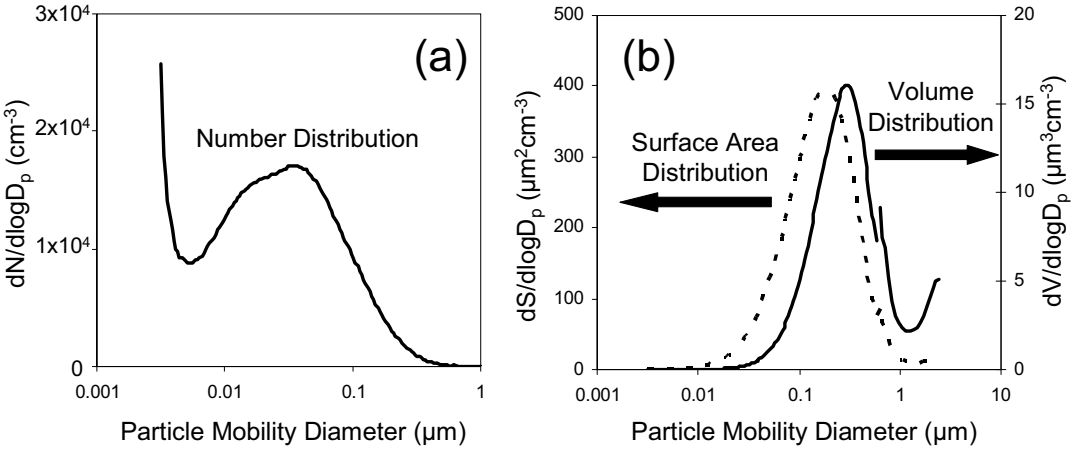

Figure 3.1 Grand average (a) number, and (b) surface area and volume distributions from the Pittsburgh Air Quality Study (7/1/2001 – 6/30/2002).

Various descriptive statistics regarding the measured size distributions are included in Table 3.1. Key points from Table 3.1 include (a) the significant difference in surface area and volume between the low RH (14%) and ambient RH (58% on average) channels of the instrument; (b) the fact that 25% of the aerosol number is less than 10 nm and 75% of the aerosol number is less than 50 nm in size; and (c) the relatively good data recovery for the SMPS instruments which operated up to 560 nm (84-92%) and relatively poor data recovery for the APS which operated from 0.5-2.5 µm (28%). The APS was removed for service for upgrading and repair early in the study, and not returned to service until late in the study.

Table 3.1 Descriptive Statistics of Particulate Matter Size Distributions Measured During the Pittsburgh Air Quality Study (Size Range 3 nm – 2.5 µm)

Attributes of Distributions – Grand Average for Pittsburgh Air Quality Study Main Site (7/1/2001 – 6/30/2002)

Distribution	Integral	Units	Mode	Mean Diameter
Low RH[1] Number	22,100	cm^{-3}	40	41
Low RH Surface Area	315	$\mu m^2/cm^3$	209	66
Low RH Volume	11.5	$\mu m^3/cm^3$	322	99
Ambient RH[2] Number	24,500	cm^{-3}	45	43
Ambient RH Surface Area	448	$\mu m^2/cm^3$	216	75
Ambient RH Volume	31.1	$\mu m^3/cm^3$	414	113

Descriptive Statistics, 24-hr Averaged cm^{-3} (Low RH Channels Only)

Size Bin	Samples	Mean	Median	Min	Max	Standard Deviation
3-10 nm	307	5600	4900	1380	25,000	3200
10-20 nm	307	4100	4100	1210	8800	1420
20-50 nm	336	6500	6100	1880	14,000	2590
50-100 nm	327	3600	3400	910	9700	1570
100-200 nm	327	1710	1510	450	4550	790
200-500 nm	327	460	361	64	1632	300
0.5 – 1 µm	102	18	11	1	67	17
1 – 2.5 µm	103	0.59	0.56	0.10	1.5	0.27

[1] Low relative humidity distributions were measured at an average relative humidity of 14%
[2] Ambient RH distributions were measured at an average relative humidity of 58%

Hourly averaged low relative humidity number concentrations from the DAASS are compared in Figure 3.2 to hourly averaged $PM_{2.5}$ values from the Tapered Element Oscillating Microbalance (TEOM, Rupprecht and Patashnick, Albany NY). The TEOM is a continuous particulate mass monitor that operated at the Pittsburgh Air Quality Study (Wittig et al., 2003) with a Sample Equilibration System (Meyer et al., 2002) to reduce the interference of water vapor on the sample while retaining as much semivolatile mass as possible. The highest number concentrations were observed during relatively clean days when the $PM_{2.5}$ concentrations were less than 25 µg m^{-3}. The number concentration is not positively correlated with the mass concentration and there is evidence of a negative correlation.

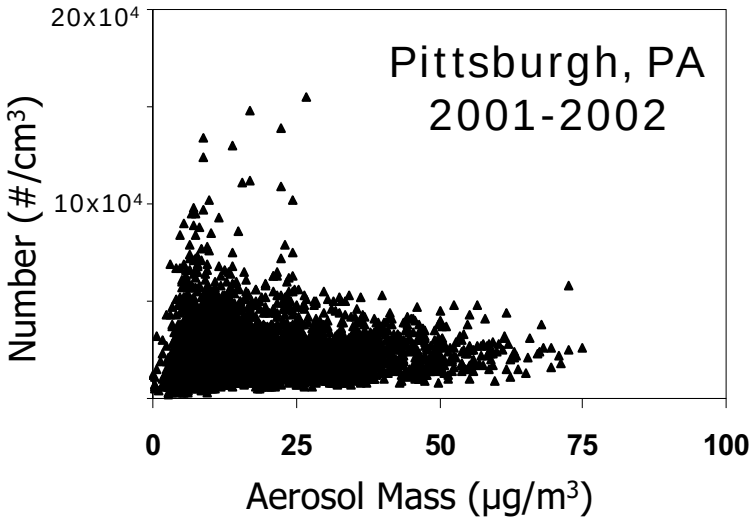

Figure 3.2 Aerosol mass versus aerosol number for the Pittsburgh Air Quality Study. Hourly average values from the TEOM (mass) are plotted against hourly number integrals from 3-560 nm measured by SMPS.

3.3.2 Temporal Trends

While the aerosol size distributions (especially the number distribution) can exhibit significant variability on the sub-hourly, hourly, and even daily timescales, the monthly average distributions are relatively stable. Figures 3 and 4 show monthly trends in properties of the size distributions for the low relative humidity and ambient relative humidity instrument channels, respectively. Figure 3.3a shows the number mean diameter, surface mean diameter, and volume mean diameter for each month. While there is little variability in the monthly averaged number mean diameter (it varies from 39 to 52 without a consistent pattern), the surface area and volume mean diameters show a clear summer maximum and winter minimum. This behavior is consistent given the summer peak in aerosol volume (and mass) in the Eastern United States (Figure 3.3c). Figure 3.3b shows the absence of a clear seasonal trend in average particle number in three different

size ranges, while Figure 3.3c shows the strong summertime maximum in aerosol volume, with summer values approximately twice winter levels.

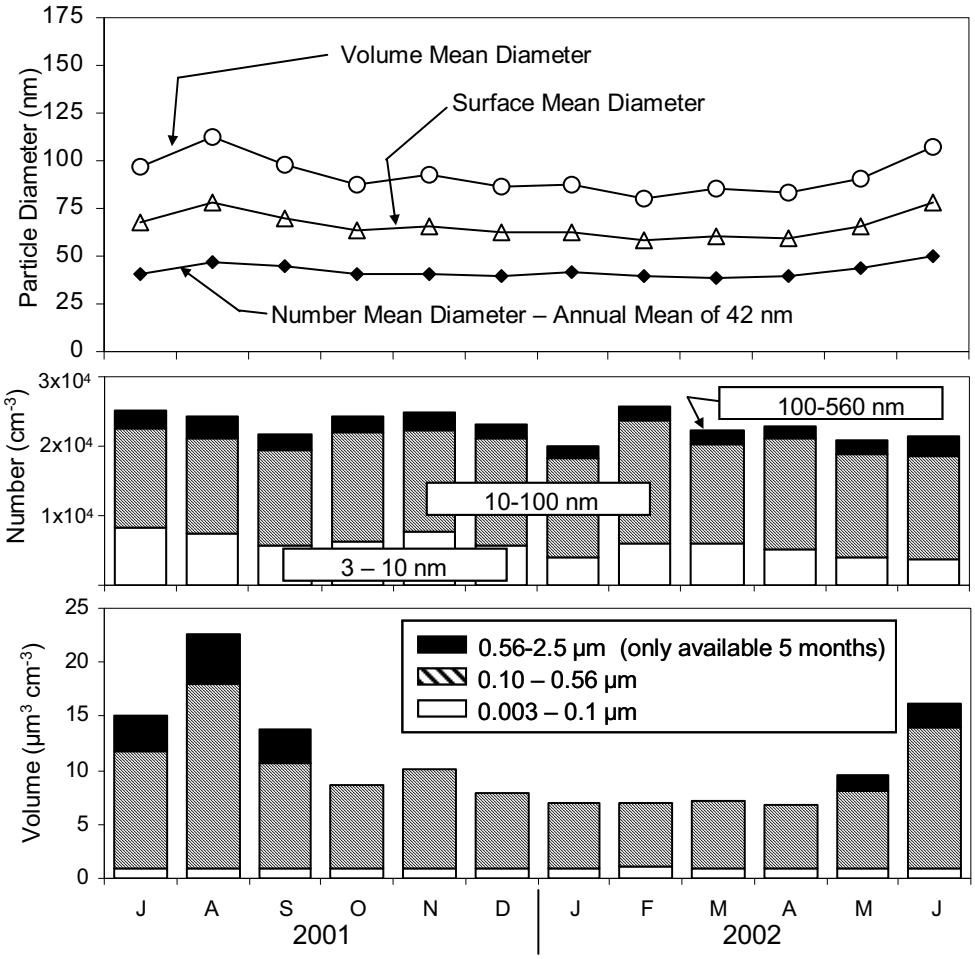

Figure 3.3 Monthly patterns in number, surface, and volume distributions for low relative humidity size distributions.

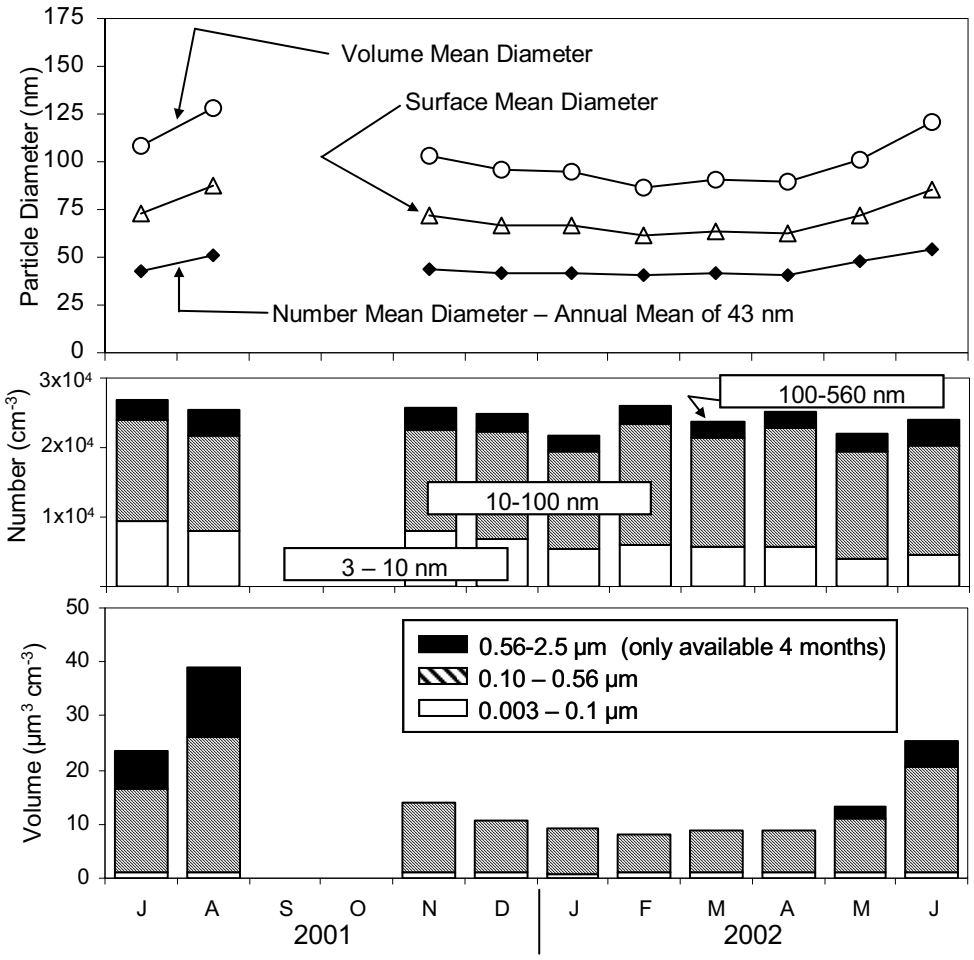

Figure 3.4 Monthly patterns in number, surface, and volume distributions for ambient relative humidity size distributions. The DAASS operated in the low relative humidity mode only during September and October 2001.

Differences in the ambient RH and low relative humidity distributions can be seen by comparing Figures 3.3 and 3.4. While there is negligible difference in ambient and low relative humidity particles counts and number mean diameter, there are significant increases in the surface and volume integrals and mean diameters. The difference is largest in summer, due to higher relative humidity and more hygroscopic aerosols (Khlystov et al., 2003b). For example, the volume mean diameter during summer months (July and August 2001 plus June 2002) for particles from 3 nm to 2.5 µm was, on average 132 nm for the ambient channel

and 113 nm for the low relative humidity channel. This corresponds to average growth ratios for the summer of 1.16 (diameter basis) and 1.60 (volume basis). The corresponding diameters for winter were 93 nm for the ambient channel and 85 for the low relative humidity channel, with ratios of 1.09 (diameter basis) and 1.30 (volume basis). The average ambient summer and winter relative humidities were both 65%. However, the organic aerosol content was significantly higher during the winter (Wittig et al., 2003).

While seasonal trends were most apparent in the aerosol volume distribution, strong diurnal trends were observed in the aerosol number distribution. The diurnal pattern of aerosol number, averaged over the entire study, is shown in Figure 3.5a. The solid line at the top of the figure is the diurnal pattern for total aerosol number, while the other lines in the figure show the diurnal pattern for specific size classes of aerosols, ranging from the nuclei mode (3-10 nm) up to part of the accumulation mode (50-100 nm). Figures 3.5b and 3.5c plot diurnal patterns for specific types of days, rather than for the average day of the entire study. Circled numbers refer to specific diurnal features discussed below in the text.

Total aerosol number, on average, peaked at midday (Figure 3.5a – feature 1). Another features apparent in the grand average diurnal trend is the minimum in 3-20 nm particles during the early morning, when their sources are at a minimum (Figure 3.5a – feature 2). Also apparent is the drop in concentration of 50-100 nm particles from dilution during the morning when the mixing height is rapidly rising (Figure 3.5a – feature 3).

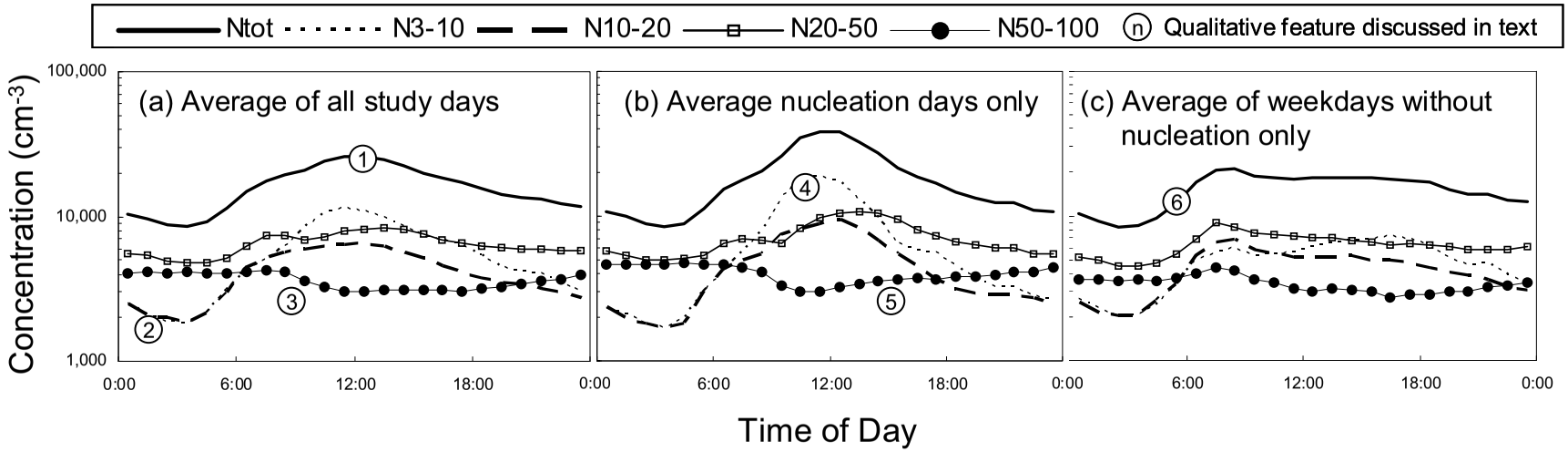

Figure 3.5 Diurnal patterns in particle number (a) average of all study days; (b) average of all study days with regional nucleation; (c) average of all weekdays without significant nucleation, showing influence of traffic. Numbered circles refer to qualitative features discussed in the text. The solid line at top of each profile is the total number, while the other lines are diurnal profile for specific size classifications. The smallest bin plotted is from 3-10 nm while the largest bin plotted is from 50-100 nm.

Two of the most representative types of days, in terms of diurnal aerosol size distribution behavior, were days with in-situ nucleation and days with a morning rush hour (weekdays) but no apparent nucleation. The former (regional nucleation) occurred on 30% of the study days and the average diurnal profile of these days is plotted in Figure 3.5b. The latter (weekday without nucleation) also occurred on approximately 30% of the study days, and is plotted in Figure 3.5c. Key features of the nucleation diurnal profile include the midday peak in nuclei mode (3-10 nm) particles (Figure 3.5b – feature 4) as well as the slow growth in the number of 50-100 nm particles during the afternoon as the small particles created earlier in the day grow to larger sizes by coagulation and condensation (Figure 3.5b – feature 5). An important feature of the non-nucleation weekday profile is the increase in particle number during the morning rush hour (Figure 3.5c – feature 6). This feature can also be seen in the grand average diurnal profile (Figure 3.5a) as a shoulder peak a few hours before the maximum from nucleation. Figure 3.5c also shows that there is no afternoon rush hour peak and no midday peak. The former is because the afternoon rush hour is more spread out in time than the morning rush hour, and the mixing height is rising during the late afternoon, diluting the emissions. The latter is because the midday peak is primarily from nucleation.

3.3.3 Rural versus Urban Distributions

During February and March of 2003, an SMPS system sampled size distributions at a rural site (Florence PA) 38 km upwind from the main sampling site. This provided information on the contribution of background aerosols, the

spatial homogeneity of aerosol processes (e.g. new particle formation from in-situ nucleation), and the difference between the "rural" and "urban" size distributions in the Pittsburgh Area. For the remainder of this work, the main site results will be referred to as urban and the Florence site will be referred to as rural. The average size distributions measured during February and March (Figure 3.6) show that number concentrations were, on average, 2-3 times higher at the urban site and that the rural site had a larger mode size (approximately 62 nm versus 32 nm at the urban site). There was little difference in the number distributions above 200 nm, consistent with the regional nature of the fine PM in the area and the similar $PM_{2.5}$ mass concentrations measured at the two sites during the study.

The rural site was impacted by nucleation very similarly to the urban site (Stanier et al., 2003b), but was not impacted nearly as strongly by traffic. Therefore, the diurnal patterns at the rural site were not as pronounced.

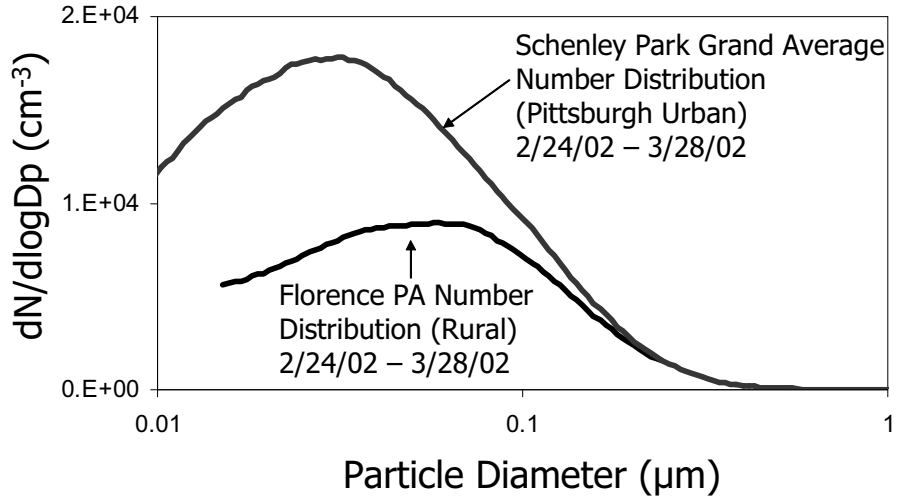

Figure 3.6 Average number size distributions from the rural site (Florence PA) and the urban site (Schenley Park, Pittsburgh PA).

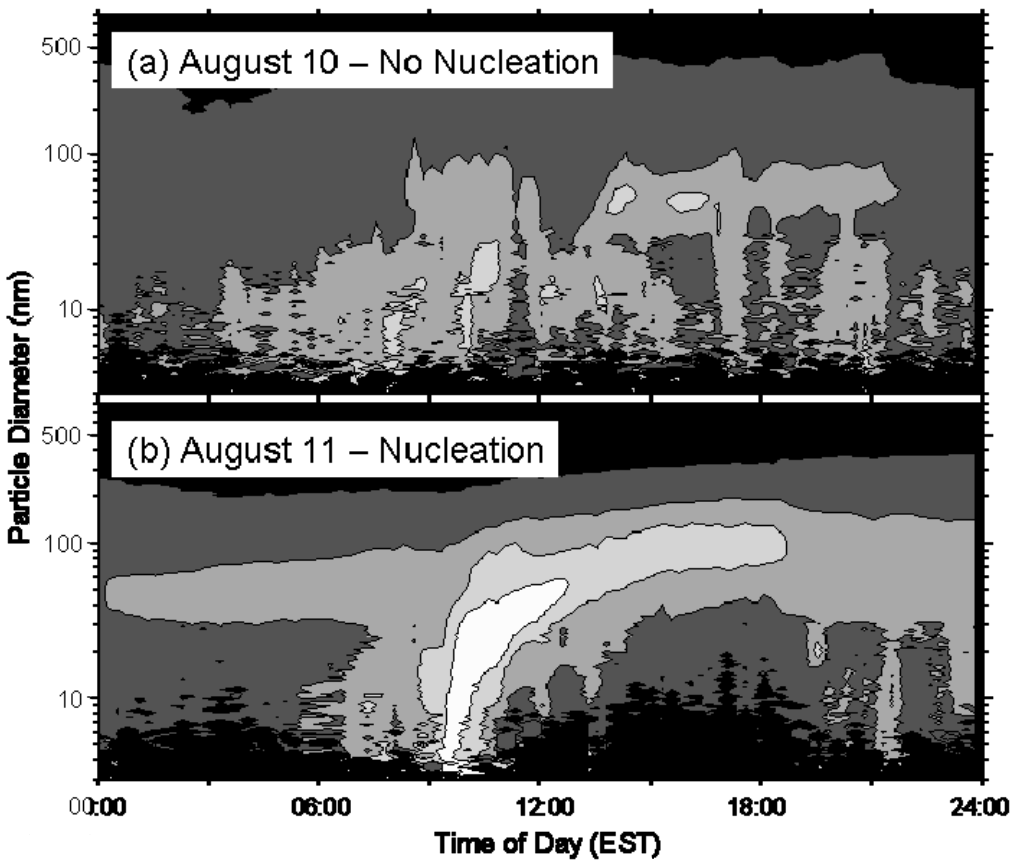

Figure 3.7 Evolution of particles size distributions on a day without nucleation (August 10) and a day with nucleation (August 11). The plots show instrument response ($dN/dlogD_p$ with units of cm^{-3}) over all size channels. Light colors are highest number concentrations and dark colors are the lowest number concentrations. Contour lines drawn at $dN/dlogD_p$ values of 10^2, 10^3, 10^4, $10^{4.5}$, and 10^5 cm^{-3}.

3.3.4 Sources of Particles

Nucleation and vehicle emissions were the most important sources of particles impacting the main (urban) sampling site. Figure 3.7 shows the evolution of the number size distribution on two consecutive days. The first day (August 10; top panel) does not exhibit nucleation behavior, while the second day (August 11; bottom panel) does. At 9 AM, there is significant new particle formation on August 11. The frequency, intensity, meteorology, and possible chemistry of such new particle formation has been analyzed (Stanier et al.,

2003b), showing that the nucleation events are associated with photochemical sulfuric acid production and occur on approximately 30% of the study days. The same type of behavior has also been witnessed in St. Louis (Shi et al., 2002).

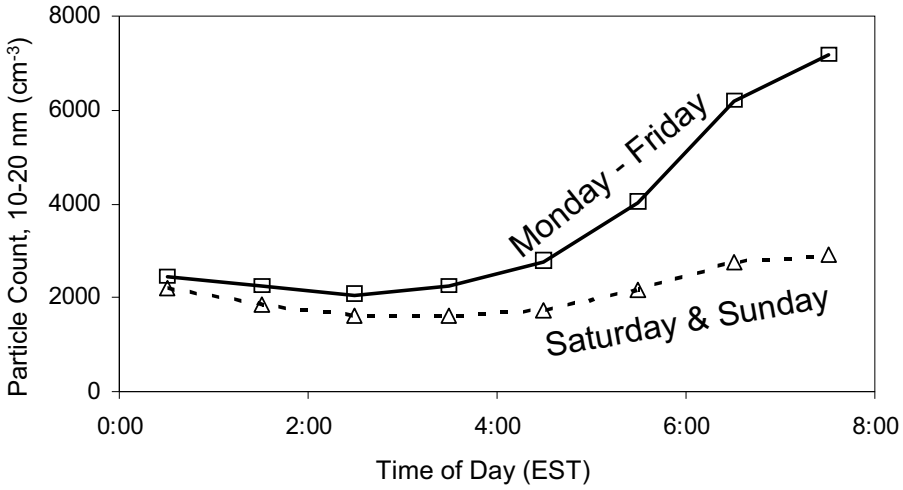

Figure 3.8 Traffic as a source of particles. 10-20 nm particle count as function of time for weekends and weekdays at the urban site.

The other major particle source impacting the urban site is traffic. On weekdays, there was a pronounced increase in particle concentrations for particles primarily in the size range from 3 nm – 30 nm (Figure 3.8) beginning at approximately 04:00 EST. The increase was much smaller, and later, on weekends. A similar analysis for daytime traffic is complicated by changes in the mixing height and nucleation activity.[8]

3.3.5 Comparison with Other Distribution Measurements

It is useful to compare the PAQS size distribution measurements to (a) other studies and (b) commonly used "typical" or model size distributions

[8] For a more complete discussion of the impact of motor vehicle traffic on particle size distributions during PAQS, see Zhou et al. (2003).

(Whitby, 1978; Jaenicke, 1993). Comparison to the sampling study of Russkanen et al. (2001) in 3 Northern European cities shows very similar results for aerosol number concentration (Table 3.2).

Table 3.2 Comparison to Other Size Distribution Measurement Campaigns

Location	Number Concentration 10-100 nm (cm^{-3})	Number Concentration 100-500 nm (cm^{-3})	Source
Alkmaar, Netherlands	18,300	2,120	Russkanen (2001)
Erfurt, Germany	17,700	2,270	Russkanen (2001)
Helsinki, Finland	16,200	973	Russkanen (2001)
Pittsburgh, Urban	14,300	2,170	This work
Pittsburgh, Rural	6,500	1,900	This work

The comparison with model distributions of Whitby and Jaenicke is shown in Figure 3.9, with number distributions in Figure 3.9a and volume distributions in Figure 3.9b. The model distributions used are Whitby's "urban average" distribution (labeled C-W1), Whitby's "average background" distribution (labeled C-W2), and Jaenicke's rural continental distribution (labeled C-J). Not shown in the figure is Jaenicke's urban distribution, which is very similar to Whitby's urban average distribution. The most general conclusion is that none of the model distributions fit either the urban or rural results from this study well. The model urban size distributions have an order of magnitude higher particle concentrations, with a strong 15 nm mode not seen in the average distributions from Pittsburgh. The model urban distributions are more appropriate for sites close to (< approximately 100 m) to traffic or Los Angeles. Based on these results, it is recommended that caution be exercised in using model distributions.

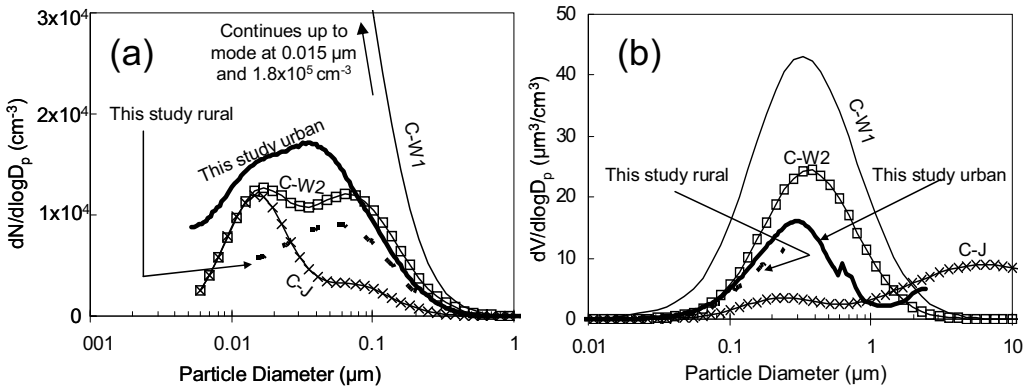

Figure 3.9 Comparison of model size distributions to Pittsburgh size distributions on an (a) number basis and (b) volume basis. Model distributions: C-W1 = Whitby (1978) urban average; C-W2 = Whitby (1978) average background; and C-J = Jaenicke (1993) rural continental.

3.4 Summary and Conclusions

Twelve months of particulate matter size distributions from the Pittsburgh Air Quality Study were summarized. The average Pittsburgh number concentration (3-500 nm) is 22,000 cm^{-3} with an average mode size of 40 nm. Seasonal patterns are not very strong for aerosol number, but are clearly evident for the aerosol volume distribution due to the summertime peak in aerosol mass concentrations. Strong diurnal patterns in number concentrations are evident as a direct effect of the sources of particles (atmospheric nucleation, traffic, and other combustion sources). Nucleation (involving sulfuric acid) is active on the 30-50% of study days and over a wide area (at least a hundred kilometers). Rural number concentrations are a factor of 2-3 lower (on average) than the urban values. Number concentrations are comparable to those found in similar sampling studies in Northern Europe, and model size distributions tested against the Pittsburgh Air Quality Study results yield a poor fit between the sampled and model distributions.

The urban and rural particulate matter size distributions measured during the Pittsburgh Air Quality Study form an excellent dataset for further research on particle sources, nucleation, and aerosol processes. To date, they have been used to address nucleation (Stanier et al., 2003b), aerosol water content (Khlystov et al., 2003b), and source-receptor relationships (Zhou et al., 2003).

3.5 References

Birmili, W., Wiedensolher, A., Heintzenber, J., and Lehmann, K., 2001. Atmospheric Particle Number Size Distribution in Central Europe: Statistical Relations to Air Masses and Meteorology. Journal of Geophysical Research 106:D23, 32,005-32018.

Cheng, M.D., Tanner, R.L., 2002. Characterization of ultrafine and fine particles at a site near the Great Smoky Mountains. Atmospheric Environment 36, 5795.

Harrison, R.M., Shi, J.P., Jones, M.R., 1999. Continuous measurements of aerosol physical properties in the urban atmosphere. Atmospheric Environment 33, 1037-1047.

Kikas, U., Mirme, A., Tamm, E., Raunemaa, T., 1996. Statistical characteristics of aerosol in Baltic Sea region. Journal of Geophysical Research 101:D14, 19,319-19,327.

Kim, S., Shen, S., Siutas, C., Zhu, Y., Hinds, W., 2002. Size distributions and diurnal and seasonal trends of ultrafine particles in source and receptor sites of the Los Angeles basin. Journal of Air and Waste Management 52:297-307.

Khlystov, A., Stanier, C., Pandis, S.N., 2003a. An algorithm for combining electrical mobility and aerodynamic size distribution data when measuring ambient aerosol. Aerosol Science and Technology, in press.

Khlystov, A., Stanier, C., Vayenas, D., Pandis, S.N., 2003b. Water content of ambient aerosols during the Pittsburgh Air Quality Study: Experimental measurements and thermodynamic modeling results. Submitted to Atmospheric Environment.

Jaenicke, R., 1993. Tropospheric aerosols, in *Aerosol-Cloud-Climate Interactions*, Ed. P.V. Hobbs. Academic Press: San Diego CA, pp. 1-31.

Lippmann, M., Ito, K., Nádas, A., Burnett, R.T., 2000. Association of particulate matter components with daily mortality and morbidity in urban populations. Research Report 95. Health Effects Institute, Cambridge MA.

Meyer, M.B., Patashnick, H., Ambs, J.L., and Rupprecht, E., 2000. Development of a sample equilibration system for the TEOM continuous PM monitor. Journal of Air and Waste Mangement *5*0:8, 1345-1349.

Morawska, L., Jayarantne, E.R., Mengersen, K., and Thomas, S., 2002. Differences in airborne particle and gaseous concentrations in urban air between weekdays and weekends. Atmospheric Environment 36: 4375-4383.

Ruuskanen, J., Tuch, Th., Ten Brink, H., Peters, A., Khystov, A., Mirme, A., Kos, G.P.A., Brunekreef, B., Wichmann, H.E., Buzorius, G., Vallius, M., Kreyling, W.G., Pekkanen, J., 2001. Concentrations of ultrafine, fine and $PM_{2.5}$ particles in three European cities. Atmospheric Environment 35: 3729-3738.

Samet, J.M., Zeger, S.L., Dominici, F., Curriero, F., Coursac, I., Dockery, D.W., Schwartz, J., Zanobetti, A., 2000. The National Morbidity, Mortality, and Air Pollution Study, Part II: Morbidity and mortality from air pollution in the United States. Research Report 94. Health Effects Institute, Cambridge MA.

Shi, Q., Sakurai, H., McMurry, P.H., 2002. Measurement of St. Louis particle size distributions: Observation of particle events. American Association of Aerosol Research Annual Meeting, Charlotte, NC.

Stanier, C., Khlystov, A., Chan, W.R., Mandiro, M., Pandis, S.N., 2003a. A method for the in-situ measurement of fine aerosol water content of ambient aerosol: the Dry-Ambient Aerosol Size Spectrometer (DAASS). Aerosol Science and Technology, in press.

Stanier, C., Khlystov, A., Pandis, S.N., 2003b. Nucleation events during the Pittsburgh Air Quality Study: Description and relation to key meteorological, gas phase, and aerosol parameters. Aerosol Science and Technology, in press.

Whitby, K.T., 1978. The physical characteristics of sulfate aerosols. Atmospheric Environment 12, 135-159.

Wichmann, H-E., Spix, C., Tuch, T., Wölke, G., Peters, A., Heinrich, J., Kreyling, W.G., Heyder, J., 2000. Daily mortality and fine and ultrafine particles in Erfurt, Germany. Part I: Role or particle number and particle mass. Research Report 98. Health Effects Institute, Cambridge MA.

Wichmann, H.-E., Peters, A., 2000. Epidememiological evidence of the effects of ultrafine particle exposure. Philosophical Transactions of the Royal Society A358:2751-2769.

Wittig, B., Anderson, N., Khlystov, A.Y., Pandis, S.N., Davidson C., Robinson A.L., 2003. Pittsburgh Air Quality Study overview and preliminary scientific findings. Submitted to Atmospheric Environment.

Woo, K.S., Chen, D.R., Pui, D.Y.H., McMurry, P.H., 2001. Measurement of Atlanta aerosol size distributions: Observations of ultrafine particle events. Aerosol Science and Technology 34, 75-87.

Zhou, L., Kim, E., Hopke, P.K., Stanier, C., Pandis, S.N., 2003. Advanced factor analysis on Pittsburgh particle size distribution data. Aerosol Science and Technology, in press.

Chapter 4 Nucleation Events During the Pittsburgh Air Quality Study: Description and Relation to Key Meteorological, Gas Phase, and Aerosol Parameters[†]

4.1 Introduction

The creation of new particles by homogenous nucleation of gas-phase atmospheric components is an important atmospheric process. Together with primary particle emission, nucleation is responsible for maintaining the number concentration of particles throughout the atmosphere. Nucleation affects climate and visibility by changing the size distribution of airborne particles (Charlson et al. 1987; Kulmala et al. 2000). The formation of ultrafine particles and the condensation of secondary aerosol components on them may impact human health, as ultrafine particles are likely to cause adverse health effects disproportionate to their mass (Oberdoster et al. 1995; Schwartz et al. 1996; Peters et al. 1997).

Until recently, nucleation was assumed to be limited to clean areas of the atmosphere such as the free troposphere. However, a number of recent studies at both rural and urban sites around the world have reported frequent nucleation events (Allen et al. 1999; Harrison et al. 1999a; Harrison et al. 1999b; Harrison et al. 2001; Shi et al. 2001; Woo et al. 2001). Woo et al. (2001) found elevated

[†] Published as "Nucleation Events During the Pittsburgh Air Quality Study: Description and Relation to Key Meteorological, Gas Phase, and Aerosol Parameters" by Charles Stanier, Andrey Khlystov, and Spyros Pandis. Aerosol Science and Technology, 2003 (in press).

levels of 3-10 nm particles in Atlanta, with highest frequencies in spring and summer. Birmili et al. (2001) measured elevated ultra-fine concentrations in continental Germany in April as well. In both the German and Atlanta studies, nucleation occurred around midday with concentrations of NO_x elevated prior to many of the nucleation events and SO_2 elevated during the events (Woo et al. 2001).

Atmospheric homogeneous nucleation has been the subject of many theoretical and experimental studies. It is recognized that there are two important steps to the production of new particles that can grow to detectable size (Zhang and Wexler 2002; Kerminen 1999). The first step is the formation of an initial nucleus, and the second step is the growth of the particles to larger sizes. A number of mechanisms have been proposed as candidates for the initial nucleus formation step based on observations and theoretical considerations, including (a) homogeneous binary nucleation of sulfuric acid and water (Weber et al. 1999); (b) homogeneous ternary nucleation of ammonia-water-sulfuric acid (Eisele and McMurry, 1997; Kulmala et al. 2001a; O'Dowd et al. 1999); (c) homogenous nucleation of low vapor pressure organic compounds (O'Dowd et al. 2002); (d) ion-induced nucleation (Kim et al. 2002). The second step in forming detectable new particles, growth, is also uncertain. These particles can grow by condensation of sulfuric acid or by self-coagulation. Both of these processes are relatively inefficient and additional growth mechanisms have been proposed (Kerminen 1999). The limited experimental evidence indicates a potential role for organic compounds (Novakov and Penner 1993; Rivera-Carpio et al. 1996).

Recent work considers the potential for heterogenous reactions of SO_2 (Kerminen 1999) and organic compounds (Kerminen 1999; Jang and Kamens 2001; Zhang and Wexler 2002) to significantly contribute to growth.

Steps toward a better understanding of tropospheric nucleation include: (a) elucidation of the mechanism responsible for the initial nuclei formation in different environments; (b) identification of the chemical compounds responsible for growth; (c) determination of the geographic scope, frequency, strength and impact of tropospheric nucleation.

The goal of this work is to describe the nucleation events observed during the Pittsburgh Air Quality Study from July 2001 – June 2002. Analysis of the particle size distributions during this period shows over 100 days with nucleation activity. The gas, aerosol phase concentrations, and meteorological conditions associated with nucleation in Pittsburgh are also discussed. Identification of initial nuclei and condensing species chemistry is ongoing and will be discussed in a subsequent paper.

4.2 Experimental

All measurements were conducted as part of the Pittsburgh Air Quality Study (PAQS), a multidisciplinary air pollution study designed to characterize fine particulate matter around Pittsburgh, evaluate next-generation aerosol monitoring instrumentation, elucidate source-receptor relationships, and improve understanding of atmospheric processes governing aerosol concentrations.

The bulk of the gas and particle measurements discussed in this paper were conducted at the main PAQS sampling location in a park 5 km east

(downwind) of downtown Pittsburgh (Figure 4.1). Two SMPS systems (TSI 3936R10 and TSI 3936N25) were operated at this location continuously. These instruments measured the size distribution of particles from 3 nm to 680 nm. The SMPS systems were a part of the Dry-Ambient Aerosol Sizing System (DAASS) (Stanier et al., 2002) and were specially configured to alternate between ambient RH samples and dried samples. The Differential Mobility Analyzers and most of the inlet tubing were kept at near ambient temperature to avoid volatilization of aerosols. Portions of the inlet were maintained at above 9 ºC at all times because they shared an enclosure with the Condensation Particle Counters. This sampling location was 0.5 km from the nearest major city street and 1.1 km from the nearest highway. A small coal-fired heating plant operated 0.8 km from the site.[9] Its plume impacted the sampling site occasionally but did not typically contain nuclei mode particles.

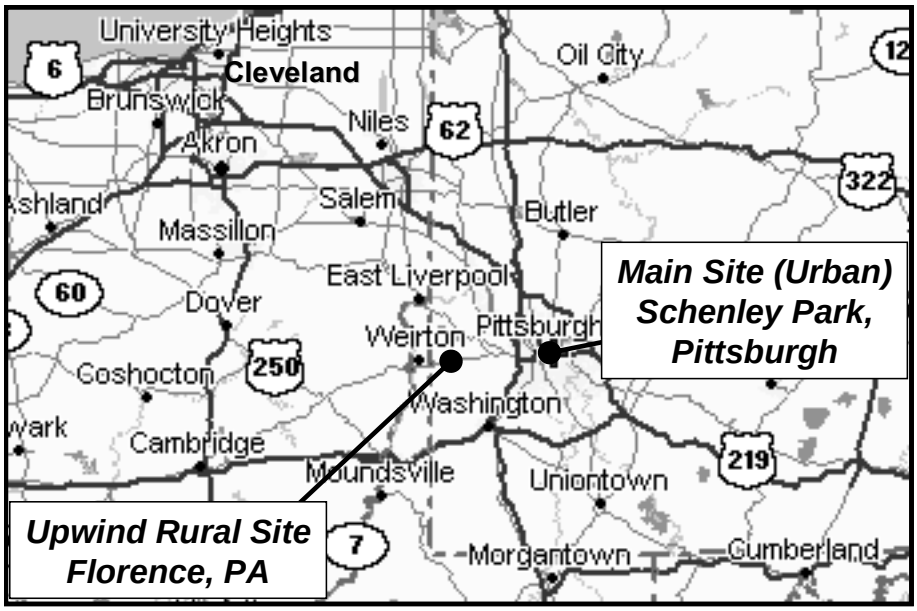

Figure 4.1 Map of Pittsburgh (main urban site) and Florence (rural upwind site)

[9] See note 7, section 3.2 for additional discussion of the site and proximity to sources.

Another SMPS system (TSI 3071/3010) was located 38 km upwind from the main site in Florence, Pennsylvania during part of winter and spring 2002. The SMPS was sampling dried aerosol size distributions in the size range 12 – 280 nm. The data from the rural site were used to assess the regional homogeneity of the events.

Table 4.1 Instruments used to examine nucleation events in this work.

Measurement	Instrument	Notes
Main supersite sampling location, Schenley Park, Pittsburgh (urban site) – Sampled 7/1/01 – 9/30/02		
Particle size distribution, 3-80 nm	TSI 3085 DMA / TSI 3025A CPC	5 min upscan; 8 scans per hour
Particle size distribution, 13-680 nm	TSI 3081 DMA / TSI 3010 CPC	5 min upscan; 8 scans per hour
Particle size distribution, 0.5-10 μm	TSI 3320 APS	Operated 7/1/01 – 10/26/01
Particle size distribution, 0.5-10 μm	TSI 3321 APS	Operated 5/26/02 – 9/30/02
$PM_{2.5}$ Mass	R&P 1400A	Running at 30 ºC with Sample Equilibration System
Ozone	API 400A	
NO & NO_x	API 200A	
SO_2	API 100A	
CO	API 300A	
Wind speed	MetOne 014A	
Wind direction	MetOne 024A	
Precipitation	MetOne 370	
Temperature and RH	Campbell HMP45C	
Barometric pressure	Campbell CS105	
Downwelling broadband radiation	Kipp & Zonen CM3 Pyranometer	
Downwelling UV radiation	Kipp & Zonen CUV3 UV Pyranometer	
Upwind sampling location, Florence, PA (rural site)		
Particle Size Distribution, 12 nm-280 nm	TSI 3071 DMA & 3010 CPC	Sampled 2/24/02 – 3/28/02

Other instruments deployed as part of the Pittsburgh Air Quality Study and used to understand nucleation in this work include: O_3, SO_2, NO_2/NO, and CO monitors, a Tapered Element Oscillating Microbalance (TEOM), solar radiation, and met station. For PAQS, 10-minute averaged $PM_{2.5}$ data were used

from the TEOM. The TEOM operated at 30 °C to minimize volatilization of nitrate and organic compounds and the Sample Equilibration System was used to dry the aerosol stream prior to the mass measurement. The complete list of instrumentation used to generate the data set for nucleation events is listed in Table 4.1.

4.3 Results and Discussion

Around 50 percent of the study days (July 2001 – June 2002) were characterized by nucleation events. Of these, about 60% showed a characteristic growth pattern from the nuclei mode to 30-100 nm over the course of several hours. During the other 40% of the nucleation events the sub-10 nm particles did not appear to grow to larger sizes. The events varied in intensity from weak increases in the ultrafine and nuclei mode particle counts to intense events which increased the overall number concentration from 10,000 - 20,000 per cm^3 to over 100,000 per cm^3 in a few hours. As an example of the contrast between days with and without nucleation, Figure 4.2 depicts the size distributions measured during August 10 and August 11, 2001. Figures 4.2a and 4.2b show evolution of the size distributions, while Figure 4.2c indicates the integrated particle concentration. On August 10 there was no detectable nucleation activity, while an intense nucleation event was observed around 9 AM EST on August 11 followed by rapid growth of the particles to a size around 100 nm. Missing size distributions in Figure 4.2 correspond to maintenance of the particle sizing instruments in some cases, and data flagged as invalid in other cases. Data was typically flagged invalid due to

occasional communication errors between the data acquisition system and the particle sizing instruments.

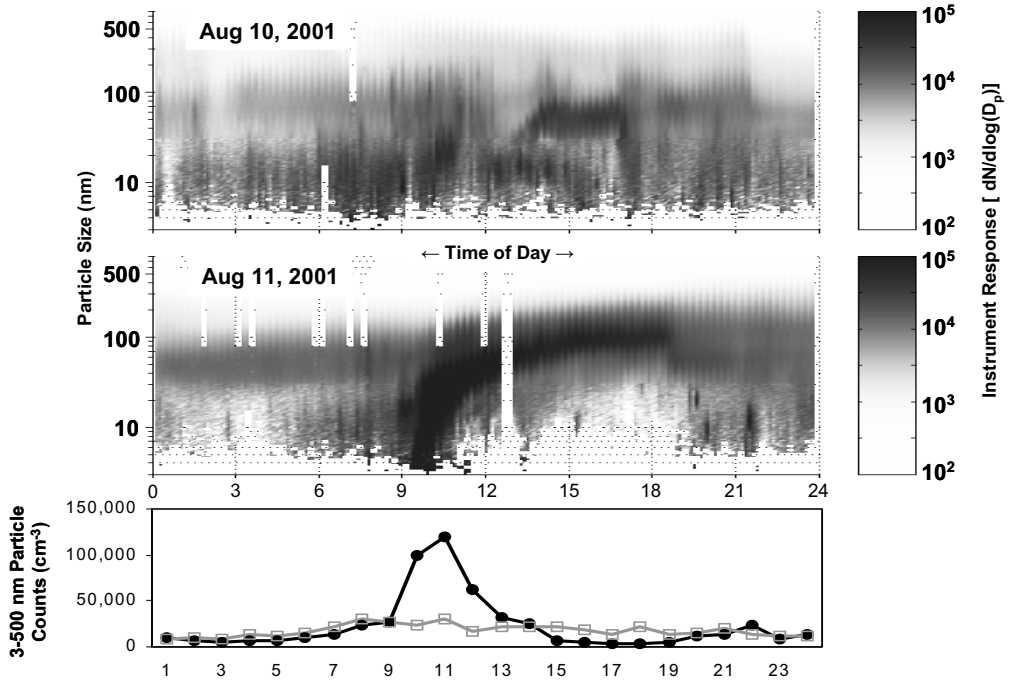

Figure 4.2 Evolution of particle size distributions and particle concentration on a day without nucleation (Aug 10) and a day with nucleation (Aug 11). The top two plots show instrument response over all size channels. The bottom plot shows the integrated particle concentration time series. Nucleation is apparent at 9 AM EST on Aug 11.

4.3.1 Classification of Events

The size distributions from the study were first analyzed to determine the frequency of nucleation events. The analysis was done by examining the evolution of size distributions on each day of the study and various time series, including those of total number concentration, nuclei mode number concentration, aerosol mass (TEOM), meteorological parameters, and gas phase concentrations of CO, NO, NO_2, O_3, and SO_2.

The most important marker for nucleation was a significant increase in the nuclei mode particle count, defined as particles from the lower detection limit of 3

nm up to 10 nm, referred to as N_{10} in this work. Once a significant increase in N_{10} was seen in the particle count time series, additional characteristics of the data were examined to rule out primary particle sources, such as vehicular traffic, which also produce particles smaller than 10 nm. Traffic was fairly easy to screen out, as it has usually a weaker signal than most nucleation events. Diurnally averaged number concentrations during nucleation days and non-nucleation weekdays and weekends are shown in Figure 4.3. The mode of the traffic-related size distribution was consistently from 15 to 20 nm, with most of the contribution to N_{10} between 6 and 10 nm. The traffic influence usually increased N_{10} from a background level of around 2,000 cm^{-3} to an early morning level of 7,500 cm^{-3} (Figure 4.3a). Finally, traffic was usually correlated with NO and CO (Zhou et al., 2003) and independent of solar radiation.

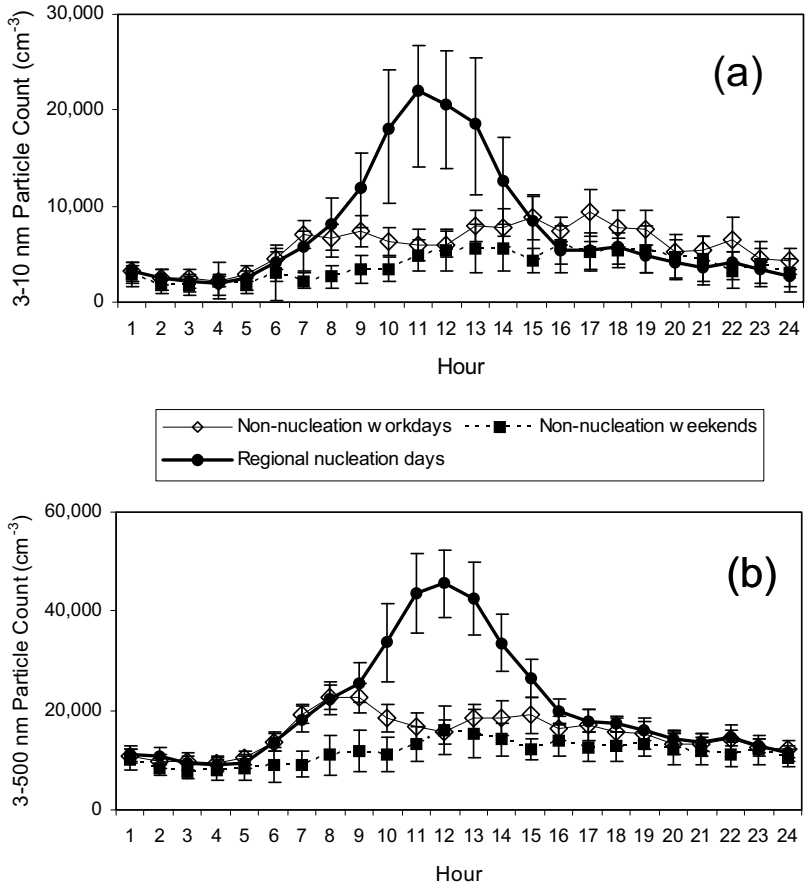

Figure 4.3 Diurnal averaged number concentrations July – November 2001. Error bars signify the 95% confidence interval on the mean. (a) particles between 3 and 10 nm, N_{10} and (b) particles smaller than 500 nm, N_{500}

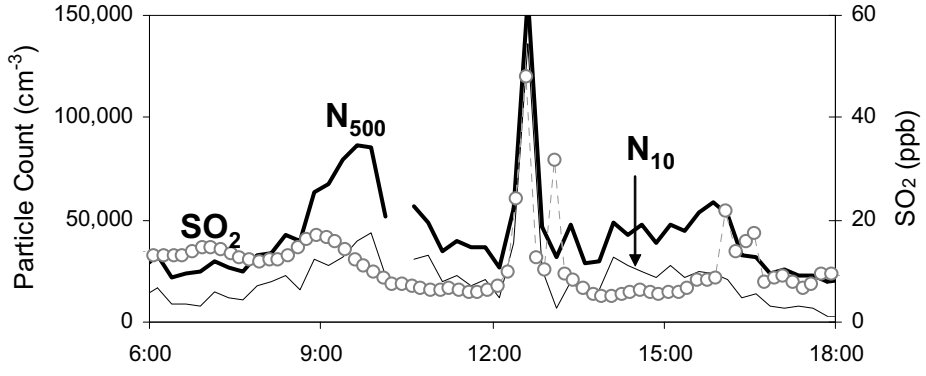

Figure 4.4 Example of a short lived nucleation event on July 5, 2001.

Once vehicular traffic was ruled out as the cause of a particular increase in N_{10}, the event was classified as a "short-lived" event, or a "regional" event following the approach by Shi et al. (2002). Regional events were characterized by an increase in N_{10} followed by the growth of the nuclei mode to larger sizes, such as that shown in Figure 4.2 for August 11. These growth events, lasting several hours, are called regional because throughout the day different air parcels are arriving at the site. If nucleation happened at a given time, but was confined to a small area close by the site, the growing mode would disappear once air parcels began arriving at the site from outside the nucleation zone. The other group classified as "short-lived" events, were characterized by an increase and then a decrease in N_{10}, but without the growth of the nuclei mode to larger sizes. These increases in N_{10} were often shorter than 1-hour and correlated with SO_2, indicating local plumes. An example of a short lived event is shown in Figure 4.4. Alternately, a regional event interrupted by precipitation, significant change in wind direction, or front would be classified as a short-lived event.

Regional nucleation events were further classified as "weak", "moderate", and "strong" depending on the net rate of increase in N_{10} during the first hour of the event. The divisions were as follows: $dN_{10}/dt > 4{,}000$ $cm^{-3}hr^{-1}$ was classified as weak, dN_{10}/dt from 4,000 to 15,000 cm^{-3} hr^{-1} was classified as moderate, and $dN_{10}/dt > 15{,}000$ $cm^{-3}hr^{-1}$ was classified as strong nucleation. It should be noted that dN_{10}/dt is not the nucleation rate, typically defined as the number of nuclei clusters growing larger than 1 nm. Rather, this is a rough measure of the intensity

of the event and also of its impact on the particle number and size distribution in the region.

One final challenge in distinguishing nucleation from primary particle emission was the observation of growth events beginning with particles larger than 6 nm, rather than the expected situation of nucleation accompanied by particles down to the instrument detection limit of 3 nm. In these cases, the increase in N_{10} was rather modest and difficult to distinguish from the increase in N_{10} associated with traffic. In all other respects, the events look like the other nucleation events, including an increase in N_{50} (number concentration of particles smaller than 50nm) significantly above levels seen on days without nucleation and the characteristic growth of the new mode to 30-100 nm in size. An explanation for these events is that nucleation is occurring near the sampling site, but not directly at the site, and the particles travel to the site while growing and coagulating. Another possible explanation is that these are primary particles from vehicle emissions that are growing by condensation, and that the increase in N_{50} is explained by an increased lifetime of primary particles due to their larger sizes. Our results support the former explanation for two reasons. First, the sources of primary particles in the 10-20 nm size range are mainly vehicles in and around the city of Pittsburgh. The size of the grown primary particles as sampled would depend on the source distance from the site, the condensational growth rate, and the wind speed. Since the sources are at a constant distance from the site, and the condensational growth rate varies with photochemical activity, one would expect an initial increase in the size of the grown primary particles, and then a decrease

later in the day. Such behavior was not observed. The second reason is that the observed increases in N_{50} for stable wind directions are too rapid to be accounted for by increased lifetimes of particles as they grow in size. Therefore, these events have been classified as nucleation events.

Figure 4.5 shows the overall frequency of days with nucleation activity from July 2001 to June 2002 according to the classification scheme described above. The overall nucleation frequency, counting all event types, was 53%, or 181 of 345 study days. The regional nucleation events occurred during 31% of the study days. Regional nucleation seemed to be more frequent during the spring and fall, and less active in summer and winter. Table 4.2 summarizes key gas phase, meteorological, and aerosol variables during strong, regional nucleation events.

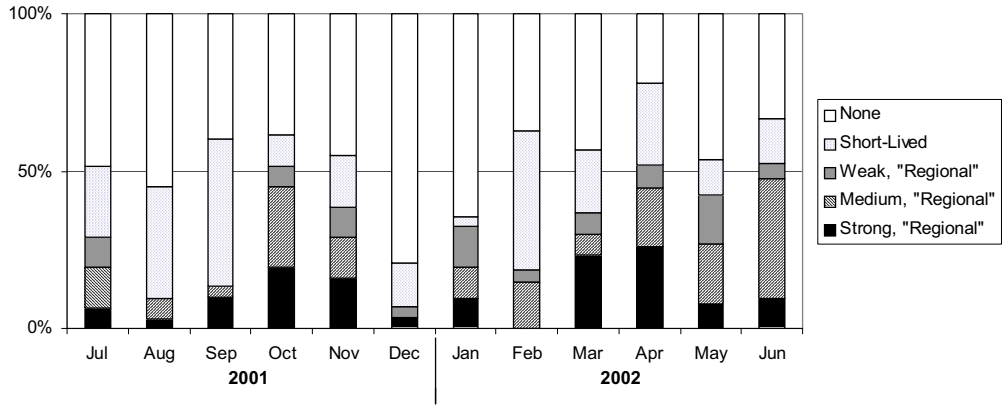

Figure 4.5 Overall Frequency of Nucleation. Days are classified by the occurrence of nucleation activity. Weak, medium, and strong refer to the rate of increase of N_{10} during the first hour of the event. $dN_{10}/dt > 4{,}000$ cm^{-3}hr^{-1} was classified as weak, dN_{10}/dt from 4,000 to 15,000 cm^{-3}hr^{-1} was classified as moderate, and $dN_{10}/dt > 15{,}000$ cm^{-3}hr^{-1} was classified as strong nucleation. Short-lived events refer to nucleation without growth to larger sizes.

Table 4.2 Summary of conditions during strong, regional nucleation events

											Num. Conc. (#/cc)			NO (ppb)			SO_2 (ppb)		
Date	Time	Strong Inversion[a]	RH %	Temp °C	Wind Direct. degree	Wind speed m/s	$PM_{2.5}$ TEOM $\mu g/m^3$	Conden. Sink cm^{-2}	UV W/m^2	Before[b]	During[b]	% Change	Before[b]	During[b]	% Change	Before[b]	During[b]	% Change
7/14/01	8:00	Y	72	17.8	318	1.5	10.8	0.021	7.2	2.8E+04	7.2E+04	157	10.0	3.6	-64	15.5	4.7	-70
7/27/01	6:00	N	64	14.2	31	0.9	8.5	0.013	1.5	1.3E+04	4.8E+04	269	0.6	3.2	446	5.8	7.1	23
8/11/01	9:00	N	67	22.6	331	1.1	8.3	0.021	8.0	na	1.1E+05	na	2.3	3.9	71	14.3	41.3	188
9/15/01	8:00	N	78	10.1	85	0.0	5.7	0.018	5.9	2.1E+04	6.9E+04	229	8.9	10.0	12	0.0	4.4	na
9/16/01	10:15	N	59	17.3	345	1.7	8.6	0.020	22.8	2.0E+04	8.1E+04	305	10.4	3.1	-70	0.0	13.8	na
10/8/01	10:30	Y	48	8.3	256	1.5	6.0	0.019	18.4	3.3E+04	6.0E+04	82	54.8	8.1	-85	21.8	13.9	-36
10/9/01	10:00	N	45	11.5	135	1.7	22.3	0.042	16.3	3.8E+04	3.9E+04	3	75.7	25.7	-66	19.5	46.7	139
10/10/01	9:30	N	44	14.6	162	2.1	13.9	0.023	14.3	2.5E+04	4.1E+04	64	22.0	7.1	-68	4.7	7.4	58
10/13/01	9:45	N	73	21.2	129	3.0	9.7	0.020	15.6	2.8E+04	na	na	20.9	8.9	-57	11.6	22.2	92
10/15/01	8:45	N	72	10.9	263	2.7	9.4	na	9.0	2.4E+04	5.5E+04	129	9.4	7.9	-16	9.6	10.0	4
10/18/01	11:45	Y	42	10.7	224	1.9	4.1	0.013	23.4	2.5E+04	4.8E+04	92	12.0	5.2	-57	1.2	5.4	347
11/3/01	11:00	Y	54	13.6	289	2.5	9.7	0.022	17.2	3.1E+04	4.4E+04	42	19.8	5.9	-70	24.2	9.5	-61
11/4/01	9:00	Y	59	9.5	203	1.8	7.3	0.016	7.2	1.7E+04	5.5E+04	224	12.2	4.3	-65	5.7	7.8	38
11/10/01	8:45	N	59	6.5	219	3.0	na	0.020	5.4	1.6E+04	6.1E+04	281	5.8	10.5	83	25.8	32.8	27
11/22/01	9:00	N	57	4.9	160	2.1	15.2	0.020	5.1	1.8E+04	3.9E+04	117	18.4	10.9	-41	11.7	11.6	-1
12/3/01	11:30	Y	40	12.6	182	2.5	4.0	0.015	13.9	3.0E+04	6.3E+04	110	36.8	10.8	-71	11.7	12.9	10
1/25/02	11:30	N	58	2.9	265	3.0	9.0	na	14.6	2.6E+04	3.9E+04	50	13.0	10.2	-22	14.2	7.6	-46
1/26/02	9:15	N	56	2.1	183	2.4	9.6	na	5.2	1.6E+04	4.1E+04	156	7.4	11.3	54	16.0	15.9	-1
1/27/02	11:00	N	46	10.2	214	2.8	10.1	na	13.7	9.8E+03	2.9E+04	196	8.2	8.6	5	12.1	13.7	14
3/7/02	10:30	N	34	10.5	19	0.4	20.1	0.026	10.4	2.4E+04	4.3E+04	79	12.0	6.7	-44	18.2	15.1	-17
3/9/02	10:00	N	46	17.7	287	4.2	18.5	0.018	15.1	1.7E+04	5.9E+04	247	5.9	4.5	-23	6.6	12.8	94
3/15/02	10:45	N	48	19.4	45	5.2	14.9	0.016	18.0	2.3E+04	5.7E+04	148	3.9	3.8	-5	8.1	13.0	60
3/23/02	8:00	N	55	-2.4	35	4.3	6.9	0.013	6.1	1.4E+04	7.7E+04	450	2.7	4.3	59	6.6	6.9	5
3/24/02	8:00	N	45	3.4	263	0.1	10.9	0.019	5.0	1.2E+04	3.1E+04	158	3.1	4.8	55	12.6	16.1	28
3/29/02	11:00	N	36	17.0	309	2.1	11.8	0.025	26.3	2.2E+04	5.9E+04	168	8.2	5.3	-35	9.7	21.6	123
4/2/02	10:45	Y	32	16.3	201	3.6	8.9	0.013	27.1	2.5E+04	4.3E+04	72	20.1	5.2	-74	14.6	6.8	-54
4/11/02	10:30	Y	28	17.8	141	4.3	10.2	0.012	27.6	1.9E+04	5.2E+04	174	11.4	5.0	-56	5.3	2.6	-52
4/12/02	9:15	N	43	15.0	150	0.5	16.5	0.024	14.7	2.4E+04	3.9E+04	63	11.7	8.8	-24	7.1	21.6	203
4/16/02	9:15	Y	54	24.6	220	0.4	26.0	0.026	19.1	3.0E+04	7.8E+04	160	23.8	10.0	-58	11.8	17.8	51
4/17/02	9:00	N	52	24.9	249	0.5	31.7	0.029	16.6	na	6.4E+04	na	84.4	10.1	-88	20.4	17.3	-15
4/18/02	8:45	N	61	22.3	na	0.0	22.8	0.026	12.8	3.1E+04	5.7E+04	84	20.0	15.4	-23	11.2	18.7	67
4/27/02	9:15	N	41	11.0	25	0.9	13.4	0.016	18.0	1.4E+04	4.5E+04	221	10.5	7.0	-34	4.5	14.1	215
5/11/02	9:30	Y	34	15.0	99	1.8	11.2	0.012	25.3	1.6E+04	9.2E+04	475	6.6	4.3	-35	3.5	18.5	427
5/30/02	10:00	Y	57	24.9	288	0.2	26.0	0.027	24.6	4.4E+04	5.2E+04	18	6.9	5.5	-20	8.5	17.8	109
6/3/02	8:45	Y	48	16.6	na	0.0	13.5	0.021	8.1	7.6E+04	1.3E+05	71	12.0	8.9	-26	7.8	19.8	153
6/22/02	9:00	Y	52	25.2	187	1.5	31.0	na	16.4	na	na	na	10.2	4.7	-54	10.8	16.0	49
6/24/02	9:00	Y	55	27.0	199	1.2	32.3	na	15.1	na	na	na	22.6	11.5	-49	25.5	54.1	112

[a] Y refers to days when a clear breaking of the nighttime inversion could be identified at approximately the same time as the inception of nucleation. Breaking of the inversion was identified as a sharp drop in ground level $PM_{2.5}$, NO, relative humidity, and CO (Table 4.9). N refers to days when the inversion layer was either not present or not significant enough to detect by analyzing the time series.

[b] Before is calculated as the average of the 2 hour period prior to nucleation. After is calculated as the average of the 2 hour period beginning with the nucleation event

4.3.2 Spatial Scale of Nucleation

The spatial scale of nucleation was investigated by operating an SMPS in Florence, Pennsylvania (Figure 4.1) during parts of February and March of 2002. This site was 38 km to the west of the main site. Although the lower limit of the size distributions was at 10 nm, the growth portion of the nucleation events was clearly evident and coincided in time well with the events at the main site (Figure 4.6). On other days of the study, no nucleation occurred at both sites. Of the 34 days of parallel sampling, all of the stronger nucleation events except one happened at both sites at nearly the same time. Only 5 days show qualitative disagreement between the two sites, usually with weak nucleation at one site but not the other.

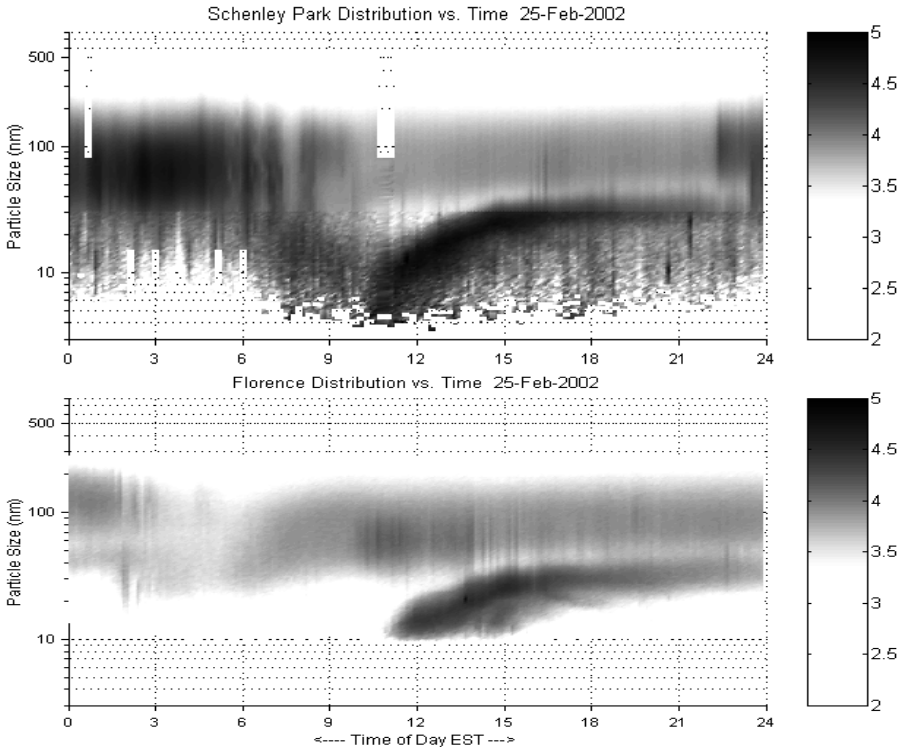

Figure 4.6 Graphical representation of instrument response for two sites. The top plot shows results at an urban sampling location in Pittsburgh, PA and the bottom graph shows results for the same time period from an upwind, rural site 40 km away. Nucleation is apparent at around 10 AM local time.

4.3.3 Conditions Favorable to Nucleation

Nucleation occurred most frequently on sunny days with below average $PM_{2.5}$ concentrations (Table 4.2). This often occurred on days after the passage of a cold front through the area with subsequent high pressure and clear skies. Although this general pattern held, no simple relationship between sunlight, preexisting aerosols, and nucleation was identified. During summer, regional nucleation was mostly associated with light northwesterly winds, while in fall and winter it was mostly associated with stronger southwesterly winds. During spring, the wind direction for nucleation was highly variable.

The hypothesis that these events are due to sulfuric acid nucleation was explored by correlating nucleation activity and H_2SO_4 production. This correlation, based on the ideas of Pirjola et al. (1999) and Wexler et al. (1994), was developed to see how well the observed nucleation events, both short-lived and regional, could be explained in terms of condensation and nucleation of H_2SO_4. As neither OH nor H_2SO_4(g) were measured during PAQS, the product of ultraviolet light and SO_2 was used as a surrogate parameter for H_2SO_4 production. The condensational sink, CS, was calculated from the measured size distribution at near-ambient relative humidity using the formula:

$$CS = \int_{3nm}^{500nm} D_p \beta(D_p) n(D_p) dD_p \qquad (4.1)$$

where β is the transitional correction factor (Fuchs and Sutugin 1970), D_p is particle diameter, and $n(D_p)$ is the measured number size distribution[10]. The condensational sink is only integrated through 500 nm, because the size

[10] The physical interpretation and units of the condensational sink are discussed in the glossary.

distributions extending beyond this size are not available for all time periods of the study. Therefore, this is a low estimate of the actual condensational sink, especially when aged aerosols are sampled.

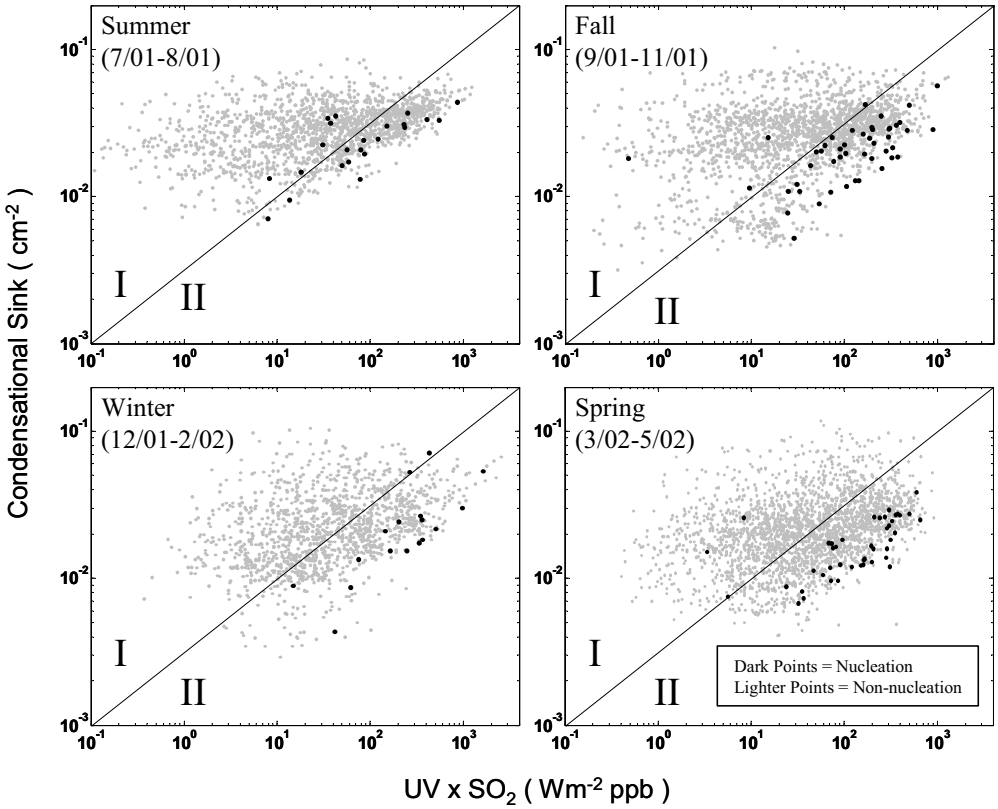

Figure 4.7 Correlation showing UV * SO_2 vs. condensational sink for four different seasons. Condensational sink (y-axis) is plotted against the product of ultraviolet light intensity and SO_2 concentration (x-axis), a proxy for sulfuric acid production. . 15-minute averaged values are plotted for all time periods of the study. The black symbols correspond to onset of nucleation. The grey symbols correspond to periods when nucleation is not observed. The 45 degree line roughly divides the each plot into two regions – the upper left region I where nucleation is not generally observed, and the lower right region II where nucleation is more common.

The result of the correlation is shown in Figure 4.7. The panels of Figure 4.7 can be divided into 2 qualitative regions. The upper left portion of each figure (Region I), dominated by grey points, is where nucleation is relatively rare, because the sulfuric acid production is too slow, or there is too much area available for condensation. The second region is where the bulk of the black

points are, indicating conditions more favorable to nucleation. As the UV*SO2 product increases and the condensational sink decreases, the ratio of nucleation points (in black) to non-nucleation point (in grey) increases. The nucleating conditions do not form a sharp line in this plot. While this is partly due to measurement errors and difficulty in assigning a precise start time to nucleation, it is probably mostly due to additional predictive variables that are important to nucleation. During summer nucleation takes place at higher condensational sink values for the same value of UV*SO2. Known variables that should be important include temperature and relative humidity.

The nucleation measurements made during this study are compared to model-based correlations of Pirjola et al. (1999) and Wexler et al. (1994) in Figure 4.8. Condensational sink (y-axis) is plotted against the product of ultraviolet light intensity and SO_2 concentration (x-axis), a proxy for sulfuric acid production. These models were designed to predict the required H_2SO_4 production rates for nucleation and growth by H_2SO_4 as a function of condensational sink, relative humidity, and temperature. The observed nucleation events are plotted as solid black circles, while the black lines are the correlation-based thresholds for H_2SO_4 nucleation, with nucleation expected to the right of the lines and not expected to the left. These thresholds are calculated at representative ground level relative humidity and temperature values. The lines are calculated using some assumptions, including (1) a proportional relationship between UV and OH, with full summer sun of 36 Wm^{-2} UV corresponding to an OH concentration of 10^7 molec cm^{-3}; and (2) a SO_2 deposition characteristic time

of 10^4 s (Wexler et al. 1994). With our assumed OH levels, both of the correlations suggest that the ground level conditions are several orders of magnitude cleaner than those required to induce binary nucleation and growth of fresh particles by sulfuric acid.

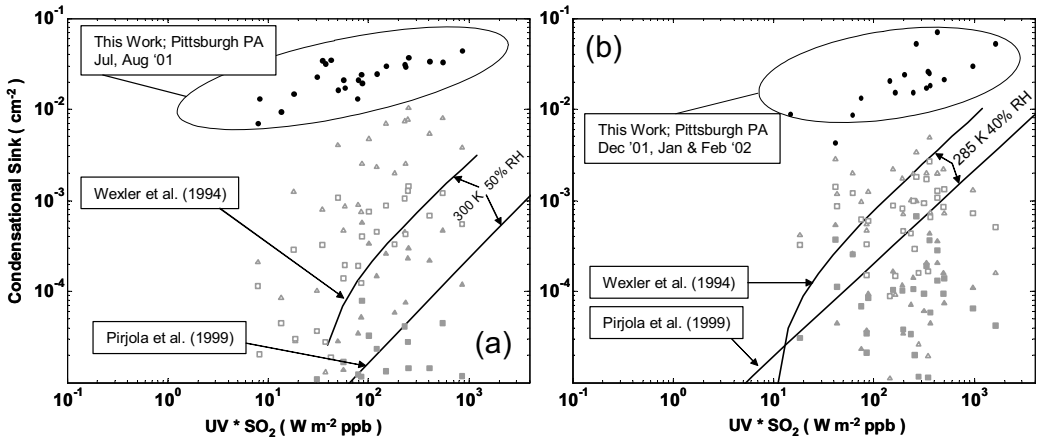

Figure 4.8 Comparisons of conditions during summer (a) and winter (b) nucleation to model-based correlations for sulfuric acid particle formation from Pirjola et al. (1999) and Wexler et al. (1994). Condensational sink (y-axis) is plotted against the product of ultraviolet light intensity and SO_2 concentration (x-axis), a proxy for sulfuric acid production. Measured nucleation events (dark circles) are found at the highest condensational sink values. Solid lines refer to correlation predictions for the nucleation threshold at a representative ground-level RH and temperature (nucleation favored to the right of the lines, and not expected to the left). Additional correlation predictions (grey data points) are plotted to see if data-model agreement improves when specific RH and temperature values for each nucleation event are used in the models (triangles = Wexler et al. 1994; squares = Pirjola et al. 1999). Filled symbols refer to RH and temperature at ground level while unfilled symbols refer to estimated conditions at the top of the boundary layer.

Also plotted are grey points, which are model predictions for the critical condensational sink level at OH, SO_2, temperature, and relative humidity levels matching those of the specific nucleation events. This provides a better comparison of models to observations, because a representative relative humidity and temperature is not needed. Each observation (black circle) is matched by 4 grey points, at the same point on the x-axis, but with different condensational sink values. Grey points refer to the correlations of Wexler et al., 1994 (triangles) and

Pirjola et al., 1999 (squares). Filled grey symbols are calculated at ground level meteorological conditions while open grey symbols are calculated at reduced temperatures and elevated relative humidities corresponding to the top of the mixed layer. This is done to check if conditions at the top of the mixed layer would be sufficient for sulfuric acid induced nucleation. Key assumptions included constant vertical profiles of dewpoint, OH, and SO_2 in the mixed layer, summertime afternoon mixing heights of 2000 m, wintertime afternoon mixing heights of 800 m, and adiabatic cooling of air parcels at a rate of 9.8 °C km^{-1}. Using these assumptions, the gap between model predicted and observed condensational sink levels during nucleation narrowed, but did not close.

The conclusions that can be drawn from comparing the nucleation models with the PAQS observations (Figure 4.8) are as follows: (1) Observed nucleation is occurring at significantly higher levels of preexisting aerosol surface area and/or lower levels of sulfuric acid production than predicted by the models; (2) this gap between models and observations is narrowed, but not removed, when lower temperatures and higher relative humidities at the top of the mixing layer are taken into account; and (3) the observations are not nearly as dependent on meteorology and sulfuric acid production rate as the models are. These conclusions suggest that additional factors, currently absent from the models, such as ammonia chemistry or growth by organic compounds, are involved in the nucleation events.

Many nucleation events were seen to coincide in time with the breakup of the morning inversion. In Table 4.2, nucleation events where this was especially

prominent are noted in the inversion column. Nucleation concurrent with inversion layer breakup is most common in spring and fall. It is not common in winter, possibly due to higher average wind speeds during nucleation events. Figure 4.9 shows the average diurnal profile for regional nucleation events associated with inversion breakup. The key features of Figure 4.9 are the unusually high morning peak of NO, significant decrease in $PM_{2.5}$ during the morning, and increase in SO_2 as NO decreases. This indicates the possibility of nucleation occurring aloft in a SO_2 enriched and low $PM_{2.5}$ stable layer, followed by the mixing downward of the nuclei.

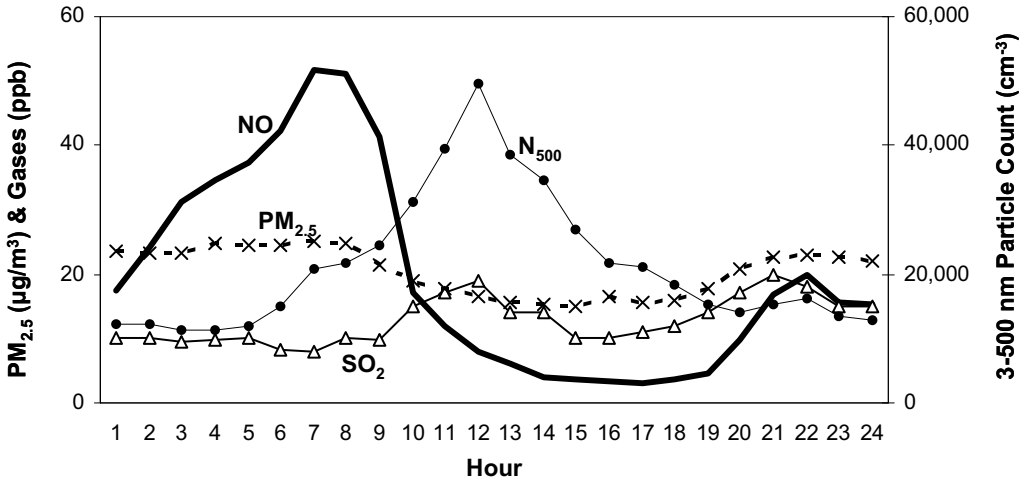

Figure 4.9 Diurnal profile for inversion-related nucleation. Inversion-related nucleation events from July – November, 2001 are averaged. Boundary layer mixing height increases during the mornings, with decreases in $PM_{2.5}$ and NO, increases in SO_2 levels, and nucleation activity.

4.4 Summary and Conclusions

Continuous particle size distribution measurements for one year during the Pittsburgh Air Quality Study indicate a high frequency of nucleation activity in the region, with nucleation occurring on about 50% of days, and regional nucleation events occurring on 30% of days on average. Nucleation occurred

during all seasons but was most intense during spring and fall. The nucleation events are more probable during bright sunny conditions with elevated SO_2 concentrations and low preexisting aerosol surface area. This relationship was analyzed using a simple correlation of UV*SO_2 versus condensational sink and compared to existing correlations for binary H_2SO_4-H_2O nucleation. The correlation indicated that nucleation occurs under higher aerosol loading conditions and/or with lower H_2SO_4 production rates than expected. A few events that did not follow the overall pattern appear to be influenced by conditions that made classification of the events problematic, such as a weak nucleation rate or a frontal passage. The correlation between H_2SO_4 production and nucleation activity provides strong evidence that sulfate plays a major role in new particle formation in Western Pennsylvania. The difference between the model-predicted and observed nucleation frequencies indicates that additional compounds, such as ammonia or organics, are possibly involved in the nuclei formation and/or growth in addition to sulfuric acid.

4.5 Acknowledgements

This research was conducted as part of the Pittsburgh Air Quality Study which was supported by US Environmental Protection Agency under contract R82806101 and the US Department of Energy National Energy Technology Laboratory under contract DE-FC26-01NT41017. The authors also wish to thank Hiromu Sakurai, Peter McMurry, and the Minnesota Particle Technology Laboratory for their help with the Ultrafine CPC testing.

4.6 Reference

Allen, A.G., Grenfell, J.L., Harrision, R.M., James, J., and Evans, M.J. (1999). Nanoparticle Formation in Marine Airmasses: Contrasting Behaviour of the Open Ocean and Coastal Environments, Atmos. Res. 51: 1-14.

Birmilie. W., Wiedensohler, A., Heintzenber, J., and Lehmann, K. (2001). Atmospheric Particle Number Size Distribution in Central Europe: Statistical Relations to Air Masses and Meteorology, J. Geophys. Res. 106 (D23): 32,005 – 32,018.

Charlson, R.J., Lovelock, J.E., Andreae, M.O., and Warren, S.G. (1987). Ocean Phytoplankton, Atmospheric Sulfur, Cloud Albedo and Climate, Nature 326: 655-661.

Eisele, F.L., and McMurry, P.H. (1997). Recent Progress in Understanding Particle Nucleation and Growth, Philos. Trans. R. Soc. London, Ser. B. 352(1350): 191-200.

Fuchs, N.A., and Sutugin, A.G. (1970). Highly Dispersed Aerosols. Ann Arbor Science, Ann Arbor, MI.

Harrison, R.M., Jones, M., and Collins, G. (1999). Measurements of the Physical Properties of Particles in the Urban Atmosphere, Atmos. Environ. 33: 309-321.

Harrison, R.M., Shi, J.P, and Jones, M.R. (1999). Continuous Measurement of Aerosol Physical Properties in the Urban Atmosphere, Atmos. Environ. 33: 1037-1047.

Harrison, R.M., Grenfell, J.L., Allen, A.G., Clemitshaw, K.C., Penkett, S.A., and Davison, B. (2000). Observations of New Particle Production in the Atmosphere of a Moderately Polluted Site in Eastern England, J. Geophys. Res. 105: 17,819-17,832.

Jang, M.S., and Kamens, R.M. (2001). Atmospheric Secondary Aerosol Formation by Heterogeneous Reactions of Aldehydes in the Presence of a Sulfuric Acid Aerosol Catalyst, Environ. Sci. Technol., 35(24): 4758-4766.

Kerminen, V.M. (1999). Roles of SO_2 and Secondary Organics in the Growth of Nanometer Particles in the Lower Atmosphere, J. Aerosol Sci. 30(8): 1069-1078.

Kim, C.S., Adachi, M., Okuyama, K., and Seinfeld, J.H. (2002). Effect of NO_2 on Particle Formation in SO_2/H_2O/air Mixtures by Ion-Induced and Homogenous Nucleation, Aerosol Sci. Technol. 36(9): 941-952.

Kulmala, M., Pirjola, L., Makela, J.M. (2000). Stable Sulphate Clusters as a Source of New Atmospheric Particles, Nature 404: (6773) 66-69.

Kulmala, M., et al. (2001). Overview of the International Project on Biogenic Aerosol Formation in the Boreal Forest (BIOFOR), Tellus. Ser. B, 53, 324-343.

Novakov, T., and Penner, J.E. (1993). Large Contribution of Organic Aerosols to Cloud Condensation Nuclei Concentrations, Nature 365: 823-826.

Oberdorster, G., Gelein, R.M., Ferin, J., and Weiss, B. (1995). Association of Particulate Air Pollution and Acute Mortality: Involvement of Ultrafine Particles, Inhal. Toxicol. 7: 111-124.

O'Dowd, C. D., Lowe, J.A., and Smith, M.H. (1999). Coupling Sea-Salt and Sulphate Interactions and its Impact on Cloud Droplet Concentration Predictions, Geophys. Res. Lett. 26(9): 1311-1314.

O'Dowd, C.D., Aalto, P., Hmeri, K., Kulmala, M., and Hoffmann, T. (2002). Aerosol Formation: Atmospheric Particles From Organic Vapours, Nature 416: 497-498.

Peters, A., Wichmann, E., Tuch, T., Heinrich, J., and Heyder, J. (1997). Respiratory Effects are Associated with the Number of Ultrafine Particles, Am. J. Respir. Crit. Care Med. 155: 1276-1383.

Pirjola, L., Kulmala, M., Wilck, M., Bischoff, A., Stratmann, F., and Otto, E. (1999). Formation of Sulphuric Acid Aerosols and Cloud Condensation Nuclei: An Expression For Significant Nucleation and Model Comparison, J. Aerosol Sci. 30(8): 1079-1094.

Rivera-Carpio, C.A., Corrigan, C.E., Novakov, T., Penner, J.E., Rogers, C.F., and Chow, J.C. (1996). Derivation of Contributions Sulfate and Carbonaceous

Aerosols to Cloud Condensation Nuclei From Mass Size Distributions, J. Geophys. Res. 101: 19,483-19,493.

Schwartz, J., Dockery, D.W., and Neas, L.M. (1996). Is Daily Mortality Associated Specifically with Fine Particles?, J. of the Air & Waste Management Association 46: 927-939.

Shi, J.P., Evans, D.E., Khan, A.A., and Harrison, R.M. (2001). Source and Concentration of Nanoparticles (<10 nm diameter) in the Urban Atmosphere, Atmos. Environ. 35: 1193-1202.

Shi, Q., Sakurai, H., and McMurry, P.H. (2002). Measurement of St. Louis Particle Size Distributions: Observation of Particle Events. American Association of Aerosol Research Annual Meeting, Charlotte, NC.

Weber, R.J., McMurry, P.H., Mauldin, L., Tanner, D., Eisele, F., Clarke, A.D., and Kapustin, V.N. (1999). New Particle Formation in the Remote Troposphere: A Comparison of Observations at Various Sites, Geophys. Res. Lett. Atmos. Sci. 26, 307-310.

Wexler, A.S., Lurmann, F.W., and Seinfeld, J.H. (1994). Modelling Urban and Regional Aerosols – I. Model Development, Atmos. Environ. 28(3): 531-546.

Woo, K.S., Chen, D.R., Pui, D.Y.H., and McMurry, P.H. (2001). Measurement of Atlanta Aerosol Size Distributions: Observations of Ultrafine Particle Events, Aerosol Sci. Technol. 34: 75-87.

Zhang, K.M., and Wexler, A.S. (2002) A Hypothesis for Growth of Fresh Atmospheric Nuclei. Accepted for publication in J. Geophys. Res.

Zhou, L., Kim, E., Hopke, P.K., Stanier, C., Pandis, S.N., 2003. Advanced factor analysis on Pittsburgh particle size distribution data. Aerosol Science and Technology, in press.

Chapter 5 An Algorithm for Combining Electrical Mobility and Aerodynamic Size Distributions Data When Measuring Ambient Aerosol[†]

5.1 Introduction

Ambient aerosol plays an important role in the atmosphere influencing visibility, affecting global climate, and participating in atmospheric chemistry (Seinfeld and Pandis 1998). Recently, increased concentrations of ambient aerosol smaller than 2.5 μm ($PM_{2.5}$) have been associated with increased morbidity and mortality rates (Swartz and Dockery, 1992; Dockery et al. 1993). Size distribution of atmospheric particles spans a wide size range from a few nanometers to several micrometers. In order to study aerosol dynamics in such a broad size range a combination of several separate instruments is necessary. Typical combinations have been that of an SMPS (Scanning Mobility Particle Sizer, TSI Inc., St. Paul, MN) with an APS (Aerodynamic Particle Sizer, TSI Inc.). For example, such a combination was employed in several recent studies to measure ambient aerosol (Shen et al. 2002; Hand and Kreidenweis, 2002; Shi et al. 2001). The integrated volume concentration measured with the SMPS-APS can be used to estimate the mass concentration using an assumed bulk aerosol density

[†] Published as "An Algorithm for Combining Electrical Mobility and Aerodynamic Size Distributions Data When Measuring Ambient Aerosol" by Andrey Khlystov, Charles Stanier, and Spyros Pandis, *Aerosol Science and Technology*, 2003 (in press).

(Shen et al. 2002). If this approach proves accurate, the SMPS-APS can be used as high time resolution substitution for the filter based mass measurements.

The SMPS and the APS have different measurement principles. The SMPS classifies particles according to their mobility in an electric field (Wang and Flagan 1989). The electrical mobility size depends on the particle cross-section and for a spherical particle is the same as the physical size. Unlike the SMPS, the APS measures aerodynamic size. Particles are accelerated in a nozzle and their time-of-flight is related to their aerodynamic size (Armendariz and Leith 2002). The aerodynamic size is proportional to the physical size and the square root of particle density (Hinds, 1999). Thus, for a sphere the aerodynamic size is equal to the physical size only for unit density particles.

Because of the different measurement principles (e.g. electrical mobility vs. aerodynamic sizing) difficulties arise in attempts to create a single size spectrum from the data measured with the SMPS and APS. Some researchers have approached this problem by selecting data from each instrument such that the SMPS is used up to a certain size beyond which the APS is used (Shen et al. 2002). Hand and Kreidenweis (2002) have developed an algorithm that combines electrical mobility, optical particle counter (OPC) and APS data into a single spectrum. The OPC data are first matched with the SMPS spectrum by finding an optimal refractive index. Then the APS data are matched to the modified OPC spectrum by finding an effective density that would provide the best fit with the OPC. The reason for matching the APS to the OPC and not directly to the SMPS was that the size overlap between the APS and the SMPS is rather small.

In this study we attempted to fit the APS size distribution to the SMPS distribution in the absence of an optical particle counter. A simple algorithm was developed to combine the aerodynamic and electrical mobility spectra into a single distribution. The algorithm provides a ratio of the particle density to the shape factor of particles in the 540 nm – 800 nm size range where the SMPS and the APS measurement ranges overlap. The ratio of aerosol density to its shape factor is usually called the "effective" density. However, the algorithm does not provide means of separating the density and the shape factor. It should also be noted that the particle shape factor and density may differ through the aerosol spectrum, as the composition and the physical properties of ambient particles usually vary with size. Instead of concentrating on the narrow overlap size range we have determined the average (bulk) aerosol "effective" density during a month of ambient aerosol measurements within the Pittsburgh Air Quality Study (PAQS).

The measurements were carried out at the central site of the PAQS, in an urban park approximately 5 km from the downtown Pittsburgh.[11] The aerosol originated from both urban and long-range sources. Ammonium salts of sulfate were the dominant aerosol components, comprising approximately 50% of the $PM_{2.5}$ aerosol mass, carbonaceous material was the second largest component, contributing approximately 25% to the mass of fine particles (Wittig et al., 2003). The results obtained with the SMPS-APS system were compared to the simultaneous measurements of the aerosol $PM_{2.5}$ mass concentration using a

[11] See note 7, section 3.2 for additional discussion of the site and proximity to sources.

TEOM (R&P Co., Albany NY) and size-fractionated mass measurements using MOUDI (MSP Co., Minneapolis, MN) cascade impactor. The comparison of the $PM_{2.5}$ particle volume concentration from the merged SMPS-APS distribution with the TEOM $PM_{2.5}$ mass concentration has provided us with an estimate of a bulk "effective" particle density.

5.2 Experimental

5.2.1 General Description of the SMPS-APS System

The SMPS-APS system used in the Pittsburgh Air Quality Study was a part of the Dry-Ambient Aerosol Size Spectrometer (DAASS), described in Stanier et al. (2003). The system consists of an ultra-fine SMPS system for 3 – 80 nm (TSI 3936N25), an SMPS for 13 – 680 nm (TSI 3936L10), and an Aerosol Particle Sizer (TSI APS 3320) covering 0.5 – 10 μm. In this study we used data up to 2.5 μm in aerodynamic diameter. The DAASS system is equipped with a number of computer-controlled solenoid valves that direct the sample and sheath flows of the instruments either directly to the instruments or through nafion driers (Perma Pure Inc.). Single channel nafion dryers in stainless steel casing were used in the sample lines to minimize particle losses. The sheath lines were equipped with multi-channel dryers, because of the higher capacity needed to dry larger flows and because particle loss is not an issue in particle-free flows. To avoid losses of semi-volatile aerosol components the whole system was maintained at a temperature that was within $2^{o}C$ of the ambient temperature. When the aerosol is sampled through the dryers, the DAASS provides measurements of dried ambient aerosol (at the relative humidity of 10-35%). When the sample bypasses the

dryers, the system measures the aerosol at ambient relative humidity. Four dried and four "ambient" (or "wet") size distributions are measured each hour.

No impactor was used in front of the SMPS systems. It was found that the cut-off characteristics of the TSI impactor change as the sampling progresses because of accumulation of material on the impactor plate. Even with daily cleaning, it was observed that the impactor was cutting into progressively smaller than nominal sizes. The purpose of the impactor in SMPS systems is to facilitate the data inversion. The impactor is to remove particles larger than the measurement range of the SMPS, such that there is no contribution of multiply-charged particles to the last channels of the instrument. If no impactor is used, the concentration in the last channels will be overestimated due to the contribution of multiple-charge particles from particles larger than the upper instrument size limit.

The effect of multiple charging was minimal in the present study. During this study the ambient aerosol number concentration was rapidly declining with size for the particles larger than 100 nm, with the number size distribution at those sizes closely following the power law function of -3 to -6 power. In other words, when moving a factor of 2 in size the concentration drops by 2^{-3} to 2^{-6} (there are 8 to 32 times less particles). If an SMPS channel measures 700 nm single-charge particles, it will also measure approximately 2 times larger double-charge particles. Even though the charging for single charge at 700 nm is approximately equal to that for double-charge particles at 1400 nm, the maximum contribution of double charge particles to the last SMPS channel would be about 10%. A more

rigorous analysis of the possible error due to the presence of multiple-charge particles in the last SMPS channels was done using MICRON software package (Wolfenbarger and Seinfeld 1991). The results confirm that the error due to the presence of multiple-charge particles at sizes larger than the upper size limit of the SMPS is less than 10% in this study. It should be also noted, that the SMPS is not designed to allow a 100% penetration of particles larger than 1 μm. Particle losses of the super-micrometer particles will further reduce the error due to multiple-charge particles outside the SMPS size range.

The APS can be operated in two modes: "summed", in which the time-of-flight (TOF) and the optical signals are saved separately, and "correlated", in which the TOF and optical signal are saved together on a per particle basis. Since less memory storage is required in the summed mode, more bits of the TOF information can be stored. Thus, the size resolution of the instrument in that mode is better. In this study the APS was operated in the summed mode, because the correlated mode has been reported to have problems at low aerosol concentrations (Armendariz and Leith 2002).

To facilitate the matching of electrical-mobility size distributions with the aerodynamic size data, the APS was "mobility" calibrated using ammonium sulfate aerosol. Ammonium sulfate was chosen because it is the dominant aerosol component in ambient aerosol in the Pittsburgh area (Rees et al. 2003). The almost mono-disperse ammonium sulfate aerosol was produced by selecting a narrow mobility range with a Differential Mobility Analyzer (DMA 3081, TSI Inc.) from a wider spectrum of artificially generated ammonium sulfate particles.

The artificial aerosol was produced by spraying aqueous ammonium sulfate solution with a constant output atomizer (Model 3076, TSI Inc.) and drying it with a silica-gel diffusion drier. After passing the drier the aerosol was fed to the DMA. The sheath and aerosol flows of the DMA were set to be 2 l min^{-1} and 0.2 l min^{-1}, respectively. This was done to extend the size range of the DMA to about a 1.2 μm mobility diameter. The mono-disperse output of the DMA was diluted with 0.8 l min^{-1} of clean filtered air. The resulting flow of 1 l min^{-1} containing the mono-disperse aerosol was fed directly to the inner inlet nozzle of the APS. The size of the mono-disperse particles was adjusted by changing the voltage of the DMA. Mono-disperse ammonium sulfate aerosol with sizes from 0.4 to 1 μm was used to calibrate the APS. The DMA output contained smaller amounts of double- and triple-charge particles, that have approximately 2 and 3 times larger sizes than the main peak of single-charge particles. Because the original poly-disperse aerosol size distribution was rapidly decreasing with size and because the size resolution of the APS is substantially better than a factor of 2 in size, these double- and triple-charge particle peaks were not interfering with the analysis of calibration results. Since it was impossible to produce particles larger than 1.2 μm with the DMA, the calibration curve obtained at smaller sizes was extrapolated to the larger sizes.

Sizing precision of the SMPS was checked using mono-disperse PSL aerosol as well as by sizing mono-disperse ammonium sulfate in 14 different size ranges from 20 nm to 900 nm. The mono-disperse ammonium sulfate particles were produced using a DMA. Similarly to the APS, the double- and triple-charge

particles did not interfere with the analysis of the calibration results. Differences in particle sizing were less than 3% across the entire size range.

Prior to the ambient study the APS was tested in the laboratory using artificial ammonium sulfate aerosol. The merging algorithm, as will be shown later, requires the counting efficiency of the SMPS and the APS to be equal in the overlap range. The integrated counting efficiency of the SMPS was compared to that of a standalone condensation particle counter (CPC Model 3025, TSI Inc) and was found to be within 10% of that of the CPC. The counting efficiency of the APS in the summed mode relatively to that of the SMPS was assessed by comparing its counts with those of the SMPS in the overlap size range of 0.5 – 1 μm in mobility diameter. The APS was mobility calibrated with mono-disperse ammonium sulfate aerosol, as described above, and the calibration information for this laboratory inter-comparison was stored in the APS with the particle density and the shape factor set both to 1. In this way, no post processing of the data was required for the APS data: the APS was reporting "mobility-equivalent" size of ammonium sulfate particles.

5.2.2 Merging of the SMPS and APS Size Distributions

Data obtained with the SMPS/APS were combined into one single size distribution in two ways. In the first approach, similarly to Shen et al. (2002), the APS data were merged with the SMPS assuming the aerodynamic size is the same as the physical size. In the second, similarly to Hand and Kreidenweis (2002), a size correction factor was searched for the APS data to be merged with the SMPS data. Unlike Hand and Kreidenweis (2002), who used optical counter

measurements as an intermediate to match the distributions, we converted the APS data to the mobility spectrum by finding a size correction factor that gives the best least squares fit directly with the SMPS in the overlap size range.

The fitting of the APS to the SMPS was done in the following way. The SMPS and APS systems overlapped from 542 to 680 nm for unit density particles. The SMPS data were fitted with a power-law (Junge size distribution) function (Willeke and Baron 1997) in this overlap size range. A size correction was then found for the APS size distribution, expressed as dN/dLog(D), to have the least squares fit with the power-law approximation of the SMPS data. Applying the correction factor preserves the shape of the APS distribution, while shifting it along the dLog(D)-axis to achieve a good fit with the SMPS size distribution. Given the narrow size range of the overlap region, the size correction factor is assumed to be constant within the overlap size range.

The size correction factor is selected to minimize the difference between the SMPS and shifted APS size distributions, with the objective function S^2 shown in the following equation.

$$S^2(x) = \frac{1}{n_2 - n_1} \sum_{i=n1}^{n2} [\log(N_s(D_i)) - \log(N_a(D_i x))]^2 \qquad (5.1)$$

in which N_s is the power-law function representing the smoothed dN/dLog(D) size distribution measured by the SMPS, and N_a is the APS size distribution; x is the size correction factor; n_1 and n_2 are the numbers of the first and the last APS channel that fit, after applying the correction, into the 540 nm – 800 nm mobility size range. The first two channels of the APS were not used for the fitting

procedure because of their unreliable counting. The logarithms of the size distribution values are used to give the same relative weight to all points in the overlap range.

It should be noted that a dN/dLog(D) distribution should be used for the minimization procedure. If a dN/dD distribution is used, the APS distribution will need to be shifted not only along the abscissa, but also vertically:

$$\left(\frac{dN}{dD_p}\right)_{SMPS} = \left(\frac{dN}{dD_a}\right)_{APS} \frac{dD_a}{dD_p} = \left(\frac{dN}{dD_a}\right)_{APS} x \tag{5.2}$$

in which D_a is the aerodynamic size, D_p is the physical size and x is the size correction factor ($D_a = x\ D_p$). In contrast, under the assumption that the shift factor does not vary within the overlap size range, the dN/dLog(D) distribution does not need a vertical shift:

$$\left(\frac{dN}{d\log D_p)}\right)_{SMPS} = \left(\frac{dN}{d\log D_a)}\right)_{APS} \frac{d\log D_a)}{d\log D_p)} = \left(\frac{dN}{d\log D_a)}\right)_{APS} \frac{d\log D_p x)}{d\log D_p)} = \left(\frac{dN}{d\log D_a)}\right)_{APS} \tag{5.3}$$

The size correction factor relates to the ratio of the aerosol density to its shape factor in the size range used for the fitting, and is usually called an "effective" density (Hand and Kreidenweis 2002). This relationship can be seen from the formula relating the mobility size to the aerodynamic size (Hinds, 1999):

$$D_p = D_a \sqrt{\chi \frac{C_s(D_a)}{C_s(D_p)} \frac{\rho_0}{\rho_p}} \tag{5.4}$$

in which D_p and D_a are the mobility and the aerodynamic diameters, respectively, C_s is the Cunnigham slip correction factor, ρ_0 is the reference density (1 g cm^{-3}), ρ_p is the density of the particle, and χ is the shape factor. At sizes of the APS-

SMPS overlap size range the slip correction can be neglected: for the particle density of 2 g cm^{-3}, the shape factor of 1 and the physical diameter of 500 nm the error in calculating the aerodynamic diameter is 4%. At lower particle densities and larger shape factors the error will be even smaller. Neglecting the slip correction, Equation 5.4 becomes:

$$D_p = D_a \sqrt{\chi \frac{\rho_0}{\rho_p}} = \frac{D_a}{x} \tag{5.5}$$

Thus, the size correction factor is:

$$x = \sqrt{\frac{\rho_p}{\chi \rho_0}} \tag{5.6}$$

The size correction factor depends on both the particle density and the shape factor in the overlap size range. Consequently, it is not possible to determine each of these parameters from the size correction factor without complementary measurements. However, the particle density in the overlap size range may differ from the average bulk aerosol density, which will introduce errors in determination of the shape factor from the size correction factor. This problem can be avoided by using mass measurements within the narrow overlap size range. For practical purposes, however, it is more useful to obtain integrated aerosol properties in the $PM_{2.5}$ size range, such that, for example, the aerosol volume measured with the SMPS-APS can be converted to the aerosol mass, substituting filter-based measurements, and the volume size distribution can be converted to the aerodynamic size distribution to substitute cascade impactor measurements. For this reason we concentrated our efforts to find the bulk $PM_{2.5}$

aerosol effective density from comparisons of the SMPS-APS with a TEOM and a MOUDI cascade impactor.

It should be noted that errors may be introduced into the merged size distribution, if the SMPS and the APS have different counting efficiencies in the overlap size range. To demonstrate the magnitude of the errors due to miscounting, a short analysis is performed here. As an example we will assume the SMPS to be correct and the APS is counting Z times lower than the SMPS. If the dN/dLog(D) size distribution follows the power-law function proportional to D^{-B}, it can be shown that the merging procedure would shift the APS distribution by $Z^{1/B}$ times extra, relative to what the correction factor should be if the APS is correct. If the size distribution in physical sizes is $f_p(D) = A\ D^{-B}$, then the size distribution in aerodynamic sizes, $f_a(D)$, will be:

$$f_a(D) = AD_p^{-B} = A\left(xD_a\right)^{-B} = x^{-B} f_p(D) \tag{5.7}$$

Consequently, the size correction factor is:

$$x = \left(\frac{f_p(D)}{f_a(D)}\right)^{\frac{1}{B}} \tag{5.8}$$

An error in concentration measurements of aerodynamic distribution of a factor of Z will translate to an error in the correction factor of a factor $Z^{1/B}$. In other words, a flatter distribution (lower B) will have a larger error in the shift factor. However, if the APS is miscounting with a constant factor throughout its size range and the distribution is power-law, there will be no error in the volume concentration measurements after the merging procedure.

5.2.3 Comparison of the SMPS-APS with TEOM and MOUDI measurements

The SMPS-APS were compared with the Tapered Element Oscillating Microbalance (TEOM Model 1400a, R&P Co.) and MOUDI cascade impactor (Model 110, MSP Co., Minneapolis, MN) during measurements of ambient aerosol in Pittsburgh, PA during July 2001.

The integrated aerosol volume concentrations in the $PM_{2.5}$ size range were compared to the simultaneous measurements with the TEOM. Dried (low relative humidity) measurements of the DAASS were used for this comparison, because the relative humidity conditions were close to those of the TEOM (below 30%RH). The TEOM was operated at 30^{o}C and was equipped with a Nafion diffusion dryer Sample Equilibration System (SES, R&P Co.) to minimize evaporative losses of volatile aerosol components. During the study, the TEOM has shown a very good agreement with the Federal Reference Method (FRM). The TEOM was on average 1.5% higher than the FRM, both instruments giving readings within 10% of each other during the whole study (Rees et al. 2003). Because of the relatively small fraction of ammonium nitrate in July in Pittsburgh, and because the TEOM was operated at 30^{o}C, the volatilization artifact in the TEOM was relatively small during this study. The accuracy and the artifacts of the FRM observed during the study are discussed in detail in Rees at al. (2003).

For comparison with the TEOM two combined spectra were calculated from the SMPS-APS measurements: 1) without converting the APS data to mobility diameter, similarly to Shen et al. (2002), or 2) with the conversion of APS data to the mobility size using the procedure described in the Experimental

section. These two spectra were used to calculate the volume concentrations in $PM_{2.5}$ range. These volume concentrations were compared to the $PM_{2.5}$ mass measured with the TEOM.

The MOUDI was operated with 47 mm ring-supported Teflon membrane filters (7592-104, Whatman) as the stage substrates to reduce bounce during the sampling. The mass size distribution of the aerosol collected with the MOUDI was determined gravimetrically by pre- and after-weighing of the MOUDI stages using a precision micro-balance (UMX2, Mettler-Toledo, Columbus, OH). The MOUDI stages were weighed in a controlled relative humidity (35±2%RH) and temperature (22±1^{o}C) glove box. Prior to the weighing the stages were equilibrated for 24 hours at the conditions of the weighing box. The combined accuracy of determination of the mass was ±5 μg per impactor stage.

The $PM_{2.5}$ mass collected with the MOUDI agreed well with the FRM measurements (Cabada et al. 2003). It was, however, found that volatile material was lost from the MOUDI stages. During the summer more than 70% of nitrate was lost from the MOUDI stages (Cabada et al. 2003). The nitrate contribution to the $PM_{2.5}$ mass in summer is small in the Pittsburgh region, so the effect of nitrate loss on the fine mass is negligible. No evident losses of organic carbon from Teflon MOUDI substrates were observed.

The MOUDI was sampling at ambient conditions (temperature and relative humidity). Because of the hygroscopic growth at high relative humidities (especially at night), the aerosol mass size distribution is shifted to larger sizes relatively to low relative humidity conditions. For the comparison with MOUDI

size distributions, merged dried SMPS-APS distributions need to be converted to aerodynamic size and corrected for the hygroscopic growth. This was done in the following way.

The DAASS measures both dried and wet size distributions. Comparing the integrated volumes from the dried and ambient measurements provides us with the increase in volume due to water accretion. Assuming volume additivity, the aerosol density at ambient conditions is:

$$\rho_a = \rho_w + (\rho_d - \rho_w)\frac{V_d}{V_a} \tag{5.9}$$

in which ρ_d and ρ_a are the dried and ambient aerosol densities, respectively; ρ_w is the density of water; V_d and V_a are the dried and ambient aerosol integrated volumes. The aerodynamic size at ambient relative humidity was then found using the following equation (slip correction is ignored here):

$$D_a = D_p\left(\frac{V_a}{V_d}\right)^{1/3}\sqrt{\rho_a} \tag{5.10}$$

in which D_p is the physical size and D_a is the corresponding size at ambient relative humidity.

The dry density of 1.5 g cm^{-3} was used (Tuch et al., 1997; Hand and Kreidenweis, 2002). As will be shown in the Results section, this value of the aerosol density is also applicable to this study. Because during this study the ambient aerosol contained water even at low relative humidities (Stanier et al. 2003), the particles are expected to be spherical and, thus, the shape factor of 1 was used to convert physical to aerodynamic size.

The geometric mean diameters and geometric mean standard deviations of the distributions in the $PM_{2.5}$ range measured with the MOUDI and the SMPS-APS were compared to assess the size-distribution comparability of the two instruments. To compare the SMPS-APS data with the size fractionated mass measurements of the MOUDI, the SMPS-APS data have been summed up to match the MOUDI stage size ranges. Then, values from individual stages have been summed up such that the PM2.5 range is divided into 4 fractions: < 0.1 μm, 0.1 – 0.3 μm, 0.3 – 1 μm, 1 – 2.5 μm. The grouping corresponds to summing 2 impactor stages. The values found with the MOUDI and the SMPS-APS within these size fractions are compared.

5.3 Results and Discussion

5.3.1 Laboratory Tests of the APS

The counting efficiency of the APS in the sub-micrometer size range is assessed by comparing it to the SMPS in the overlap size range. The APS was mobility calibrated using ammonium sulfate aerosol. The calibration information was stored with the density and the shape factor being both one. In this way the APS was measuring the mobility equivalent size of ammonium sulfate particles and no further data reduction was needed. The APS was found to agree well with the SMPS in the overlap size range of 580 - 720 nm (mobility equivalent size), with the counting efficiency differences of no more than 10% (Figure 5.1). The first APS channel, however, had a lower efficiency of about 70%. Armendariz and Leith (2002) suggested that the counting efficiency was steadily going up from about 30% at 0.5 μm to about 90% at 1 μm. However, they did not test the

efficiency between these sizes. Our results indicate, however, that the counting efficiency is constant and close to 100% except for the first APS channel.

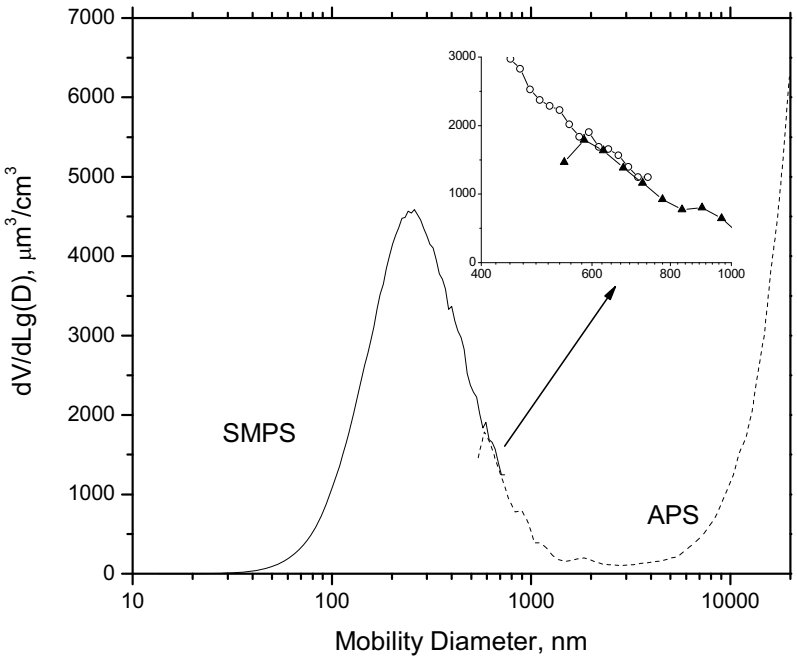

Figure 5.1 Comparison of the APS and the SMPS in the overlap size range using ammonium sulfate aerosol.

5.3.2 Comparison with TEOM

Figure 5.2 shows a comparison of the integrated ambient volume concentrations with the TEOM measurements. The agreement between the SMPS/APS and the TEOM is considerably improved when the APS is fitted to the SMPS distribution. The ratio of the aerosol mass to the aerosol volume is a measure of the aerosol effective density, which is equal to the bulk aerosol density if the shape factor is 1. If the APS data are used without any corrections, the density is unrealistically low (often below 1 g cm^{-3}). However, when the APS is fitted to the SMPS, the estimated density is 1.52 g cm^{-3}, which is very close to the values reported in the literature, around 1.5 g cm^{-3} (Tuch et al., 1997; Hand and

Kreidenweis, 2002). The density data appear to be normally distributed around the mean value with the standard deviation of 0.26 g cm^{-3}. It is thus concluded that the SMPS-APS size distribution data, in which the APS data are fitted to the SMPS, can be used to estimate the PM2.5 mass concentration with an average standard error of about 20% by using an average aerosol density of 1.5 g cm^{-3}.

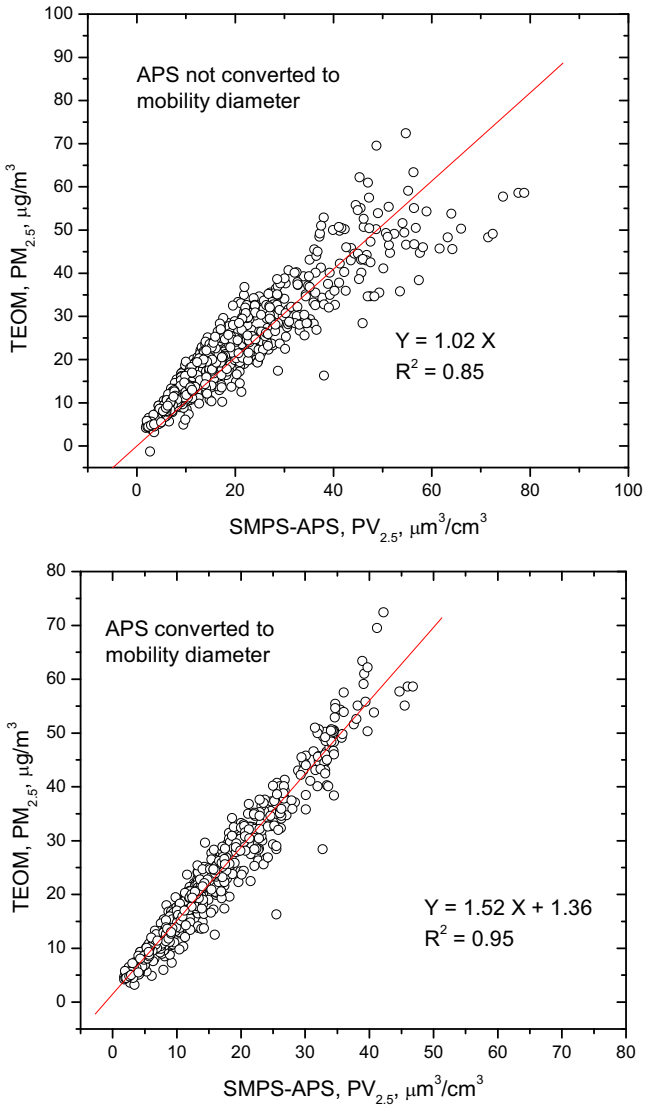

Figure 5.2 Comparison of mass concentrations with volume concentration in the $PM_{2.5}$ range. A) APS size distributions were not converted to electrical mobility; B) APS size distributions were converted to electrical mobility using the algorithm.

The estimated density is in good agreement with the density estimated from the average chemical composition of the aerosol during this study. The aerosol consisted for about 50% of ammonium salts of sulfate, 25% organic carbon, 3% elemental carbon, 2% nitrate, and 2% crustal material (Wittig et al. 2003). It was also shown that the FRM and the TEOM retained water, which comprised on average about 20% of the aerosol mass measured with those instruments. Assuming the density of organic carbon to be 1.4 g/cm^3 and the density of crustal material and elemental carbon to be 2 g/cm^3, and taking the density of salts of ammonium to be 1.8 g/cm^3, the average density of the aerosol according to its chemical composition is estimated to be 1.56 g/cm^3, which is close to the density estimated from the SMPS-APS and TEOM comparison. This suggests that the aerosol during this study had the shape factor close to 1.

5.3.3 Comparison with MOUDI

Comparisons of the geometric mean diameters (GMD) and the geometric mean standard deviations (GSTD) of the ambient aerosol size distributions measured with the MOUDI and the SMPS-APS converted to the aerodynamic size and corrected for the hygroscopic growth are shown in Figure 5.3 and Figure 5.4, respectively. Both the GMD and GSTD show a good correlation between the instruments. The slope of the regression line for GMD is virtually 1. A shape factor of 1 was used to convert the SMPS-APS distributions to aerodynamic sizes. The equality of the GMDs suggests that the shape factor of 1 is justified for this study. During this study the aerosol was found to be always wet (i.e. contain water), even at relative humidities as low as 30%. Thus, particles are expected to

be spherical droplets and have the shape factor of 1, which explains our observation.

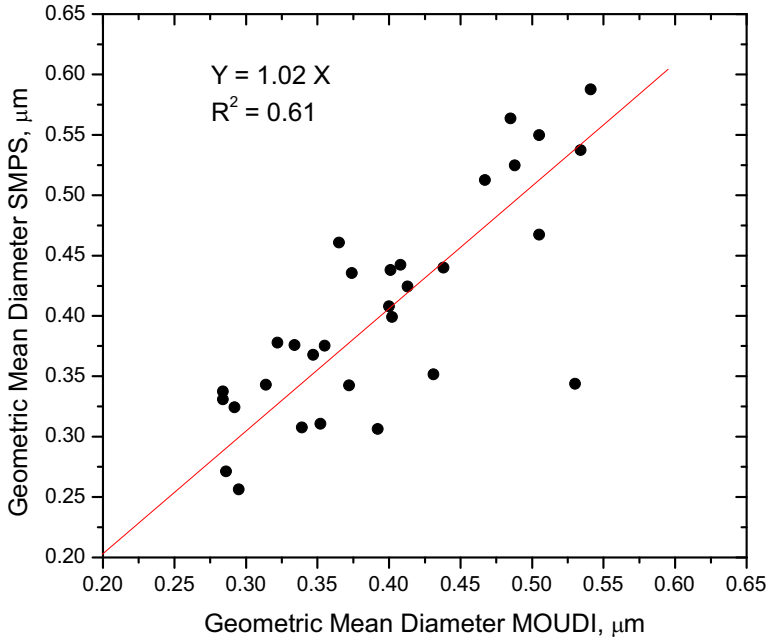

Figure 5.3 Comparison of geometric mean diameters.

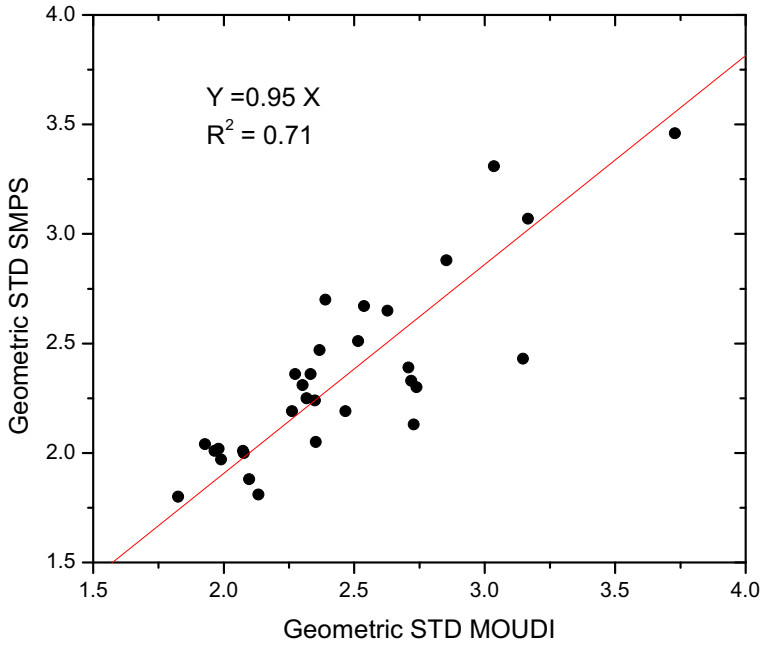

Figure 5.4 Comparison of geometric standard deviations.

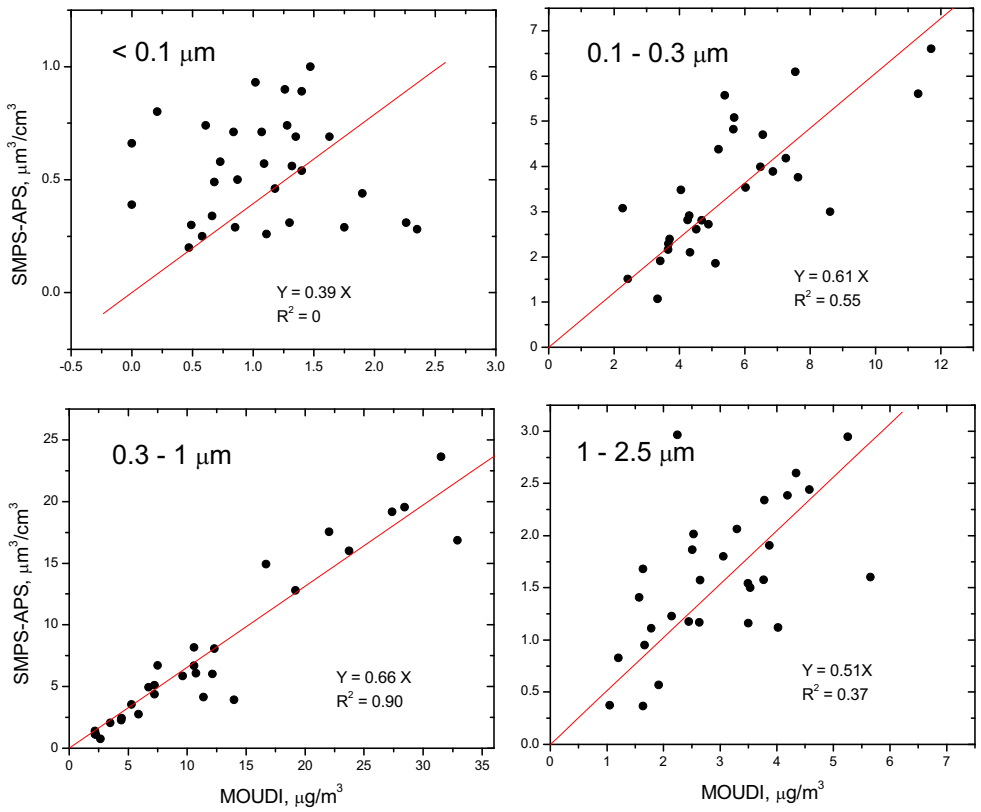

Figure 5.5 Comparison of size fractionated mass concentrations from MOUDI and volume concentrations from SMPS-APS.

Figure 5.5 shows a size-fractionated comparison of the MOUDI and the SMPS-APS. With the exception of the lowest stages (below 0.1 μm) the MOUDI and the SMPS-APS appear to be well correlated. The R^2 values are similar or higher than those found during the similar study by Shen et al. (2002). The slopes for the stages between 0.1 and 1 μm are 0.61 – 0.66. Such slopes correspond to aerosol densities between 1.52 and 1.64 g cm^{-3}, which again are close to the ones reported in the literature and to the density found during the comparison with the TEOM. The slope for the 1 – 2.5 μm range indicates a density of about 2 g cm^{-3}, which is probably due to a larger contribution of the crustal material to this size range.

The absence of correlation between the SMPS-APS and the MOUDI below 0.1 μm is similar to the observations by Shen et al. (2002). Similarly, we found that the MOUDI measures on average more than the SMPS-APS in that size range. A possible explanation for this observation is the particle bounce from the upper stages of the MOUDI (Pak et al. 1992). The mass loading on the last stages of the MOUDI is usually small and even a small contribution due to the bounce would introduce a large relative error on those stages, while losses from the larger stages will probably remain insignificant.

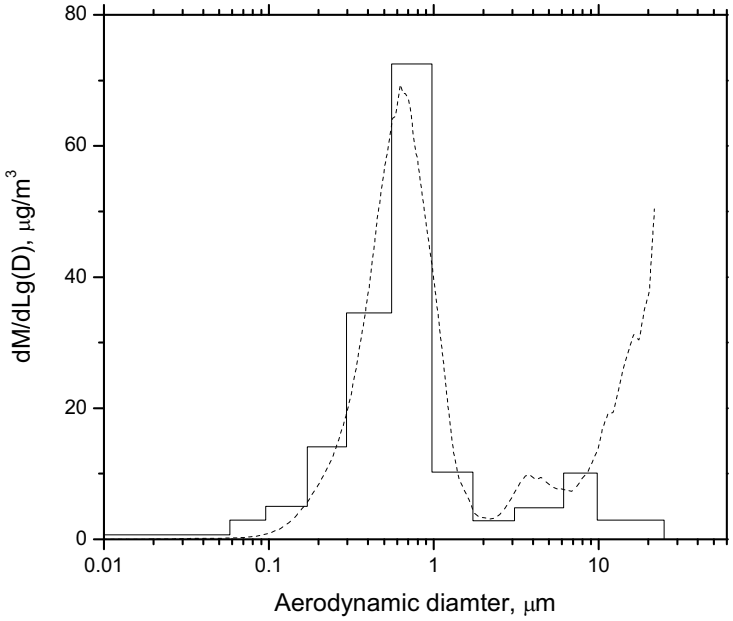

Figure 5.6 Comparison of size distributions measured with SMPS-APS and MOUDI.

The comparison of representative size distributions measured with the SMPS-APS and the MOUDI is shown in Figure 5.6. The SMPS-APS distribution was converted to the mass size distribution in aerodynamic space using the density of 1.5 g cm^{-3} and correcting for the hygroscopic growth as explained in the Experimental section. Qualitatively similar distributions are measured with the

two instruments. The sharp increase in the volume concentration after 7 μm measured with the SMPS-APS is most probably due to the well documented artifact counts in the APS in the large size range (Stein et al. 2002). In this study, however, these artifact counts were not observed to contribute significantly to the $PM_{2.5}$ range.

5.4 Conclusions

A simple algorithm was developed to combine electrical mobility and aerodynamic size distribution data into a single size distribution. This algorithm was tested during a month of ambient aerosol measurements by comparing size distributions measured using an SMPS-APS combination with simultaneous measurements using a MOUDI cascade impactor and $PM_{2.5}$ mass concentration measurements using a TEOM.

Size distributions obtained by using the algorithm have better correlations with PM2.5 measurements than do size distributions in which aerodynamic sizes were not converted to electrical mobility diameters.

A comparison of the TEOM $PM_{2.5}$ mass concentrations with the volume concentrations from the SMPS-APS data indicates that the ambient aerosol during the study had an effective density of 1.52 ± 0.26 g cm^{-3}. This density is close to 1.56 g cm^{-3}, the density estimated from the average aerosol chemical composition during this study. This suggests that the aerosol shape factor during this study is close to 1.

The SMPS-APS size distributions obtained using the algorithm agree with the mass distributions measured with MOUDI cascade impactors within 0.1 – 2.5

μm size range, if a density of 1.5 g cm^{-3} and a shape factor of 1 are used, and the hygroscopic growth of aerosol is taken into account. However, there was no agreement below 0.1 μm, probably due contamination of the low impactor stages because of the bounce of large particles, and / or a different shape factor based on the composition in this size range, which may affect particle mobility of ultra-fine particles.

5.5 Acknowledgements

This research was conducted as part of the Pittsburgh Air Quality Study which was supported by US Environmental Protection Agency under contract R82806101 and the US Department of Energy National Energy Technology Laboratory under contract DE-FC26-01NT41017. This paper has not been subject to EPA's required peer and policy review, and therefore does not necessarily reflect the views of the Agency. No official endorsement should be inferred.

5.6 References

Armendariz, A. J., and Leith, D. (2002). Concentration measurement and counting efficiency for the aerodynamic particle sizer 3320. J. Aerosol Sci. 33, 133-148.

Cabada, J.C., Rees, S., Takahama, S., Khlystov, A., Pandis, S.N., Davidson, C. and Robinson, A.L. (2003) Mass size distributions and size resolved chemical composition of fine particulate matter at the Pittsburgh Supersite. Submitted to Atmos.Environ.

Dockery, D.W., Pope, C.A., Xu, X., Splengler, J.D., Ware, J.H., Ferris,B.G. and Speizer, F.E. (1993) Mortality risks of air pollution: a prospective cohort study. New England Journal of Medicine 329, 1753-1759.

Hinds, W.C. (1999) Aerosol Technology: Properties, Behavior and Measurements of Airborne Particles, 2nd ed., John Wiley & Sons, New York.

Hand, J.L. and Kreidenweis, S.M. (2002) A new method for retrieving particle refractive index and effective density from aerosol size distribution data, Aerosol Sci. Technol. 36: 1012-1026.

Pak, S.S., Liu., BY.H., and Rubuw, K.L. (1992) Effect of coating thickness on particle bounce in inertial impactor, Aerosol Sci. Technol. 16:141-150.

Rees, S.L, Robinson, A.L., Khlystov, A., Stanier, C.O. and Pandis, S.N. (2003) Performance of the U.S. Federal Reference Method for PM2.5 in Pittsburgh, PA, Submitted to Atmos. Environment.

Seinfeld, J.H. and Pandis, S.N. (1998) *Atmospheric Chemistry and Physics: From Air Pollution to Climate Change*. John Wiley & Sons, Inc., New York.

Schwartz, J. and Dockery, D.W. (1992) Increased mortality in Philadelphia associated with daily air pollution concentration, American Journal Of Epidimeology 135, 12-19.

Shen, S., Jaques, P.A., Zhu, Y., Geller, M.D., and EN.REFLISTSiuotas C. (2002) Evaluation of the SMPS-APS system as a continuous monitor for measuring $PM_{2.5}$, PM_{10} and coarse $PM_{2.5-10}$. Atmos. Environ., 36: 3939-3950.

Shi, J. P., Harrison, R. M., and Evans, D. (2001) Comparison of ambient particle surface area measurement by epiphaniometer and SMPS/APS. Atmos.Environ., 35: 6193-6200.

Stanier, C. O., Khlystov, A., Chan, W.R., Mandiro, M., and Pandis, S.N. (2002) A method for the in-situ measurement of aerosol water content of ambient aerosols: the Dry-Ambient Aerosol Size Spectrometer (DAASS). Submitted to Aerosol Science and Technology.

Stein, S.W., Turpin, B.J., Cai, X.P., Huang, C.P.E., and McMurry, P.H. (1994) Measurements of relative humidity-dependent bounce and density for atmospheric particles using the DMA-impactor technique, Atmos. Environ. 28:1739-1746.

Stein, S.W., Gabrio, B.J., Oberreit, D., Hairston, P., Myrdal, P.B., and Beck, T.J. (2002) An evaluation of mass-weighted size distribution measured with the model 3320 Aerodynamic Particle Sizer. Aerosol Sci. Technol. 36: 845-854.

Tuch, Th., Brand, P., Wichmann, H.E.; Heyder, J. (1997) Variation of particle number and mass concentration in various size ranges of ambient aerosols in Eastern Germany. Atmos. Environ. 31: 4193-4197.

Wang, S.C. and Flagan, R.C. (1989) Scanning Electrical Monbility Spectrometer. J. Aerosol Sci., 20:1485-1489.

Wittig, B., Anderson, N., Khlystov, A.Y., Pandis, S.N., Davidson C. and Robinson A.L. (2003) Pittsburgh Air Quality Study overview and preliminary scientific findings, Submitted to Atmos. Environ.

Wolfenbarger, J.K. and Seinfeld, J.H. (1991) Regularized solutions to the aerosol data inversion problem. SIAM J. Sci. Stat. Comput. 12: 342-361.

Chapter 6 Water Content of Ambient Aerosol During the Pittsburgh Air Quality Study

6.1 Introduction

Absorption of water by aerosol particles has a major effect on many of their properties. Water increases particle size and thus alters the particle's lifetime in the atmosphere. The light scattering, and consequently, the visibility reduction and direct climate forcing by the aerosol particles strongly depends on the amount of water present in the particles (Ramaswamy, 2001). The presence of water changes the partitioning of semi-volatile species between the gas and aerosol phases (Ansari and Pandis, 2000). In addition, water provides a medium for numerous chemical reactions in the atmosphere (Seinfeld and Pandis, 1998).

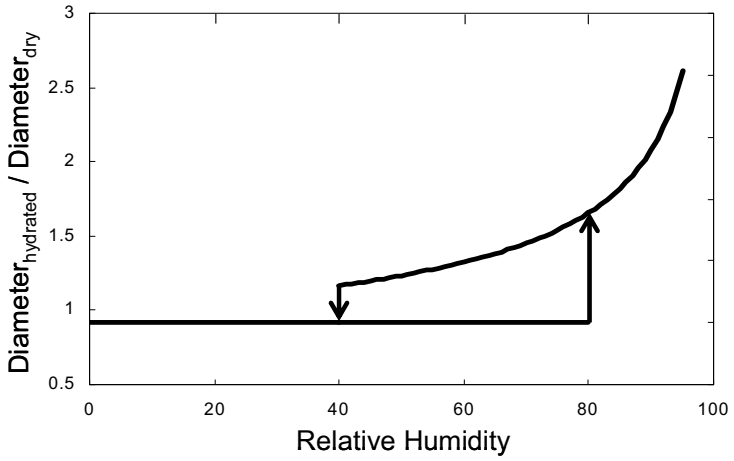

Figure 6.1 Ammonium sulfate hygroscopic growth and hysteresis.

The hygroscopic behavior (absorption of water) of aerosol particles exhibits a hysteresis effect as shown in Figure 6.1. A dry single-salt particle becomes wet only at a certain relative humidity, the so-called deliquescence relative humidity. For example, the deliquescence point of ammonium sulfate is

80% RH (Tang and Munkelwitz, 1993). After becoming wet, the particle will absorb more water if the relative humidity is increased. If the relative humidity is decreased, the particle will release some of the absorbed water to equilibrate with the new conditions. However, if the relative humidity is decreased below the deliquescence point, the particle will not crystallize, but rather will remain wet until a substantially lower RH is reached (e.g., 35-40% for ammonium sulfate). Ammonium sulfate is a major component of the ambient aerosol, and other inorganic species present in the ambient aerosol have been shown to exhibit a similar behavior (Tang, 1997). Because of the hysteresis effect there is a wide range of relative humidity (40-80%) within which the physical state (dry or wet) of the ambient particles is not known. This leads to uncertainties in predicting aerosol properties that depend on absorbed water, including partitioning of semi-volatile compounds and light scattering.

In addition to the uncertainty in the physical state of the particles, there is difficulty in predicting the amount of water that would be present in the aerosol phase at the given atmospheric conditions and chemical composition. The difficulty arises from the multi-component nature of the aerosol and high concentrations of dissolved species, especially at or below the deliquescence point.

The role of the organic aerosol fraction in water absorption is especially uncertain, with a number of recent investigations arriving at differing conclusions regarding the role of organics in water uptake. Saxena et al. (1995) reported that organics at a remote continental location increased water absorption by ~30% at

85% relative humidity, while at an urban location, organics decreased overall water absorption by ~30% at 85% relative humidity due to interactions with hygroscopic inorganic compounds. Dick et al. (2000) found, for a rural continental site, organics contributed significantly to water uptake at relative humidity below 50% and less significantly at higher relative humidities. In a modeling study, Ansari and Pandis (2000) found that a high loading (35% by mass) of secondary organic compounds increased water content by about 20% at 50% relative humidity, with lesser effects at higher relative humidities.

The hygroscopic aerosol growth is usually studied with Humidified Tandem Differential Mobility Analyzers (H-TDMA). H-TDMAs select a narrow size range of particles, equilibrate the sample in a flow tube to a certain relative humidity, and then measure the sizes of the grown particles (e.g. Cocker et al.; 2001, Weingartner 2002a,b). The H-TDMA studies typically show that particles are externally mixed with respect to their water absorption properties, i.e. there are more hygroscopic and less hygroscopic fractions. The number of fractions and their behavior vary with time, place and size (e.g., Cocker et al., 2001). The H-TDMA studies, however, can provide information on the hygroscopic properties of only a few size classes. The overall hygroscopic behavior of the full aerosol spectrum and the amount of water present in the aerosol need to be inferred from measurements of a few separate size classes.

In this work we have used the recently developed Dry and Ambient Aerosol Size Spectrometer (DAASS) that measures aerosol size distributions at ambient and low (<35% RH) relative humidity conditions (Stanier et al., 2003a).

The DAASS provides information on both the effect of ambient humidity on the whole size distribution and the amount of water present in the aerosol phase. Here we report our observations of aerosol water and hygroscopic size changes of ambient aerosol during the Pittsburgh Air Quality Study (PAQS).

Measurements of aerosol water content were carried out during July-August 2001 and January-July 2002 at the central monitoring site of the PAQS located in an urban park approximately 6 km from downtown Pittsburgh, PA. The aerosol originated from both urban and long-range sources. Ammonium salts of sulfate were the dominant aerosol components, comprising approximately 50% of the $PM_{2.5}$ aerosol mass, carbonaceous material was the second largest component, contributing approximately 25% to the mass of fine particles (Wittig et al., 2003a).

The following two hypotheses were tested during this study:

- the ambient aerosol is in its lower hysteresis branch (i.e. is dry) below 80%RH;
- the contribution of organics to water absorption by the aerosol is negligible in comparison to that of the inorganic component of the aerosol.

6.2 Experimental

6.2.1 Sampling Site

The measurements were carried out at the main sampling station of the Pittsburgh Air Quality Study. The site was located in Schenley Park,

approximately 6 kilometers east of downtown Pittsburgh, PA.[12] The site was surrounded by parkland, urban, and residential areas and roughly one kilometer of parkland exists between the site and the city in the predominant upwind direction (south and west). The site was more than several hundred meters from any major sources.

6.2.2 Dry-Ambient Aerosol Size Spectrometer (DAASS)

Measurements of water content of ambient aerosol and its hygroscopic growth were made using the Dry and Ambient Aerosol Size Spectrometer (DAASS). The design, calibration, and data reduction are described in detail in Stanier et al. (2003a). Briefly, the DAASS alternates between measuring the aerosol size distribution at ambient conditions and at low RH (10-35%) (referred to as ambient and dried, respectively). A comparison of the dried and ambient distributions provides information on both the amount of absorbed water and the change in aerosol size with RH. The amount of absorbed water can be calculated from the increase in the aerosol volume at ambient conditions relative to the low RH state. The changes in size can be deduced from the mass or number mean diameters, shifts in the position of different modes in the distribution, etc. The detailed procedure of data reduction and interpretation is given in Stanier et al. (2003a), and data reduction equations used particularly in this work are summarized in a separate section below.

Uncertainties in the DAASS measurements are described in detail in Stanier et al. (2003a). For accurate determination of water amount in the aerosol

[12] See note 7, section 3.2 for additional discussion of the site and proximity to sources.

phase, it is important that there is no significant bias between the dried and ambient channels of the DAASS. It was shown that no such significant bias exists and the channels agree within 5% of each other. The other sources of error are associated with the differences in temperature between aerosol charging and actual measurements during winter months when the ambient temperature was below 9^{o}C. It was shown that at low ambient RH (around 50%) the growth is biased positively by about 3%. The maximum error is expected at low temperatures and high relative humidity conditions. The error at -5^{o}C and 92% RH is estimated to be 14% positive.

6.2.3 Complementary Measurements

The amount of absorbed water as a function of ambient RH was related to the amount of water-soluble inorganic constituents and the amount of organic matter present in the $PM_{2.5}$ aerosol. These aerosol constituents were measured in parallel to and at the same location as the DAASS measurements. The measurements of chemical constituents are described in Wittig et al. (2003a). Aerosol sulfate and nitrate were measured with denuder filter-pack system and at a higher time resolution with Rupprecht and Patashnick Models 8400S and 8400N (R&P Co., Albany, NY). Total nitrate (sum of $PM_{2.5}$ aerosol nitrate gas phase nitric acid) and total ammonia (sum of $PM_{2.5}$ aerosol ammonium and gas phase ammonia) were measured with a steam sampler (Khlystov et al., 1995). Organic and elemental carbon content in the aerosol was measured with a denuder – filter pack system described in Subramanian et al. (2003) and at a higher frequency with Sunset Labs in-situ analyzer (Sunset Labs Co., Portland, Oregon).

Because of the differences in measurement principles and difference in accuracies between the instruments, data from the different instruments were combined to form a best estimate. This procedure is described in Wittig et al. (2003b). The instruments measuring the same component were inter-compared and the outliers identified. After the outliers were removed, a regression was found to match high-time resolution measurements with the filter-based methods. This was done because the denuder filter-pack techniques are generally considered to be the reference for newer and less widely adopted high-time resolution methods. The regression coefficients were then used to convert the high-time resolution data to "filter-equivalent" values. For comparison with the DAASS results, the chemical composition measurements were then averaged or interpolated to an hourly basis as needed.

6.2.4 Data Reduction Methods

The DAASS data reduction is reported in detail in Stanier et al. (2003a). For this work we have used two methods: (1) calculation of the amount of water in the aerosol phase, and (2) the volume-based growth factors. These methods are described briefly below.

The amount of aerosol water can be found from the comparison of integrated dried and ambient aerosol volumes. Assuming volume additivity, the increase in volume between the ambient and the dried measurements is proportional to the mass of absorbed water (the proportionality factor being the density of liquid water). Consequently, the amount of absorbed water can be calculated as:

$$m_w = \rho_w (V_{wet} - V_{dry}) \tag{6.1}$$

in which m_w is the mass concentration of water, ρ_w is the density of liquid water, V_{wet} and V_{dry} are, respectively, the ambient and dried integrated volume concentrations.

When integrating the volume concentrations, the shift in aerosol size distribution due to the hygroscopic growth needs to be accounted for. This is done by iteration, searching for the size boundaries that satisfy the following criteria:

$$GF_v = \frac{V_{wet}}{V_{dry}} \tag{6.2a}$$

$$V_{wet} = \frac{\pi}{6} \int_{Dw1}^{Dw2} D^3 n_{wet}(D) dD \tag{6.2b}$$

$$V_{dry} = \frac{\pi}{6} \int_{Dd1}^{Dd2} D^3 n_{dry}(D) dD \tag{6.2c}$$

$$D_w = D_d \sqrt[3]{GF_v} \tag{6.2d}$$

in which GF_v is the volumetric growth factor, D is the particle size, $n_{wet}(D)$ and $n_{dry}(D)$ are the number-based ambient and dried size distributions, respectively, and subscripts w and d correspond to the ambient and dried integration limits.[13]

The amount of absorbed water was calculated from the DAASS measurements for the dried size range up to 2.5 μm. This was done to allow a straightforward comparison of the amount of water to the amounts of different chemical species measured simultaneously in the $PM_{2.5}$ size range. However, due to the frequent malfunction of the Aerosol Particle Sizer (APS) in the DAASS,

[13] See section 2.4.2.1 for additional information on this calculation.

consistent measurements of water content in the $PM_{2.5}$ range are only available for July and August 2001. For the rest of the study the measurements extended only up to 0.5 μm in diameter (ambient size).

When the APS was not available, the volumetric growth factor was calculated based on the available size range. The volumetric growth factor method is less straightforward than the method described above since its interpretation requires knowledge of the particle density, as will be shown below. The volumetric growth factor is calculated according to the following formula:

$$GF_{VOL} = \frac{V_{RH2}}{V_{RH1}} = \frac{\int_0^{D_{RH2}} D^3 n^o_{N,RH2}(\log D) d\log D}{\int_0^{D_{RH1}} D^3 n^o_{N,RH1}(\log D) d\log D} \tag{6.3}$$

where D is the particle diameter, V_{RH2} and V_{RH1} are the aerosol volume concentrations measured using the ambient (RH2) and dried (RH1) inlets, $n°_{N,RH2}$ and $n°_{N,RH1}$ are the ambient and dried aerosol size distributions, and D_{RH2} and D_{RH1} are appropriately selected limits of integration.

Because in the absence of the APS the data are available only up to 0.5 μm instead of 2.5 μm, the amount of water in the $PM_{2.5}$ range can not be deduced. Instead, the mass growth factor expected from the chemical composition is compared to the volume GF from the DAASS measurements. To compare the mass with the volume GF, particle densities in the dried and ambient state need to be calculated.

The density calculations assume that the aerosol is an internal mixture consisting of inorganic matter (which may be hydrated), organic matter (assumed not to take up any aerosol water), and elemental carbon fractions (assumed not to take up any aerosol water), each with a fixed characteristic density. Densities of 1.2, 1.6, and 1.77 g cm^{-3} were assumed (Stanier et al., 2003a) for organic matter, elemental carbon aerosol, and dry inorganic aerosol, respectively, and a multiplier of 1.8 was used to calculate organic aerosol from organic carbon (to account for elements other than carbon not detected in the OC analysis).

6.2.5 Comparison with a Thermodynamic Model

The observations were compared to the GFEMN thermodynamic model (Ansari and Pandis, 1999). The model finds aerosol composition and the amount of aerosol bound water that corresponds to thermodynamic equilibrium using direct minimum of Gibbs free energy of the system, which is calculated from gas- and particle-phase compositions using an activity coefficient model. The model inputs include $PM_{2.5}$ concentrations of sulfate and sodium as well as the sum of gas and $PM_{2.5}$ concentrations of nitrate, chloride, ammonia and ammonium. The model assumes that organic carbon does not contribute to water absorption.

6.3 Results and Discussion

6.3.1 Aerosol Water Content

The volume based growth factors (the aerosol volume at ambient conditions divided by the volume at low RH, as described in the Experimental section) observed at ambient RH during different months of the study are shown in Figure 6.2. A growth factor greater than one indicates that the aerosol contains water. The aerosol was found to always contain water when the relative humidity

is above 60%. However, the aerosol water content below 60% RH exhibits a seasonal behavior. As an example we will first concentrate on July 2001 and January 2002 as the months representing summer and winter aerosol in the Pittsburgh area. Growth factor data for these months are summarized in Table 6.1. The volume growth factors for July, with a few exceptions, are above one indicating that the aerosol contained water, even at RH as low as 30%. A similar behavior was observed in June and August (Figure 6.2). It can be concluded that summer-time aerosol in the Pittsburgh area practically always contains water. During winter months, however, the volume ratios at RH below about 60% did not differ from unity within the experimental error, indicating absence of aerosol bound water. The spring months show a transitional behavior: the fraction of observations when the GF is higher than 1 below 60% RH progressively increases from March to June (Figure 6.3).

Table 6.1 Statistical Summary of Summer and Winter Growth Factor Results

July 2001 Hygroscopic Growth Data (Based on Hourly Averages)							
Ambient Channel RH Range	20-30	30-40	40-50	50-60	60-70	70-80	80-90
Growth Factor (-560 nm)*							
Mean	1.141	1.261	1.328	1.432	1.69	1.97	
95% C.I. on Mean	0.023	0.022	0.027	0.028	0.04	0.08	
Median	1.13	1.26	1.34	1.41	1.71	1.97	
10th Percentile	1.05	1.13	1.11	1.21	1.38	1.51	
25th Percentile	1.10	1.16	1.23	1.29	1.49	1.87	
75th Percentile	1.19	1.33	1.41	1.55	1.86	2.16	
90th Percentile	1.23	1.40	1.54	1.70	2.02	2.32	
Number of Values	38	105	132	175	154	46	NO DATA
Relative Humidity Averages							
Outdoor	34.9	45.5	56.8	69.1	83.0	91.5	
Ambient Channel	26.2	35.5	45.0	55.1	65.0	71.9	
Dried Channel	9.9	13.5	16.5	19.7	20.6	21.5	
Aerosol Charger, Ambient Scans	27.9	38.1	49.8	62.7	75.3	81.3	
TEOM $PM_{2.5}$ ($\mu g\ m^{-3}$)	14.4	20.2	22.7	19.1	25.8	22.7	

January 2002 Hygroscopic Growth Data (Based on Hourly Averages)							
Growth Factor (-560 nm)*							
Mean	1.008	1.020	1.034	1.118	1.340	1.63	1.89
95% C.I. on Mean	0.01	0.012	0.014	0.017	0.019	0.05	0.04
Median	1.009	1.009	1.025	1.09	1.33	1.58	1.91
10th Percentile	0.990	0.995	0.99	1.02	1.17	1.37	1.68
25th Percentile	0.998	0.998	1.00	1.05	1.25	1.50	1.78
75th Percentile	1.017	1.034	1.05	1.16	1.45	1.72	2.01
90th Percentile	1.023	1.063	1.08	1.25	1.52	1.89	2.08
Number of Values	10	36	88	143	197	92	53
Relative Humidity Averages							
Outdoor	27.6	35.8	46.0	59.3	70.7	84.1	94.3
Ambient Channel	27.4	36.0	45.5	55.8	64.5	74.4	82.3
Dried Channel	-2.0	-0.4	1.3	3.0	4.4	4.9	5.5
Aerosol Charger, Ambient Scans	19.6	26.4	49.0	41.0	42.3	48	54.7
TEOM $PM_{2.5}$ ($\mu g\ m^{-3}$)	7.1	7.8	9.2	11.1	12	13.4	11.5

*The volume growth factors reported in this table are based on an upper limit for volume integration of 560 nm (the upper limit of SMPS instrument). This corresponds to equation 6.3 with D_{RH2} at 560 nm.

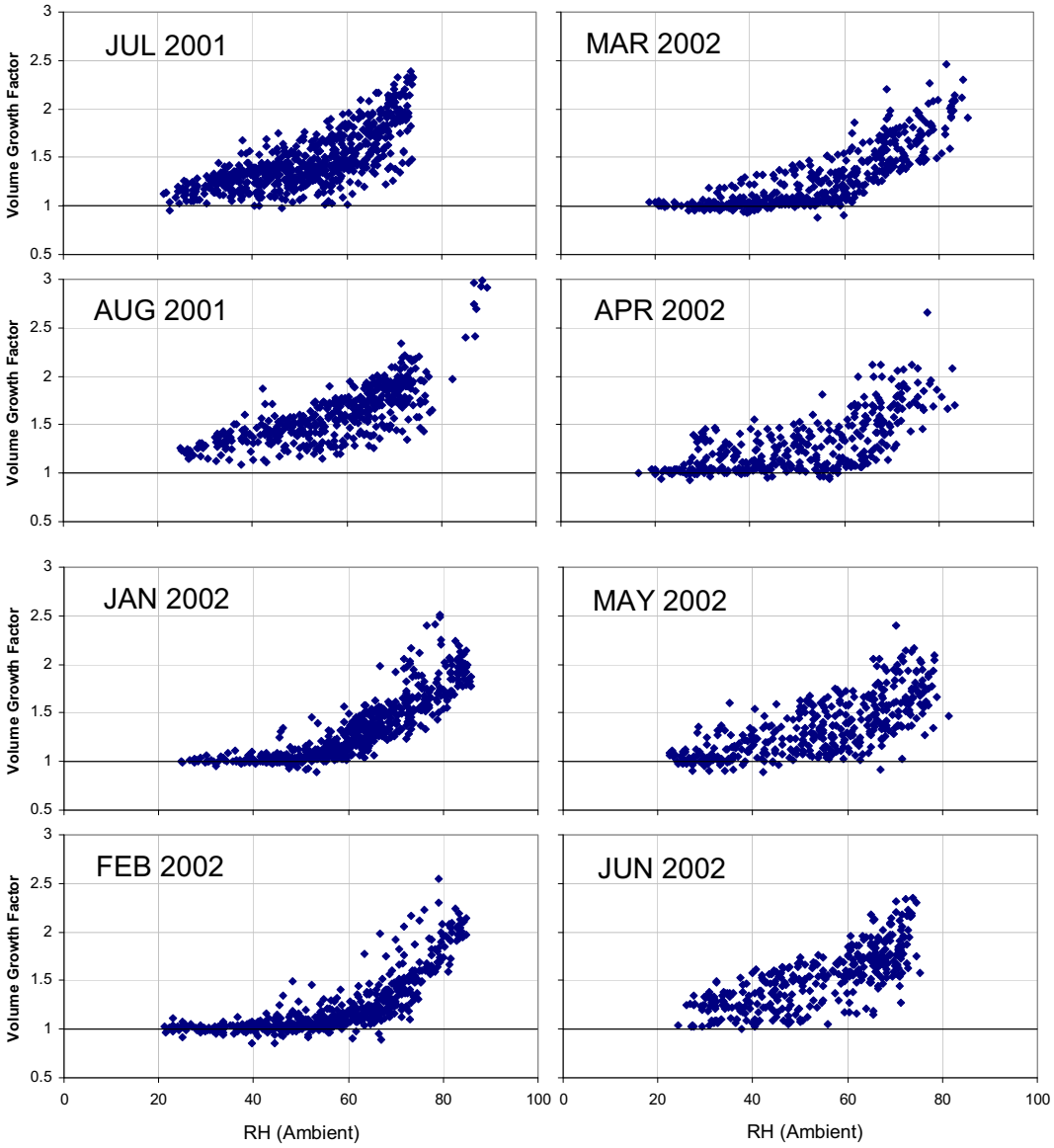

Figure 6.2 The volume GF as a function of ambient RH for different months of the study.

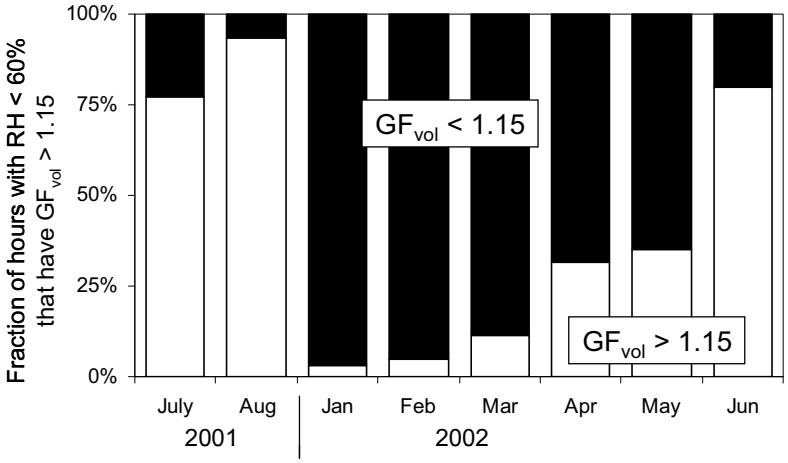

Figure 6.3 Fraction of hydrated hours with RH < 60% by month.

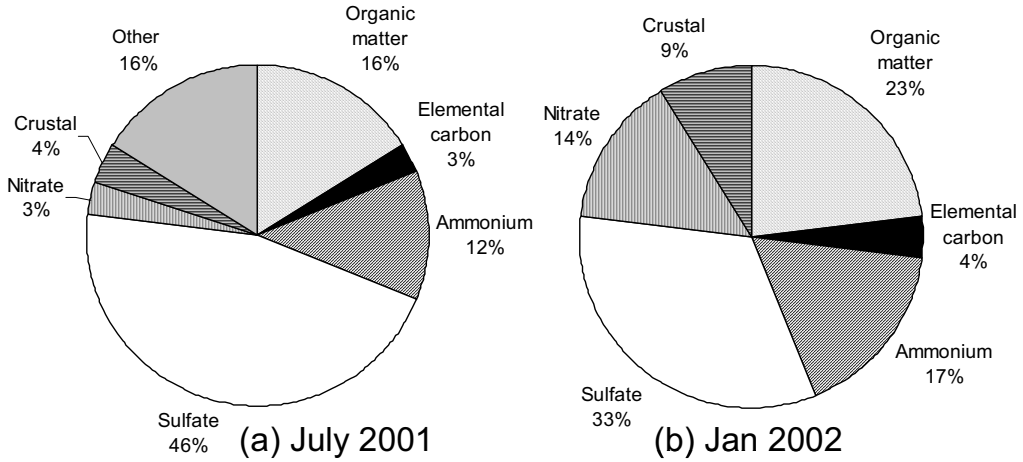

Figure 6.4 Average chemical composition during Summer (a) and Winter (b)

The seasonal behavior of aerosol bound water below 60% RH follows that of the aerosol acidity in the Pittsburgh area. Figure 6.4 shows average chemical composition for July and January in Pittsburgh as measured during PAQS. The sulfate to ammonium ratio (moles sulfate to moles ammonium) in summer is 1.4 which corresponds to an approximately equal mixture of ammonium sulfate [$(NH_4)_2SO_4$] and ammonium bisulfate [$(NH_4)HSO_4$]. The ammonium bisulfate crystallizes at about 5% RH, conditions that do not occur in the Pittsburgh region. However, the RH often exceeds the deliquescence point of ammonium bisulfate

(40%) during most nights and also may be reached at upper layers of the boundary layer during the day. Thus, the particles during their life time (a few days) have a chance to become hydrated. However, they are not subjected to RH below the crystallization point of ammonium bisulfate, thus leaving the aerosol almost always in the wet state. In contrast to summer, the ammonium to sulfate mole equivalent ratio in winter is higher than 2 indicating that all of sulfate is neutralized by ammonium (the ratio is higher than 2 because some of the ammonium is in the form of ammonium nitrate). Sulfate exists during the winter as ammonium sulfate that crystallizes at about 40% RH, which is frequently encountered during the daytime in the mixed boundary layer, providing the opportunity for crystallization. Spring months exhibit a transitional behavior as the aerosol becomes progressively more acidic.

As was mentioned in the Experimental section, in winter months during periods when the temperature was below 9^{o}C the aerosol passed through a heated enclosure before it was re-equilibrated to the ambient RH at which the measurements were done. If the aerosol crystallizes during the passage through the heated section (where the relative humidity is accordingly low) it would remain dry even after re-equilibration, unless the ambient RH is above the deliquescence point of the aerosol. This possibility was investigated by comparing growth factors of aerosols that were dried significantly (<40% RH) at the aerosol charger to those that were not. The results (Table 6.2) show that the fraction of hours with growth factors less than 1.05 depends on the ambient relative humidity, not the relative humidity at the aerosol charger. Thus aerosol

crystallization during the passage through the heated section is not thought to occur during this study, probably because of the very short residence time.

Table 6.2 Fraction of hours in January 2002 with low growth factors as a function of ambient and aerosol charger humidity

	Ambient Relative Humidity	Aerosol Charger Relative Humidity (Ambient RH Scans)	Fraction of Aerosols with $GF_{VOL} < 1.05$
CASE 1, no significant drying expected at charger	> 60%	> 60%	0%
CASE 2, aerosols expected to be dehydrated	< 40%	< 40%	88%
CASE 3, drying by aerosol charger possible	> 60%	< 40%	2%

6.3.2 Comparison with a Thermodynamic Model

The observations with the DAASS were compared to the thermodynamic model GFEMN (Ansari and Pandis, 1999). The comparison was done with two objectives: 1) assess the contribution of organic aerosol to water absorption and 2) to determine whether all particles remained wet below 60% RH. The contribution of organic material was assessed as a difference between the observations and the predictions, because the model assumes that the organic aerosol does not participate in water absorption. When the APS measurements were available (July – August 2001) the amount of aerosol water was compared. When the APS was not available (January-April 2002), the volume based growth factors were compared, as described in the Experimental section.

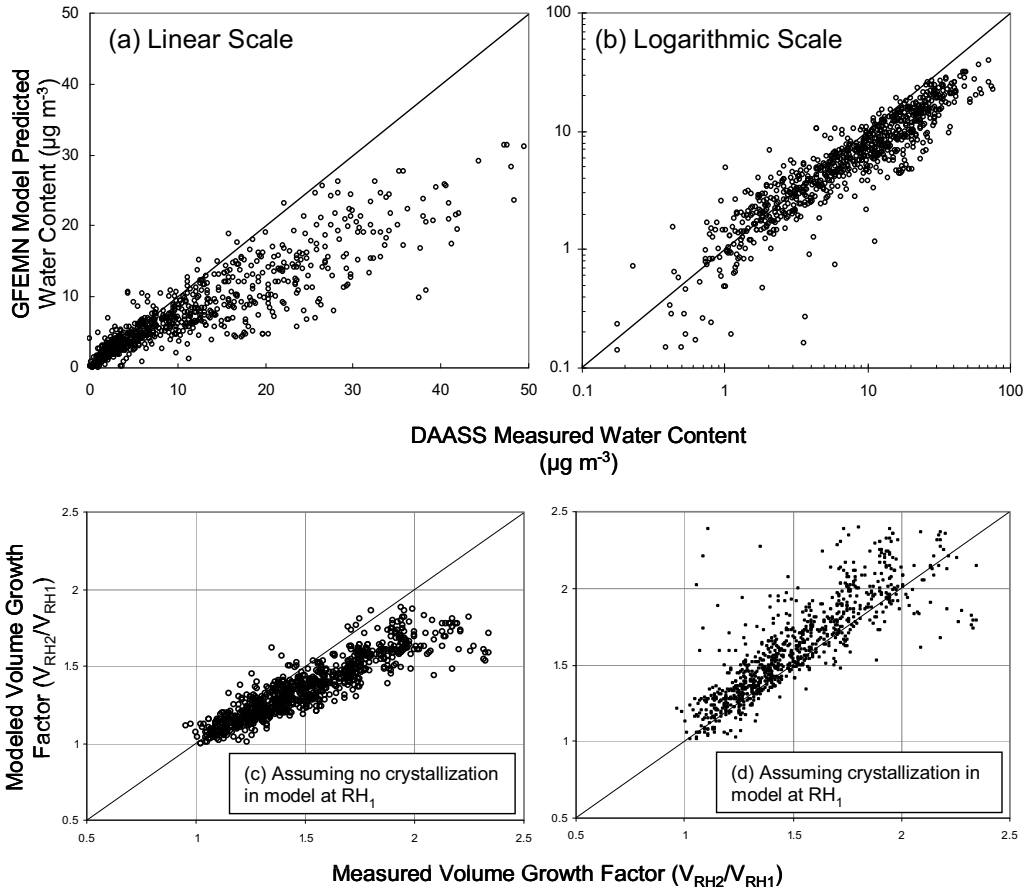

Figure 6.5 Model versus measurement for July-August 2001. The upper graphs show measured (x-axis) versus modeled (y-axis) aerosol water in µg m^{-3}. Graphs (a) and (b) are both calculated on the efflorescence branch of the model (no crystallization). The volume growth factors corresponding to graphs (a) and (b) are shown in panel (c). The larger growth factors calculated under the assumption of crystallization in the dried channel are shown in panel (d).

A comparison of the aerosol water content during July 2001 observed with the DAASS and predicted with the GFEMN is shown in Figure 6.5. The model provides two predictions: 1) assuming it remains wet during the low-RH measurements (in which case the predictions are smaller); 2) assuming the aerosol crystallizes during the low-RH measurements. Under the first assumption the observations tend to be higher than the predicted values at high water concentrations/high growth factors and in agreement at low water concentrations/low growth factors (Figure 6.5a-c). Under the second assumption

the measured growth factors are somewhat lower than the modeled ones (Figure 6.5d). Based on the lack of observations of dried (GF = 1) aerosols during the summer months and supported by the aerosol acidity and low crystallization RH for ammonium bisulfate, it is assumed that the aerosol is hydrated and moves along the efflorescence branch in a metastable state during most (but not all) time periods during the summer. Therefore, the measurement-model comparisons using the model without crystallization (Figures 6a-c) are thought to be more appropriate than the model with crystallization (Figure 6.5d).

The discrepancy between the measurements and model in July was investigated starting with the assumption that it was caused by water uptake from hygroscopic organic compounds, similar to results seen by Saxena et al. (1995) and Dick et al. (2000). This was investigated by examining if the measurement-model disagreement correlated with either the mass fraction of organic aerosols or secondary organic aerosols. To do this, we first limited the dataset to acidic periods to reduce the chance of including data with crystallization behavior in the analysis. This was done by screening out hours with aerosol acid:base equivalent mole ratios less than 1.1 (as calculated by GFEMN). Then, for each hour, a measurement-model mismatch parameter *r* was calculated:

$$r = \frac{H_2O_{measured} - H_2O_{GFEMN}}{f(RH)\sum inorganic} \tag{6.4}$$

where the $\sum inorganic$ is the sum of aerosol sulfate, nitrate, chloride, sodium, and ammonium. The function used for $f(RH)$ is $RH/(1-RH)$. The terms in the denominator serve to normalize the error parameter, an important step in

analyzing for correlations with other variables. As *f(RH)* is 1 at 50% RH, the error parameter *r* is equivalent to mass model underprediction per mass of inorganic aerosol at 50% RH. If organics (currently neglected in the model GFEMN) absorbed water in similar quantities to inorganics and were present in a mass ratio of 1 part organics to 2 parts inorganics, then we would expect an error *r* of around 0.2 g/g. Previous studies, as discussed in the introduction, have found results for water absorption that are consistent with a parameter *r* in Pittsburgh from -0.15 to around +0.2 if similar water absorption is occurring (Saxena et al., 1995, Dick et al., 2000, Ansari and Pandis 2000). The Pittsburgh data for July and August 2001 have an average error *r* of 0.3 and a median of 0.25. However, this error is only weakly correlated with the fraction of organic and secondary organic aerosols. The correlation of the error term with secondary organic / inorganic ratio, ozone, and temperature are shown in Figure 6.6.

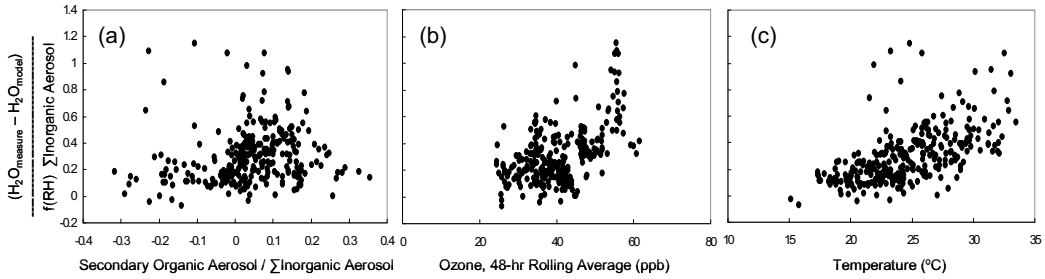

Figure 6.6 Three variables correlated with summertime water measurement-model mismatch. Negative secondary organic aerosol concentrations occur because this quantity is calculated by difference of two uncertain numbers. They are retained in the statistical analysis to avoid introducing bias in this uncertain parameter.

A linear model was used to search for variables that might be correlated in a statistically significant fashion with the error term, including relative humidity values at different points in the instrument, relative humidity differences, aerosol composition, time of day, and temperature. The model consistently found that

temperature, or variables correlated with temperature (ozone, secondary organics, time of day) were correlated with the model underprediction. Of these, temperature (Figure 6.6c) correlated most strongly (equivalent to an increase of approximately 30% in measured water for a 10 ºC temperature increase). The strong correlation with temperature does not rule out water absorption due to aerosol chemistry (e.g. organics) as the fraction of secondary organics was also positively correlated with temperature. Interestingly, if the entire measure-model mismatch is attributed to organics, secondary organics are positively correlated with water uptake, total organic matter less so, and primary organic matter is negatively correlated (with coefficients of +0.29±0.11 g/g at 50% RH for SOA, +0.16±0.09 for total organic matter, and -0.26±0.09 for primary organic matter). However, at this time, it cannot be determined which relationship(s) are causal, and which are caused by coincidence. Hypotheses for the causal mechanism include (1) water uptake by (mainly secondary) organics; (2) a temperature dependent error in the relative humidity sensor for the SMPS sheath air; (3) other (unknown) factors positively correlated with temperature.

6.4 Summary and Conclusion

Eight months of continuous aerosol water content measurements were analyzed using the Dry-Ambient Aerosol Size Spectrometer data which operated as part of the Pittsburgh Air Quality Study in Pittsburgh, Pennsylvania during 2001 and 2002. Important features regarding aerosol water content were determined in the analysis. These include: (1) the summertime aerosol is usually hydrated, even at low relative humidities, and therefore exists along in the

metastable efflorescence condition; (2) the situation is different in the winter; the aerosol is usually dry at relative humidities up to 60%; (3) this seasonal behavior is tied to aerosol acidity, with acidic condition predominating in summer; (4) the acidic compound believed to prevent crystallization is ammonium bisulfate [$(NH_4)HSO_4$], which is present during summer months but not during the winter months; (5) thermodynamic predictions of water uptake based on inorganic aerosol composition compared to measurements in July and August show good agreement at low water content (<5 $\mu g\ m^{-3}$) but underpredict water content by approximately 30% at higher concentrations; (6) the underprediction is correlated positively with ambient temperature and a number of other variables correlated with temperature, including ozone concentration and the ratio of secondary organic aerosol to inorganics; (7) the amount of water uptake by organic and secondary organic compounds cannot be determined at this time. The data is consistent with the hypothesis that organic aerosols, or at least some organic aerosols, take up modest amounts of water. However, alternative explanations cannot be ruled out

6.5 References

Ansari, A.S., and Pandis, S.N. (1999). Prediction of Multicomponent Inorganic Atmospheric Aerosol Behavior, *Atmos. Environ*. 33:745-757.

Ansari, A.S., and Pandis, S.N. (2000). Water Absorption by Secondary Organic Aerosol and Its Effect on Inorganic Aerosol Behavior, *Environ. Sci. Technol*. 34:71-77.

Cocker, D.R., III, Whitlock, N.E., Flagan, R.C., and Seinfeld, J.H. (2001) Hygroscopic Properties of Pasadena, California Aerosol, Aerosol Sci. Technol. 35:637-647.

Dick, W.D., Saxena, P., McMurry, P.H. (2000) Estimation of Water Uptake by Organic Compounds in Submicron Aerosols Measured During the Southeastern Aerosol and Visibility Study. J. Geophys. Res. 105(D1), 1471-1479.

Khlystov, A., Wyers, G.P., Slanina, J. (1995) The Steam-Jet Aerosol Collector. Atmos. Environ. 29(17), 2229-2234.

Ramaswamy, V. Radiative Forcing of Climate Change. In Climate Change 2001, The Scientific Basis: Contribution of the Working Group 1 to the Third Assessment Report of the IPCC. 2001, Ed. Houghton, J.T.; Ding, Y.; Griggs, D.J.; Noguer, M.; van der Linden, D.J.; Dai, X.; Maskell, K.; and Johnson, C.A. Cambridge University Press, Cambridge.

Saxena, P., Hildemann, L.M., McMurry, P.H., and Seinfeld, J.H. (1995) Organics Alter Hygroscopic Behavior of Atmospheric Particles. *J. Geophys. Res*. 100(D9), 18755-18770.

Seinfeld, J.H.; Pandis, S.N. *Atmospheric Chemistry and Physics*; Wiley and Sons: New York, 1998.

Stanier, C. O., Khlystov, A., Chan, W.R., Mandiro, M., and Pandis, S.N. (2003) A method for the in-situ measurement of aerosol water content of ambient aerosols: the Dry-Ambient Aerosol Size Spectrometer (DAASS). Aerosol Sci. Technol. in press.

Stanier, C.O., Khlystov, A., Pandis, S.N. (2003) Nucleation Events During the Pittsburgh Air Quality Study: Description and Relation to Key Meteorological, Gas Phase, and Aerosol Parameters. *Aerosol Sci. Technol.* In press.

Subramanium, R., Khlystov, A., Cabada, J.C., Robinson, A. (2003) Positive and Negative Artifacts in Particulate Organic Carbon Measurements with Denuded and Undenuded Sampler Configurations. *Aerosol Sci. Technol*. In press.

Tang, I.N., and Munkelwitz, H.R. (1993). Composition and Temperature Dependence of the Deliquescence Properties of Hygroscopic Aerosols, *Atmos. Environ*. 27A:467-473.

Tang, I.N. (1997). Thermodynamic and Optical Properties of Mixed-Salt Aerosols of Atmospheric Importance, *J. Geophys. Res*. 102:1883-1893.

Weingartner, W., Gysel, M., Baltensperger, U. (2002) Hygroscopicity of Aerosol Particles at Low-Temperatures. 1. New Low-Temperature H-TDMA Instrument: Setup and First Applications, *Environ. Sci. Technol.* 36, 55-62.

Weingartner, W., Gysel, M., Baltensperger, U. (2002) Hygroscopicity of Aerosol Particles at Low-Temperatures. 2. Theoretical and Experimental Hygroscopic Properties of Laboratory Generated Aerosols, *Environ. Sci. Technol.* 36, 63-68.

Wittig, B., Anderson, N., Khlystov, A.Y., Pandis, S.N., Davidson C. and Robinson A.L. (2003) Pittsburgh Air Quality Study overview and preliminary scientific findings, Submitted to Atmos. Environ.

Wittig, B., Pandis, S.N., Hering, S., Kirby, B., Khlystov, A.Y., Takahama, S., Davidson, C.I. (2003) Continuous $PM_{2.5}$ inorganic composition measurements during the Pittsburgh Air Quality Study. Submitted for publication.

Chapter 7 The Role of Temperature In Secondary Organic Aerosol Partitioning

7.1 Introduction

Secondary organic compounds are important constituents of aerosols in urban, rural, and remote areas. In an urban and regional context, organic aerosol precursors, of both manmade and biogenic sources, can have important contributions to aerosol concentrations, particularly during photochemical smog episodes and periods of reduced summertime visibility. On a global scale, the large fluxes of reactive biogenic compounds may lead to aerosol formation significant for both the direct and indirect climate effects (Müller, 1992; Guenther et al. 1995; Griffin et al. 1999).

Currently, our ability to accurately model the formation of secondary organic aerosol and its impact on air quality is limited by our understanding of its chemistry, gas-aerosol partitioning, and hygroscopic properties.

The potential for secondary organic aerosol (SOA) formation was recognized more than 40 years ago (Went, 1960). Work in environmental ("smog") chambers in the 1980s showed significant aerosol yields from oxidation reactions of compounds such as α- and β-pinene (Hatakeyama et al.,1989). These early smog chamber experiments were translated into aerosol models by assuming an aerosol yield for each precursor. For example, experiments showed an average yield of 18% for α-pinene. With additional chamber experiments, investigators showed that yields from the chamber experiments were not constant, but depended on aerosol concentration in a manner expected from equilibrium gas-

particle partitioning of organic gases over organic condensed phase mixtures (Pankow 1994a,b; Odum et al., 1996).

As more chamber experiments were performed and analyzed according to equilibrium partitioning theory, a database of empirical concentration-dependent aerosol yields was developed and implemented in some air quality models (Pandis et al., 1992; Lurmann et al., 1997; Strader et al.; 1999). During this time, secondary organic aerosol markers, both biogenic and anthropogenic, were being identified using gas chromatography-mass spectrometry, and the same techniques were used to isolate gas- and particle-phase products in chamber experiments (Yu et al., 1999; Hallquist et al., 1999; Glasius et al., 2000).

Attention then turned to the role of water vapor and temperature in determining aerosol concentrations. Temperature was recognized (Strader et al., 1999; Sheehan and Bowman, 2001) as having a potentially mixed role in influencing secondary organic aerosol (SOA) concentrations, with high temperatures favoring greater formation of species from increased reaction rates and low temperatures favoring partitioning of semivolatile species to the condensed phase. Particle volatility of a few pure components found in SOA was measured by Bilde and Pandis (2001).

This body of theoretical and experimental work on SOA formation is increasingly finding application in air quality models for use at the local, regional, and global scale. Therefore, it makes sense to check for errors as we translate experimental chamber data into simplified SOA formation expressions suitable for large scale computer models. There has been little work in this area. For

example, Bian and Bowman (2002) performed calculations showing potential errors in lumping n-component product formation data into smaller numbers of "lumped" products. It is prudent to check, as thoroughly as possible, the validity of the physical models and assumptions used to paramaterize SOA formation. Four assumptions are typically incorporated into the modeling efforts:

1. Reversible gas-particle partitioning is the mechanism for particle formation, growth, and evaporation. There are no particle-phase reactions (isomerizations, physical interactions, chemical interactions, heterogeneous reactions) that further process particles.
2. Stoichiometric yields depend on the precursor-oxidant combination only and do not depend on temperature, or the presence of additional compounds such as water.
3. Yield and saturation concentration parameters fitted from chamber experiments at high concentration adequately predict ambient aerosol yields at much lower concentrations.
4. Temperature dependence of aerosol yield can be calculated by using temperature dependent saturation concentrations; furthermore, the temperature dependence can be represented by the Clausius-Clapeyron equation with enthalpies of vaporization drawn from the literature or group contribution methods.

Consider Figure 7.1, which shows organic aerosol concentrations as a function of both temperature and precursor concentration (the Reactive Organic Gas ROG) for a typical system. The concentration and temperature of smog chamber experiments used to produce partitioning data is plotted, and lies at the high temperature-high concentration region B. However, the models that predict secondary organic aerosol for areas around the globe encounter a wide range of

reactant concentrations and temperatures, usually lower than those in the chamber experiments – sometimes by orders of magnitude. This modeling domain is shown as region A. The assumptions listed above are used, either implicitly or explicitly, to extend chamber measurements from region B to region A.

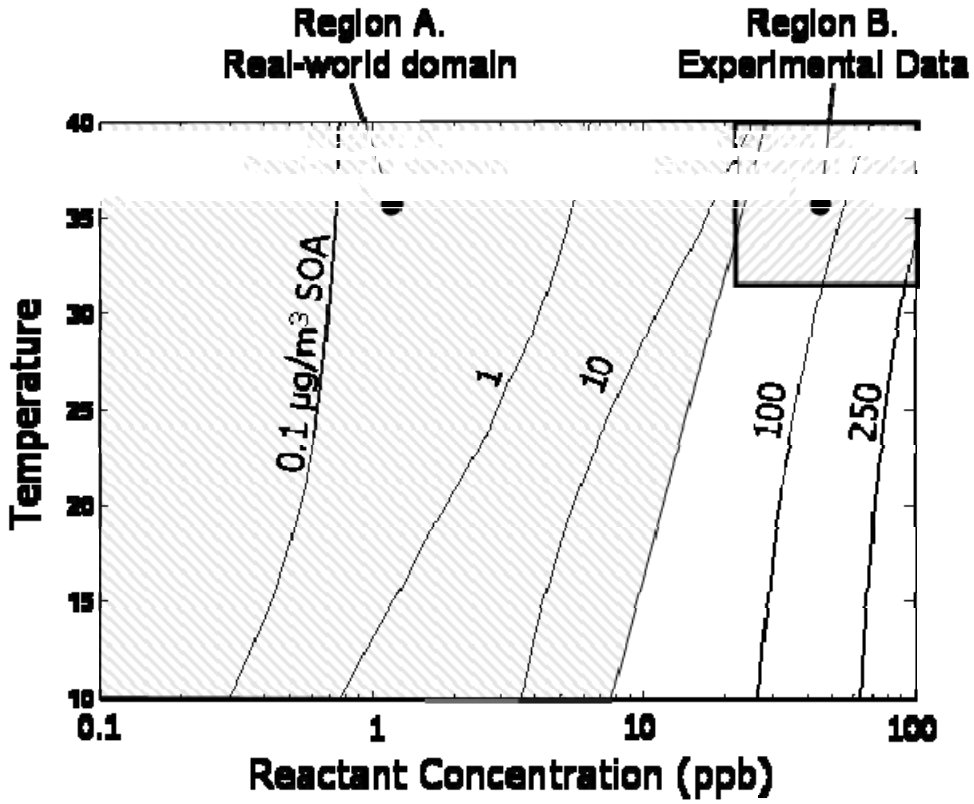

Figure 7.1 Conceptual diagram of range of potential atmospheric conditions and chamber experiments for SOA formation. Reactant concentration (x-axis) is plotted against temperature (y-axis). Contour level is the equilibrium concentration of SOA formation. The larger shaded area (A) corresponds to real-worl conditions, while the small shaded box shows laboratory values (B).

The fourth assumption, concerning temperature effects on secondary organic aerosol partitioning, is the main topic of this chapter. Assumption number four is tested directly through smog chamber experiments with the ozone oxidation products of α-pinene, β-pinene, and 3-carene, three prevalent biogenic secondary organic aerosol precursor gases.

7.2 Experimental

The laboratory SOA used in the study was generated by the reaction of volatile organic compounds and ozone inside a Teflon chamber. Two chambers were used: a 5 m^3 chamber for initial experiments, and a ~25 m^3 chamber for later experiments (Welch Fluorocarbons, Dover NH). Concentrations of VOC, ozone, and particles were monitored by a gas chromatograph (Perkin Elmer AutoSystem XL with FID and J&W Scientific DB-624 capillary column, 30 m x 0.530 mm), a continuous ozone analyzer (Dasibi 1008-PC), and a Scanning Mobility Particle Sizer (SPMS, TSI 3936), respectively. The Teflon smog chamber was positioned inside a temperature-controlled enclosure which enabled rapid temperature changes (approximately 2 minute per °C) (Figure 7.2).

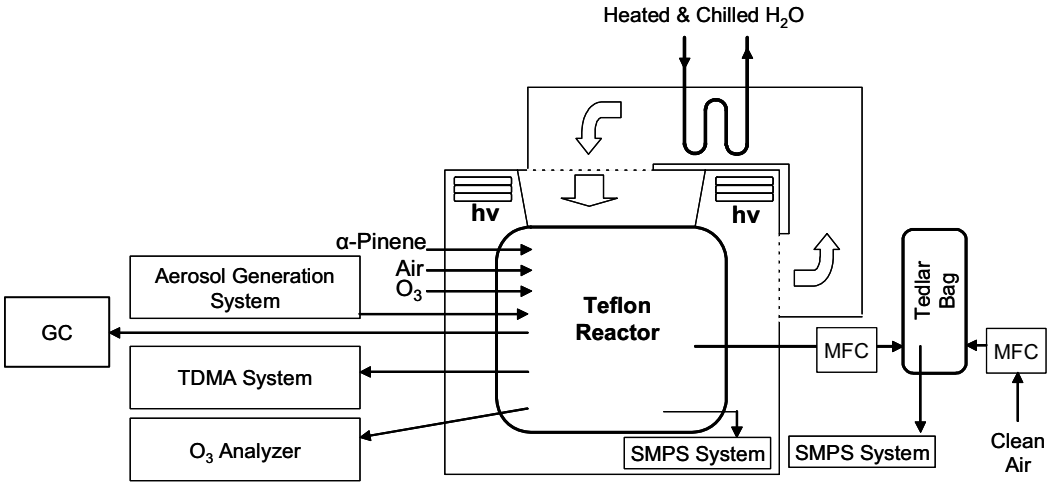

Figure 7.2 Schematic of Smog Chamber and Enclosure (Side View). Reactions are performed inside the Teflon reactor. Temperature control is provided by a large HVAC system – airflows are depicted by the large open arrows. Ultraviolet light (labeled hv) is provided by banks of fluorescent lamps. Gas- and particle-monitoring instruments are deployed around the enclosure.

Reactants included monoterpenes in the 50-150 ppb concentration range and ozone produced from an ozone generator (Azco HTU500AC). Reactions were carried out in the presence of an OH-scavenger (2-butanol) in the same concentration ratios used by Yu et al. (1999). Reagents were HPLC or ACS purity from Sigma Aldrich. Reactions were carried out under dry conditions (<10% RH) and without a seed aerosol.

Each of the experiments involved a two step process: (1) formation of SOA at room temperature (20-25 ºC); (2) perturbation of gas-particle equilibrium by heating or dilution. Step 2 was performed by one of two different techniques, (a) Tandem Differential Mobility Analysis, TDMA (Rader et al., 1987, Turner 1997); and (b) heating of the entire smog chamber. The TDMA measures the dynamic response of the particles with relatively rapid heating (up to 60 ºC/min with a time scale of 0.25-4 min, Bilde and Pandis, 2001; Cruz and Pandis, 2000). On the other hand, the whole chamber temperature change approach allows the study of temperature changes under equilibrium, as opposed to dynamic, conditions. A list of experiments analyzed in this paper is shown in Table 7.1.

Table 7.1 List of chamber experiments

Date	Reactant	Conc.	Scavenger	Perturbation
5/22/03	α-pinene	~150 ppb	Yes	Dilution
8/21/02	3-carene	~150 ppb	Yes	Chamber Temp.
8/19/02	limonene	~150 ppb	Yes	Chamber Temp.
8/9/02	β-pinene	~150 ppb	Yes	Chamber Temp.
8/8/02	α-pinene	~150 ppb	Yes	Chamber Temp.
10/03/01	α-pinene	73 ppb	Yes	Chamber Temp.
9/29/01	α-pinene	110 ppb	Yes	Chamber Temp.
1/17/01	α-pinene	~100 ppb	Yes	TDMA
1/15/01	α-pinene	~100 ppb	Yes	TDMA
1/9/01	α-pinene	~100 ppb	Yes	TDMA
10/30/00	α-pinene	~100 ppb	Yes	TDMA
6/26/00	α-pinene	> 1 ppm	No	TDMA

7.2.1 Data Reduction

Calculating volatility for single component aerosols by TDMA is well established (Bilde and Pandis 2001; Zhang et al., 1993). One can compute the reduction in diameter with time (dD_p/dt) for an evaporating particle of a compound in the transition regime in an environment of zero gas-phase concentration. The relavent equation is:

$$\frac{dD_p}{dt} = -\frac{4M_i D_{i,air} p_i^o}{\rho_i D_p RT} \exp\left[\frac{4\sigma_i M_i}{D_p \rho_i RT}\right] F(Kn_i, \alpha_i) \tag{7.1}$$

where M_i is the molar mass of species i, ρ_i is the density, R is the gas constant, T is the temperature, p_i^o is the vapor pressure of species i over a flat surface, σ_i is the surface free energy, D_p is the particle diameter, Kn_i is the Knudsen number, $D_{i,air}$ is the binary diffusivity of species i in air, and α_i is the accommodation coefficient. Several expressions have been proposed for the transition regime correction term $F(Kn_i,\alpha_i)$. The transition regime correction of Fuchs and Sutugin (1971) is used in this work. While not used in this work, the TDMA data analysis

has been extended to multicomponent mixtures (Pesci and Pandis, 1997) and may be useful in future work.

In the temperature change experiments, the aerosol size distribution is monitored by SMPS as the chamber (and aerosol) temperature changes. The SMPS system is run in recirculation mode and is located inside the heated chamber so that gas-particle equilibrium is not changed en route to or during particle sizing. The reference temperature used for the system is that of a surface-mounted thermocouple on the DMA column. The system was used to size non-volatile ammonium sulfate at temperatures from 15-40 ºC to rule out size changes due to instrument temperature alone. The time series of the aerosol size distribution is used to calculate an aerosol volume time series. The volatility of the SOA is then assessed by the amount of volume change observed during a ramp from an initial to final temperature.

The aerosol volume time series is corrected for wall losses by calculating the mass of aerosol on the wall C_w (assuming no production or loss of product C via reaction).

$$\frac{dC_w}{dt} = k_w C_p + \frac{C_w}{C_p}\left(k_w C_p + \frac{dC_p}{dt}\right) \tag{7.2}$$

where C_p is the aerosol concentration inside the chamber and k_w is a size-independent first order wall loss constant. Consider the limiting case when there is no reaction (required in the assumption) and no evaporation or condensation. Under this limiting case, the decrease in gas phase particle concentration with respect to time in the bag is simply equal to $k_w C_p$, the right hand term drops out of

the equation, and the wall "phase" concentration increases by the same amount. The wall loss rate is determined for each experiment by holding the temperature of the chamber constant and recording the rate of decay of the gas-phase aerosols. Thus, the time series of $C_p(t)$ (recorded for each experiment), and the wall loss constant (determined for each experiment), are used to calculate $C_w(t)$ and thus the total aerosol yield C_w+C_p.

Given the relatively slow temperature changes (up to 2 ºC min^{-1}), the aerosol is expected to maintain equilibrium, and the change in aerosol volume with temperature should be described by thermodynamic equilibrium only. For single components, the vapor pressure as a function of temperature is described by the Clausius-Clapyeron equation:

$$\frac{p(T)}{p(T_{ref})} = \exp\left[\frac{-\Delta H}{R}\left(\frac{1}{T_{ref}} - \frac{1}{T}\right)\right] \tag{7.3}$$

where $p(T)$ and $p(T_{ref})$ are saturation vapor pressures at the temperature in question T and a reference temperature T_{ref}. ΔH is the enthalpy of evaporation for the compound in question and R is the gas constant.

7.3 Results and Discussion

As previous investigations have shown (Yu et al., 1999, Hallquist et al., 1999, Glasius et al., 2000), SOA consists of a complex mixture of many (often 10 or more) components. Therefore, it is difficult to extract thermodynamic parameters for individual compounds, such as vapor pressures or enthalpies of vaporization, from evaporation data. However, the evaporation experiments serve two useful purposes. First, they provide a "reality check" for multiparameter

chemical-thermodynamic models. In other words, SOA models should be consistent with the evaporation behavior measured in these experiments. Second, the evaporation experiments provide a way to check the validity of the commonly made assumption of absorptive partitioning in SOA formation.

7.3.1 Results from Evaporation of SOA from ozone oxidation of monoterpenes

7.3.1.1 Temperature-ramped chamber experiments

With temperature ramps from 22 ºC to 35 ºC, aerosol volume reductions of 16%, 35%, and 35% was seen for β-pinene, α-pinene, and 3-carene, respectively. An example of one of these experiments is shown in Figure 7.3. Figure 7.4 shows aerosol volume versus temperature for 3 experiments. Although the aerosol concentrations in the chamber for the α-pinene runs are quite different due to different initial reactant concentrations, the percentage changes in aerosol volume upon heating (Figure 7.4b) are fairly similar.

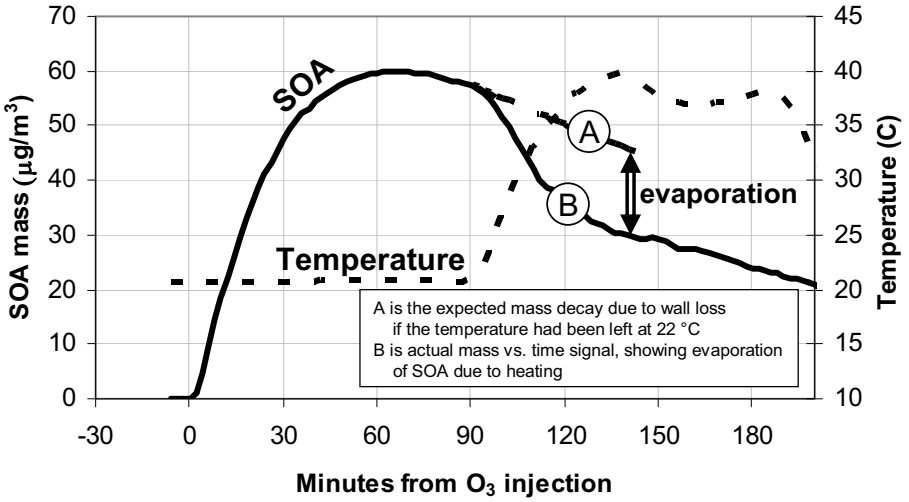

Figure 7.3 Example of time series of organic aerosol mass (actual and expected from wall-losses alone) and temperature. Experiment shows α-pinene-O3 reaction (73 ppb of α-pinene and 400 ppb ozone). Soon after ozone injection, there is a rapid increase in particle (SOA) mass. At about 60 minutes into the reaction, the formation of SOA is nearly complete and the concentration begins to decline due to wall losses. At 90 minutes into the reaction, the temperature setpoint is increased. Line A shows expected decay from wall losses while line B shows actual decay. Arrow shows amount of SOA evaporated due to temperature ramp.

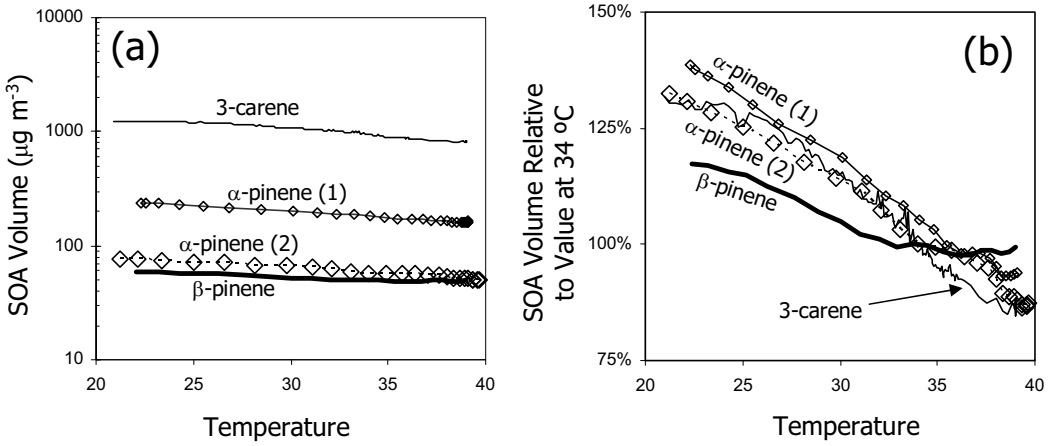

Figure 7.4. Results from smog temperature-change smog chamber experiments. Results are plotted as (a) wall-corrected concentrations in the chamber and as (b) relative concentrations, normalized to their values at 34ºC.

7.3.1.2 Tandem Differential Mobility Analyzer (TDMA) experiments

A number of smog chamber experiments with O_3 - α-pinene were conducted. Each chamber experiment generated a number of TDMA data points as residence time, temperature, particle size, and particle concentration were

varied in the TDMA system. These results are plotted together in Figure 7.5 as the effective single component vapor pressure calculated from each TDMA experiment using equation 7.1 assuming an aerosol surface tension of 0.31 J m^{-2} (see Bilde and Pandis (2001) for a discussion of sensitivity to this parameter). Most of the TDMA experiments used temperatures between 30 and 43 ºC and residence times between 14 s and 1 min. Most runs exhibited particle size change from 0-10% (diameter change). This was much smaller than expected, based on literature values of vapor pressures and saturation vapor concentrations.

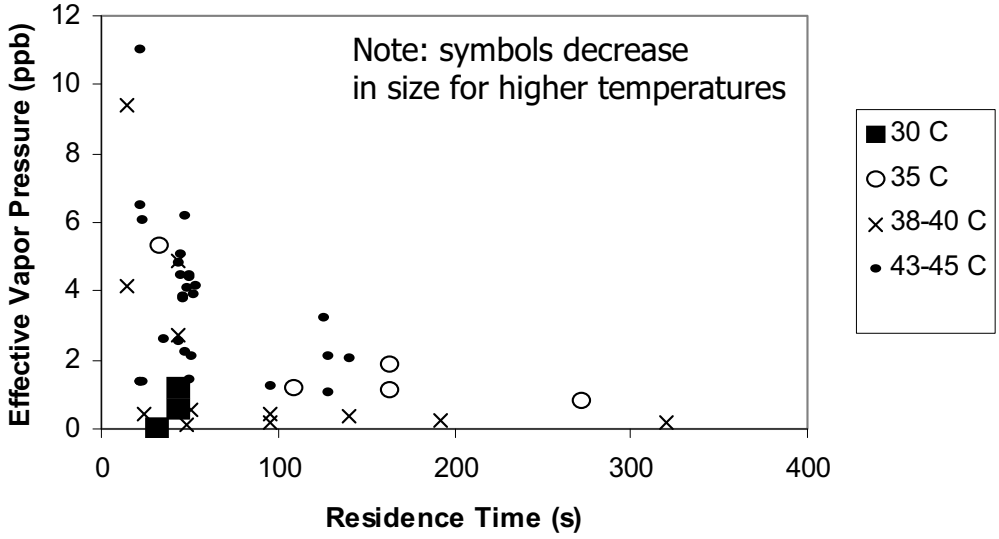

Figure 7.5. All TDMA data reduced as effective (single component) vapor pressure required for observed volume change assuming accommodation coefficient = 1 and surface tension = 0.31 J m^{-2}.

For a true single component, one would expect a constant vapor pressure with respect to residence time. However, the SOA showed a marked dropoff in the effective vapor pressure, indicating fast evaporation initially and slower evaporation later on. This is the result of the multicomponent makeup of the SOA, with small amounts of high vapor pressure compounds coming off early and lower volatility compounds coming off later.

The TDMA experimental results are tabulated in Table 7.2.

7.3.2 Parameter estimation and comparison with other investigators

7.3.2.1 Temperature-ramped chamber experiments

Temperature-ramp smog chamber experiment results for α-pinene were used to assess the validity of yields as a function of temperature *predicted* using accepted techniques and a combination of theoretical and empirical data from the literature. The predictions for evaporation of α-pinene plus O_3 SOA were made using two different models. Both assume equilibrium partitioning of organic semi-volatile species, but differ in the number of components assumed as reaction products.

The first model assumes a 9-component mixture for the SOA. Vapor pressures and yields were from Bian and Bowman (2002) who adapted them from experimental results of Yu et al. (1999). The amount of aerosol evaporation expected as a function of temperature in this system, assuming different values for the enthalpy of vaporization (assumed to be the same for all nine components in the aerosol) is shown in Figure 7.6 and indicates that ΔH_{evap} of 25-30 kcal/mol predicts the experimentally observed evaporation well.

Table 7.2 Numerical values for TDMA experiments

M_o (μg m^{-3})*	Date	Temperature	time(s)	Dp,initial (nm)	Dp,final(nm)	% Change
191	1/17/2001	43	44.5	153.9	146.6	-4.7%
			44.5	155.2	146.9	-5.3%
			49.9	155.3	147.1	-5.3%
			49.9	155.3	147.3	-5.2%
			53.2	155.0	146.9	-5.2%
			51.5	152.3	145.0	-4.8%
			46.1	152.4	145.8	-4.3%
			45.7	151.9	145.5	-4.2%
			23.3	148.5	143.2	-3.6%
			22.0	147.8	142.4	-3.7%
			128.7	154.4	144.5	-6.4%
			139.7	152.2	141.6	-7.0%
			125.4	203.0	190.7	-6.1%
			47.5	201.7	192.7	-4.5%
			22.2	195.4	187.8	-3.9%
			48.9	151.5	144.1	-4.9%
40	1/15/2001	25	32.6	92.1	92.6	0.5%
			32.6	98.4	98.7	0.3%
			32.6	148.8	148.3	-0.3%
			35.7	197.9	196.2	-0.9%
			46.6	148.5	148.3	-0.1%
			48.9	98.8	99.5	0.7%
40	1/15/2001	35	30.6	98.9	99.2	0.3%
			30.6	148.6	147.2	-0.9%
			32.6	176.6	177.1	0.3%
			48.9	178.2	175.2	-1.7%
			48.9	150.1	148.4	-1.1%
			48.9	99.9	99.3	-0.6%
40	1/15/2001	43	88.9	147.3	149.4	1.4%
			32.6	148.7	147.3	-0.9%
2	1/9/2001	30	31.8	29.7	29.7	0.0%
20	1/9/2001	35	48.9	38.7	39.3	1.6%
31	1/9/2001	38	48.9	49.2	48.6	-1.2%
38	1/9/2001	38	95.9	48.6	47.1	-3.1%
50	1/9/2001	38	95.9	69.9	67.1	-4.0%
63	1/9/2001	38	50.4	69.7	67.7	-2.9%
87	1/9/2001	38	24.5	70.5	69.8	-1.0%
112	1/9/2001	38	50.4	105.6	106.1	0.5%
127	1/9/2001	43	34.9	111.7	107.5	-3.8%
133	1/9/2001	43	50.4	111.1	106.2	-4.4%
140	1/9/2001	43	95.9	111.0	105.4	-5.0%
102	10/30/2000	35	163.0	147.1	140.2	-4.6%
			271.7	146.5	137.9	-5.9%
			108.7	152.9	148.1	-3.1%
			32.6	148.7	142.1	-4.4%
			163.0	183.3	173.5	-5.3%
150	6/26/2000	40	44.1	98.6	92.4	-6.3%
600	6/26/2000	40	14.2	98.5	95.5	-3.1%
280	6/26/2000	40	44.1	148.4	140.2	-5.6%
500	6/26/2000	40	14.2	147.8	142.7	-3.4%
700	6/26/2000	45	44.1	147.8	139.7	-5.5%
			44.1	98.5	92.8	-5.7%
700	6/26/2000	30	44.1	147.3	145.3	-1.4%
			44.1	98.4	97.2	-1.2%
700	6/26/2000	23	44.1	147.3	147.2	-0.1%

*The mass concentration of secondary organic aerosol in the chamber.

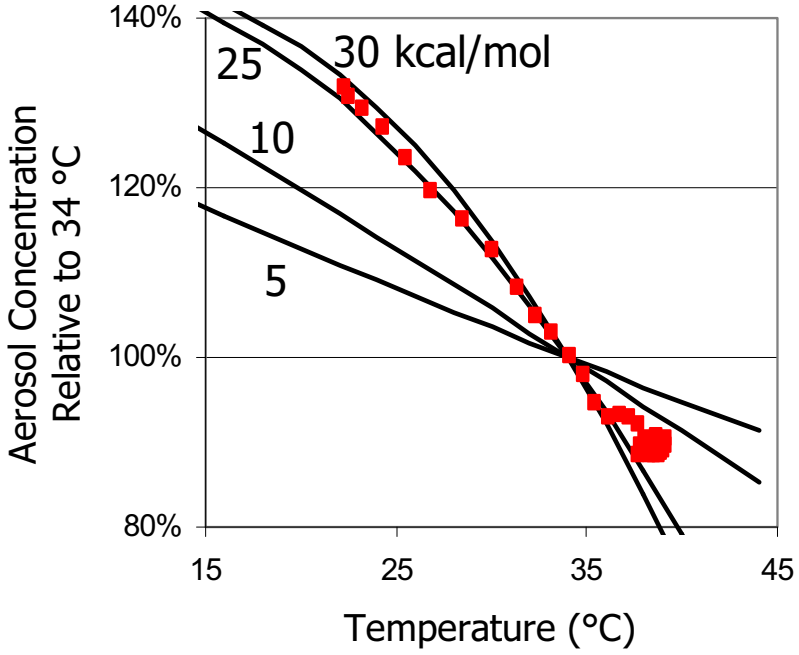

Figure 7.6 Comparison of data (points) to model prediction of evaporation behavior (lines) from secondary organic aerosol (SOA) created from ozone oxidation of 73 ppb α-pinene. Thermodynamic and yield parameters for 9 component model of the SOA from Bian and Bowman (2002) . Enthalpy of vaporization was assumed to be equal for all 9 components.

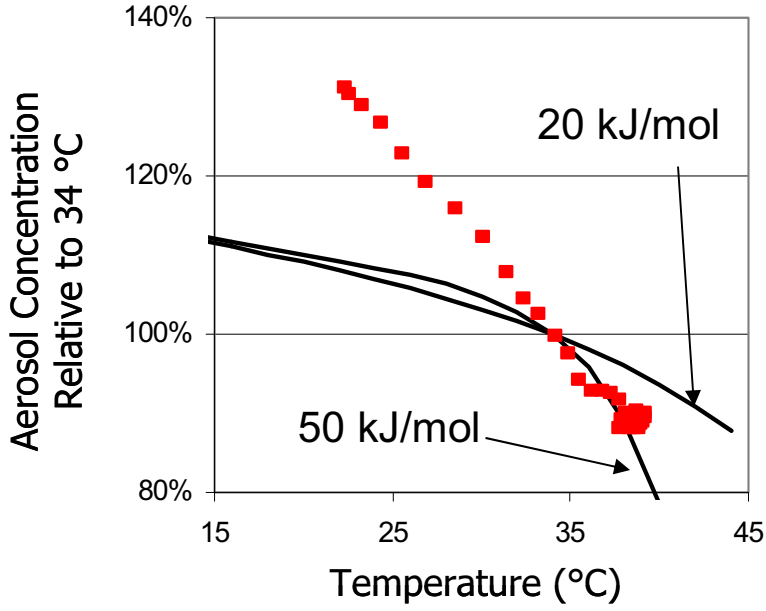

Figure 7.7 Comparison of data (points) to model prediction of evaporation behavior (lines) from secondary organic aerosol (SOA) created from ozone oxidation of 73 ppb α-pinene. Thermodynamic and yield are from Griffin et al. (1999), a common data source for air quality models.

The results were also compared with a simpler single component model with parameters from the chamber work of Griffin et al. (1999), indicating that the simpler model was not robust enough for extension to other temperatures (Figure 7.7).

7.4 Summary and Conclusion

Several new techniques with potential for improving the prediction of secondary organic aerosols were presented, including TDMA of secondary organic aerosols and temperature-ramp chamber experiments.

Changes in aerosol concentrations of 15-35% were measured in chamber experiments with temperature variations from 20 to 40 ºC, consistent with ΔH_{evap} of 25-30 kcal for the components making up the secondary organic aerosol.

While not fully exploited to date, these techniques will provide a promising tool determining secondary organic aerosol yields in the future.

7.5 Acknowledgements

I would like to thank Tim Raymond, Ray Dagastine, Mirete Bilde, and Kara Huff-Hartz for all there help with these experiments.

7.6 References

Asher, W.E.; Pankow, J.F,; Erdakos, G.B.; Seinfeld, J.H. (2002). Estimating the vapor pressures of multi-functional oxygen-containing organic compounds using group contribution methods. *Atmos. Environ.* 36, 1483-1498.

Bademosi, F.; Liu, B.Y.H. PTL Publication No. 156, Particle Technology Laboratory, University of Minnesota; Minneapolis, MN, 1971.

Bian, F., Bowman, F. (2002) Theoretical Method for Lumping Multicomponent Secondary Aerosol Mixtures. *Environ. Sci. Technol*. 36, 2491-2497.

Bilde, M., and Pandis, S.N. (2001). Evaporation Rats and Vapor Pressures of Individual Aerosol Species Formed in the Atmospheric Oxidation of α- and β-Pinene. *Environ. Sci. Technol*. 35, 3344-3349.

Cruz, C.N., and Pandis, S.N. (2000). Deliquescence and Hygroscopic Growth of Mixed Inorganic-Organic Atmospheric Aerosol. *Environ. Sci. Tech*. 34, 4313-4319.

Fuchs and Sutugin (1971) In *Topics in Current Aerosol Research*, Pergamon Press.

Glasius, M.; Lahaniati, M.; Calogirou, A.; Di Bella, D.; Jensen, N. R.; Hjorth, J.; Kotzias, D.; Larsen, B. R. Carboxylic Acids in Secondary Aerosols from Oxidation of Cyclic Monoterpenes by Ozone. *Environ. Sci. Technol.* 2000, *34*, 1001-1010.

Griffin, R.J.; Cocker, D.R. III; Seinfeld, J.H. *Geophysical Research Letters*. 1999, *26*, 2721-2724.

Guenther, A.; Hewitt, C.; Erickson, D.; Fall, R.; Geron, C.; Graedel, T.; Harley, P.; Klinger, L.; Lerdau, M.; McKay, W.; Piersce, T.; Scholes, B.; Steinbrecher, R.; Tallamraju, R.; Taylor, J.; Zimmerman, P. A Global Model of Natural Volatile Organic Compound Emissions. *J. Geophys. Res*. 1995, *100*, 8873-8892.

Hallquist, M.; Wängberg, I.; Ljungström, E.; Barnes, I.; Becker, K. H. Aerosol and Product Yields from NO_3 Radical-Initiated Oxidation of Selected Monoterpenes. *Environ. Sci. Technol.* 1999, *33*, 553-559.

Hatakeyama, S.; Izumi, K.; Fukuyama, T.; Akimoto, H. Reactions of ozone with a-pinene and b-pinene in air: yields of gaseous and particulate products. *J. of Geophys. Res.* 1989, *94*, 13,013-13,024.

Lurmann, F.W., Wexler, A.S., Pandis, S.N., Musarra, S., Kumar, N., and Seinfeld, J.H. (1997). Modelling Urban and Regional Aerosols II. Application to California's South Coast Air Basin. *Atmos. Environ*. 31, 2695-2715.

Müller, J. F. Geographical Distribution and Seasonal Variation of Surface Emissions and Deposition Velocities of Atmospheric Trace Gases. *J. Geophys. Res*. 1992, *97*, 3787-3804.

Pandis, S.N., Harley, R.A., Cass, G.R., and Seinfeld, J.H. (1992) Secondary Organic Aerosol Formation and Transport. *Atmos. Environ*. 26A, 2269-2282.

Pankow, J.F. (1994) An absorption model of gas/particle partitioning of organic compounds in the atmosphere. *Atmos. Environ.* 28, 185-188.

Pankow, J.F. (1994) An absorption model of the gas/particle partitioning involved in the formation of organic aerosols. *Atmos. Environ*. 28, 189-193.

Pesci, C.P.; Pandis, S.N. (1997) Investigating Multiple Theories for the Evaporation of Binary Liquid Particles Containing Adipic and Glutaric Acids. Term Paper, Carnegie Mellon University Dept. of Chemical Engineering.

Odum, J.R.; Hoffmann, T.; Bowman, F.; Collins, D.; Flagan, R.C.; Seinfeld, J.H. Gas/particle partitioning and secondary organic aerosol yield. *Environ. Sci. Technol*. 1996, *30*, 2580-2585.

Rader, D. J.; McMurry, P. H.; Smith, S. Evaporation Rates of Monodisperse Organic Aerosols in the 0.02- to 0.2-μm-Diameter Range. *Aero. Sci. Technol.* 1987, *6*, 247-260.

Sheehan, P.E.; Bowman, F.M. (2001). Estimated Effects of Temperature on Secondary Organic Aerosol Concentrations. *Environ. Sci. & Technol. 35*, 2129-2135.

Strader, R.; Lurmann, F.; Pandis, S.N. Evaluation of secondary organic aerosol formation in winter. *Atmos. Environ.* 1999, *33*, 4849-4863.

Tao, Y. & McMurry, P. H. Vapor Pressures and Surface Free Energies of C14-C18 Monocarboxylic Acids and C5 and C6 Dicarboxylic Acids. *Environ. Sci. Technol.* 1989, *23*, 1519-1523.

Turner, F. C. Evaporation Rates of Secondary Organic Aerosol. (1997) M.S. Thesis, Carnegie Mellon University, Pittsburgh, PA.

Yu, J.; Cocker D.R.; Griffin, R.J.; Flagan, R.C.; Seinfeld, J.J.; Blanchard, P. (1999) Gas-Phase Ozone Oxidation of Monoterpenes: Gaseous and Particulate Products *J. Atmos. Chem*. 34, 207-258.

Went, F.W. (1960) Blue hazes in the atmosphere. *Nature* 187, 641-643.

Zhang, S.H., Seinfeld, J.H., Flagan, R.C. (1993) Determination of Particle Vapor Pressures Using the Tandem Differential Mobility Analyzer *Aero. Sci. Technol*. 19, 3-14.

Chapter 8 Summary and Future Work

8.1 Summary

Several important field and laboratory results regarding the formation and properties of fine and ultrafine aerosols were shown. Key field results included (1) the importance of in situ new particle formation in Western Pennsylvania; (2) production of a high quality dataset of ambient aerosol size distributions; (3) measurement of the ambient aerosol liquid water content; and (4) discovery of large seasonal differences in aerosol water content during the Pittsburgh Air Quality Study. The key laboratory result was the direct measurement of secondary organic aerosol volatility at thermodynamic equilibrium.

The realization of these experimental and field results required the development of new aerosol measurement systems and data processing tools. The most important contributions in these areas were (1) the design, development, and demonstration of the Dry-Ambient Aerosol Spectrometer; (2) the algorithm for merging Scanning Mobility Particle Sizer and Aerosol Particle Sizer data; (3) equations and computer programs for automated computation of aerosol water content from size distributions; and (4) the development of the temperature-change smog chamber experimental method for determination of aerosol volatility.

8.2 Future Work

Future work in the area of ultrafine particles is grouped into at least three categories. The first category is in the health effects of the particles. This body of research guides and motivates much of the fundamental and applied research regarding ultrafine particles. As health effects research on issues such as the relative toxicity of particles as a function of size and composition progresses, the priorities for additional research in aerosol science are refined accordingly.

The second group of future work is in applied research, often taking the form of better predictive models to help in the management of air quality and development of air pollution control strategies and regulations. The models range in scale from air quality around a single factory to global models that evaluate climate change. Accurate modeling of ultrafine particles often involves generalization, simplification, and parameterization of field and laboratory data.

The third group of future work is fundamental research, probing the chemistry, physics, and thermodynamics of aerosols. This often involves hypothesis testing and clever experimental design.

With respect to ultrafine aerosols, all three of these require further research. While future avenues in aerosol health effects research is beyond the scope of this thesis, some promising projects in applied and fundamental research regarding ultrafine aerosols are described below.

8.2.1 Particle Sources

8.2.1.1 Determine the chemistry of new particle formation

A number of mechanisms have been proposed as candidates for new particle formation based on observations and theoretical considerations, including (a) homogeneous binary nucleation of sulfuric acid and water; (b) homogeneous ternary nucleation of ammonia-water-sulfuric acid; (c) homogenous nucleation of low vapor pressure organic compounds; (d) and ion-induced nucleation. However, because of difficulties in determining the chemical composition of sub-10 nm particles, it has been difficult to tell the mechanism(s) responsible for the observed nucleation.

New techniques such as sensitive mass spectrometry techniques for both short- and long-lived atmospheric constituents will be an important tool in determining the new particle formation chemistry, as will chamber experiments and monitoring of ultrafine aerosols in additional different places around the world.

8.2.1.2 Develop a predictive model for new particle formation

As nucleation data sets from field studies such as the Pittsburgh Air Quality Study are fully analyzed, elucidation of the nucleation mechanism and development of predictive nucleation models will become possible. These can then be used in conjunction with chemical transport models to assess the impact of nucleation on climate (via aerosol-cloud interactions) and on human health (via the inhalation of ultrafine particles).

8.2.2 Aerosol Water Content

8.2.2.1 Resolve differences seen in water uptake by organic compounds

Analysis of water content data from the Pittsburgh Air Quality Study showed an uncertain water uptake from organic compounds. The water uptake of organic compounds could be investigated more precisely by (1) sampling at rural locations to reduce the impact of local sources which increase the uncertainty in DAASS water measurements; (2) deployment of a combination of instruments for a water-specific study including an aerosol mass spectrometer, relative-humidity controlled nephelometer, in situ organic carbon analyzer, Dry-Ambient Aerosol Size Spectrometer, Hygroscopic Tandem Differential Mobility Analyzer, and organic speciation filters; (3) repeated deployment of identical instruments (to reduce impact of bias) at different locations such as Western Pennsylvania (sulfate dominated), Blue Ridge Mountains (biogenic organic influenced), and downwind of LA (anthropogenic organic dominated).

8.2.2.2 Next generation Dry-Ambient Aerosol Size Spectrometer

As with any first-generation instrument, several potential improvements to the Dry-Ambient Aerosol Size Spectrometer were identified during the Pittsburgh Air Quality Study. A list of specific improvements for increased accuracy, reliability, and ease of operation are included in the Appendix.

8.2.2.3 Test recently proposed organic-water-salt thermodynamic models

Recently, several methods for calculating organic water uptake have been published. These need to be tested against real datasets. As discussed above, the organic water uptake is relatively small and existing measurements of aerosol water content and chemical composition may not be able to discriminate between

small differences in modeled water content from alternate models. However, large discrepancies between models and measurement could be identified at this point and specific areas of model disagreement could be identified, leading to better targeted field experiments.

8.2.3 Secondary Organic Aerosols

8.2.3.1 Extend and generalize this work for use in mathematical models

This work shows that, especially with respect to temperature and concentration, existing parameterizations of smog chamber data for prediction of secondary organic aerosols in the atmosphere may lead to significant errors. There are a large number of reactive organic gases in the urban atmosphere, and these produce an even larger number of semivolatile organic products (many of which are unknown). Therefore, at this time, these reaction products cannot be incorporated explicitly into chemical transport models for prediction of aerosol formation. New parameterization schemes are required that reflect the temperature and concentration dependence of organic aerosol yields more accurately.

Glossary

Arranged alphabetically, including terms from all chapters of thesis:

APS, Aerosol Particle Sizer: Instrument (TSI Model 3320 and 3321) for determining the aerodynamic size (number) distribution of aerosol particles from 0.5 to 20 μm. Instrument sizes particles by time of flight while under flow-induced acceleration. Particles are detected in the APS by light scattering using a red laser.

CPC, Condensation Particle Counter: Instrument (TSI Model 3010 and 3025) that measures the number concentration of particles in air down to sizes of about 3 nm. CPCs operate exposing the aerosols to a supersaturation of butanol vapor, which condenses on the aerosols to form optically detectable (> 0.5 μm) particles. Used as the detector in SMPS systems.

CS, Condensational Sink: A proportionality constant in the rate of condensation that is a function of particle surface area, particle size, and particle concentration, the mean free path of the condensing molecule, and the accommodation coefficient. Its physical interpretation is as follows: The rate of condensation of a supersaturated vapor *a* to the particle phase is (Pirjola et al. 1999, full reference in Chapter 4):

$$\frac{dM_{a,particle}}{dt} = 4\pi \, \mathrm{CS} \, D_{a-air} \left(M_{a,\infty} - M_{a,saturation} \right)$$

where dM_a/dt is the change in the particle phase concentration of *a* (μg $m^{-3}s^{-1}$), CS is the condensational sink (cm^{-2}), $D_{a\text{-}air}$ is the diffusivity of *a* in air (cm^2 s^{-1}), $M_{a,\infty}$ is the gas-phase concentration of *a* in the bulk gas (far from the particles), and $M_{a,saturation}$ is the equilibrium saturation concentration of *a* (μg m^{-3}). From dimensional analysis, the rate of condensation for a single particle is proportional to particle surface area (L^2), diffusivity of the condensing vapor ($L^2 T^{-1}$), the supersaturation driving force ($M L^{-3}$), and inversely proportional to the thickness of the mass transfer layer (L), giving units of the condensation rate of mass per time or $M T^{-1}$. Comparing this dimensional analysis with the equation above, the condensational sink for a single particle is proportional to its surface area divided by the mass transfer layer thickness, for units of L^1. Furthermore, the condensational sink "concentration" for a group of N particles then has units of $L^1 L^{-3}$ or L^{-2}. Accordingly, the condensational sink values used in this work (e.g. plots in Chapter 4) have units of cm^{-2}. For a single particle in the continuum regime (D_p > 10 μm), CS is proportional to D_p^1. This has a physical interpretation of the mass transfer layer thickness being proportional to the particle size. For particles in the kinetic regime (< 10 nm), CS is proportional to D_p^2 and mass transfer is more

efficient (on a per surface area basis). This has the physical interpretation of a constant (particle size independent) mass transfer layer thickness. For particles in the transition regime, CS is proportional to D_p^x where x is between 1 and 2, depending on particle size.

CRH, Crystallization Relative Humidity: RH at which a supersaturated hydrated aerosol reaches a critical supersaturation, nucleation of a solid phase occurs, and the aerosol dehydrates spontaneously forming a solid particle (Figure 6.1).

DAASS, Dry-Ambient Aerosol Size Spectrometer: Instrument described in Chapter 2 which measures the size (number) distribution of ambient aerosols from 3 nm to 20 μm at both ambient and dried relative humidities. Results from the DAASS are used in Chapters 3-6. Designed and deployed for the Pittsburgh Air Quality Study, DAASS was a combination of specially-configured commercial instruments and in-house elements.

DMA, Differential Mobility Analyzer: Device which separates particles according electrical mobility (related to particle size). The DMA is widely used in aerosol studies and is mentioned throughout this work in several contexts. DMAs have two operational modes. They can either be used to select particles of a specific size (classification) or they can be used in conjunction with a particle detector to measure the size distribution of an aerosol sample (SMPS). Sold by TSI (Model 3071, 3081, and 3083). Length of the flow path is a key path in determining the size range accessible to the instrument. Two sizes were used in this work, and they are referred to as the *Long*-DMA (LDMA, TSI Models 3071 and 3081), and *Nano*-DMA (NDMA, TSI Model 3083).

$dN/d\log(D_p)$: Units for the ordinate (y-value) aerosol number size distribution. Used rather than the simpler dN/dD_p for clarity of presentation. See Chapter 7 of Seinfeld and Pandis, *Atmospheric Chemistry and Physics*, 1998, John Weily and Sons.

DRH, deliquescence relative humidity: RH where a solid particle spontaneously absorbs water vapor to form a saturated aqueous solution. See figure 6.1.

efflorescence: crystallization from an evaporating aqueous solution.

efflorescence branch: part of the aerosol humidigraph (Figure 6.1) where aerosol is hydrated and supersaturated, and thus metastable. This occurs between the crystallization (CRH) and deliquescence (DRH) relative humidities.

GMD, Geometric Mean Diameter: Property of an aerosol size distribution. For a measurement with n size bins each with a number of particles N_i and size D_i, the GMD is given by:

$$\mathrm{GMD} = \left[\prod_{i=1..n} D_i^{N_i} \right]^{1/\sum N_i}$$

alternately, logarithms can be used to compute the GMD is the product in the above formula is too large.

GSTD, Geometric Standard Deviation: Property of an aerosol size distribution. For a measurement with n size bins each with a number of particles N_i and size D_i, the GSTD is given by:

$$\mathrm{GSTD} = 10^{\sqrt{\frac{\sum_{i=1..n} N_i \left(\log(D_i) - \log(\mathrm{GMD})\right)^2}{\left[\sum N_i\right] - 1}}}$$

GF, Growth Factor: The ratio of particle size at two different relative humidities. Can be calculated on a size-basis or volume-basis. Volume growth factors are used throughout this work unless otherwise mentioned.

ΔH_{evap}: Enthalpy of evaporation, with units of kJ/mol or kcal/mol.

H-TDMA, Hygroscopic Tandem Differential Mobility Analysis: See entry for TDMA.

LDMA, Long Differential Mobility Analyzer: see entry for DMA.

NDMA, Nano-Differential Mobility Analyzer: see entry for DMA.

PAQS, Pittsburgh Air Quality Study: a multi-investigator air quality field investigation conducted during 2001-2002 focused on the sources, concentrations, and chemistry of fine particulate matter in and around Pittsburgh, PA.

PM, Particulate Matter: Solid or liquid particles suspended in air.

$PM_{2.5}$: Particulate matter smaller than 2.5 μm. Sometimes referred to as *fine* particulate matter. Sometimes used to indicate the mass concentration in air

of particulate matter smaller than 2.5 μm (aerodynamic diameter) as measured by specific techniques approved by the U.S. Environmental Protection Agency (EPA) and usually reported in units of μg m^{-3}. EPA limits for $PM_{2.5}$ are 15 μg m^{-3} for an annual average and 65 μg m^{-3} for a 24-hour average.

primary: see SOA.

PSL, Polystyrene Latex Spheres: Commercially available (Duke Scientific) spheres in solution used for instrument calibration.

secondary: see SOA.

SMPS, Scanning Mobility Particle Sizer: Instrument (TSI Model 3936) that measures the size (number) distribution of aerosol particles from as low as 3 nm to up to about 1 μm. SMPS is actually a combination of an aerosol charger (TSI 3077), DMA (for size classification), and a CPC (for particle detection). Specific choice of the DMA geometry, flow settings, and CPC determine the actual size range analyzed. In this work size ranges are indicated by a prefix: *Nano*-SMPS = 3 – 80 nm while SMPS refers to 15-680 nm.

SOA, Secondary Organic Aerosol: Aerosol particles, or portions of aerosol particles, formed in the atmosphere from gas-to-particle conversion. Gas vapors that are supersaturated relative to their equilibrium concentrations condense or nucleate, forming secondary particulate matter. If the vapor is organic, then the secondary aerosol is referred to as secondary organic aerosol (SOA). The other source classification for particulate matter is *primary*, meaning emitted directly in solid or liquid from sources such as stacks, tailpipes, vegetation, and soil. Aerosols that form from gas-to-particle conversion in cooling exhaust plumes of combustion sources (e.g. vehicle and power plant plumes) are an exception to the rule stated above; they are considered primary particles.

TDMA, Tandem Differential Mobility Analysis: Technique for studying aerosol physical and chemical properties by monitoring the size change of a mono-disperse group of aerosols after exposure to controlled conditions such as elevated temperature or exposure to water (or other) vapor. The technique has

three main steps: (1) creation of a mono-disperse population of aerosols using a DMA; (2) residence time to allow size change under controlled conditions; (3) measurement of size distribution by SMPS. When the size change of the aerosol is due to evaporation or absorption of water vapor, it is called Hygroscopic-TDMA or H-TDMA.

ROG, Reactive Organic Gas: Gases that are susceptible to degradation by atmospheric oxidants such as OH, NO_3, and O_3.

VOC, Volatile Organic Compound: Organic compounds that are found in the gas phase. Compounds are classified as volatile and semi-volatile based on vapor pressure, but threshold vapor pressures for classifications are not standardized.

Appendices

Appendix A Daily Graphs of PAQS Size Distributions

All colorplots depict evolution of number size distribution from midnight to midnight as measured by DAASS at the Schenley Park station. Y-axis is in nm. X-axis is in hours (EST). Z-axis is in $dN/dlogD_p$ (cm^{-3}). A key is shown here:

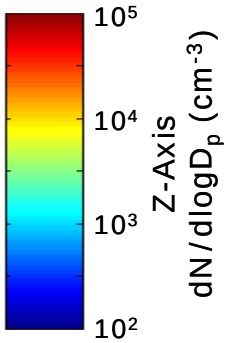

JULY 2001

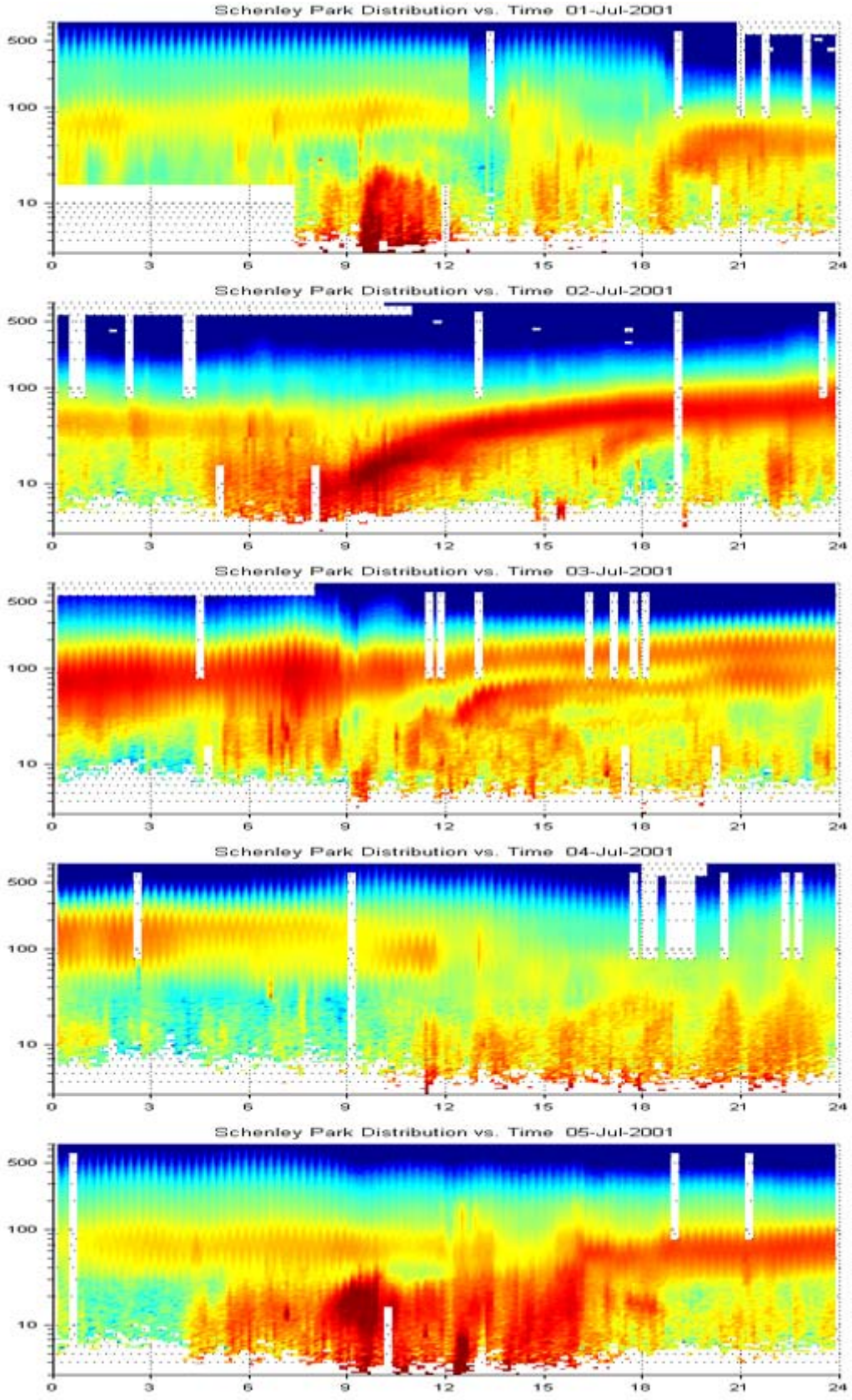
Schenley Park Distribution vs. Time 01-Jul-2001
Schenley Park Distribution vs. Time 02-Jul-2001
Schenley Park Distribution vs. Time 03-Jul-2001
Schenley Park Distribution vs. Time 04-Jul-2001
Schenley Park Distribution vs. Time 05-Jul-2001
500
100
10
0
3
6
9
12
15
18
21
24

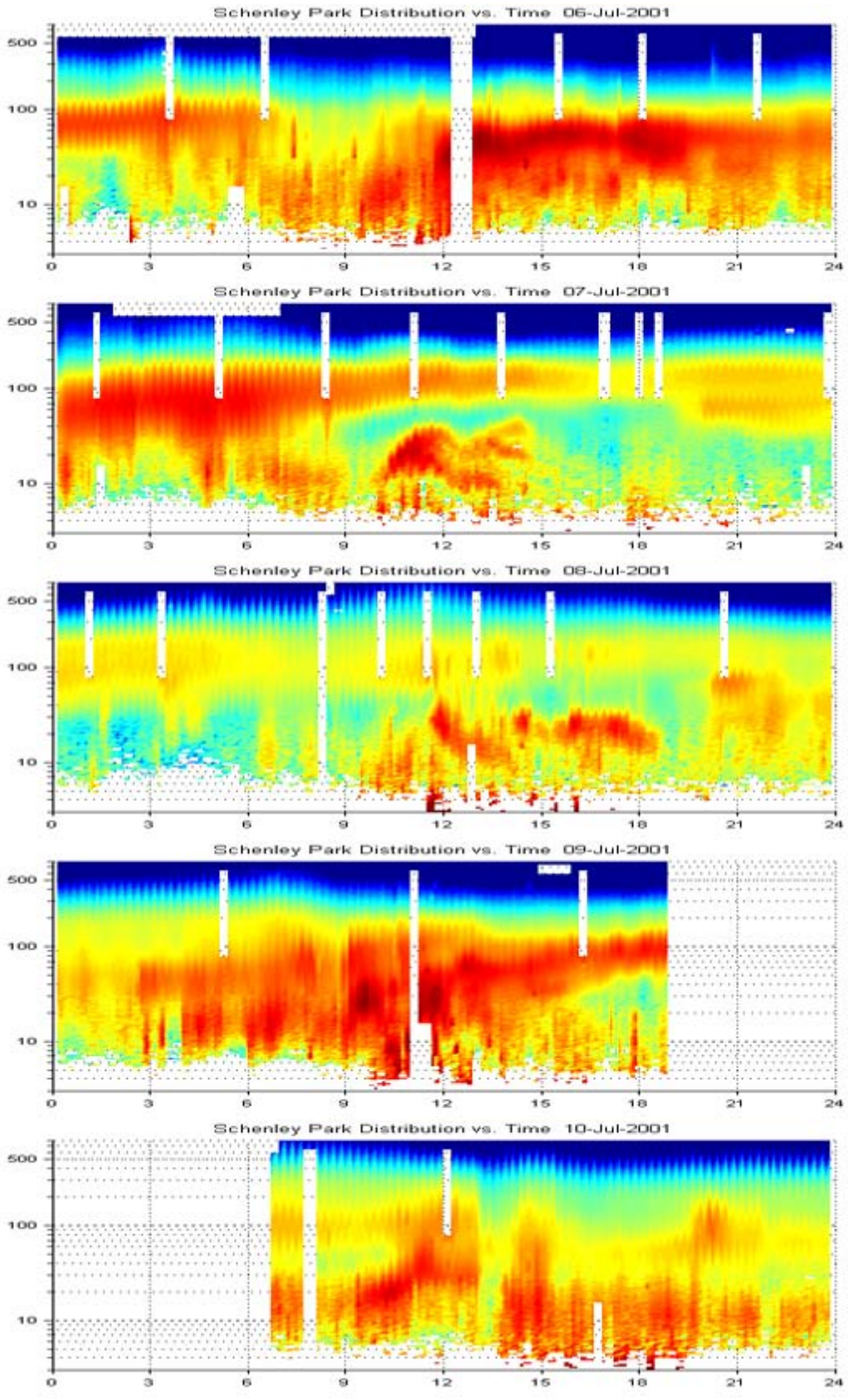
Schenley Park Distribution vs. Time 06-Jul-2001
Schenley Park Distribution vs. Time 07-Jul-2001
Schenley Park Distribution vs. Time 08-Jul-2001
Schenley Park Distribution vs. Time 09-Jul-2001
Schenley Park Distribution vs. Time 10-Jul-2001
500
100
10
0
3
6
9
12
15
18
21
24

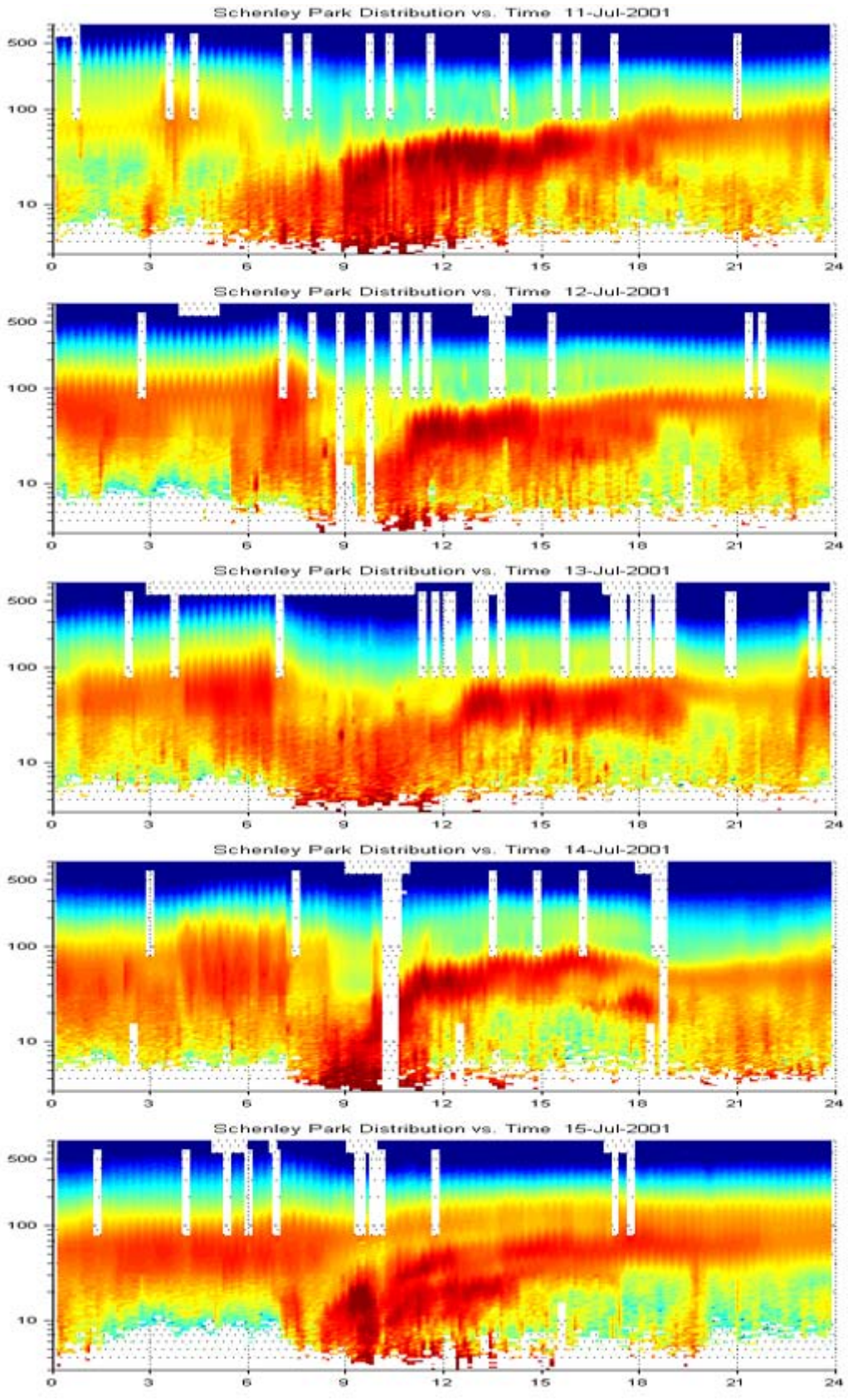
Schenley Park Distribution vs. Time 11-Jul-2001
Schenley Park Distribution vs. Time 12-Jul-2001
Schenley Park Distribution vs. Time 13-Jul-2001
Schenley Park Distribution vs. Time 14-Jul-2001
Schenley Park Distribution vs. Time 15-Jul-2001
500
100
10
0
3
6
9
12
15
18
21
24

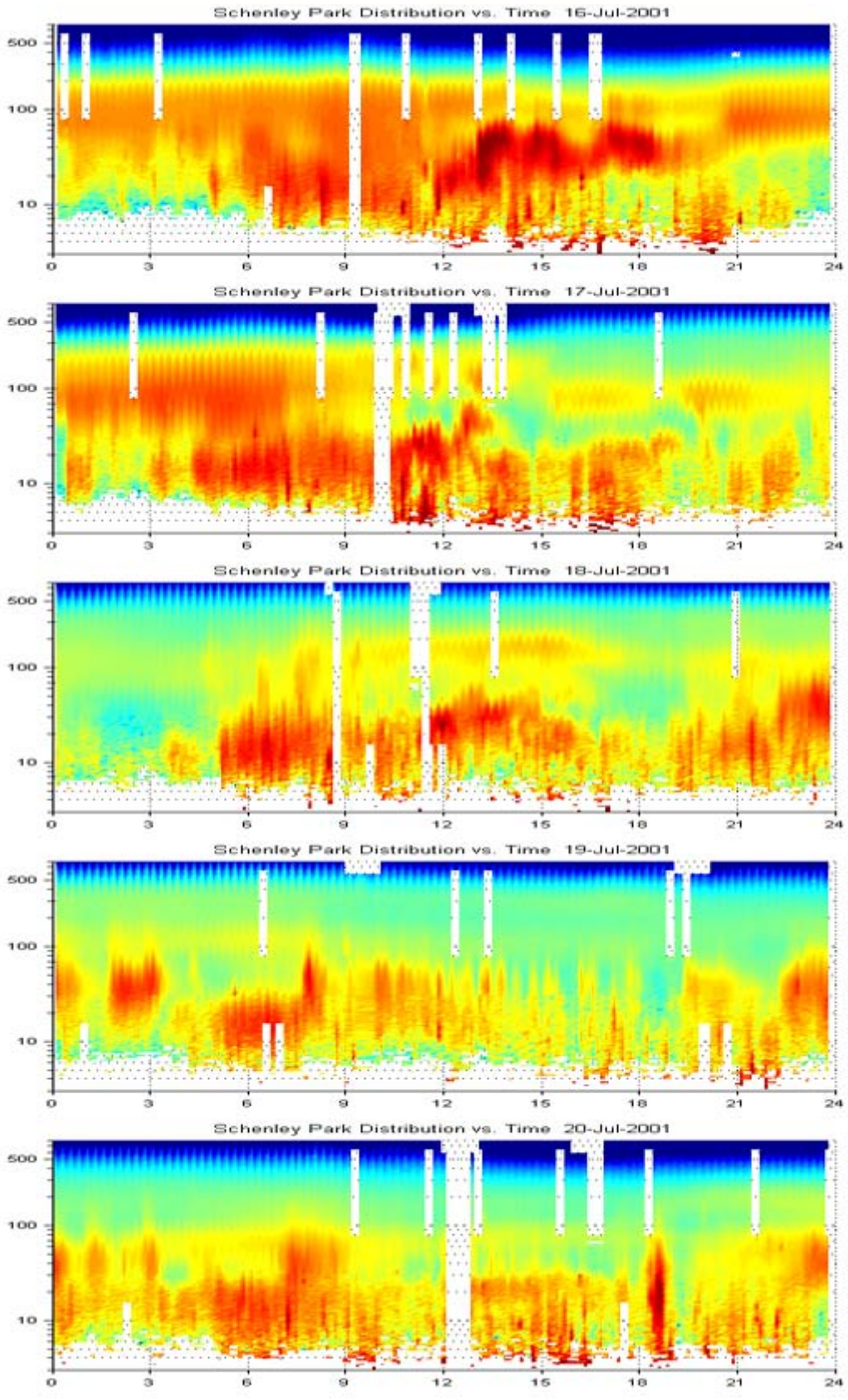
Schenley Park Distribution vs. Time 16-Jul-2001
Schenley Park Distribution vs. Time 17-Jul-2001
Schenley Park Distribution vs. Time 18-Jul-2001
Schenley Park Distribution vs. Time 19-Jul-2001
Schenley Park Distribution vs. Time 20-Jul-2001
500
100
10
0
3
6
9
12
15
18
21
24

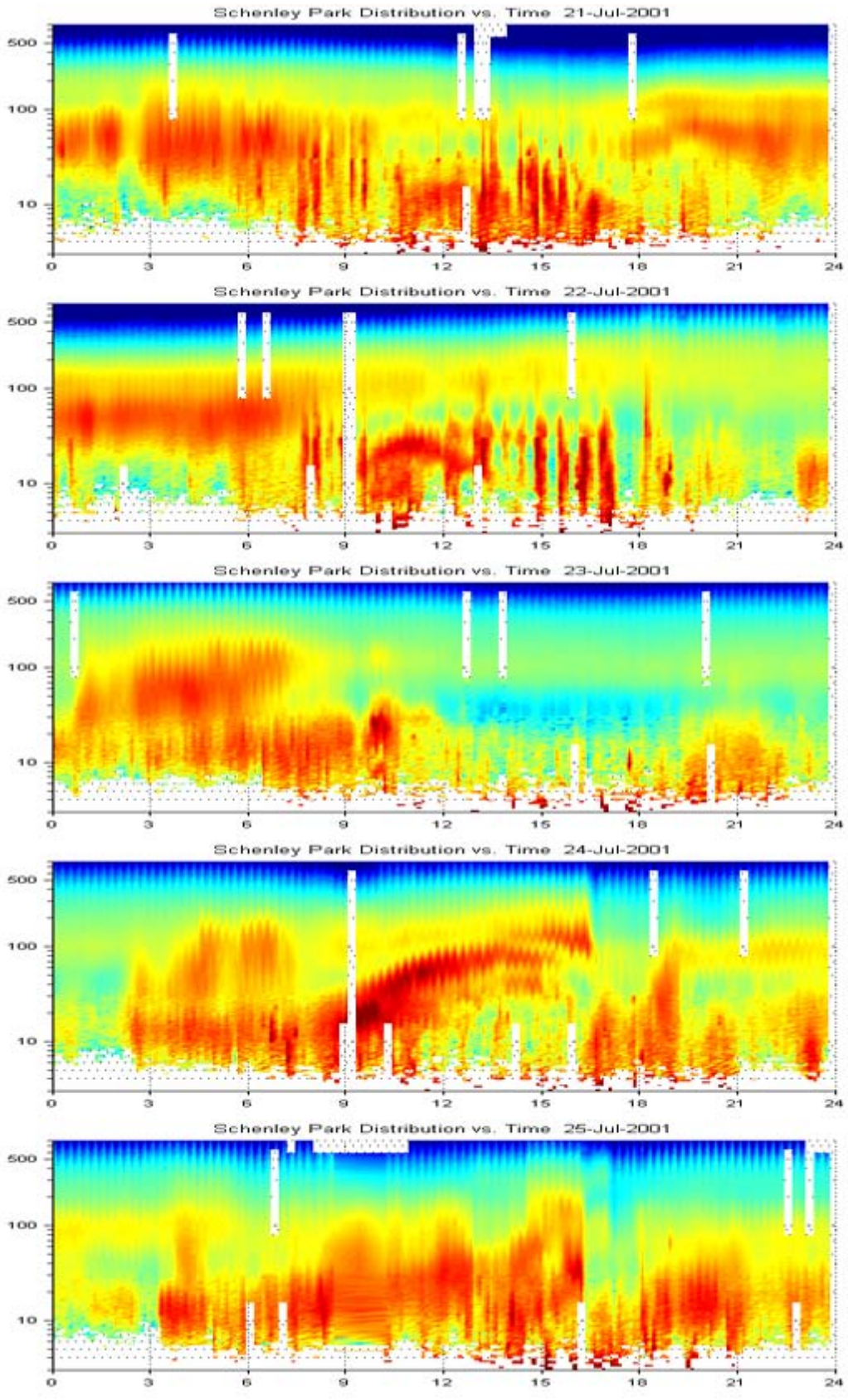
Schenley Park Distribution vs. Time 21-Jul-2001
Schenley Park Distribution vs. Time 22-Jul-2001
Schenley Park Distribution vs. Time 23-Jul-2001
Schenley Park Distribution vs. Time 24-Jul-2001
Schenley Park Distribution vs. Time 25-Jul-2001
500
100
10
0
3
6
9
12
15
18
21
24

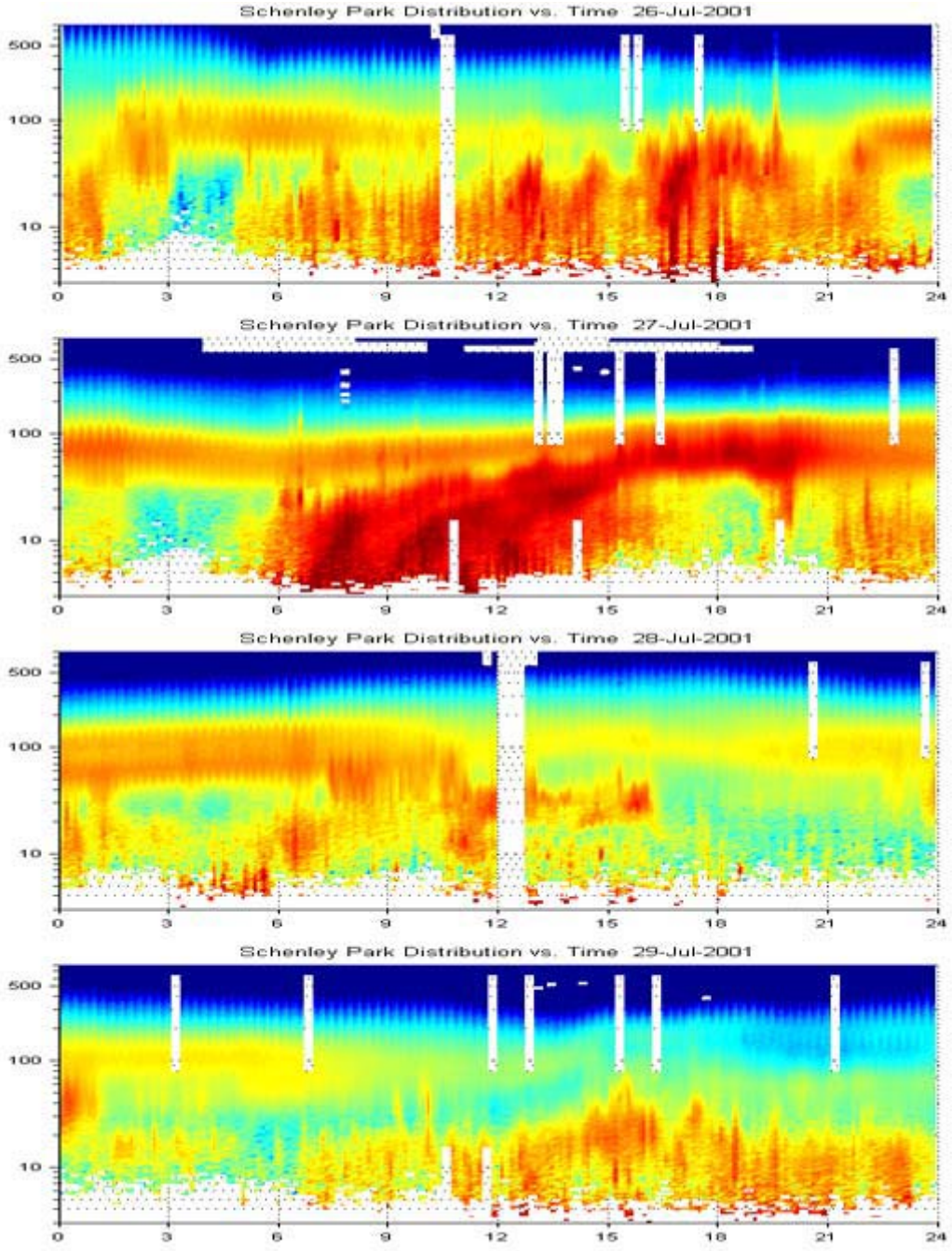
Schenley Park Distribution vs. Time 26-Jul-2001
Schenley Park Distribution vs. Time 27-Jul-2001
Schenley Park Distribution vs. Time 28-Jul-2001
Schenley Park Distribution vs. Time 29-Jul-2001
500
100
10
0
3
6
9
12
15
18
21
24

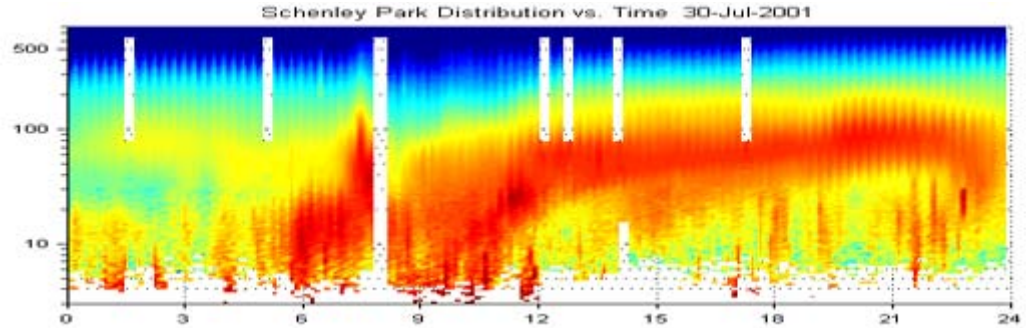
Schenley Park Distribution vs. Time 30-Jul-2001
500
100
10
0
3
6
9
12
15
18
21
24

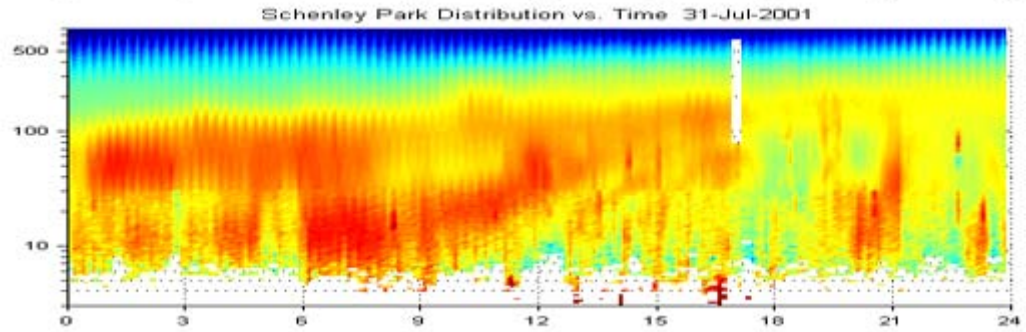
Schenley Park Distribution vs. Time 31-Jul-2001
500
100
10
0
3
6
9
12
15
18
21
24

AUGUST 2001

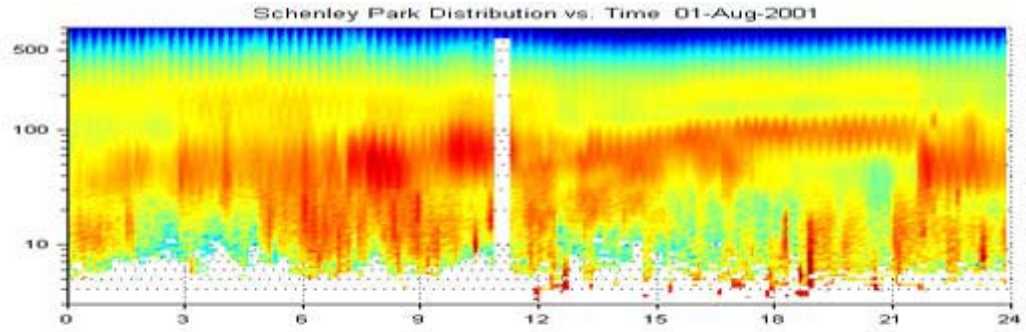
Schenley Park Distribution vs. Time 01-Aug-2001
500
100
10
0
3
6
9
12
15
18
21
24

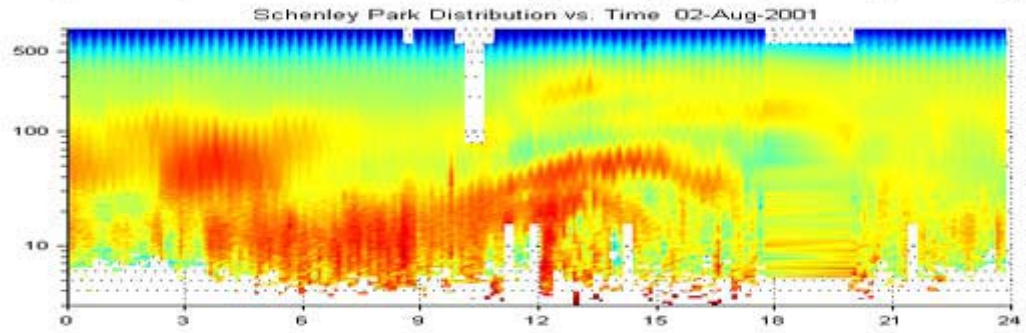
Schenley Park Distribution vs. Time 02-Aug-2001
500
100
10
0
3
6
9
12
15
18
21
24

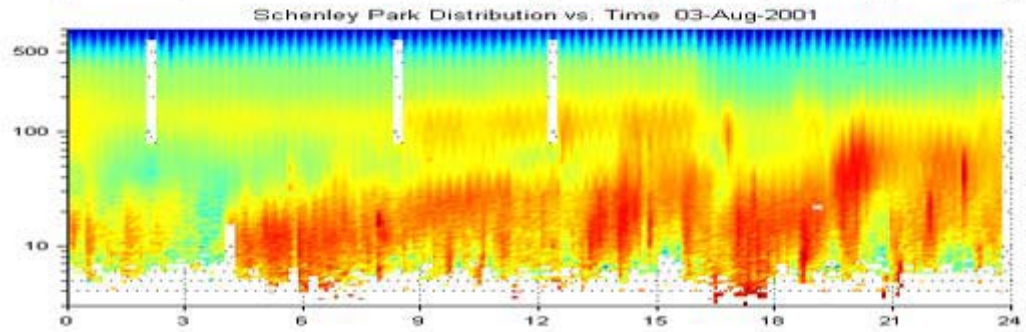
Schenley Park Distribution vs. Time 03-Aug-2001
500
100
10
0
3
6
9
12
15
18
21
24

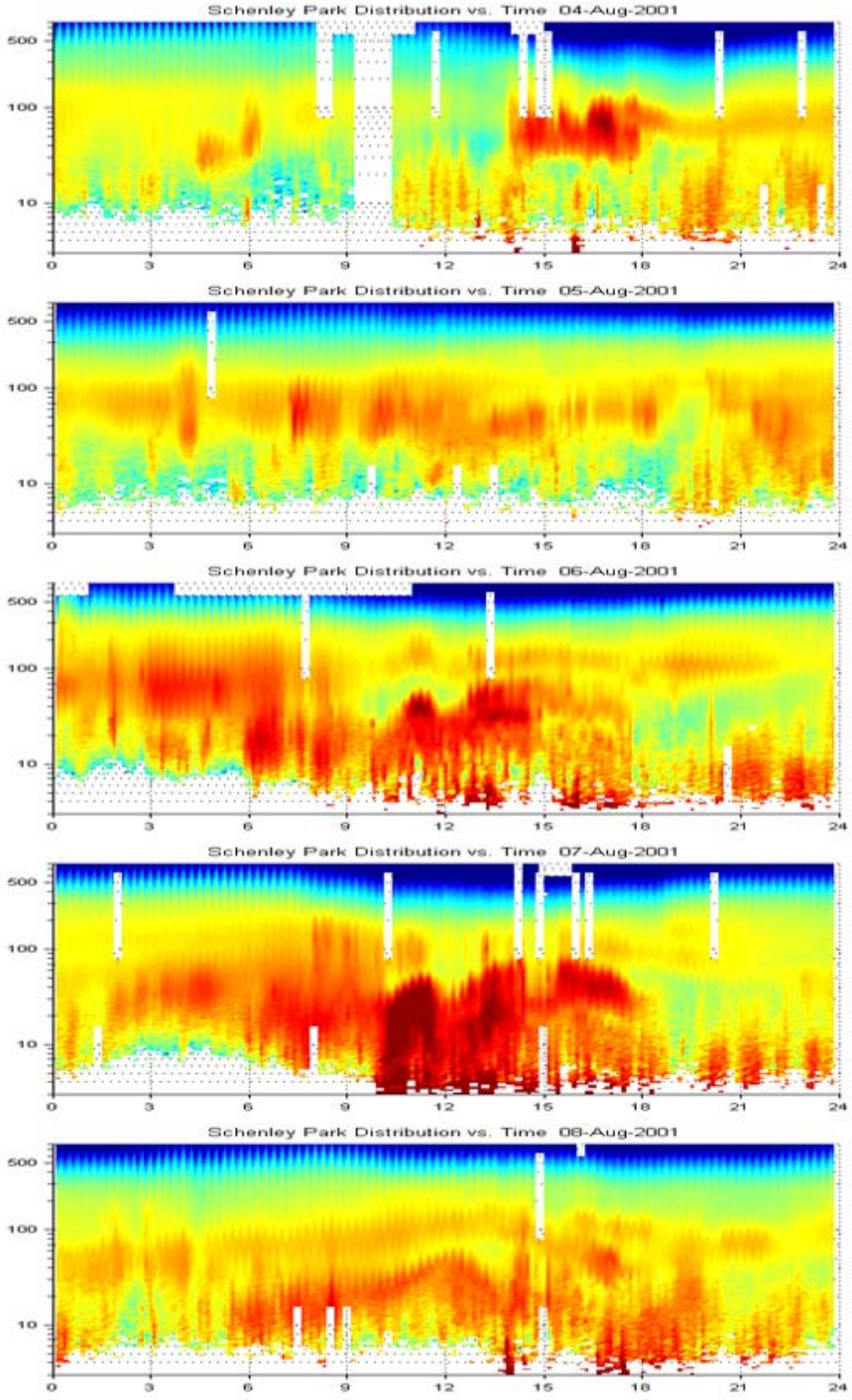
Schenley Park Distribution vs. Time 04-Aug-2001
Schenley Park Distribution vs. Time 05-Aug-2001
Schenley Park Distribution vs. Time 06-Aug-2001
Schenley Park Distribution vs. Time 07-Aug-2001
Schenley Park Distribution vs. Time 08-Aug-2001
500
100
10
0
3
6
9
12
15
18
21
24

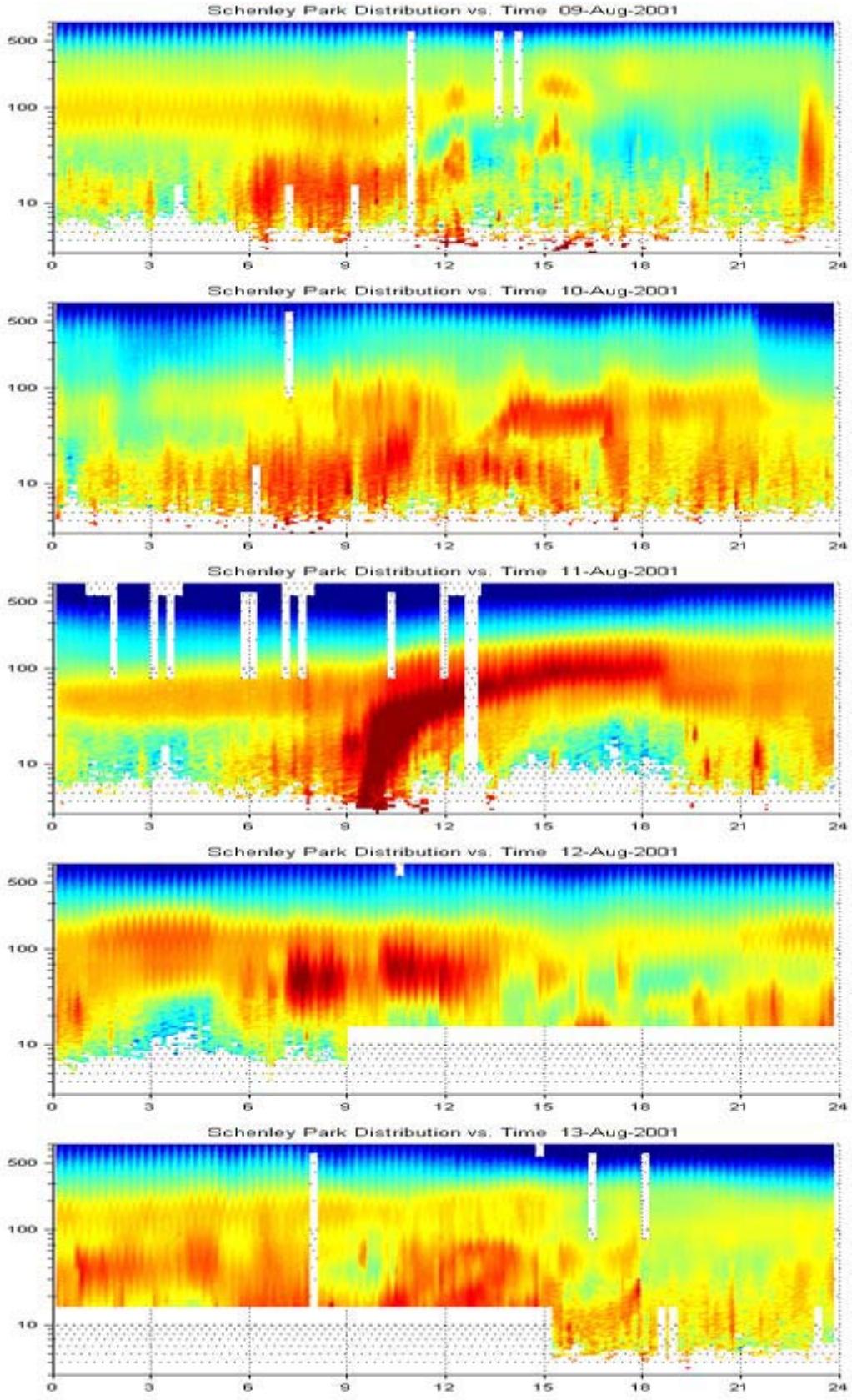
Schenley Park Distribution vs. Time 09-Aug-2001
Schenley Park Distribution vs. Time 10-Aug-2001
Schenley Park Distribution vs. Time 11-Aug-2001
Schenley Park Distribution vs. Time 12-Aug-2001
Schenley Park Distribution vs. Time 13-Aug-2001
500
100
10
0
3
6
9
12
15
18
21
24

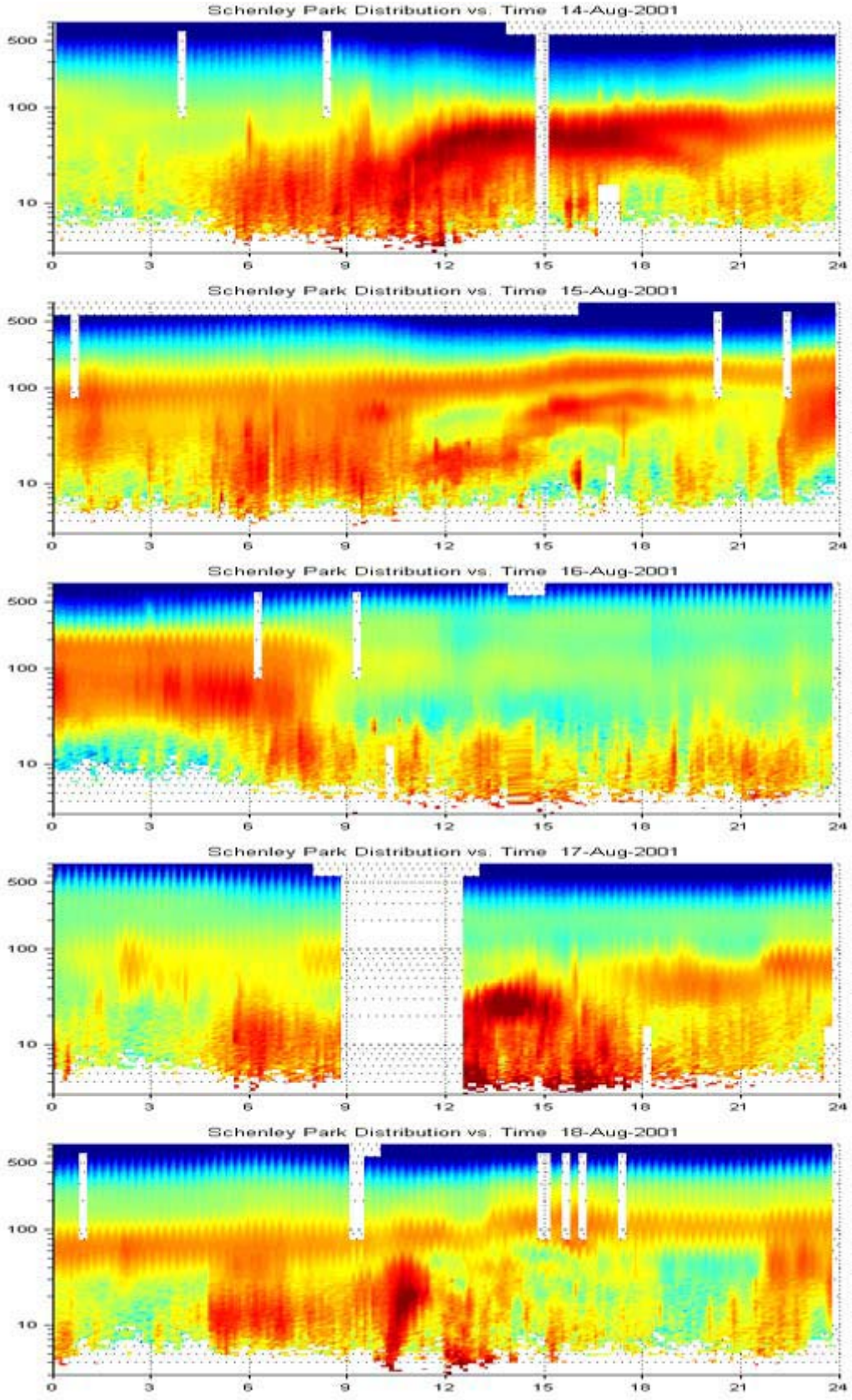
Schenley Park Distribution vs. Time 14-Aug-2001
Schenley Park Distribution vs. Time 15-Aug-2001
Schenley Park Distribution vs. Time 16-Aug-2001
Schenley Park Distribution vs. Time 17-Aug-2001
Schenley Park Distribution vs. Time 18-Aug-2001
500
100
10
0
3
6
9
12
15
18
21
24

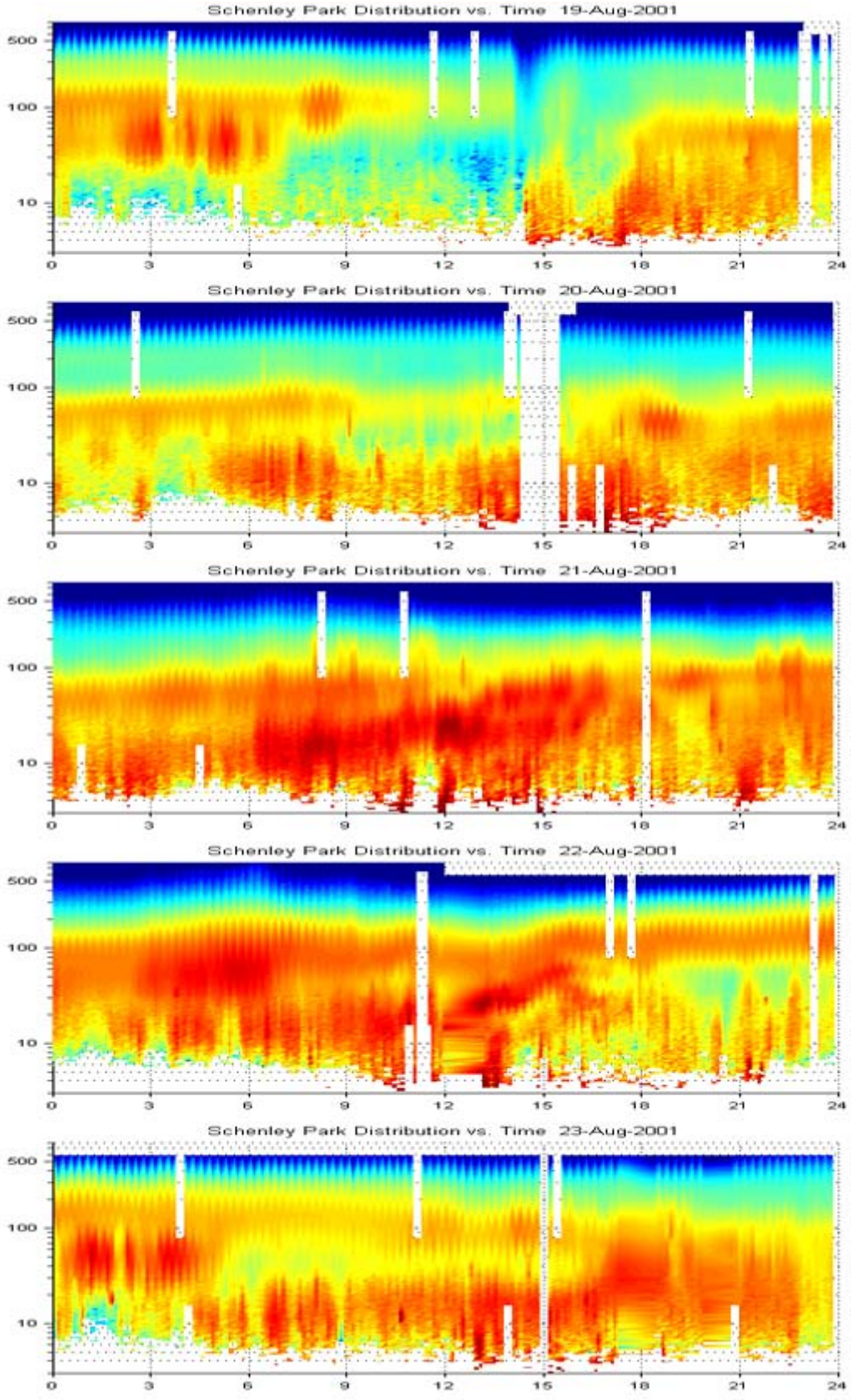
Schenley Park Distribution vs. Time 19-Aug-2001
Schenley Park Distribution vs. Time 20-Aug-2001
Schenley Park Distribution vs. Time 21-Aug-2001
Schenley Park Distribution vs. Time 22-Aug-2001
Schenley Park Distribution vs. Time 23-Aug-2001
500
100
10
0
3
6
9
12
15
18
21
24

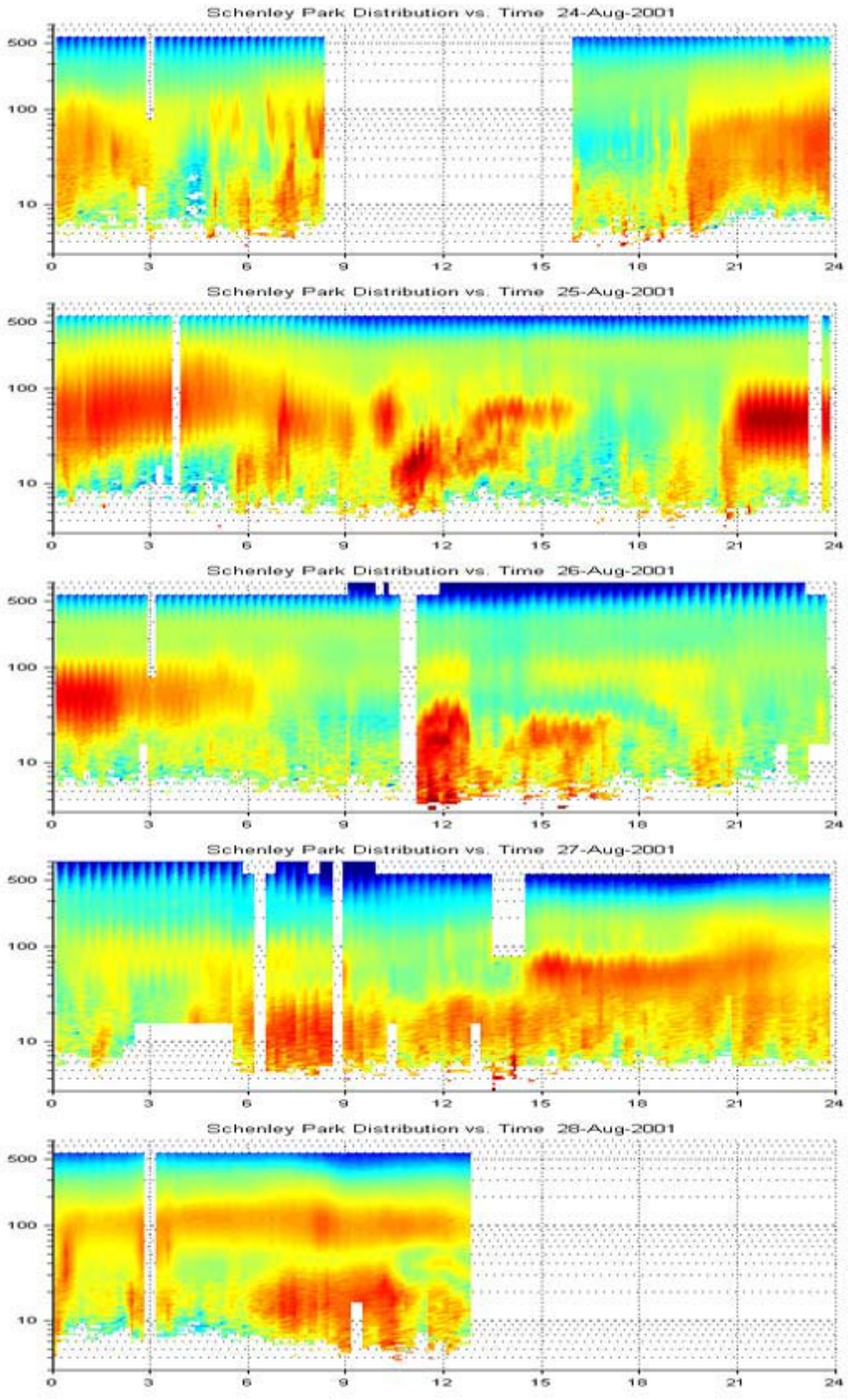
Schenley Park Distribution vs. Time 24-Aug-2001
Schenley Park Distribution vs. Time 25-Aug-2001
Schenley Park Distribution vs. Time 26-Aug-2001
Schenley Park Distribution vs. Time 27-Aug-2001
Schenley Park Distribution vs. Time 28-Aug-2001
500
100
10
0
3
6
9
12
15
18
21
24

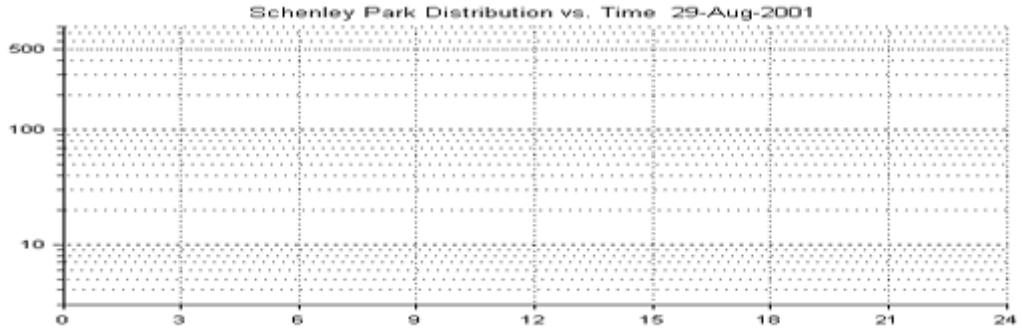

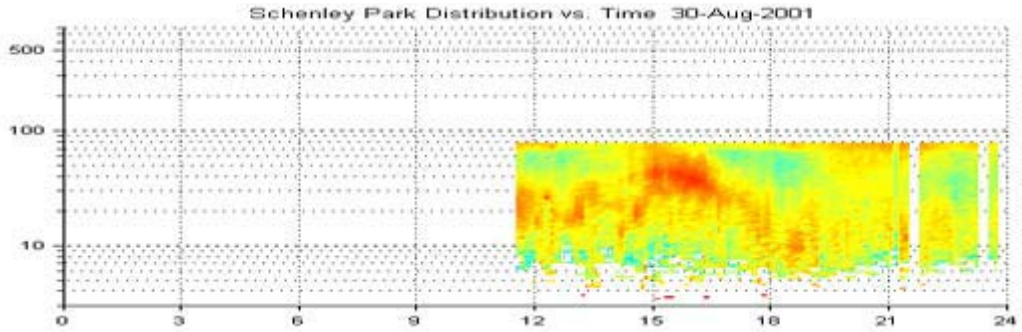

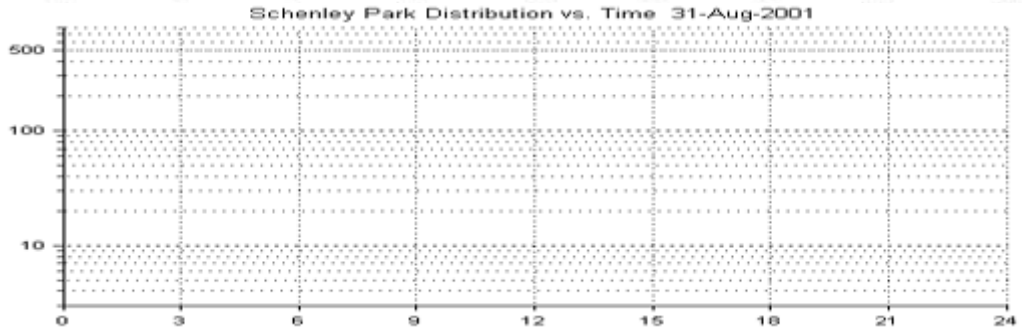

SEPTEMBER 2001

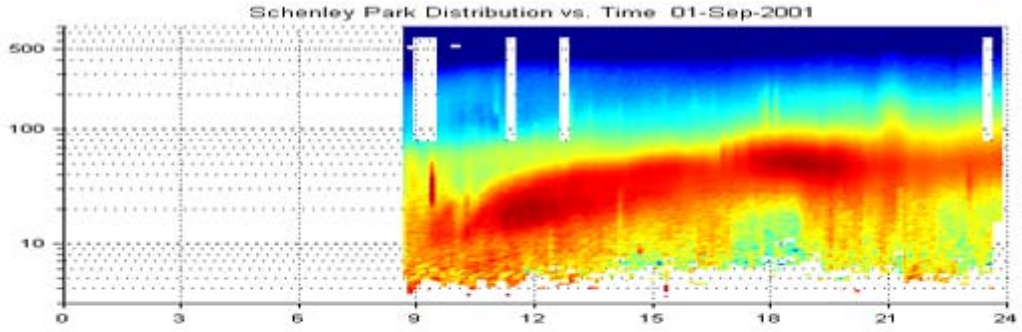

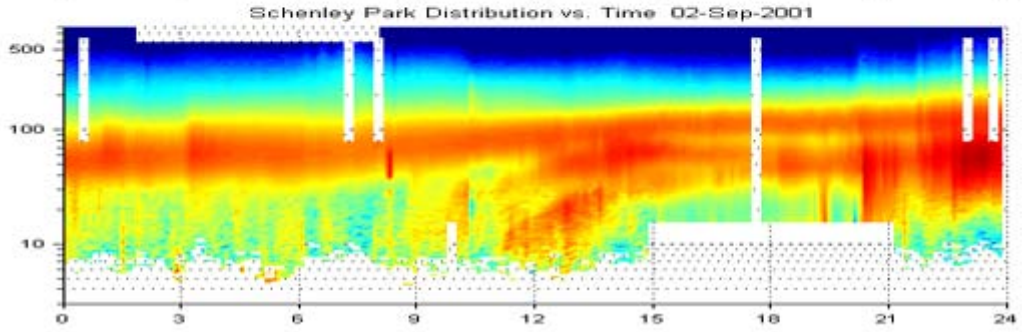

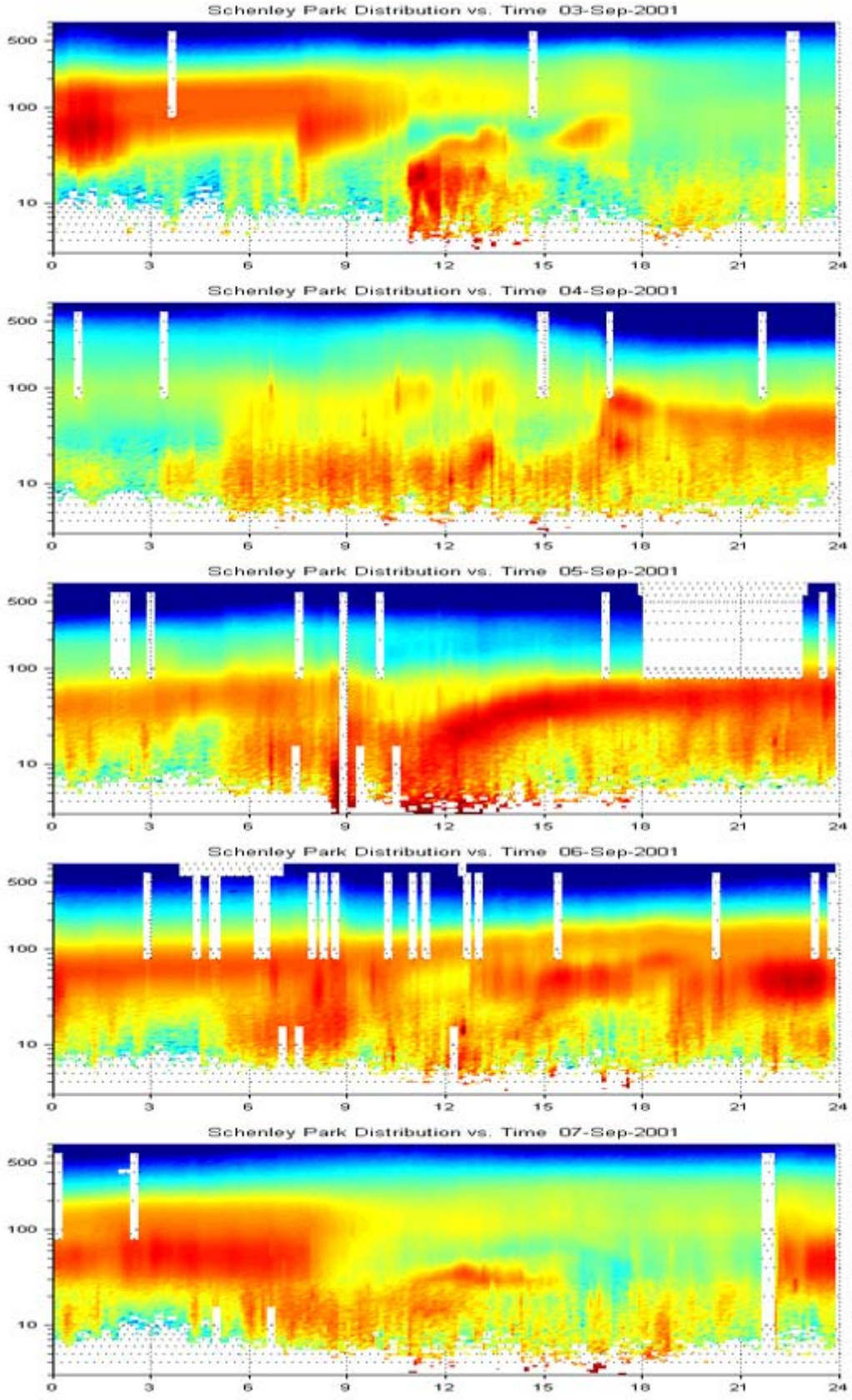
Schenley Park Distribution vs. Time 03-Sep-2001
Schenley Park Distribution vs. Time 04-Sep-2001
Schenley Park Distribution vs. Time 05-Sep-2001
Schenley Park Distribution vs. Time 06-Sep-2001
Schenley Park Distribution vs. Time 07-Sep-2001
500
100
10
0
3
6
9
12
15
18
21
24

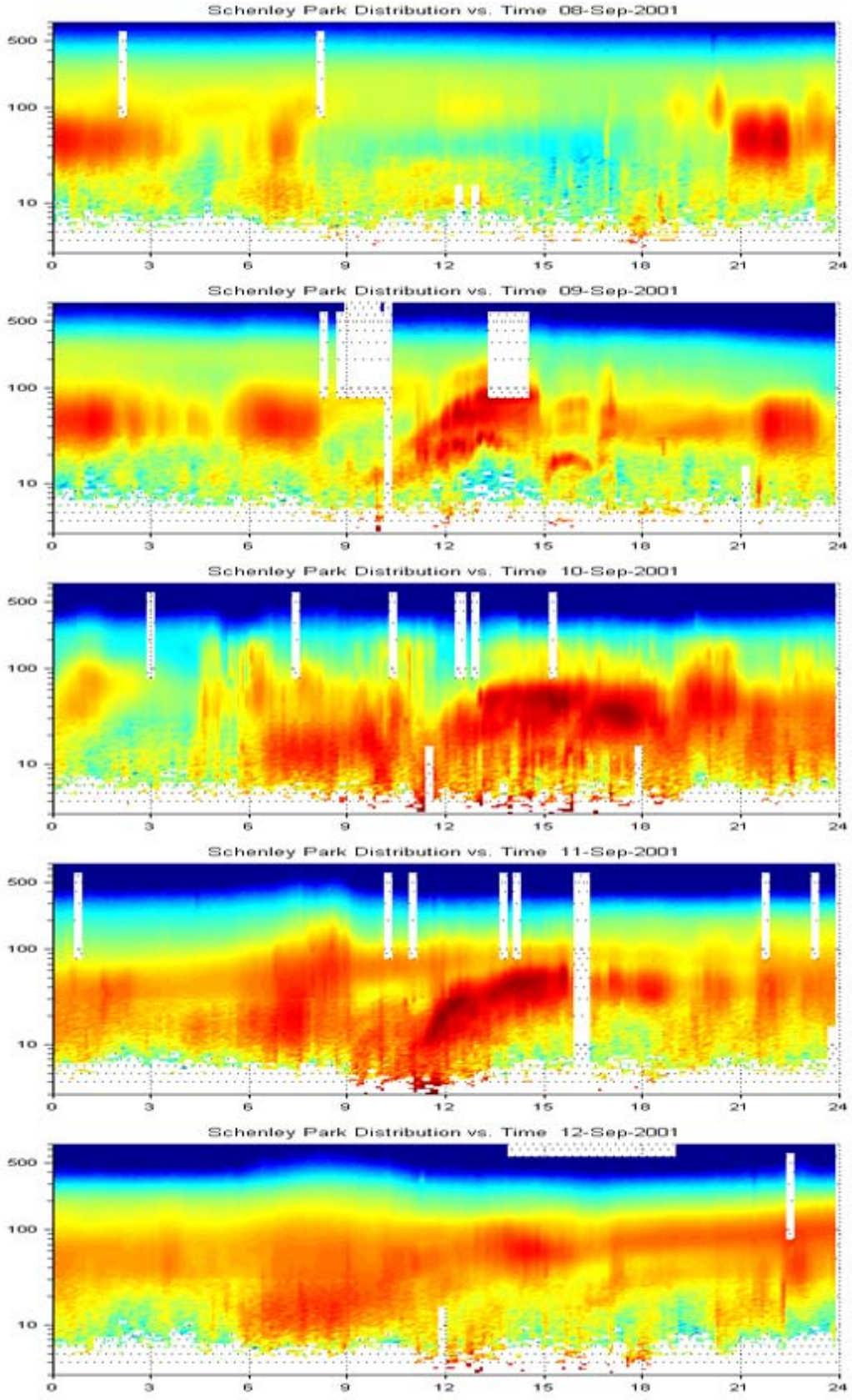
Schenley Park Distribution vs. Time 08-Sep-2001
Schenley Park Distribution vs. Time 09-Sep-2001
Schenley Park Distribution vs. Time 10-Sep-2001
Schenley Park Distribution vs. Time 11-Sep-2001
Schenley Park Distribution vs. Time 12-Sep-2001
500
100
10
0
3
6
9
12
15
18
21
24

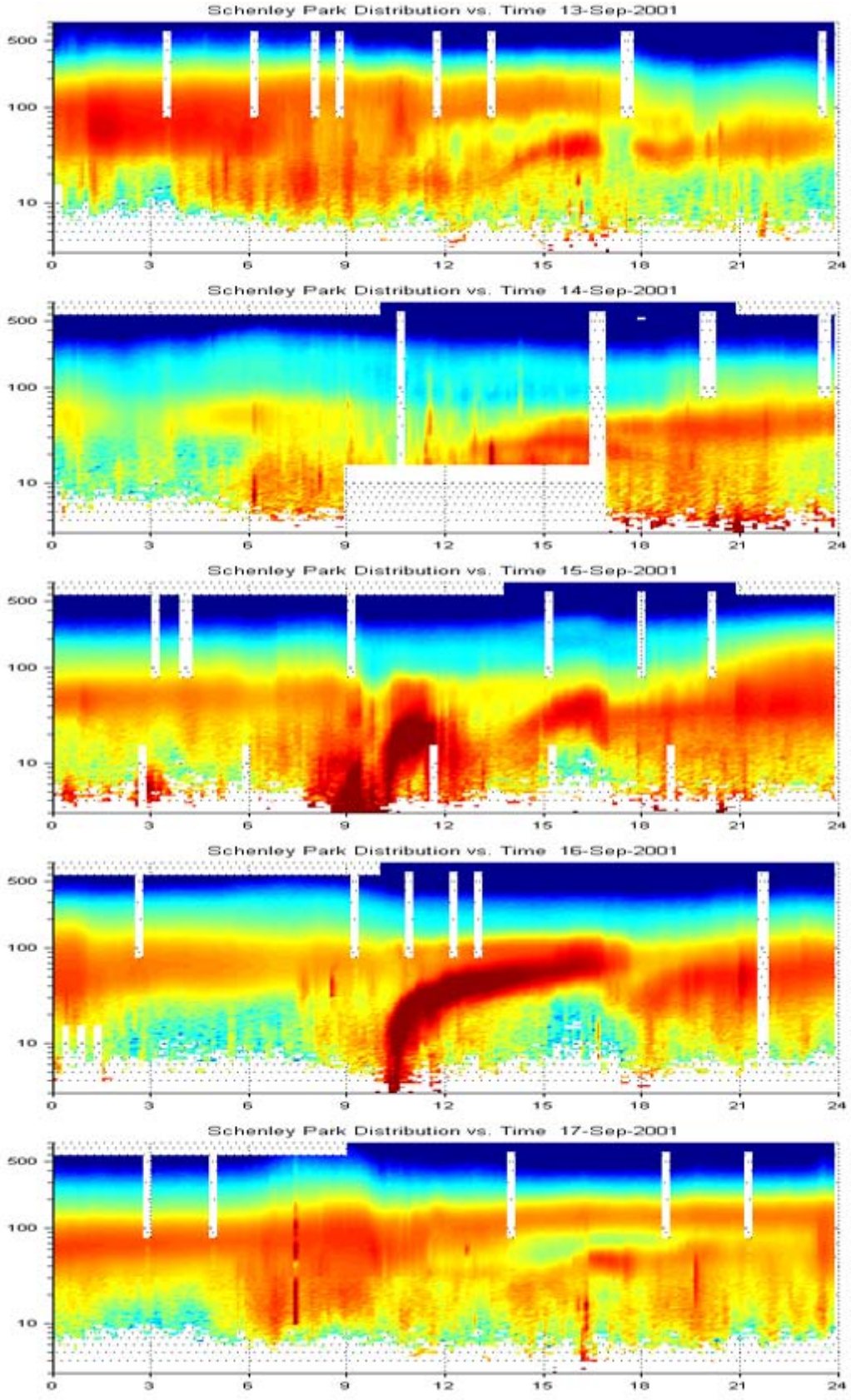
Schenley Park Distribution vs. Time 13-Sep-2001
Schenley Park Distribution vs. Time 14-Sep-2001
Schenley Park Distribution vs. Time 15-Sep-2001
Schenley Park Distribution vs. Time 16-Sep-2001
Schenley Park Distribution vs. Time 17-Sep-2001
500
100
10
0
3
6
9
12
15
18
21
24

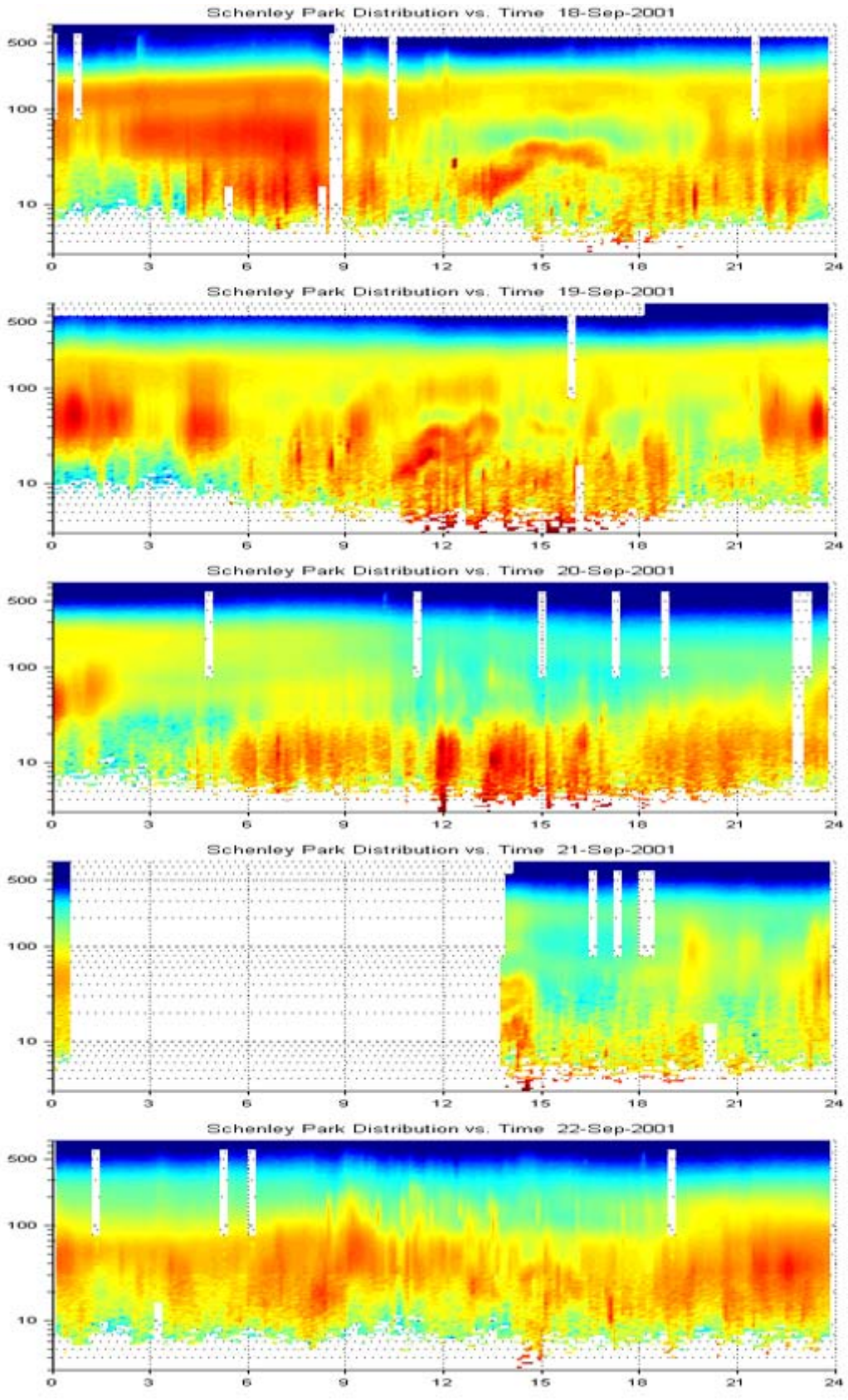
Schenley Park Distribution vs. Time 18-Sep-2001
Schenley Park Distribution vs. Time 19-Sep-2001
Schenley Park Distribution vs. Time 20-Sep-2001
Schenley Park Distribution vs. Time 21-Sep-2001
Schenley Park Distribution vs. Time 22-Sep-2001
500
100
10
0
3
6
9
12
15
18
21
24

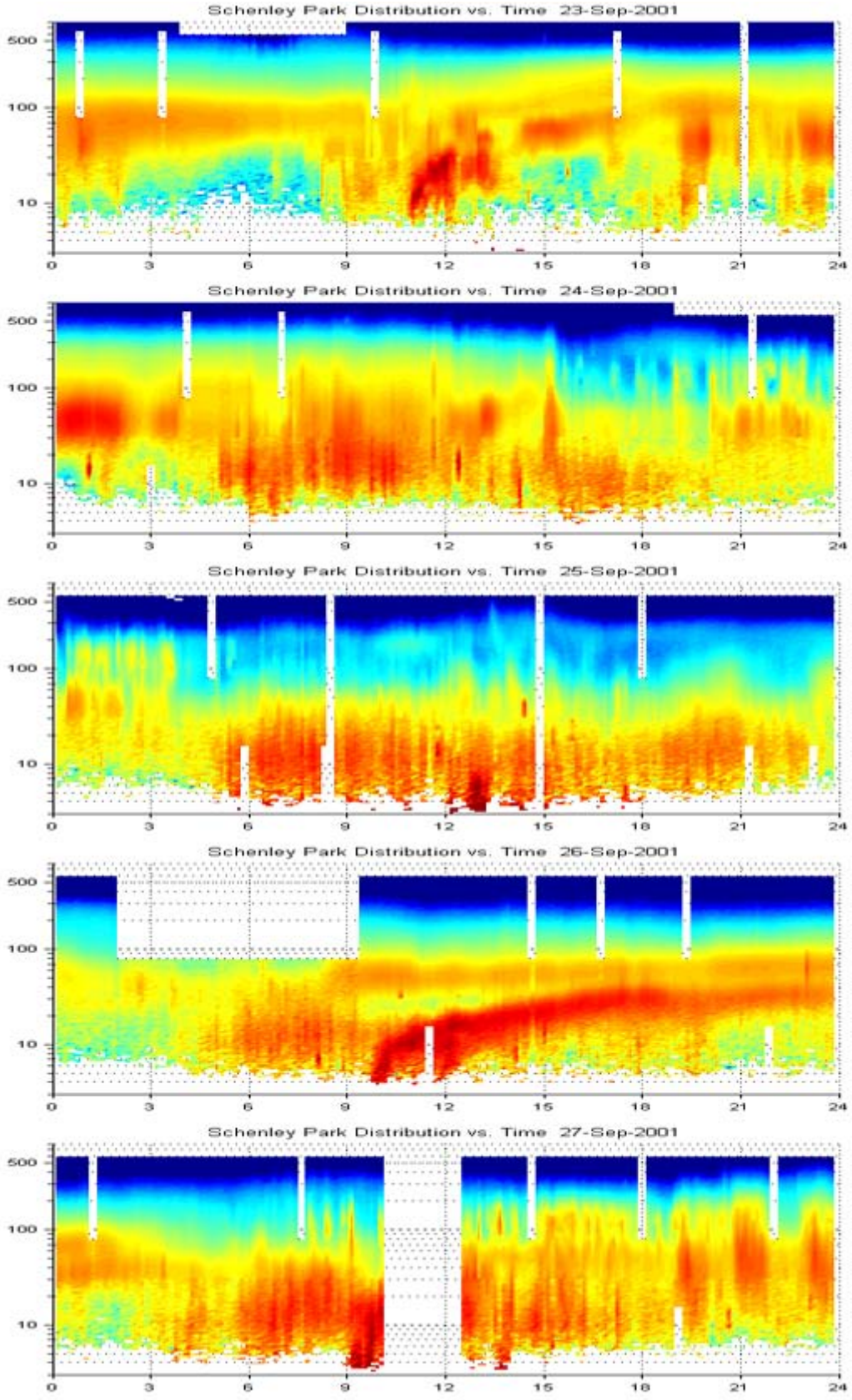
Schenley Park Distribution vs. Time 23-Sep-2001
Schenley Park Distribution vs. Time 24-Sep-2001
Schenley Park Distribution vs. Time 25-Sep-2001
Schenley Park Distribution vs. Time 26-Sep-2001
Schenley Park Distribution vs. Time 27-Sep-2001
500
100
10
0
3
6
9
12
15
18
21
24

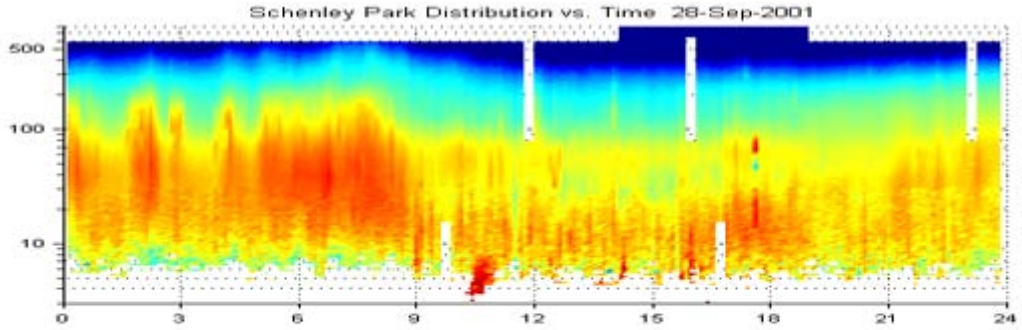

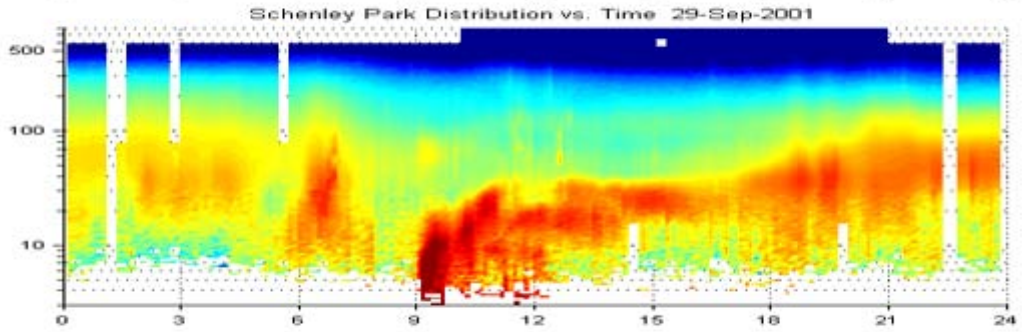

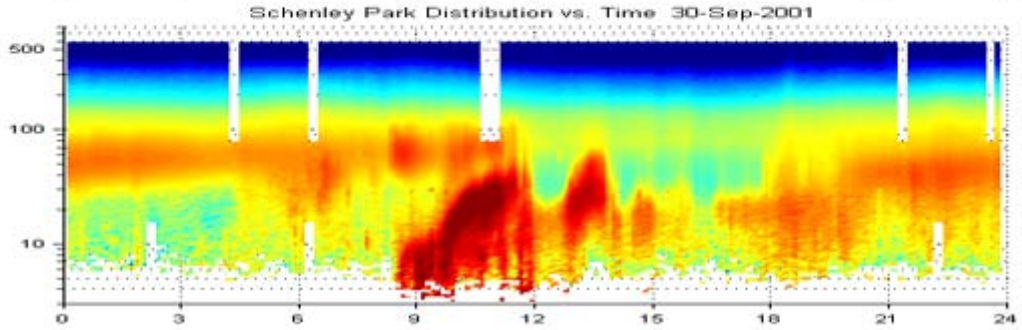

OCTOBER 2001

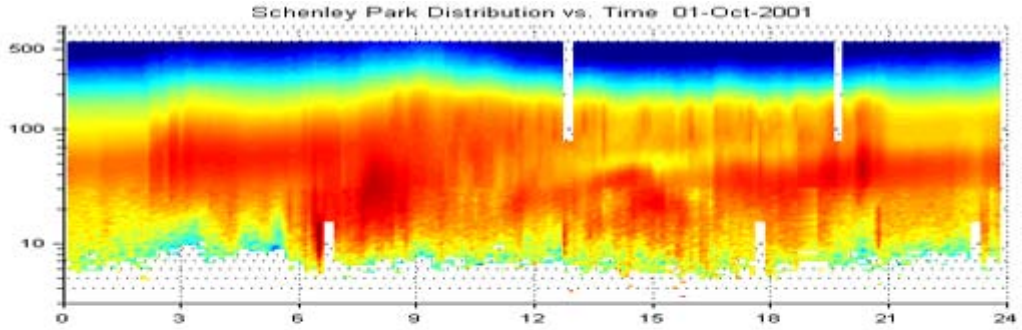

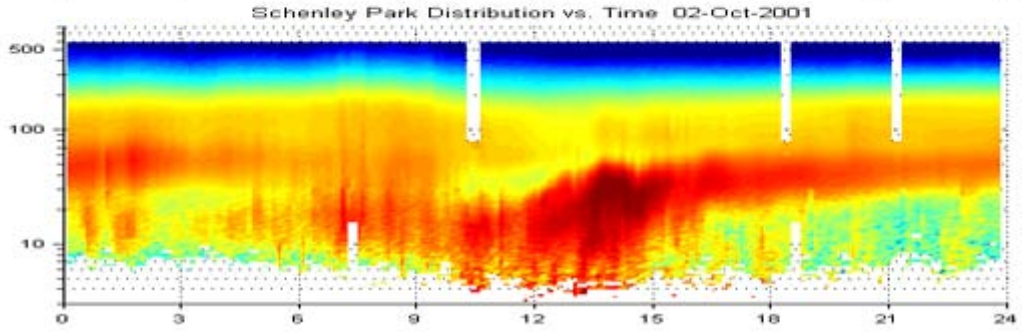

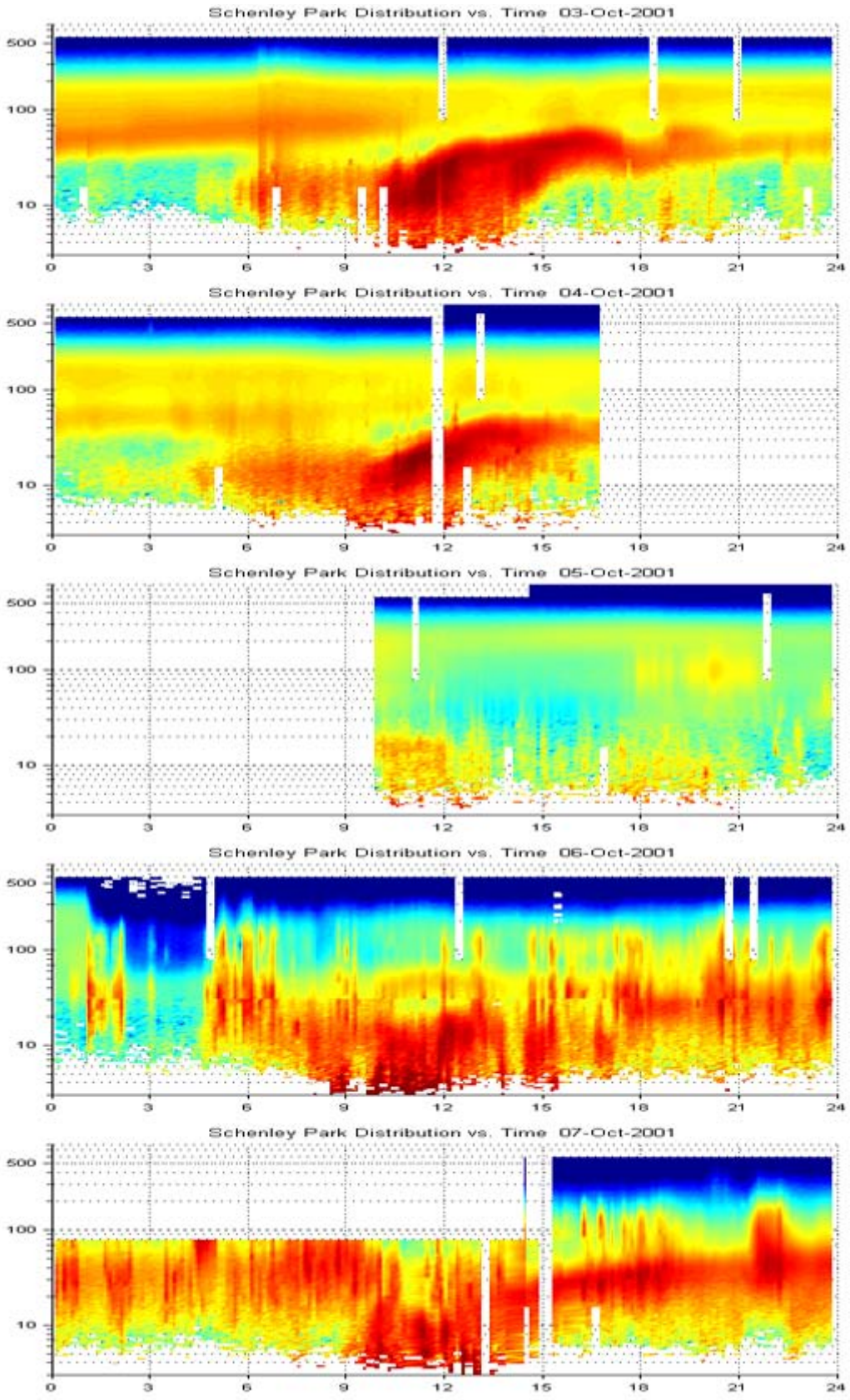
Schenley Park Distribution vs. Time 03-Oct-2001
Schenley Park Distribution vs. Time 04-Oct-2001
Schenley Park Distribution vs. Time 05-Oct-2001
Schenley Park Distribution vs. Time 06-Oct-2001
Schenley Park Distribution vs. Time 07-Oct-2001
500
100
10
0
3
6
9
12
15
18
21
24

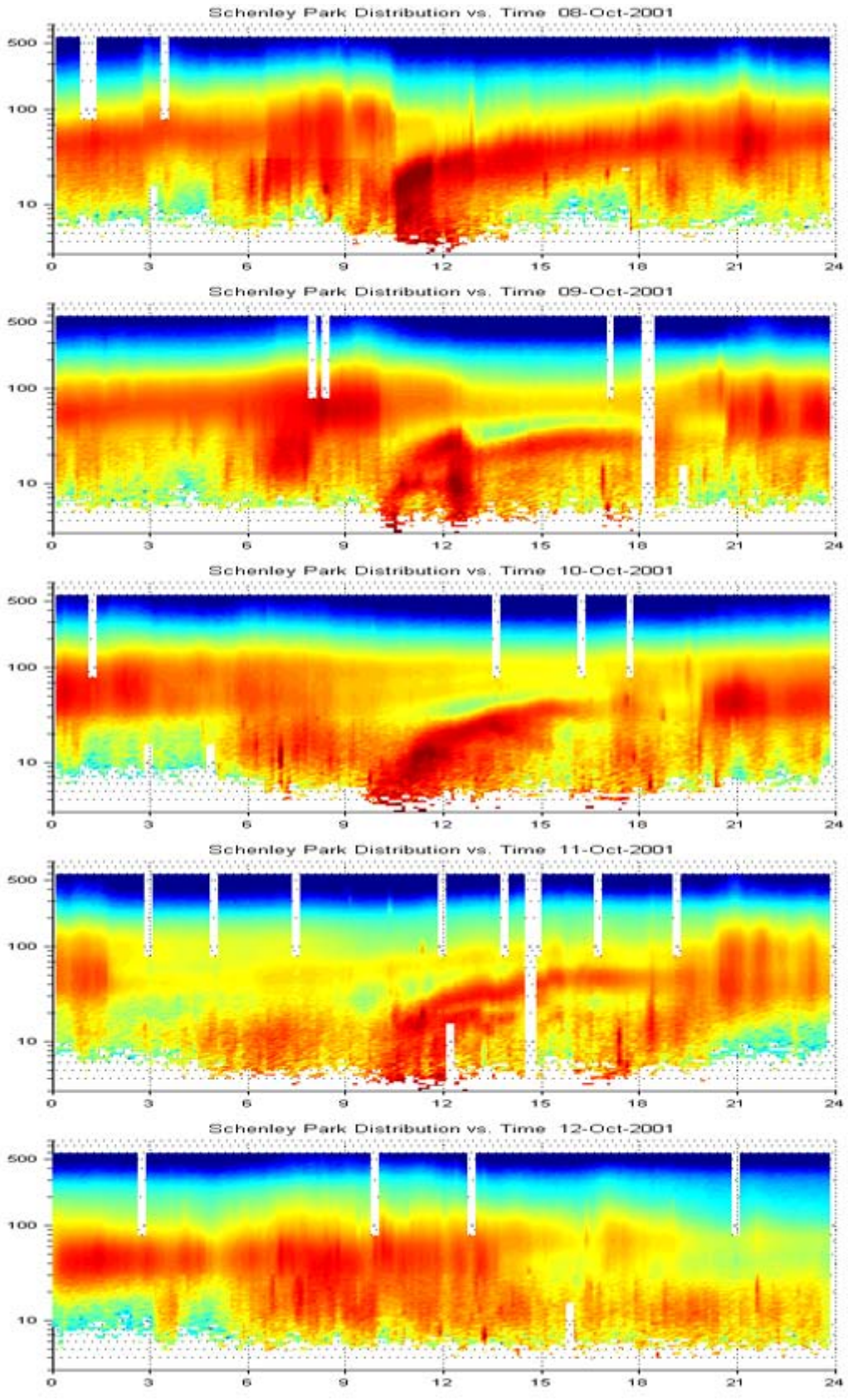
Schenley Park Distribution vs. Time 08-Oct-2001
Schenley Park Distribution vs. Time 09-Oct-2001
Schenley Park Distribution vs. Time 10-Oct-2001
Schenley Park Distribution vs. Time 11-Oct-2001
Schenley Park Distribution vs. Time 12-Oct-2001
500
100
10
0
3
6
9
12
15
18
21
24

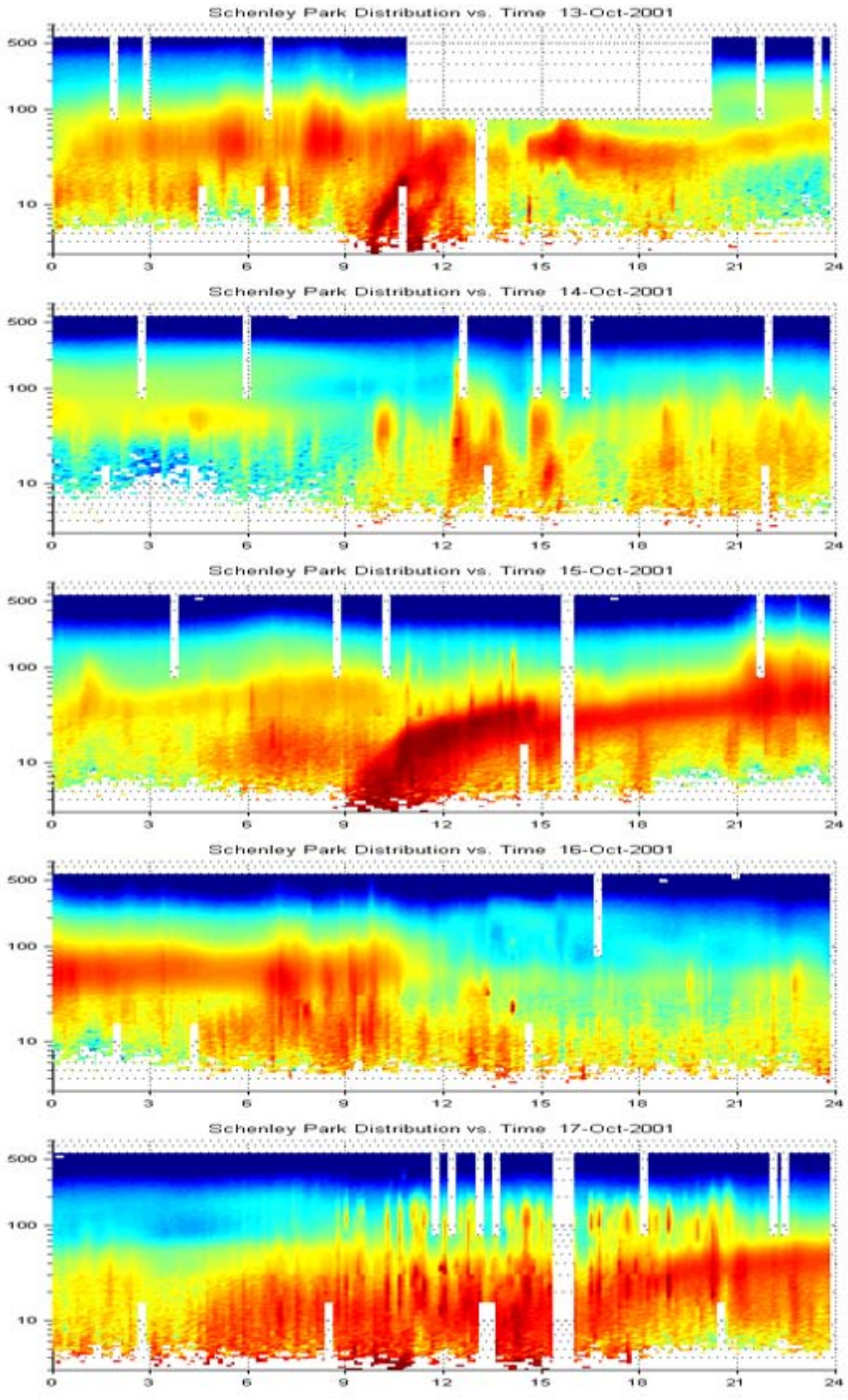
Schenley Park Distribution vs. Time 13-Oct-2001
Schenley Park Distribution vs. Time 14-Oct-2001
Schenley Park Distribution vs. Time 15-Oct-2001
Schenley Park Distribution vs. Time 16-Oct-2001
Schenley Park Distribution vs. Time 17-Oct-2001
500
100
10
0
3
6
9
12
15
18
21
24

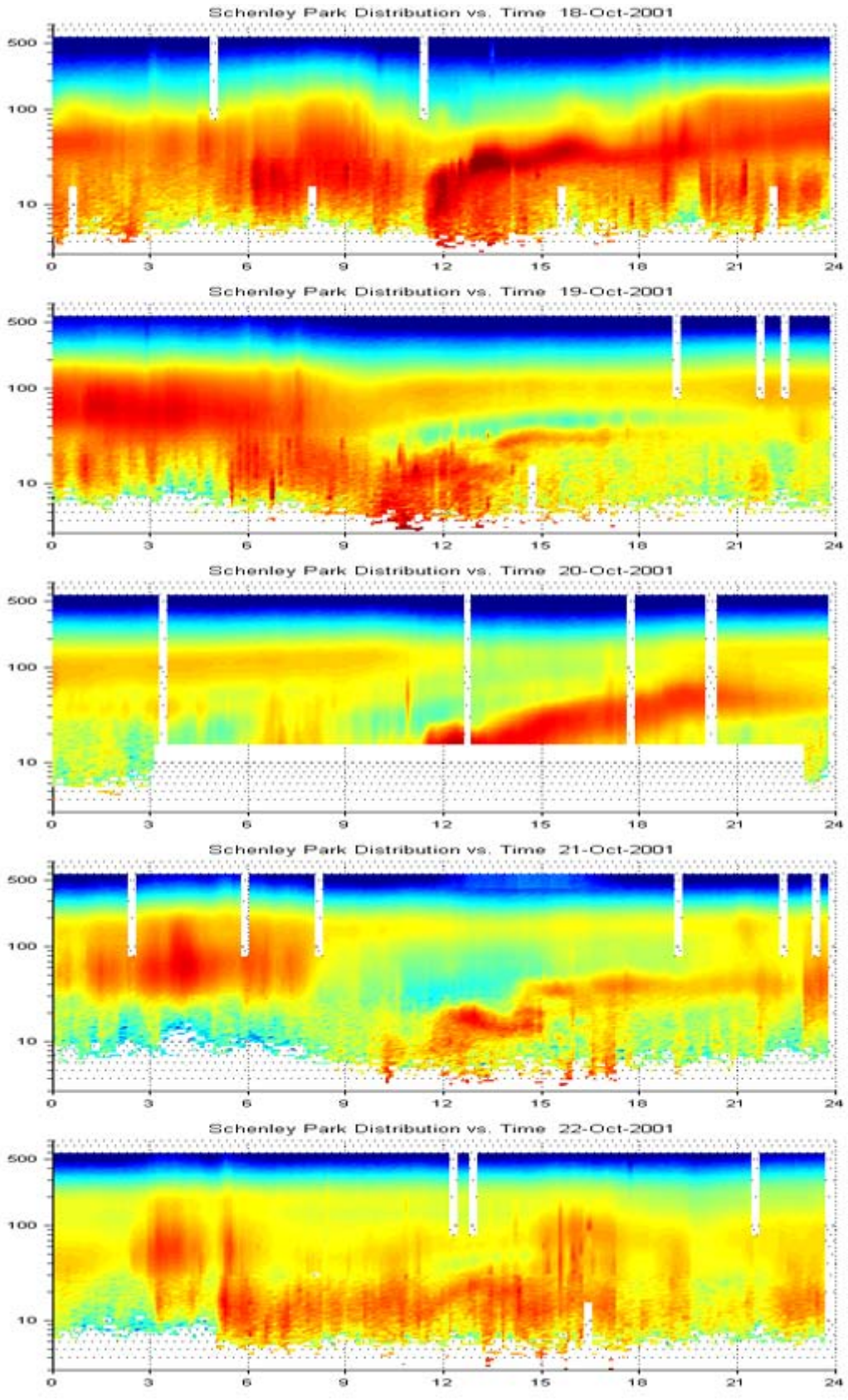
Schenley Park Distribution vs. Time 18-Oct-2001
Schenley Park Distribution vs. Time 19-Oct-2001
Schenley Park Distribution vs. Time 20-Oct-2001
Schenley Park Distribution vs. Time 21-Oct-2001
Schenley Park Distribution vs. Time 22-Oct-2001
500
100
10
0
3
6
9
12
15
18
21
24

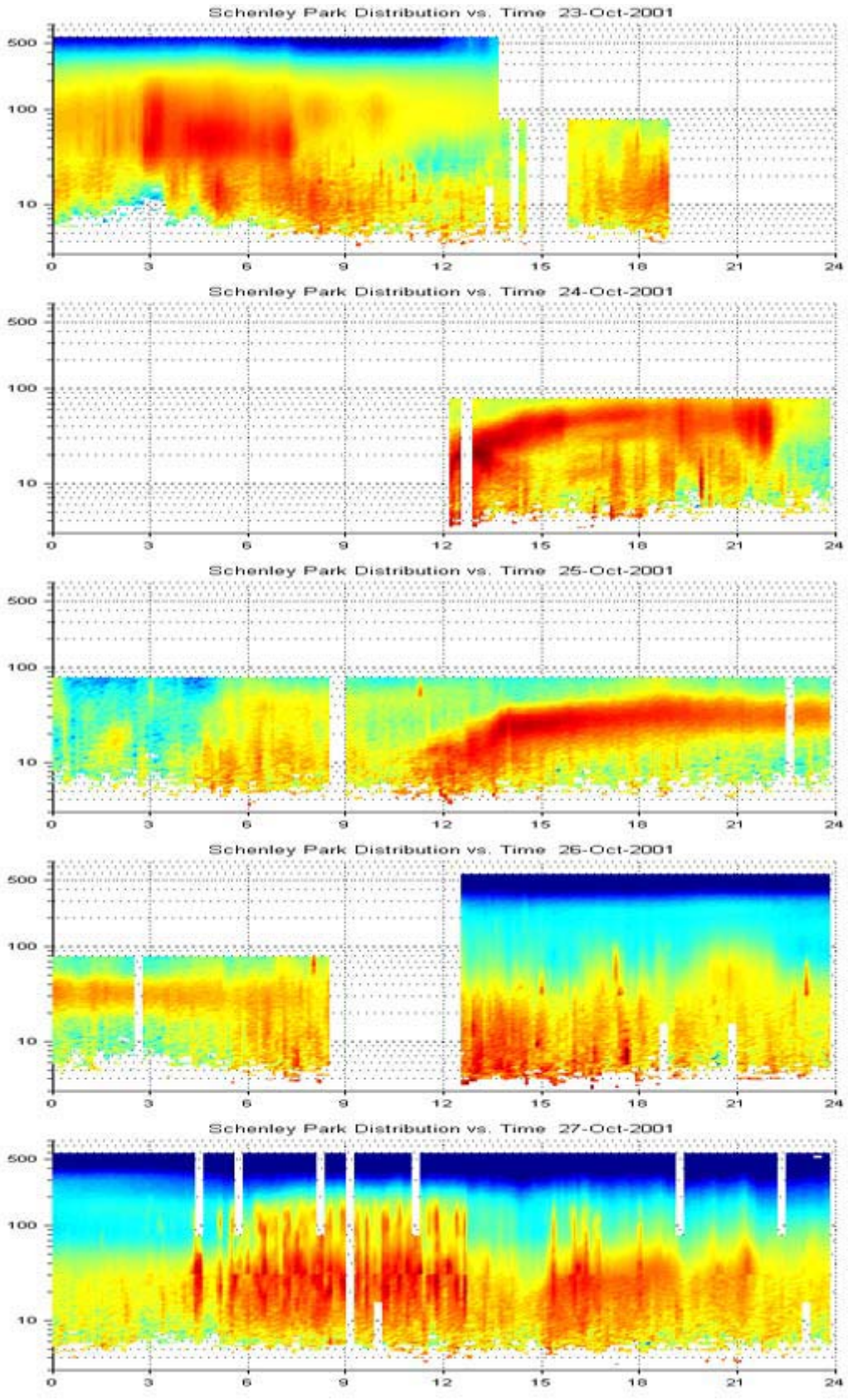
Schenley Park Distribution vs. Time 23-Oct-2001
Schenley Park Distribution vs. Time 24-Oct-2001
Schenley Park Distribution vs. Time 25-Oct-2001
Schenley Park Distribution vs. Time 26-Oct-2001
Schenley Park Distribution vs. Time 27-Oct-2001
500
100
10
0
3
6
9
12
15
18
21
24

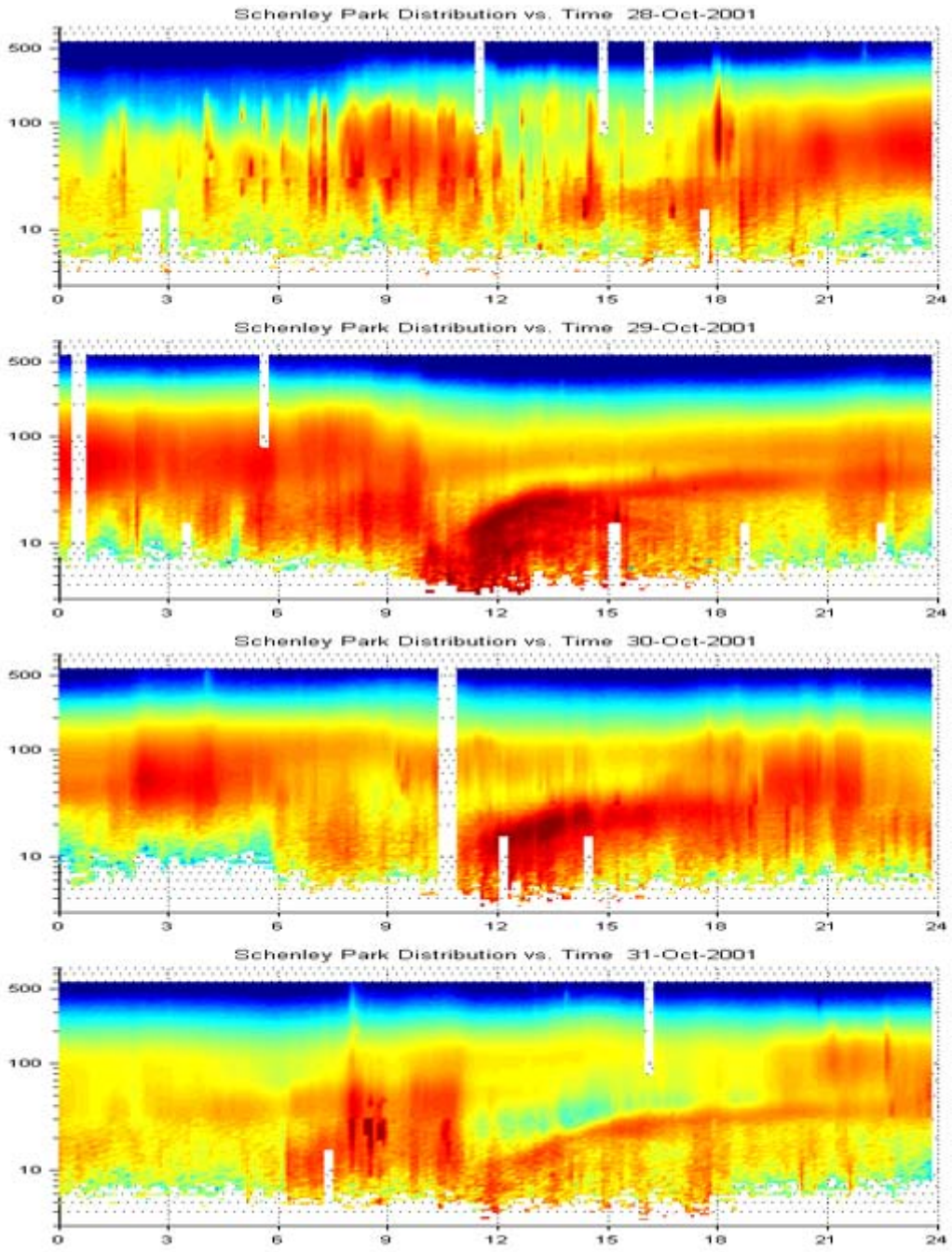

NOVEMBER 2001

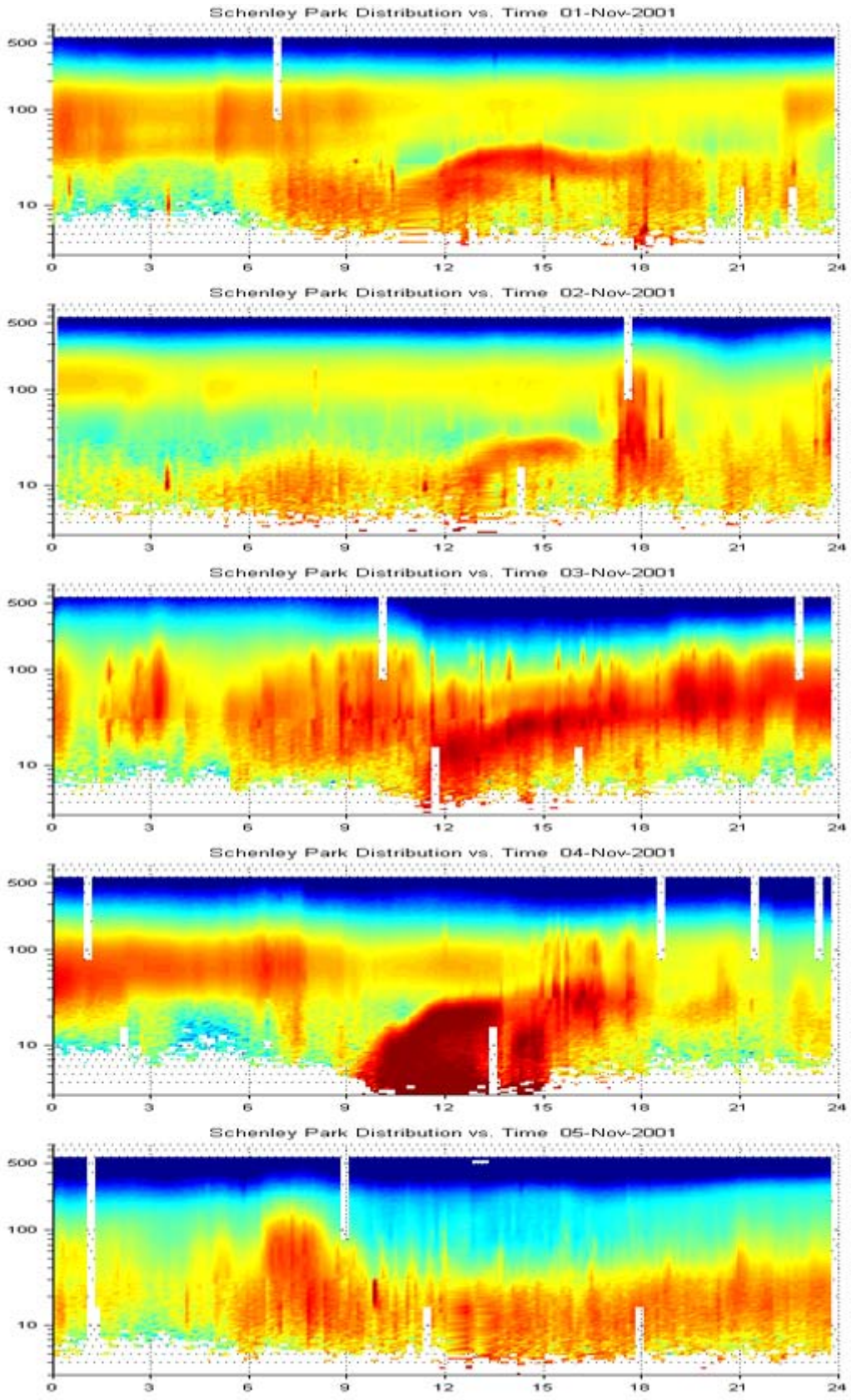
Schenley Park Distribution vs. Time 01-Nov-2001
Schenley Park Distribution vs. Time 02-Nov-2001
Schenley Park Distribution vs. Time 03-Nov-2001
Schenley Park Distribution vs. Time 04-Nov-2001
Schenley Park Distribution vs. Time 05-Nov-2001
500
100
10
0
3
6
9
12
15
18
21
24

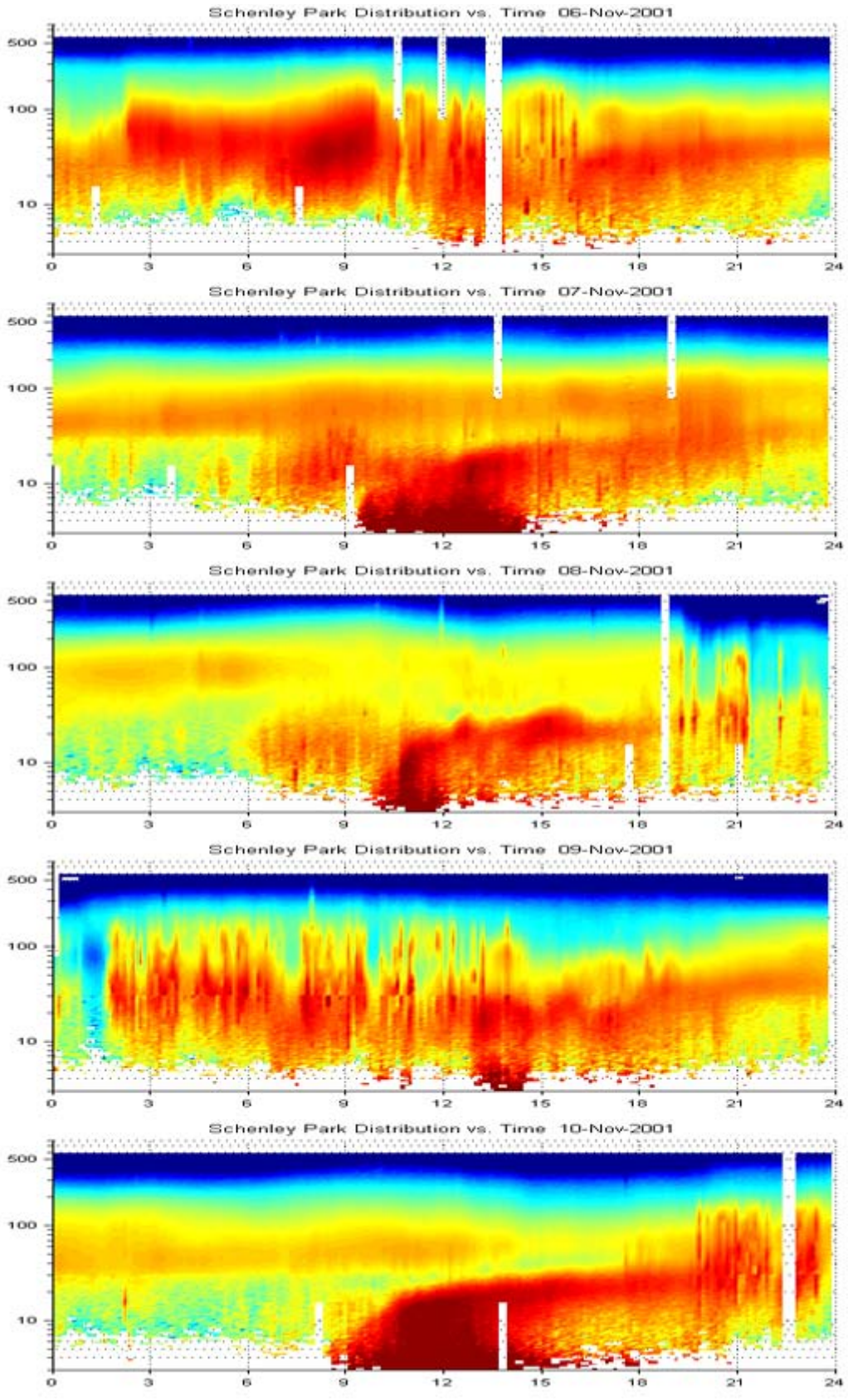
Schenley Park Distribution vs. Time 06-Nov-2001
Schenley Park Distribution vs. Time 07-Nov-2001
Schenley Park Distribution vs. Time 08-Nov-2001
Schenley Park Distribution vs. Time 09-Nov-2001
Schenley Park Distribution vs. Time 10-Nov-2001
500
100
10
0
3
6
9
12
15
18
21
24

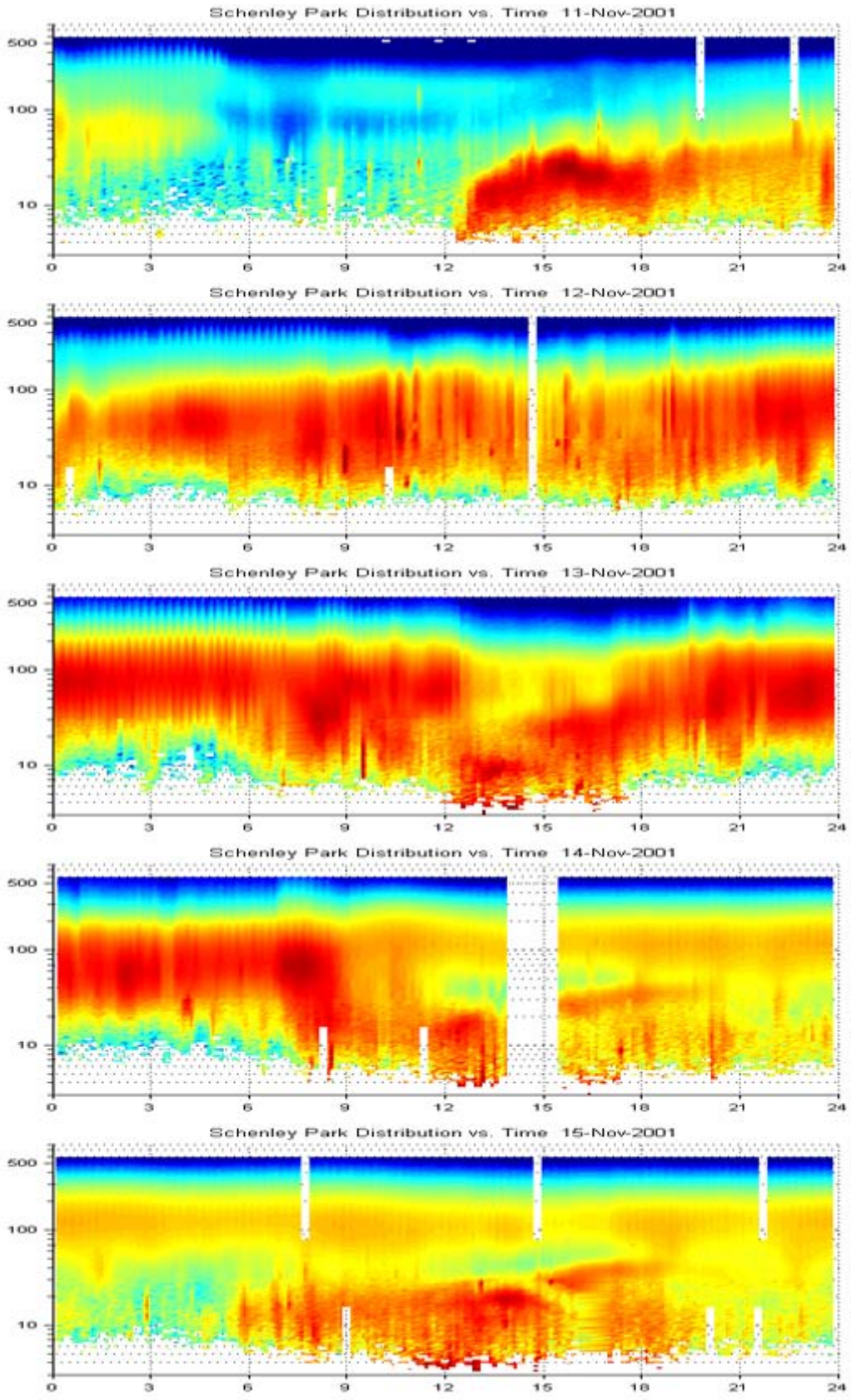
Schenley Park Distribution vs. Time 11-Nov-2001
Schenley Park Distribution vs. Time 12-Nov-2001
Schenley Park Distribution vs. Time 13-Nov-2001
Schenley Park Distribution vs. Time 14-Nov-2001
Schenley Park Distribution vs. Time 15-Nov-2001
500
100
10
0
3
6
9
12
15
18
21
24

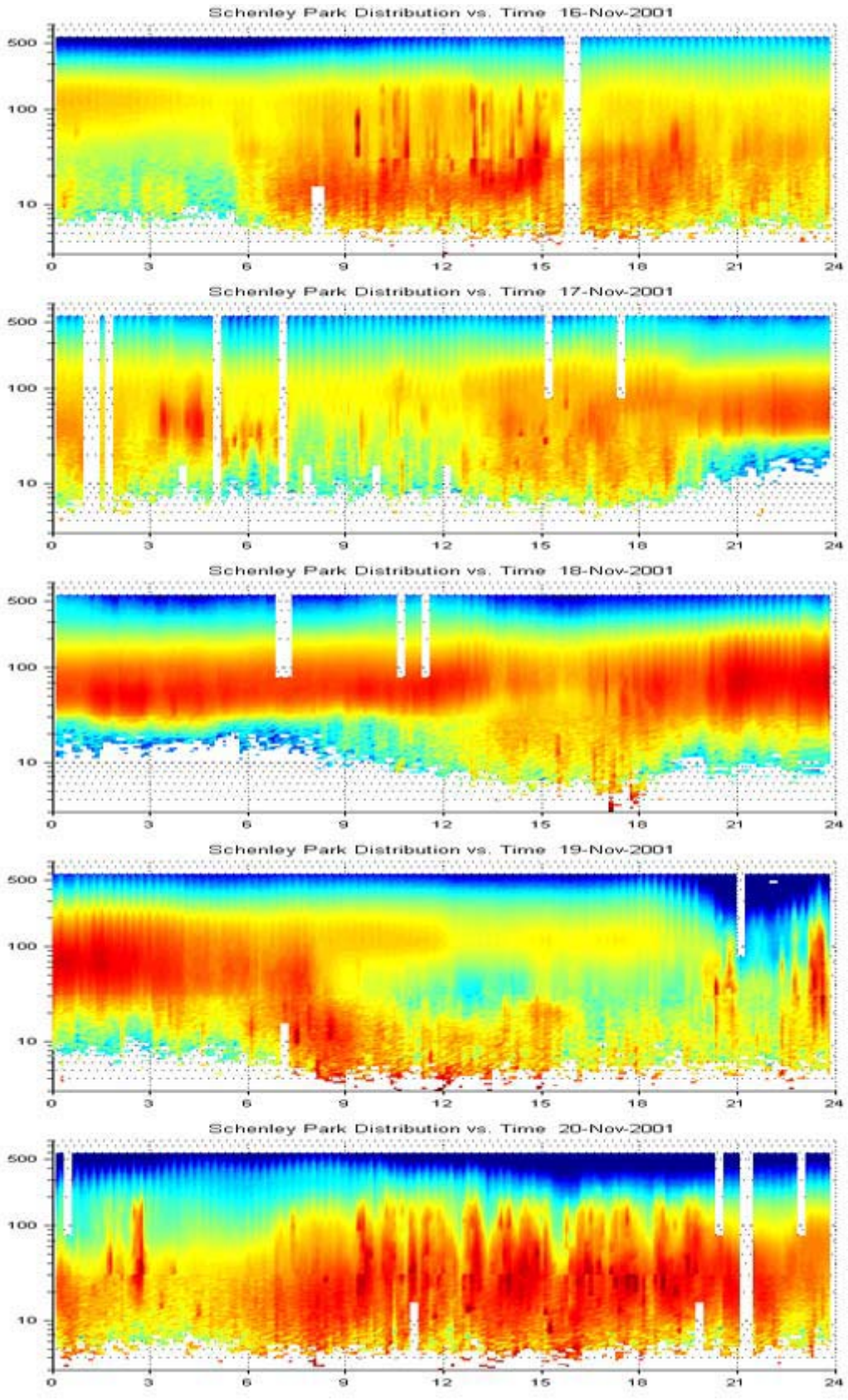
Schenley Park Distribution vs. Time 16-Nov-2001
Schenley Park Distribution vs. Time 17-Nov-2001
Schenley Park Distribution vs. Time 18-Nov-2001
Schenley Park Distribution vs. Time 19-Nov-2001
Schenley Park Distribution vs. Time 20-Nov-2001
500
100
10
0
3
6
9
12
15
18
21
24

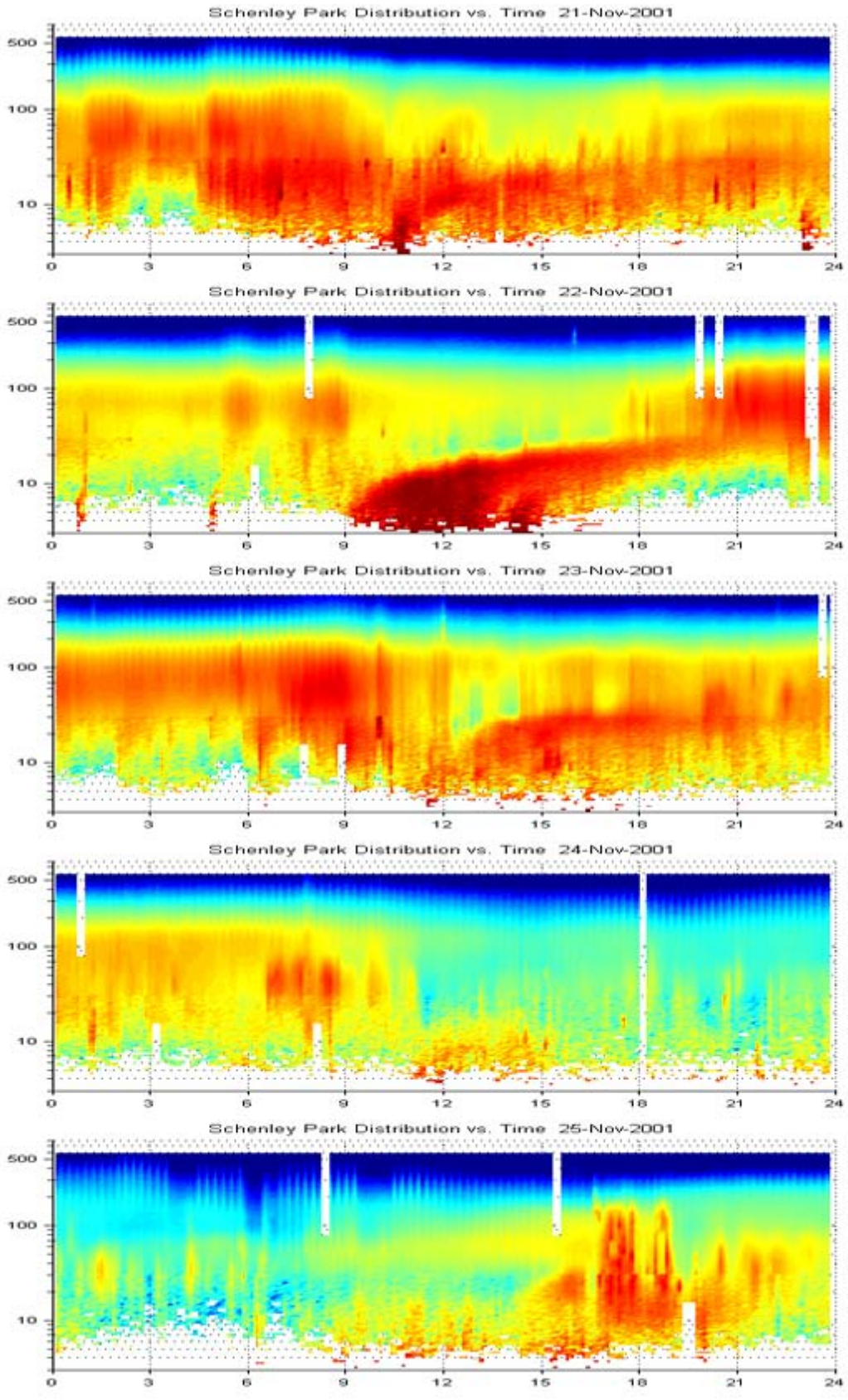
Schenley Park Distribution vs. Time 21-Nov-2001
Schenley Park Distribution vs. Time 22-Nov-2001
Schenley Park Distribution vs. Time 23-Nov-2001
Schenley Park Distribution vs. Time 24-Nov-2001
Schenley Park Distribution vs. Time 25-Nov-2001
500
100
10
0
3
6
9
12
15
18
21
24

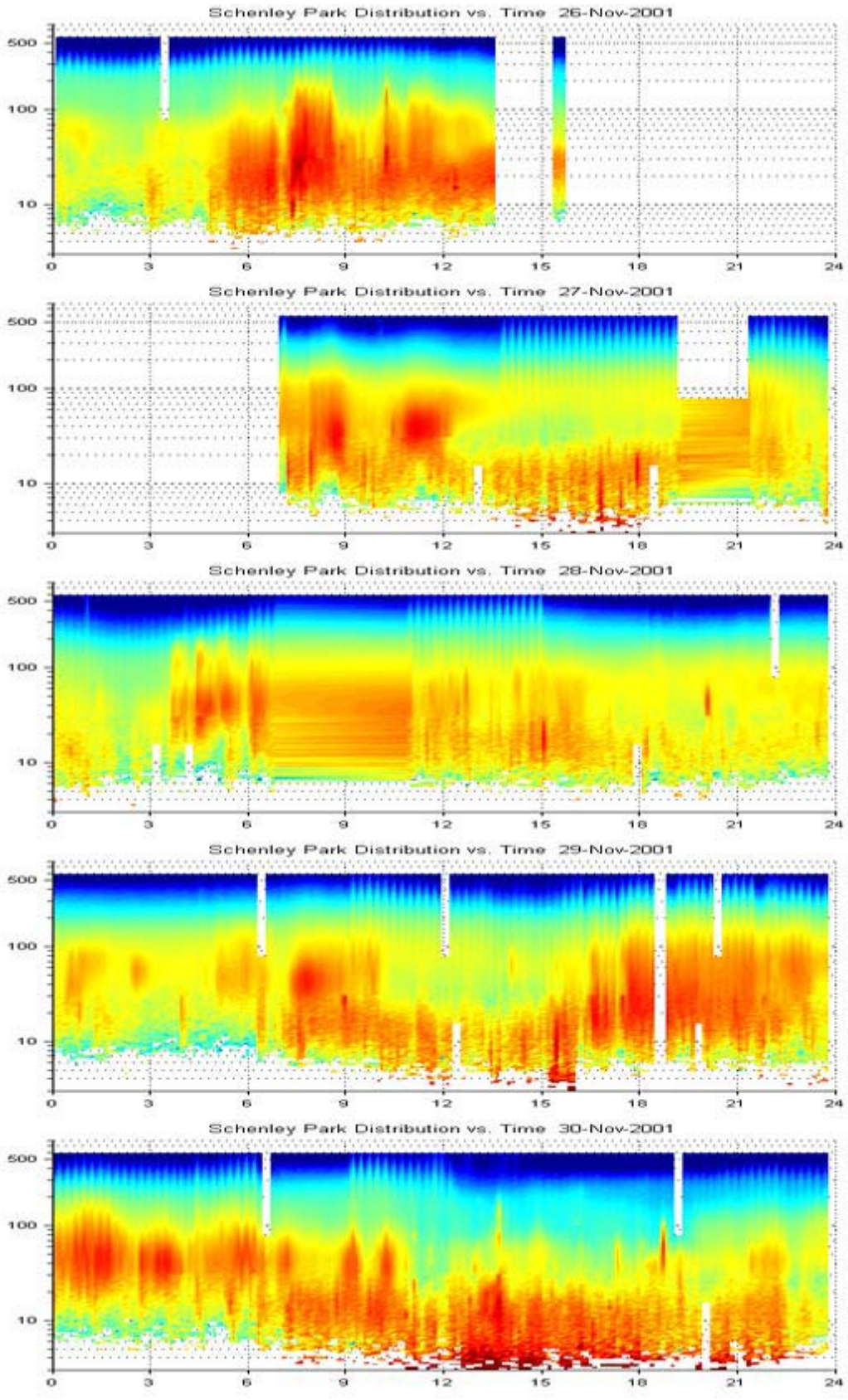
Schenley Park Distribution vs. Time 26-Nov-2001
Schenley Park Distribution vs. Time 27-Nov-2001
Schenley Park Distribution vs. Time 28-Nov-2001
Schenley Park Distribution vs. Time 29-Nov-2001
Schenley Park Distribution vs. Time 30-Nov-2001
500
100
10
0
3
6
9
12
15
18
21
24

DECEMBER 2001

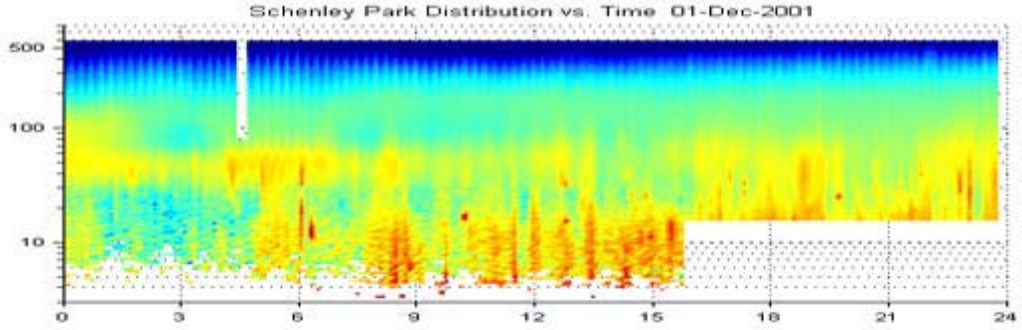

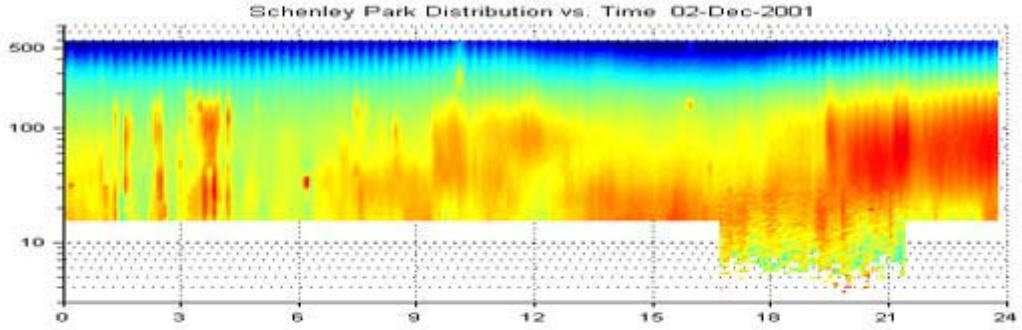

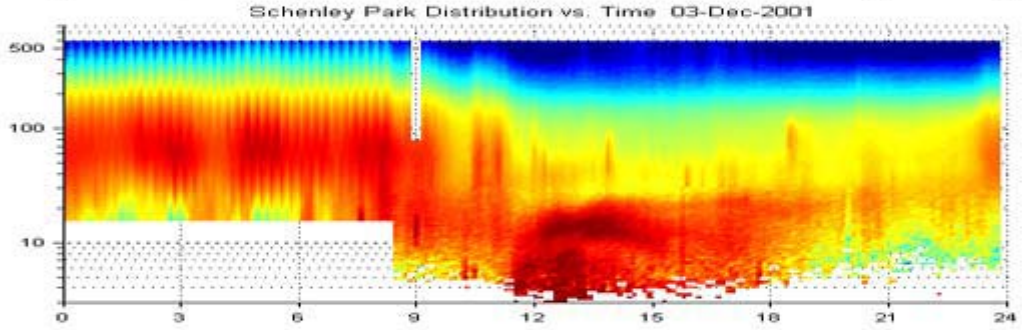

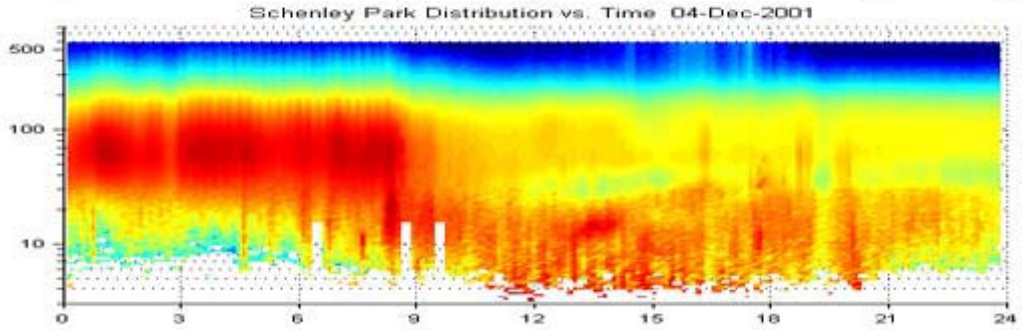

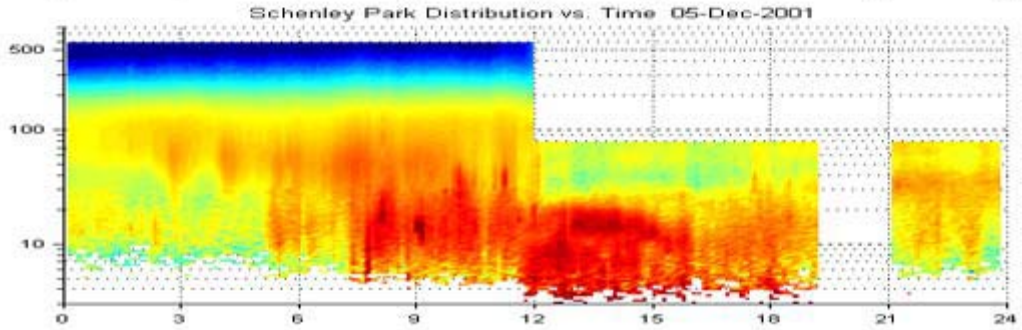

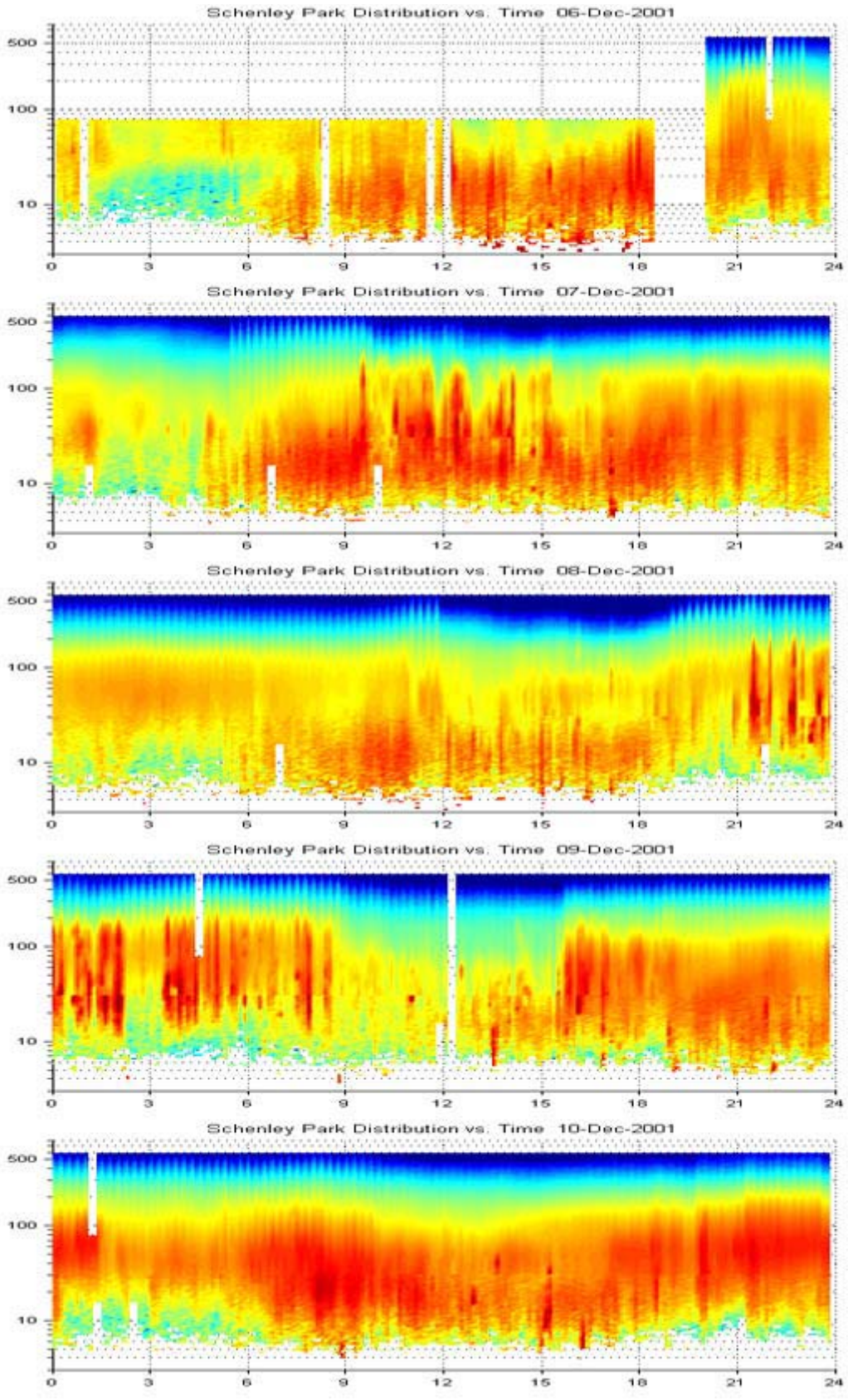
Schenley Park Distribution vs. Time 06-Dec-2001
Schenley Park Distribution vs. Time 07-Dec-2001
Schenley Park Distribution vs. Time 08-Dec-2001
Schenley Park Distribution vs. Time 09-Dec-2001
Schenley Park Distribution vs. Time 10-Dec-2001
500
100
10
0
3
6
9
12
15
18
21
24

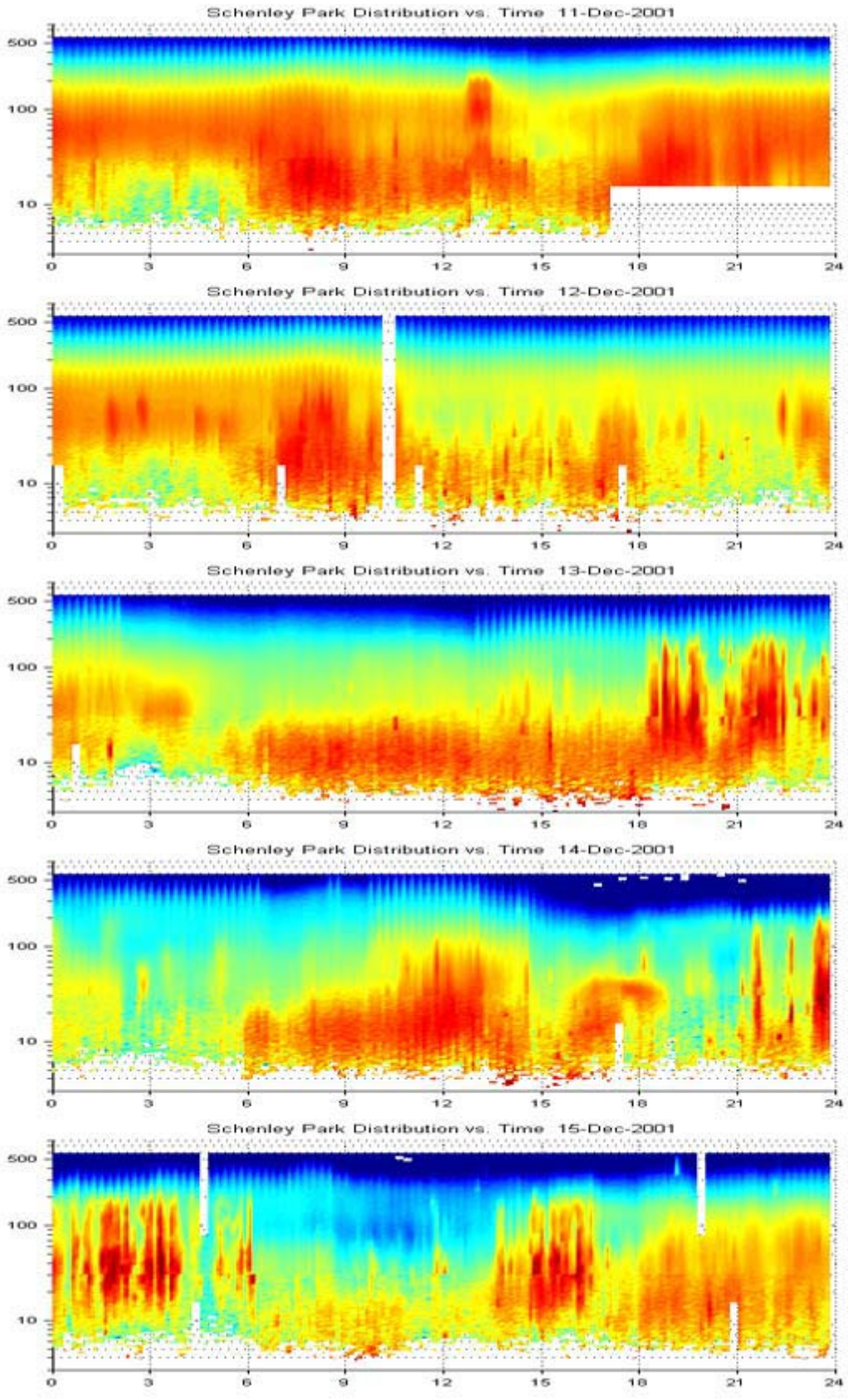
Schenley Park Distribution vs. Time 11-Dec-2001
Schenley Park Distribution vs. Time 12-Dec-2001
Schenley Park Distribution vs. Time 13-Dec-2001
Schenley Park Distribution vs. Time 14-Dec-2001
Schenley Park Distribution vs. Time 15-Dec-2001
500
100
10
0
3
6
9
12
15
18
21
24

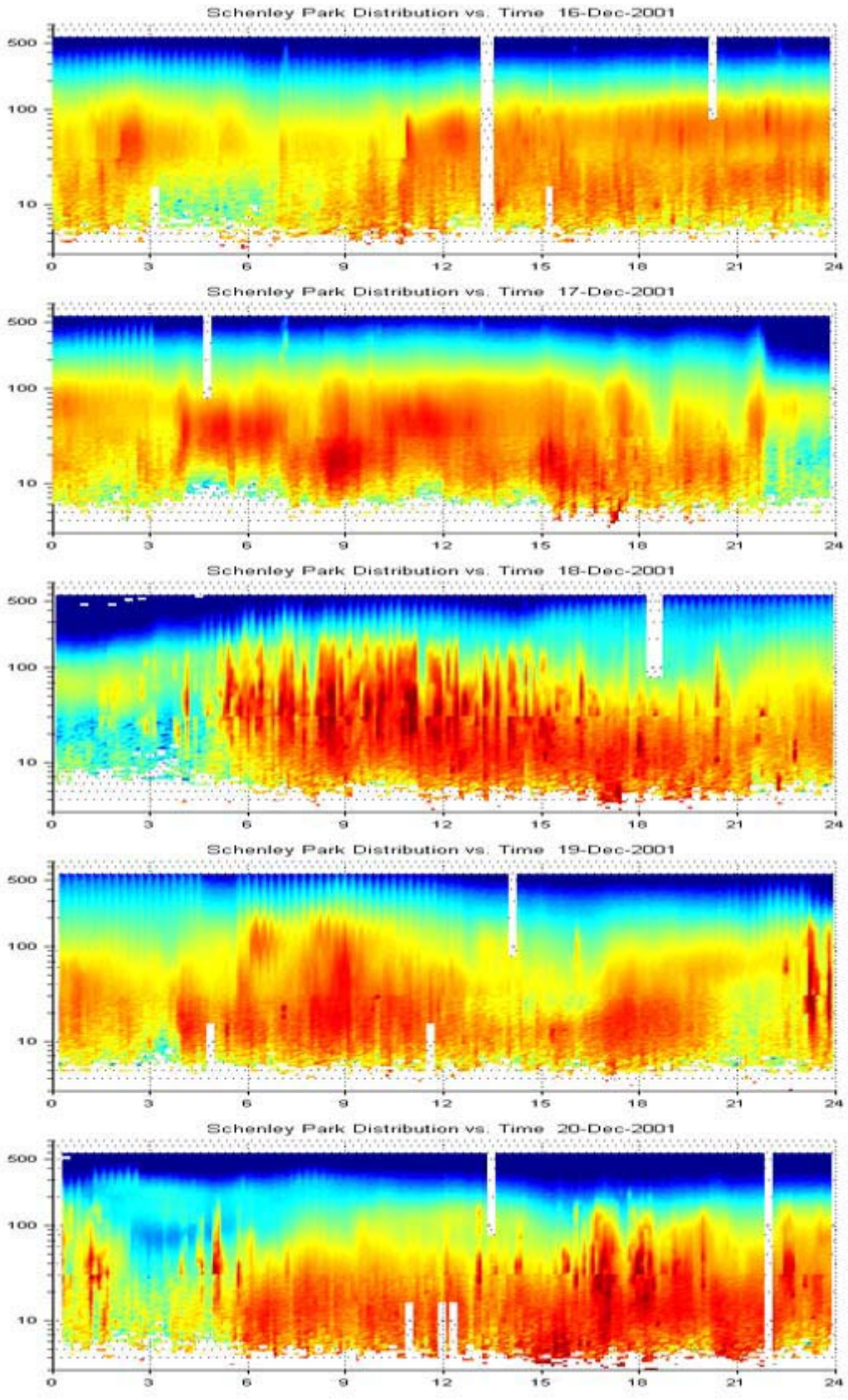
Schenley Park Distribution vs. Time 16-Dec-2001
Schenley Park Distribution vs. Time 17-Dec-2001
Schenley Park Distribution vs. Time 18-Dec-2001
Schenley Park Distribution vs. Time 19-Dec-2001
Schenley Park Distribution vs. Time 20-Dec-2001
500
100
10
0
3
6
9
12
15
18
21
24

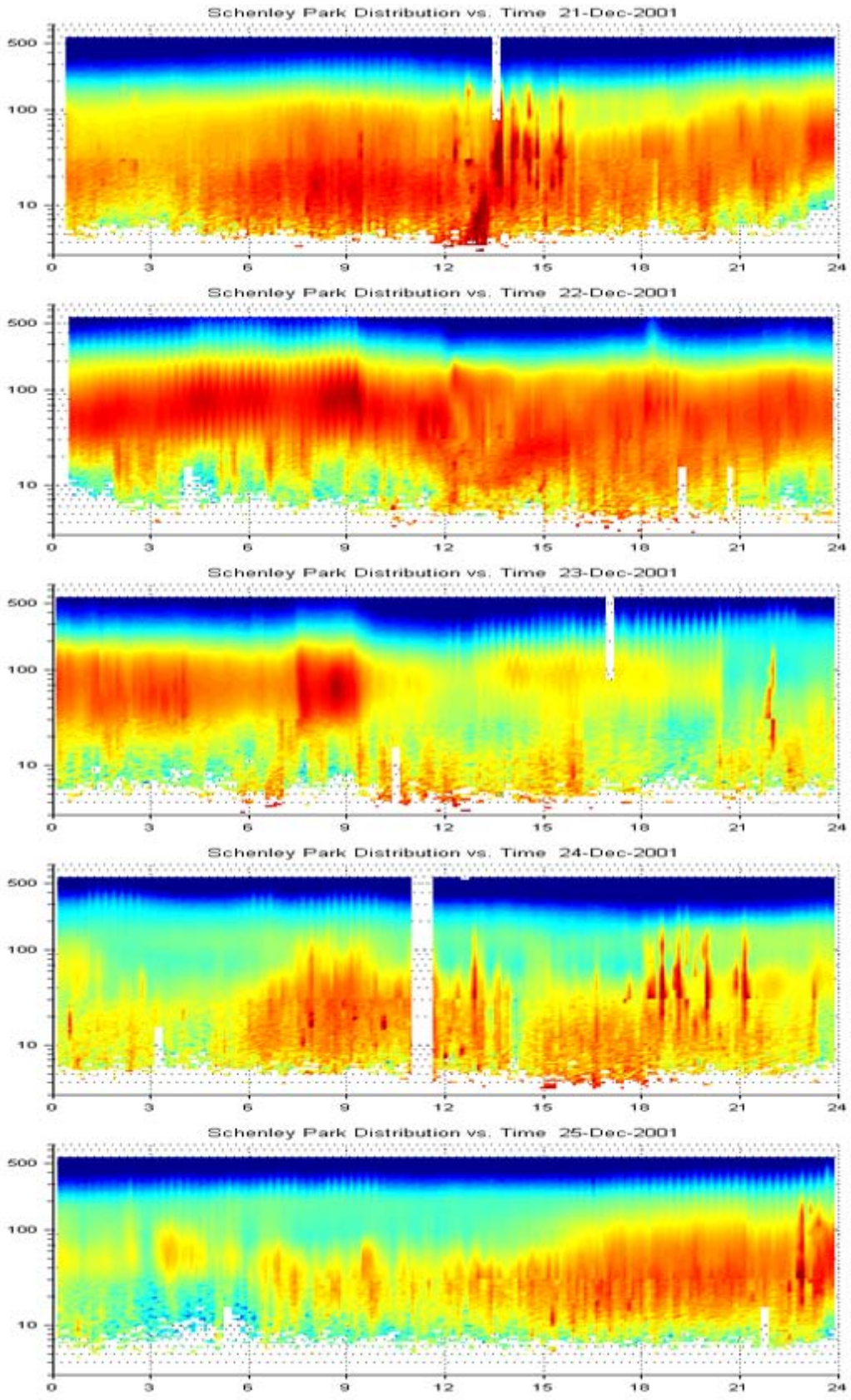
Schenley Park Distribution vs. Time 21-Dec-2001
Schenley Park Distribution vs. Time 22-Dec-2001
Schenley Park Distribution vs. Time 23-Dec-2001
Schenley Park Distribution vs. Time 24-Dec-2001
Schenley Park Distribution vs. Time 25-Dec-2001
500
100
10
0
3
6
9
12
15
18
21
24

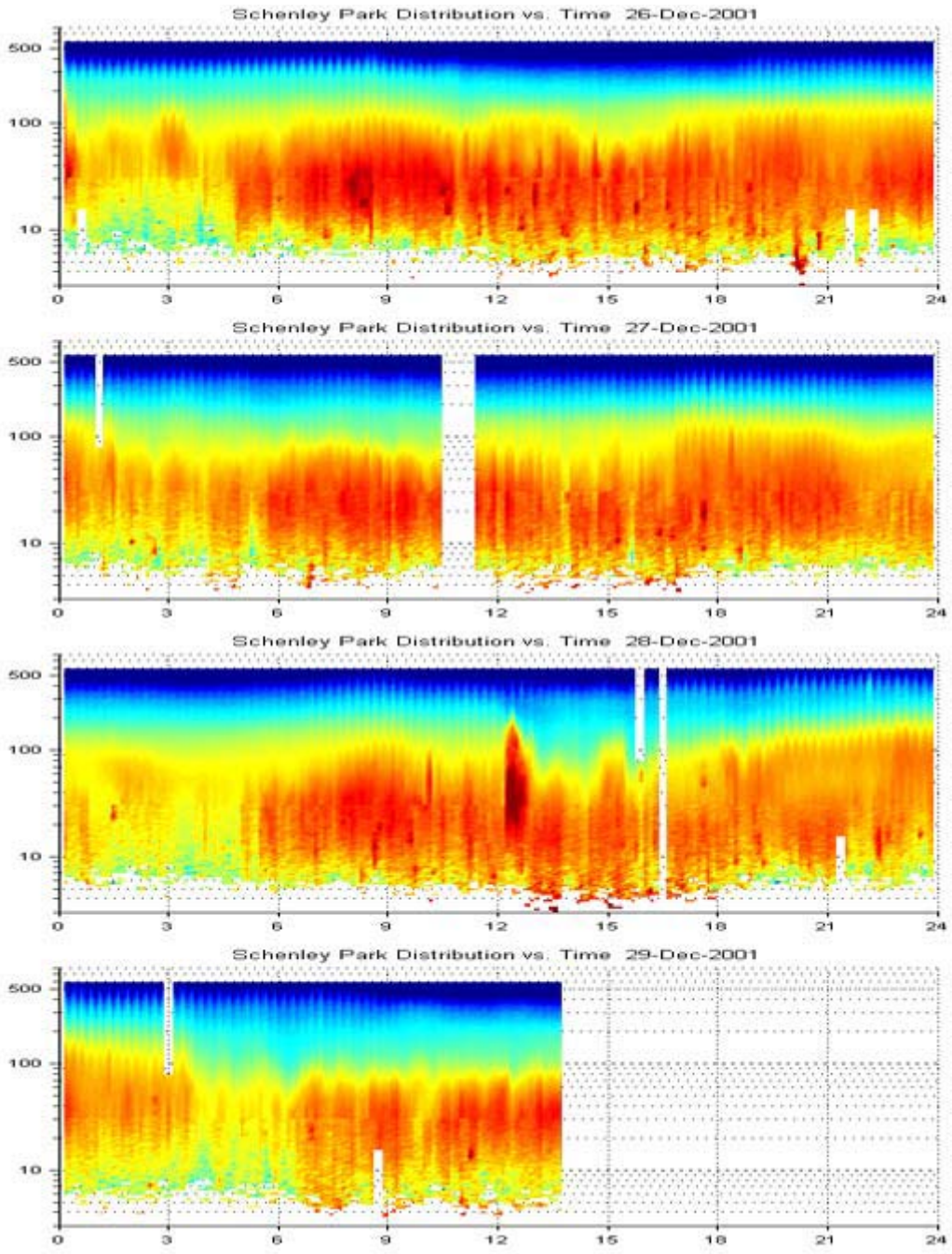

NO DATA TAKEN ON 12/30/01

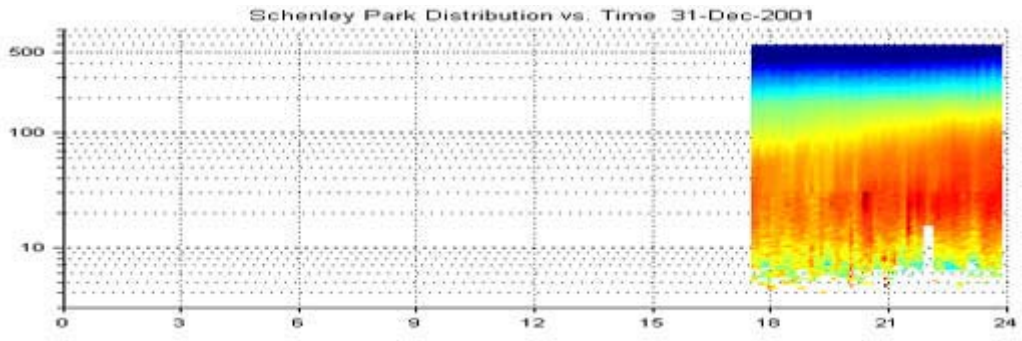
Schenley Park Distribution vs. Time 31-Dec-2001
500
100
10
0
3
6
9
12
15
18
21
24

JANUARY 2002

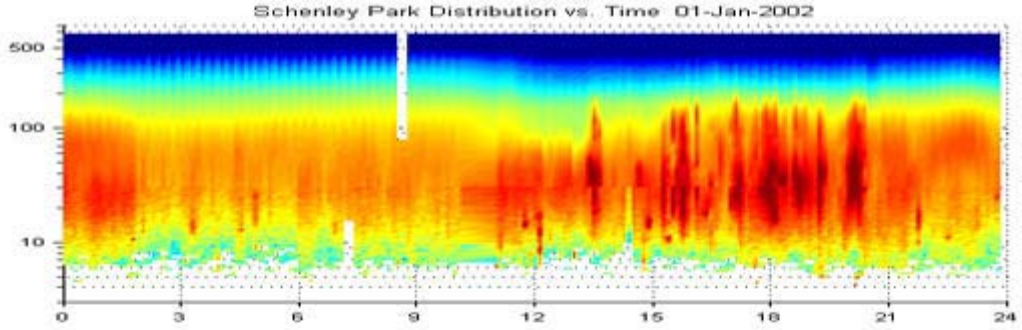

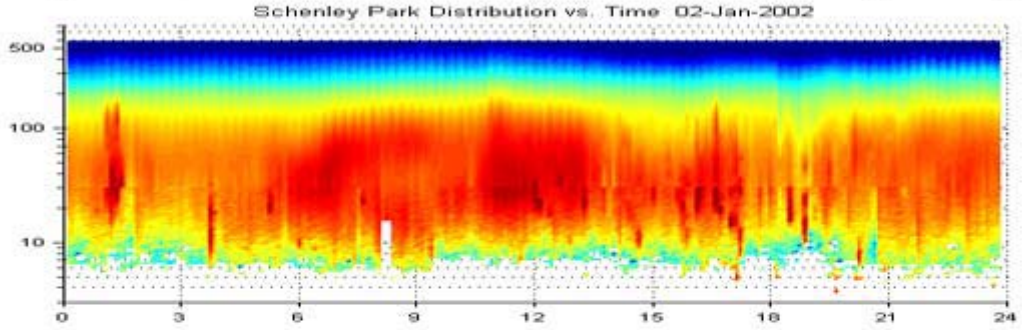

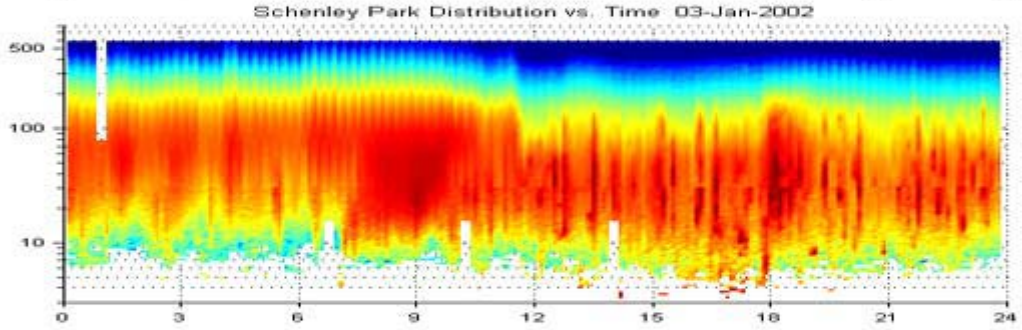

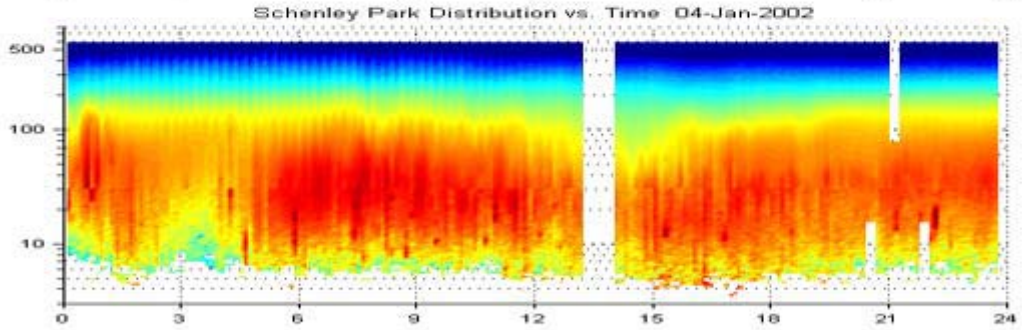

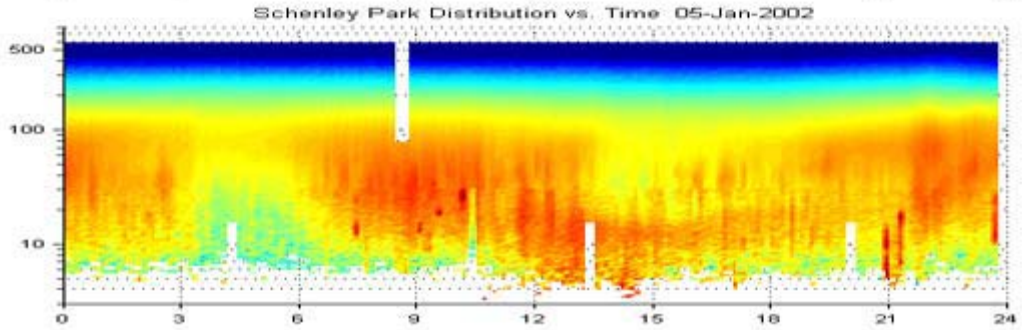

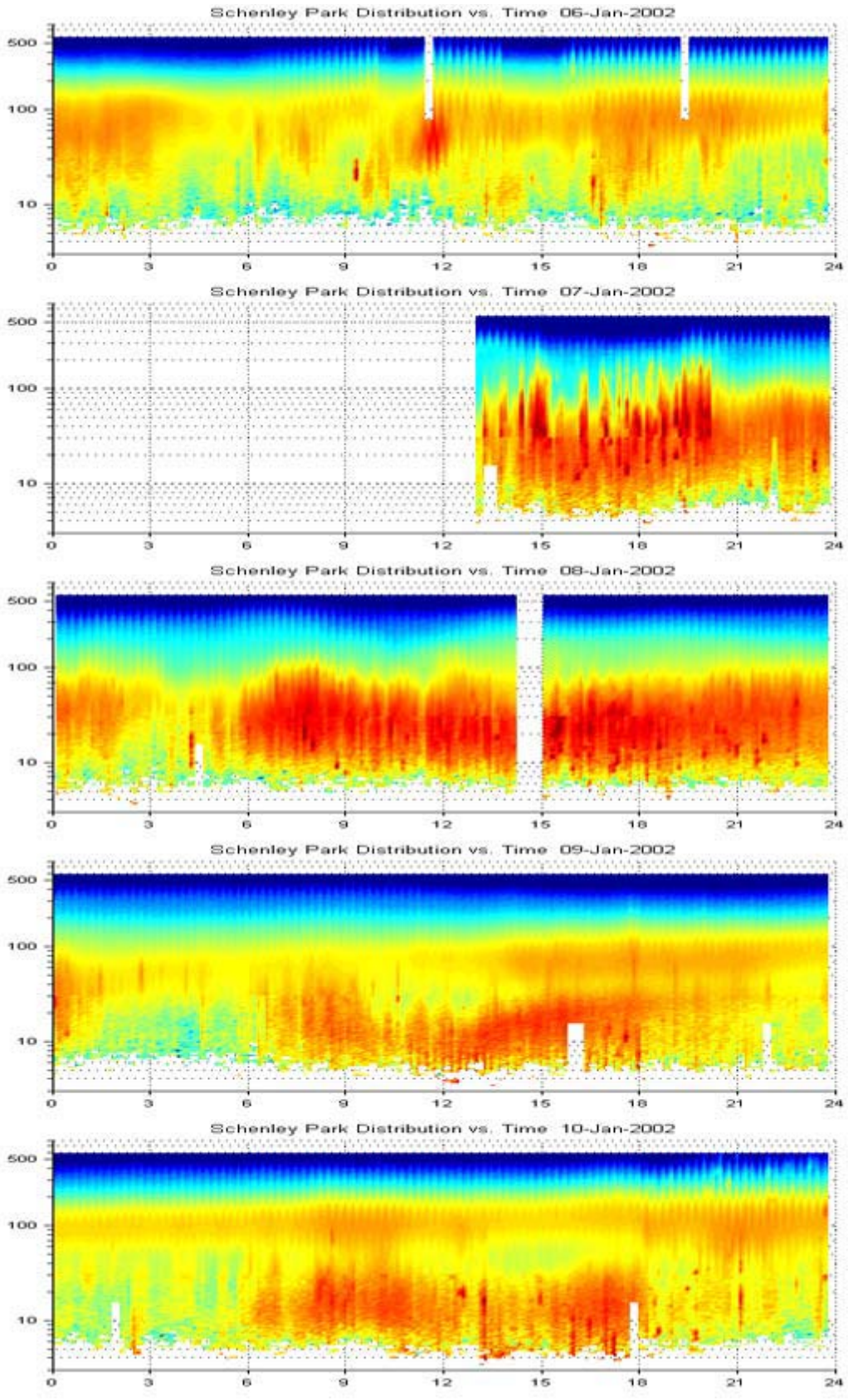
Schenley Park Distribution vs. Time 06-Jan-2002
Schenley Park Distribution vs. Time 07-Jan-2002
Schenley Park Distribution vs. Time 08-Jan-2002
Schenley Park Distribution vs. Time 09-Jan-2002
Schenley Park Distribution vs. Time 10-Jan-2002
500
100
10
0
3
6
9
12
15
18
21
24

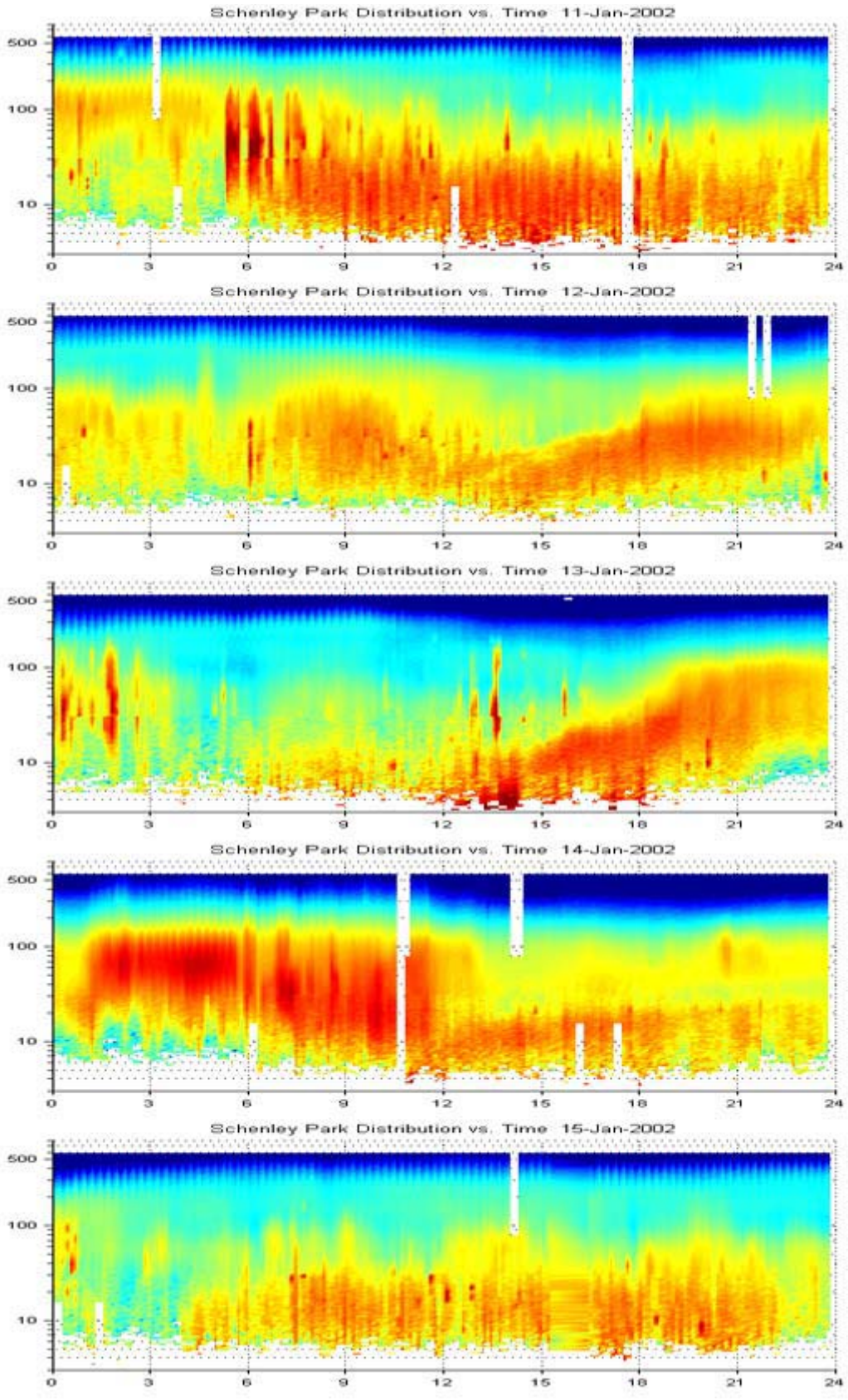
Schenley Park Distribution vs. Time 11-Jan-2002
Schenley Park Distribution vs. Time 12-Jan-2002
Schenley Park Distribution vs. Time 13-Jan-2002
Schenley Park Distribution vs. Time 14-Jan-2002
Schenley Park Distribution vs. Time 15-Jan-2002
500
100
10
0
3
6
9
12
15
18
21
24

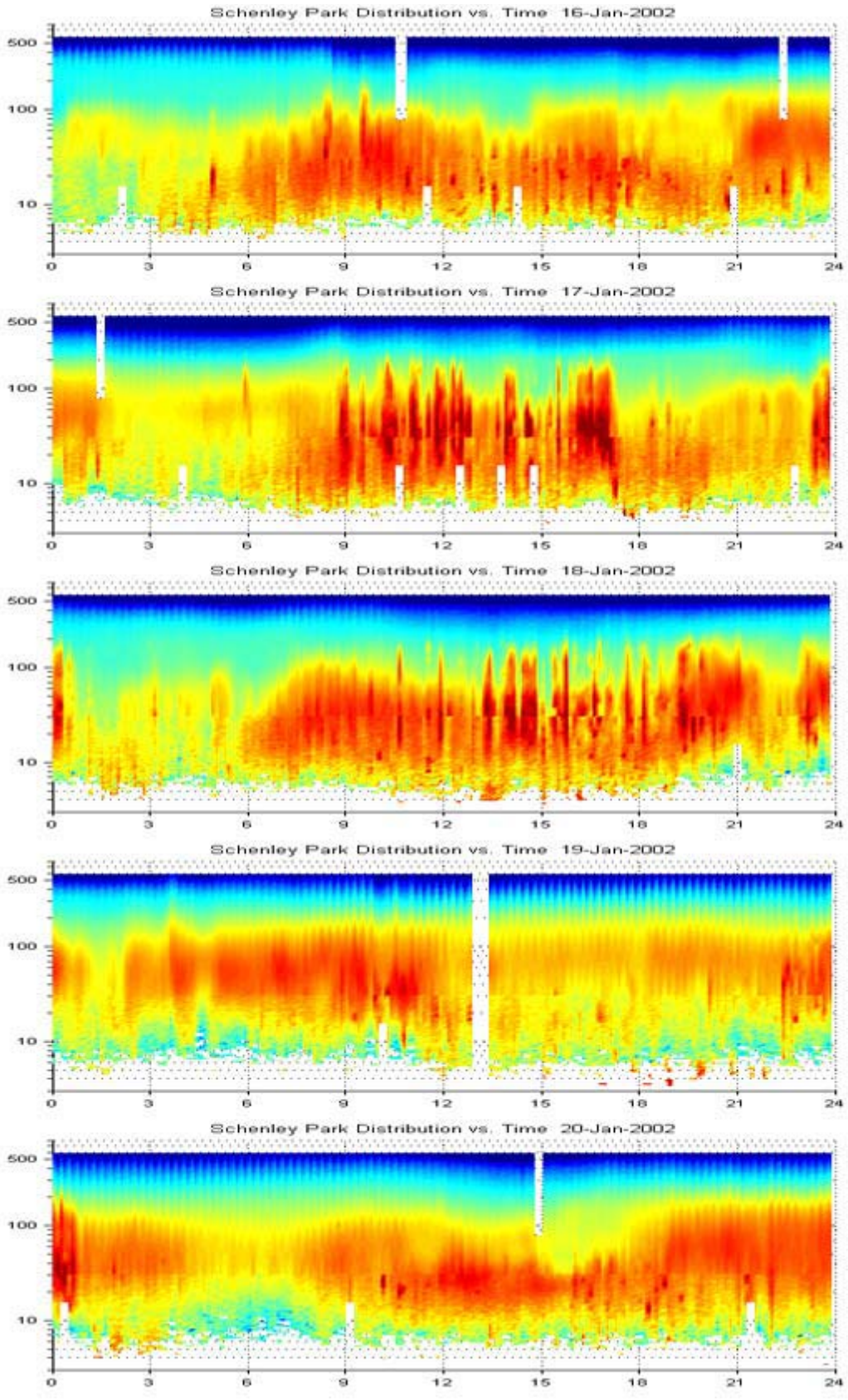
Schenley Park Distribution vs. Time 16-Jan-2002
Schenley Park Distribution vs. Time 17-Jan-2002
Schenley Park Distribution vs. Time 18-Jan-2002
Schenley Park Distribution vs. Time 19-Jan-2002
Schenley Park Distribution vs. Time 20-Jan-2002
500
100
10
0
3
6
9
12
15
18
21
24

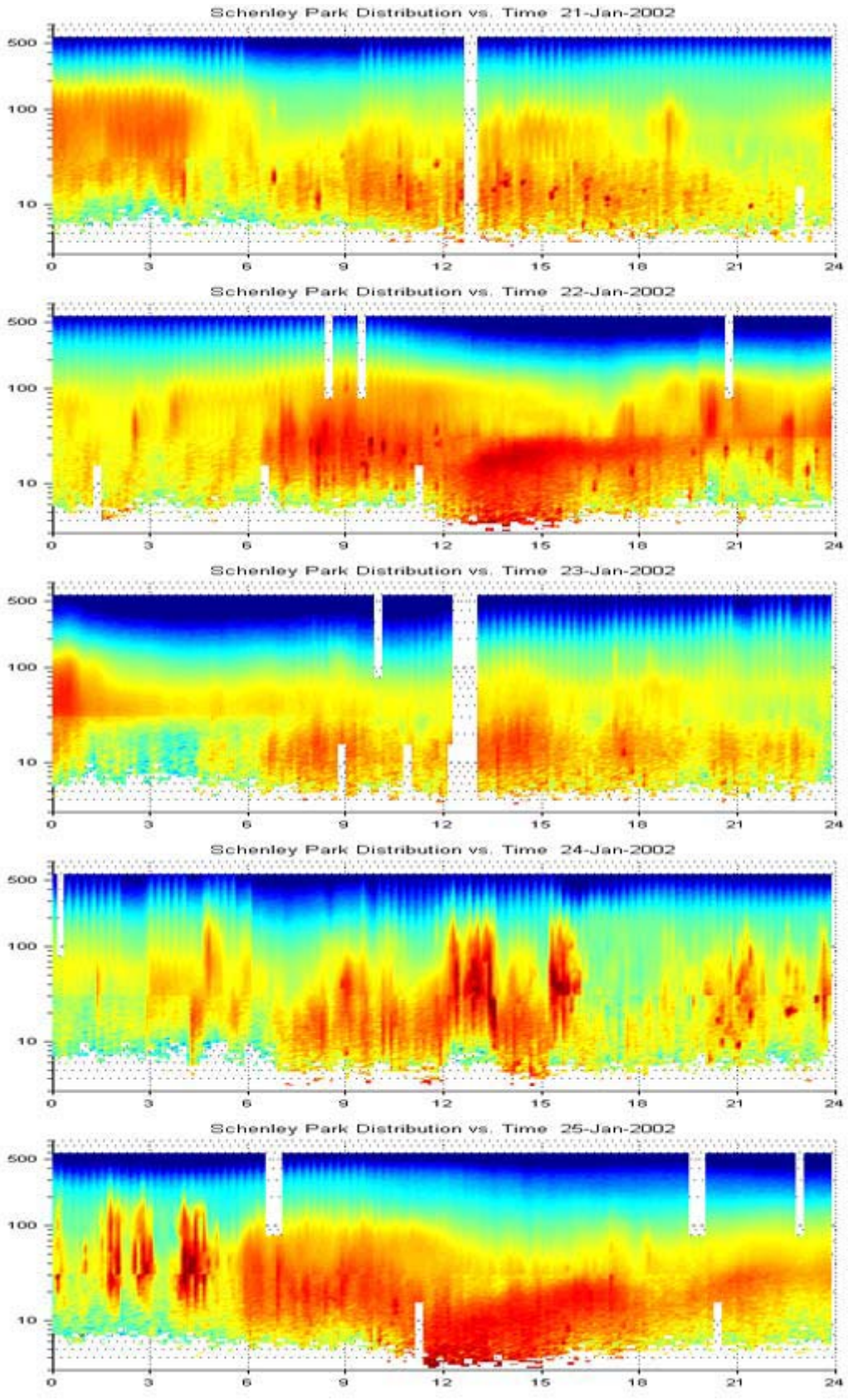
Schenley Park Distribution vs. Time 21-Jan-2002
Schenley Park Distribution vs. Time 22-Jan-2002
Schenley Park Distribution vs. Time 23-Jan-2002
Schenley Park Distribution vs. Time 24-Jan-2002
Schenley Park Distribution vs. Time 25-Jan-2002
500
100
10
0
3
6
9
12
15
18
21
24

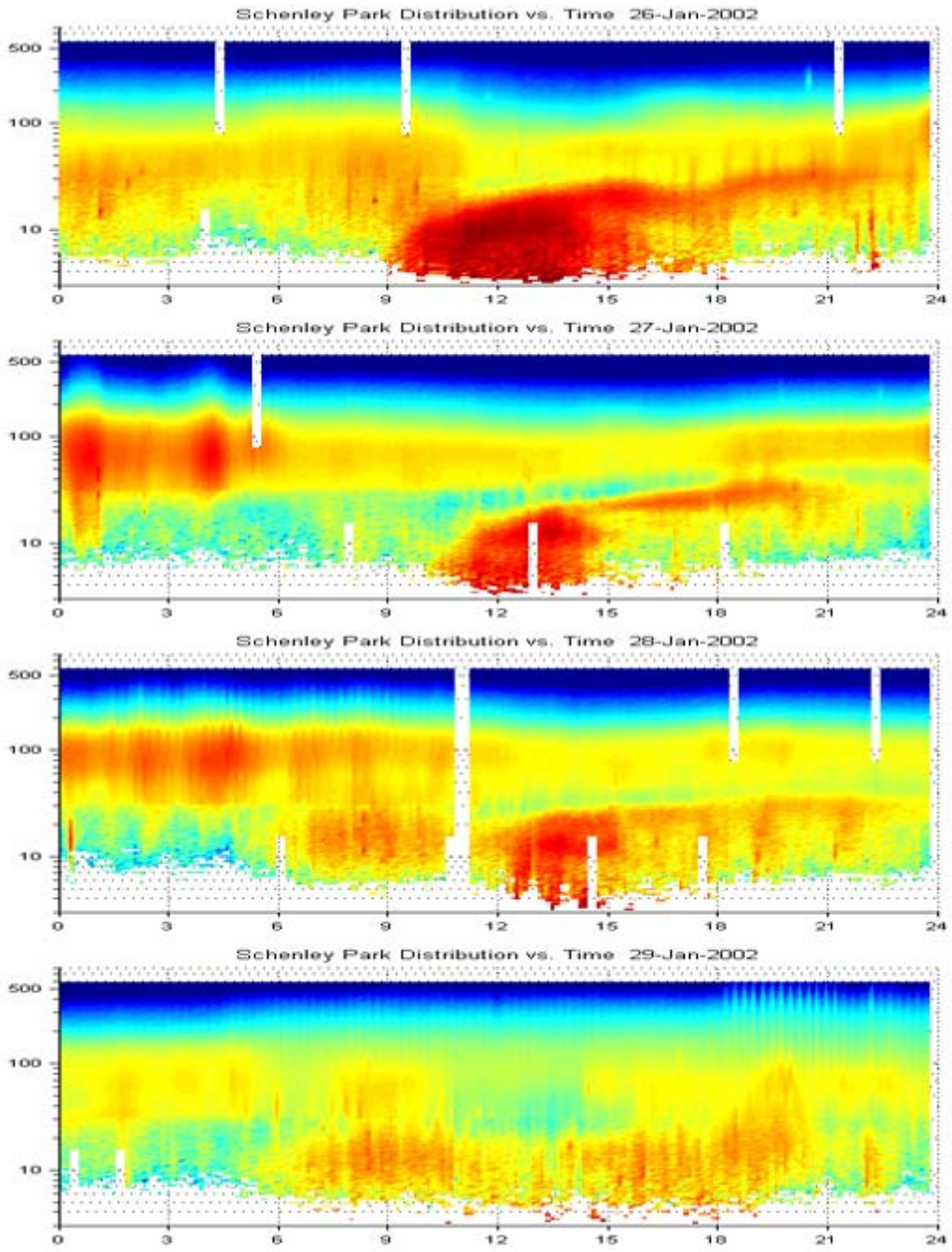
Schenley Park Distribution vs. Time 26-Jan-2002
Schenley Park Distribution vs. Time 27-Jan-2002
Schenley Park Distribution vs. Time 28-Jan-2002
Schenley Park Distribution vs. Time 29-Jan-2002
500
100
10
0
3
6
9
12
15
18
21
24

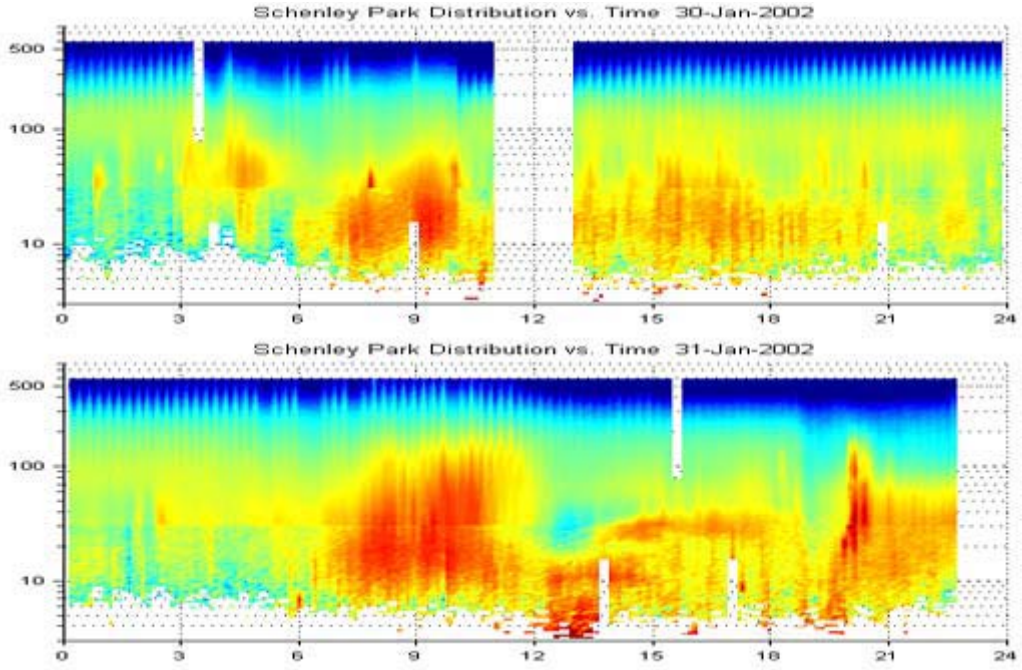

FEBRUARY 2002

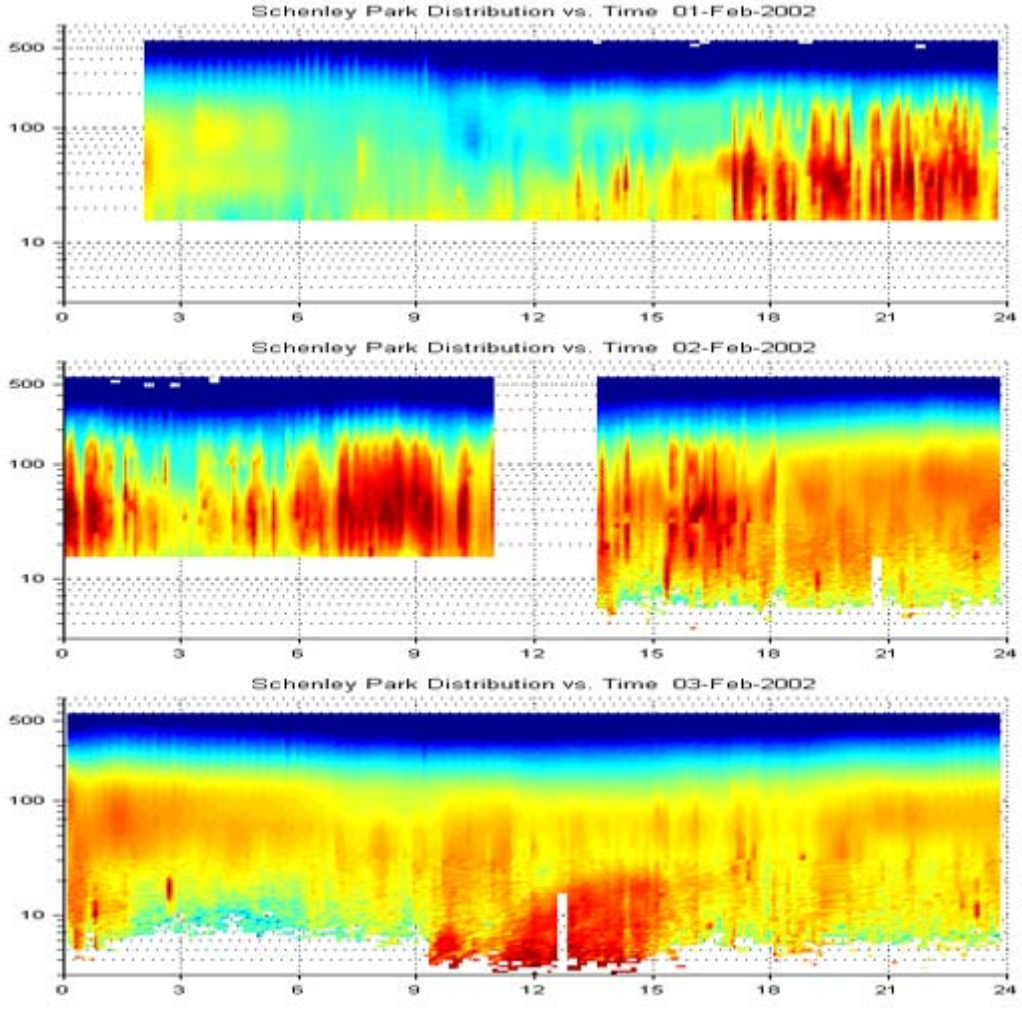

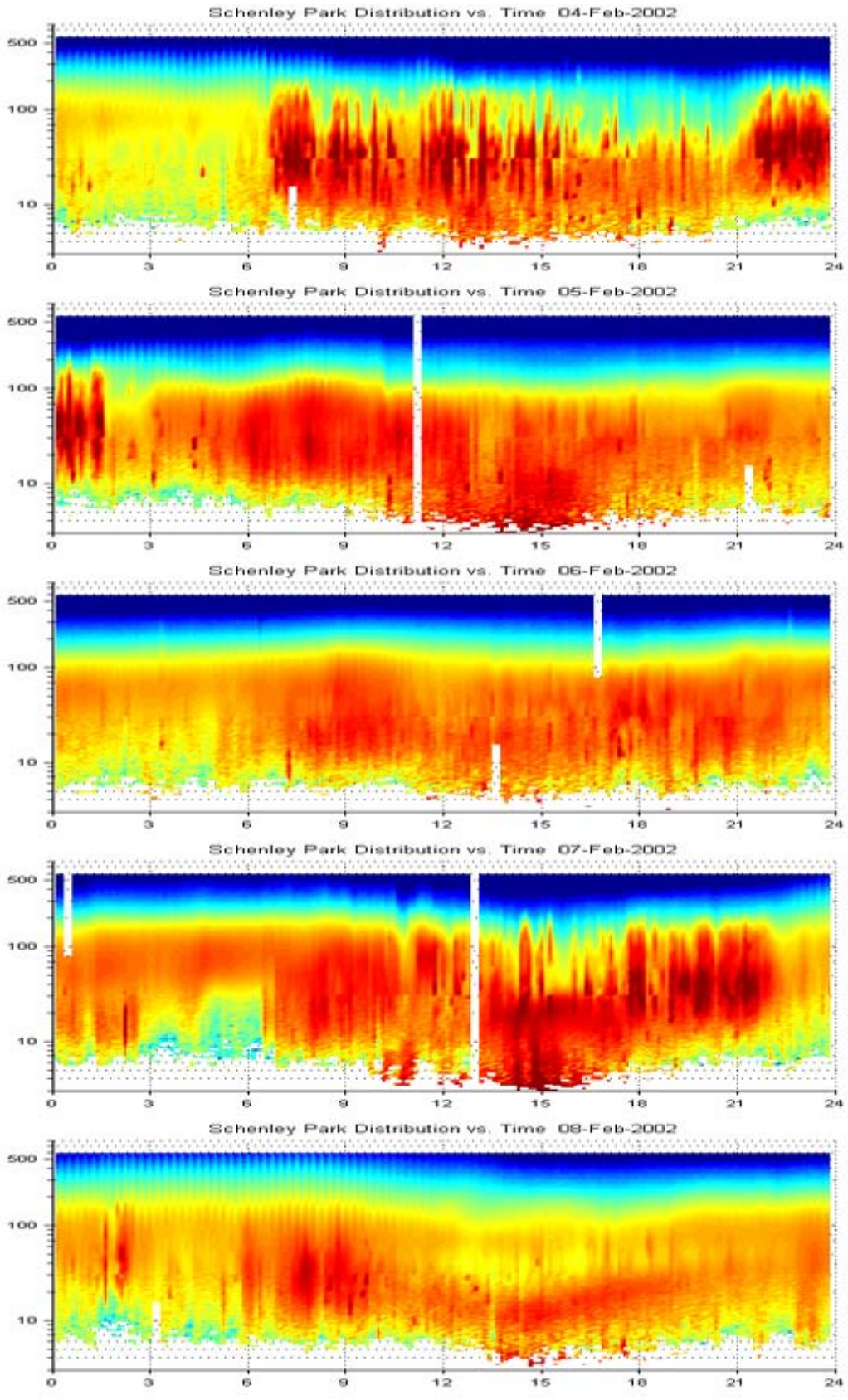
Schenley Park Distribution vs. Time 04-Feb-2002
Schenley Park Distribution vs. Time 05-Feb-2002
Schenley Park Distribution vs. Time 06-Feb-2002
Schenley Park Distribution vs. Time 07-Feb-2002
Schenley Park Distribution vs. Time 08-Feb-2002
500
100
10
0
3
6
9
12
15
18
21
24

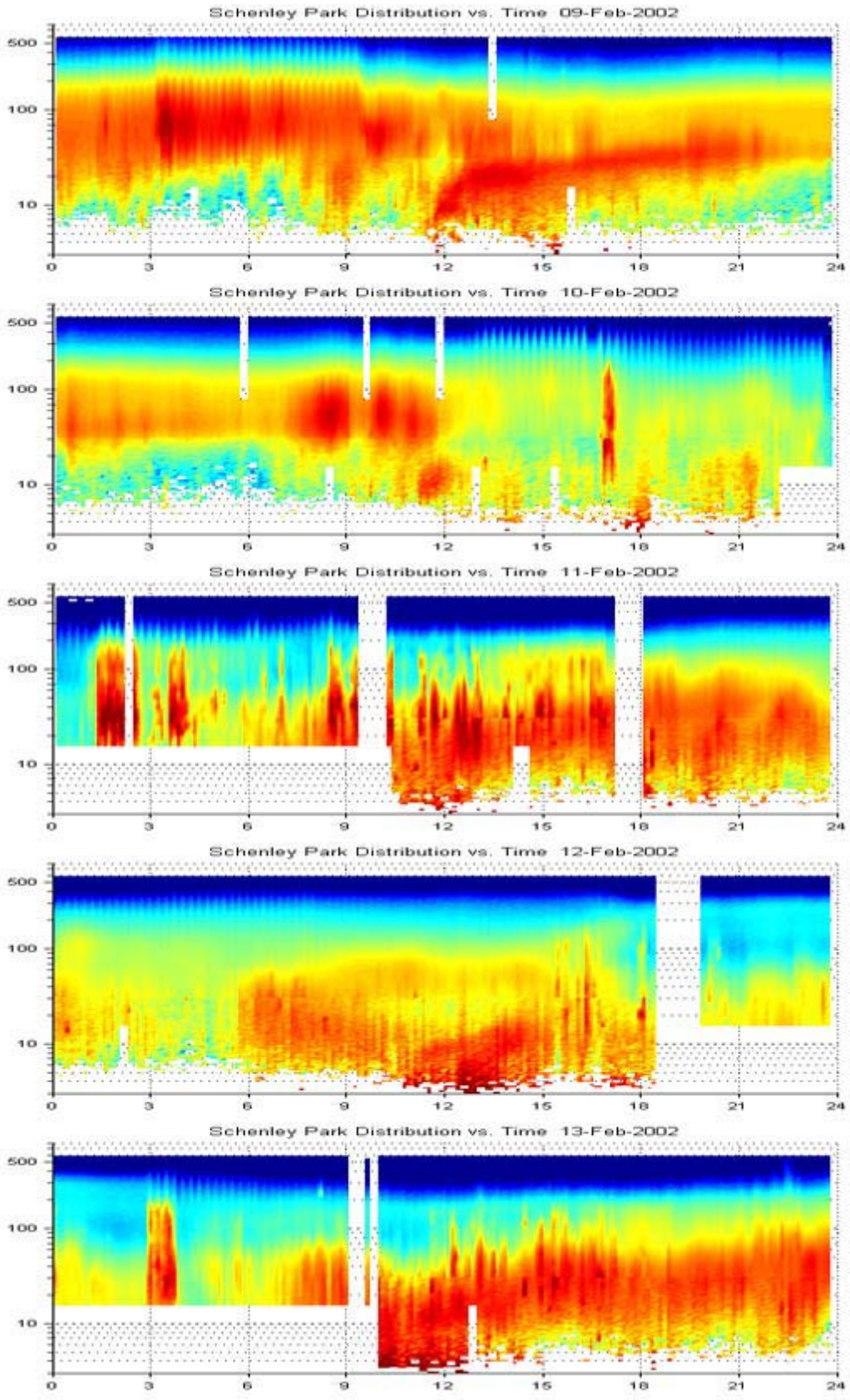
Schenley Park Distribution vs. Time 09-Feb-2002
Schenley Park Distribution vs. Time 10-Feb-2002
Schenley Park Distribution vs. Time 11-Feb-2002
Schenley Park Distribution vs. Time 12-Feb-2002
Schenley Park Distribution vs. Time 13-Feb-2002
500
100
10
0
3
6
9
12
15
18
21
24

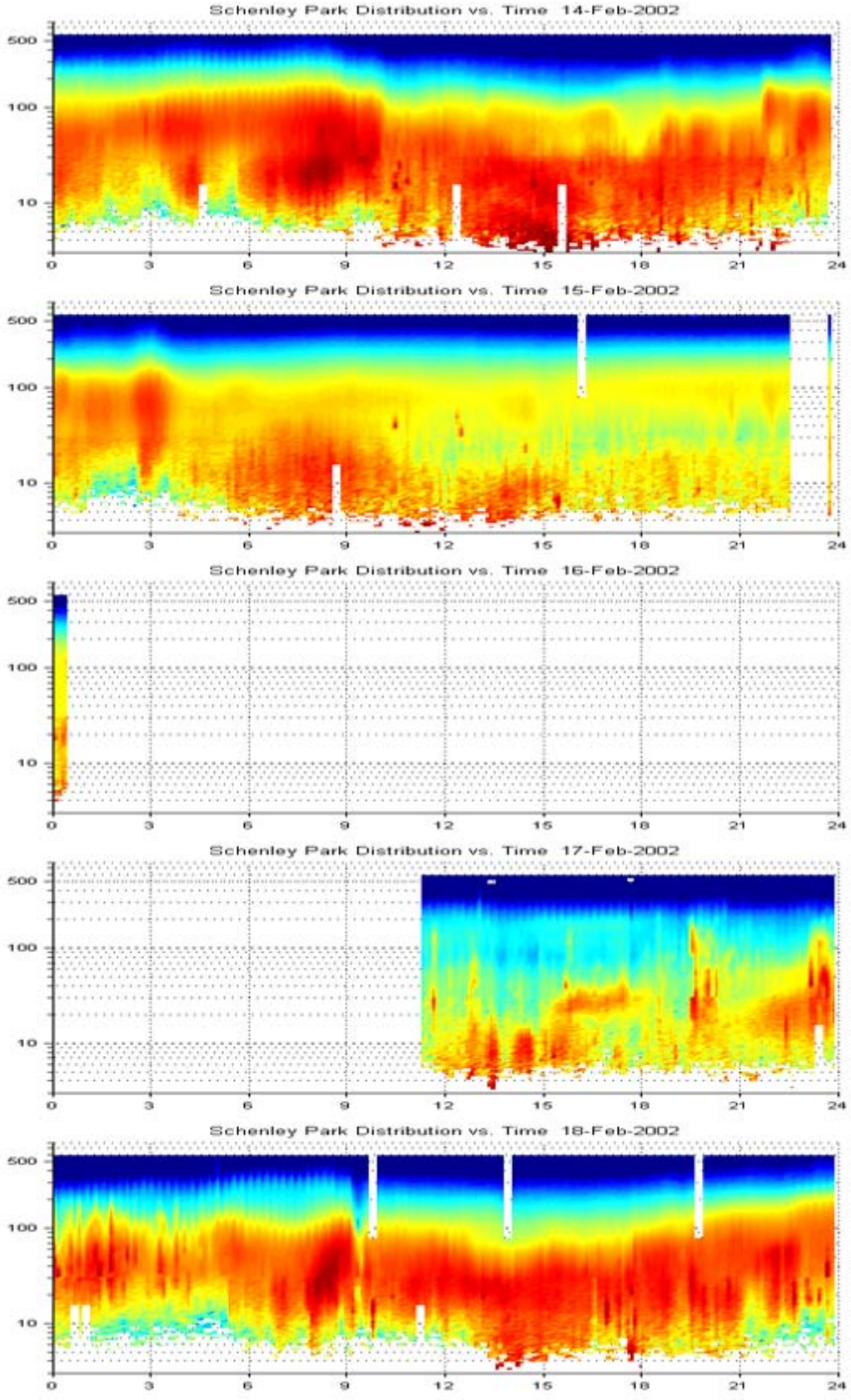
Schenley Park Distribution vs. Time 14-Feb-2002
Schenley Park Distribution vs. Time 15-Feb-2002
Schenley Park Distribution vs. Time 16-Feb-2002
Schenley Park Distribution vs. Time 17-Feb-2002
Schenley Park Distribution vs. Time 18-Feb-2002
500
100
10
0
3
6
9
12
15
18
21
24

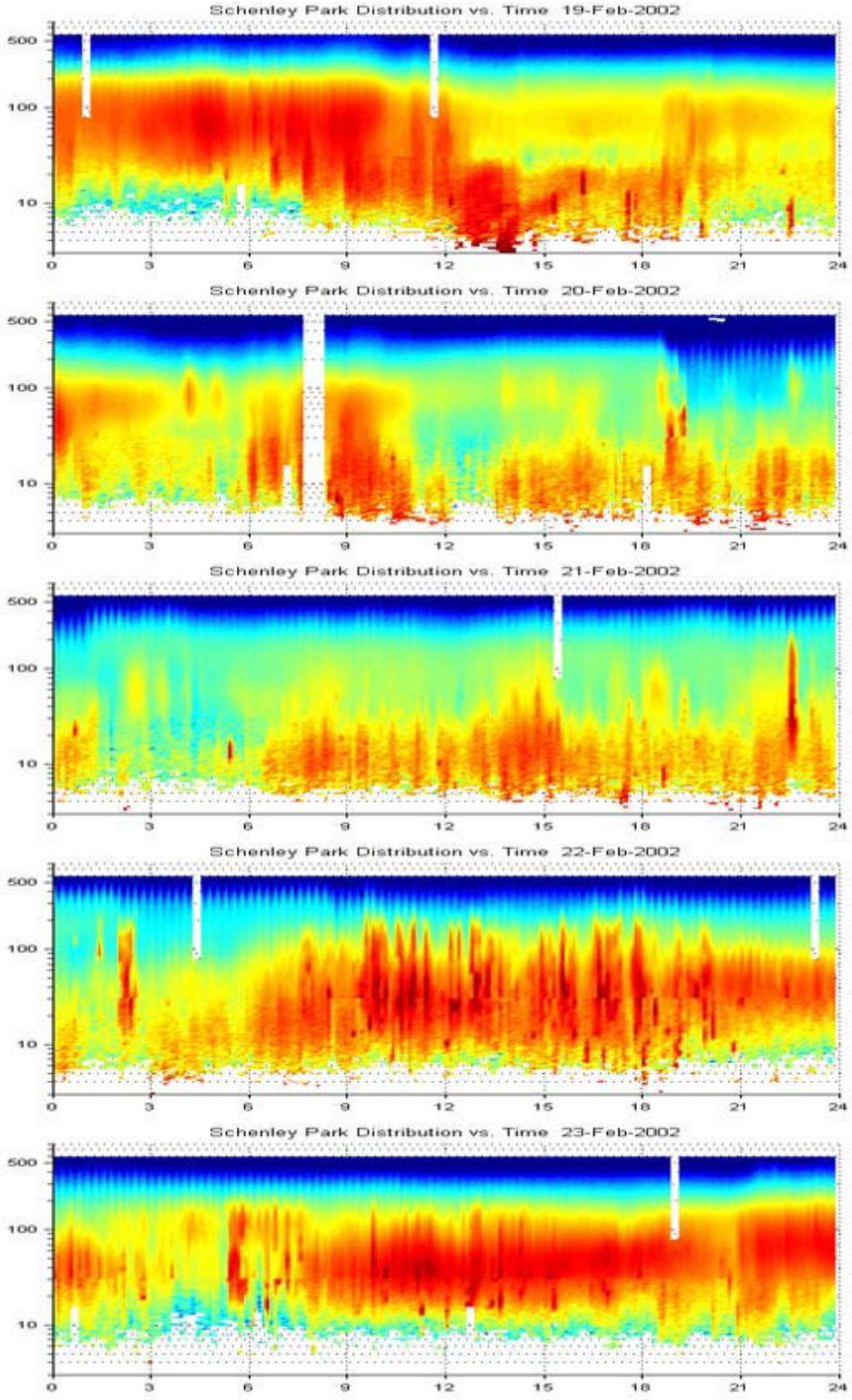
Schenley Park Distribution vs. Time 19-Feb-2002
Schenley Park Distribution vs. Time 20-Feb-2002
Schenley Park Distribution vs. Time 21-Feb-2002
Schenley Park Distribution vs. Time 22-Feb-2002
Schenley Park Distribution vs. Time 23-Feb-2002
500
100
10
0
3
6
9
12
15
18
21
24

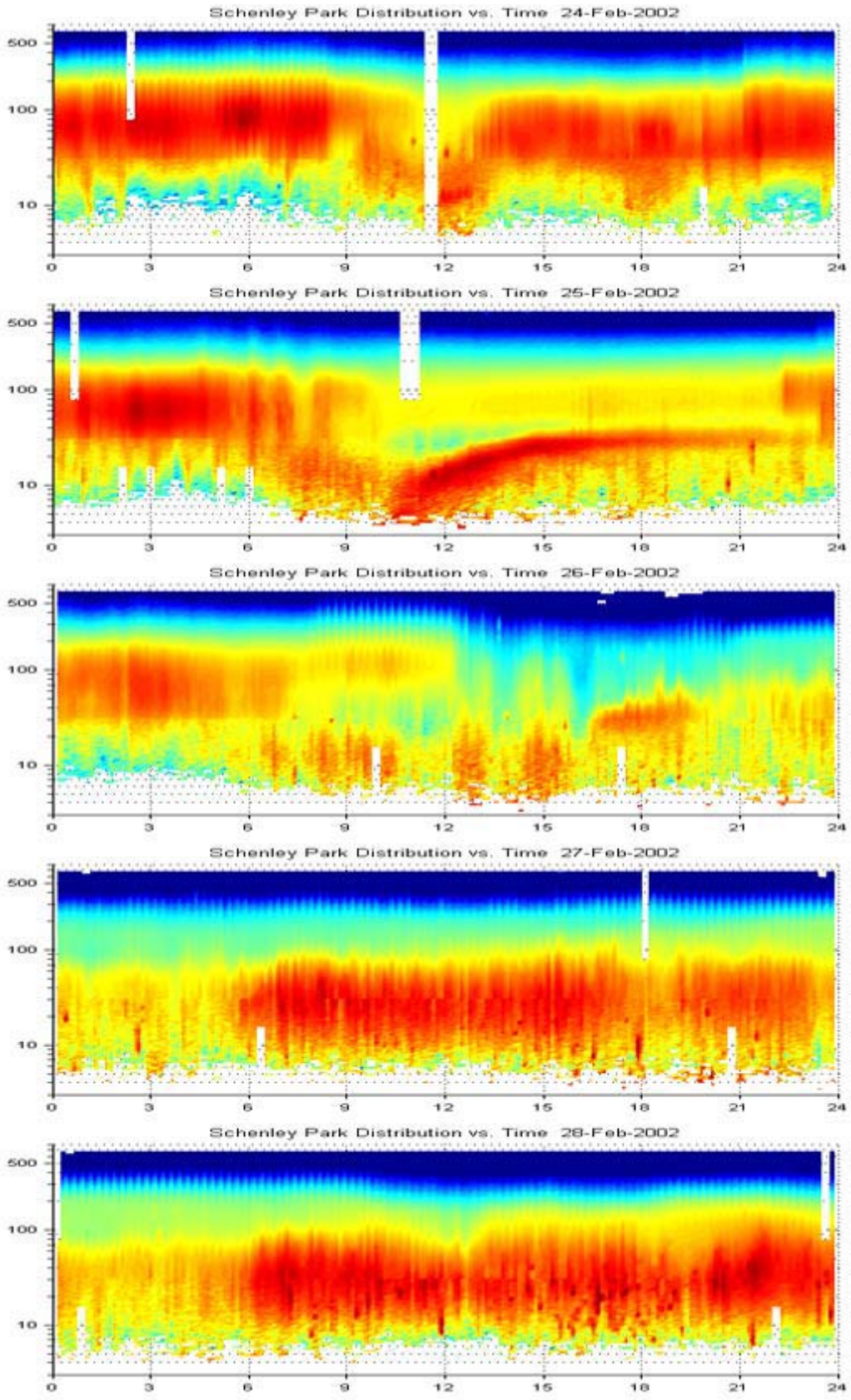
Schenley Park Distribution vs. Time 24-Feb-2002
Schenley Park Distribution vs. Time 25-Feb-2002
Schenley Park Distribution vs. Time 26-Feb-2002
Schenley Park Distribution vs. Time 27-Feb-2002
Schenley Park Distribution vs. Time 28-Feb-2002
500
100
10
0
3
6
9
12
15
18
21
24

MARCH 2002

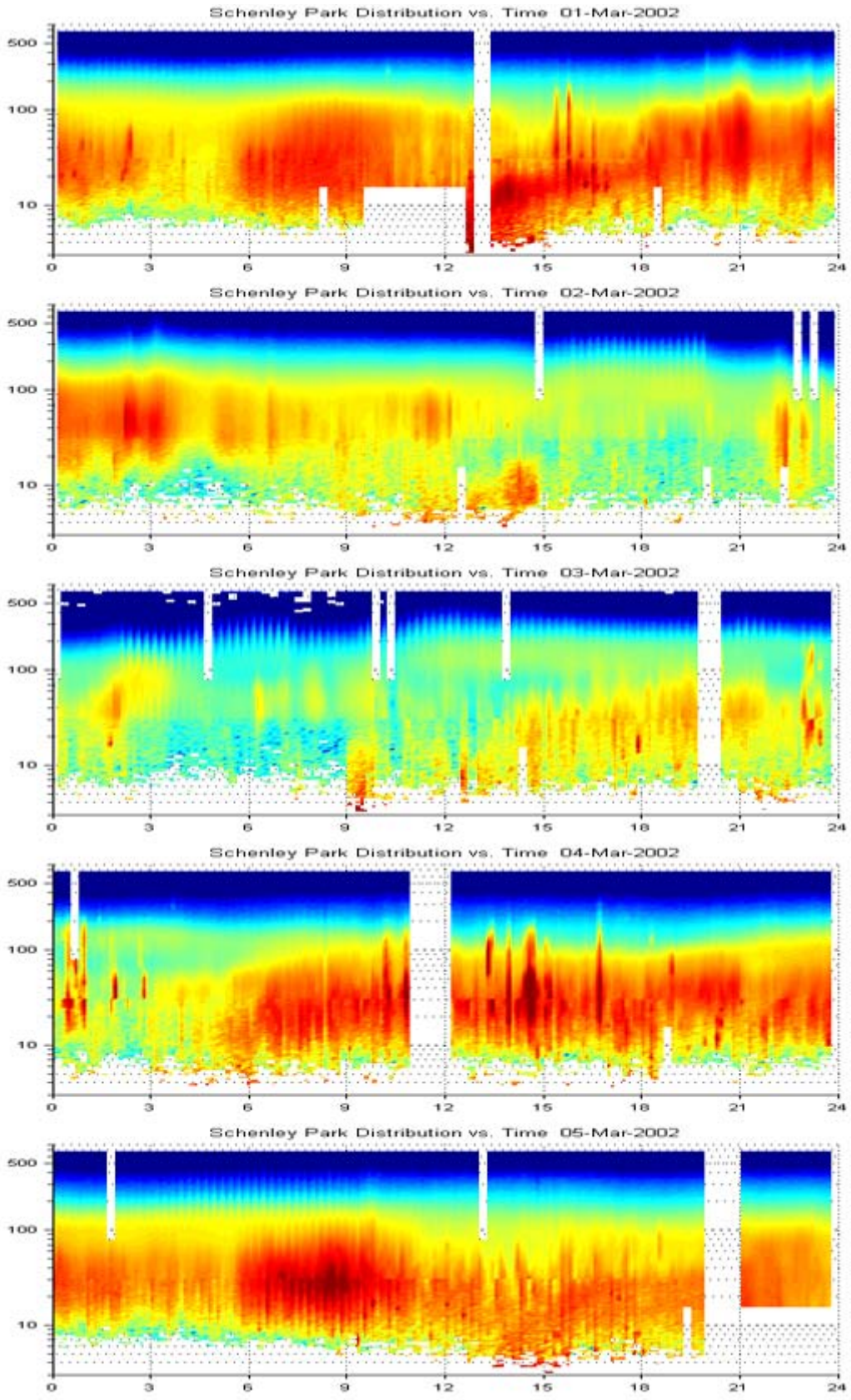
Schenley Park Distribution vs. Time 01-Mar-2002
Schenley Park Distribution vs. Time 02-Mar-2002
Schenley Park Distribution vs. Time 03-Mar-2002
Schenley Park Distribution vs. Time 04-Mar-2002
Schenley Park Distribution vs. Time 05-Mar-2002
500
100
10
0
3
6
9
12
15
18
21
24

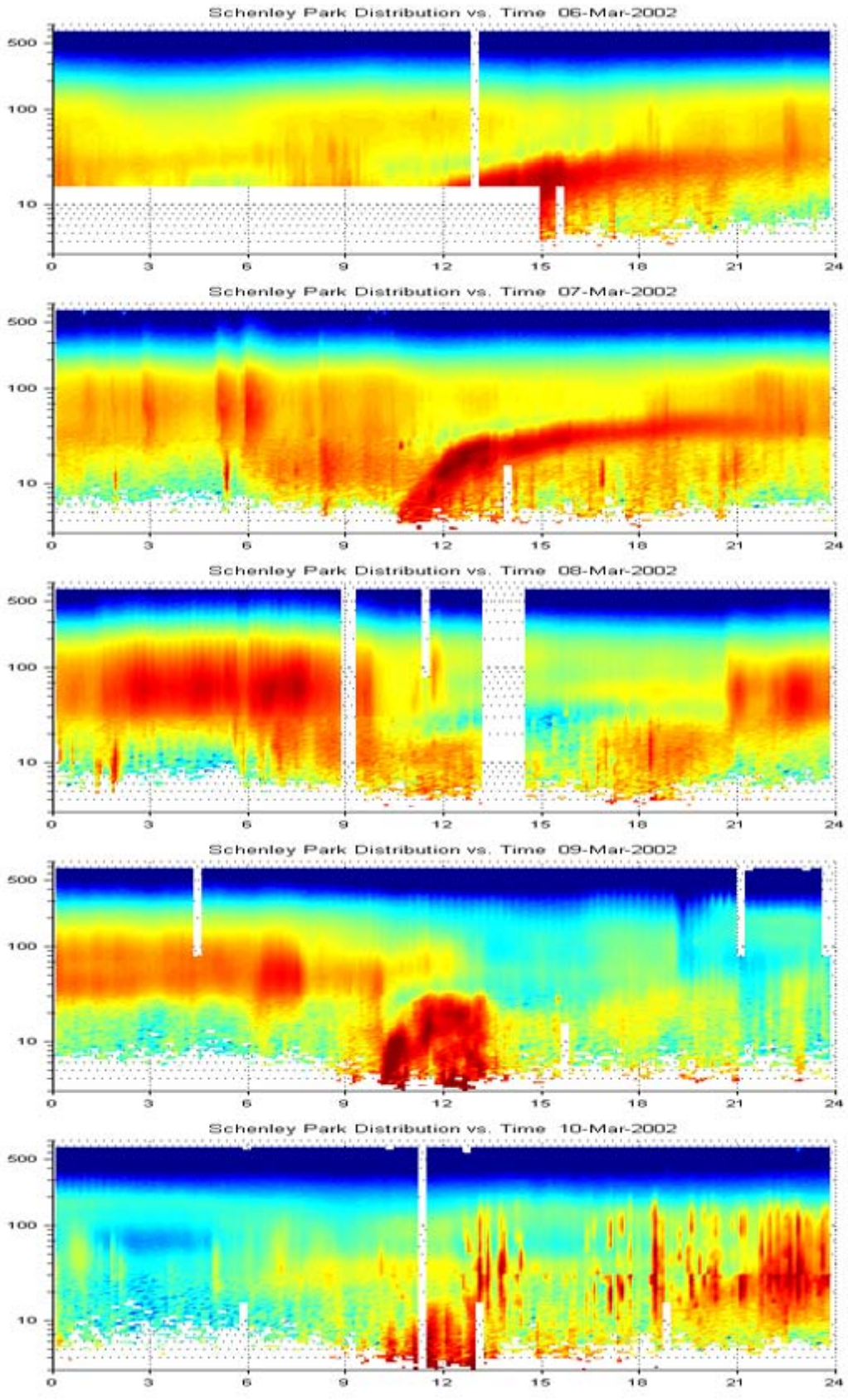
Schenley Park Distribution vs. Time 06-Mar-2002
Schenley Park Distribution vs. Time 07-Mar-2002
Schenley Park Distribution vs. Time 08-Mar-2002
Schenley Park Distribution vs. Time 09-Mar-2002
Schenley Park Distribution vs. Time 10-Mar-2002
500
100
10
0
3
6
9
12
15
18
21
24

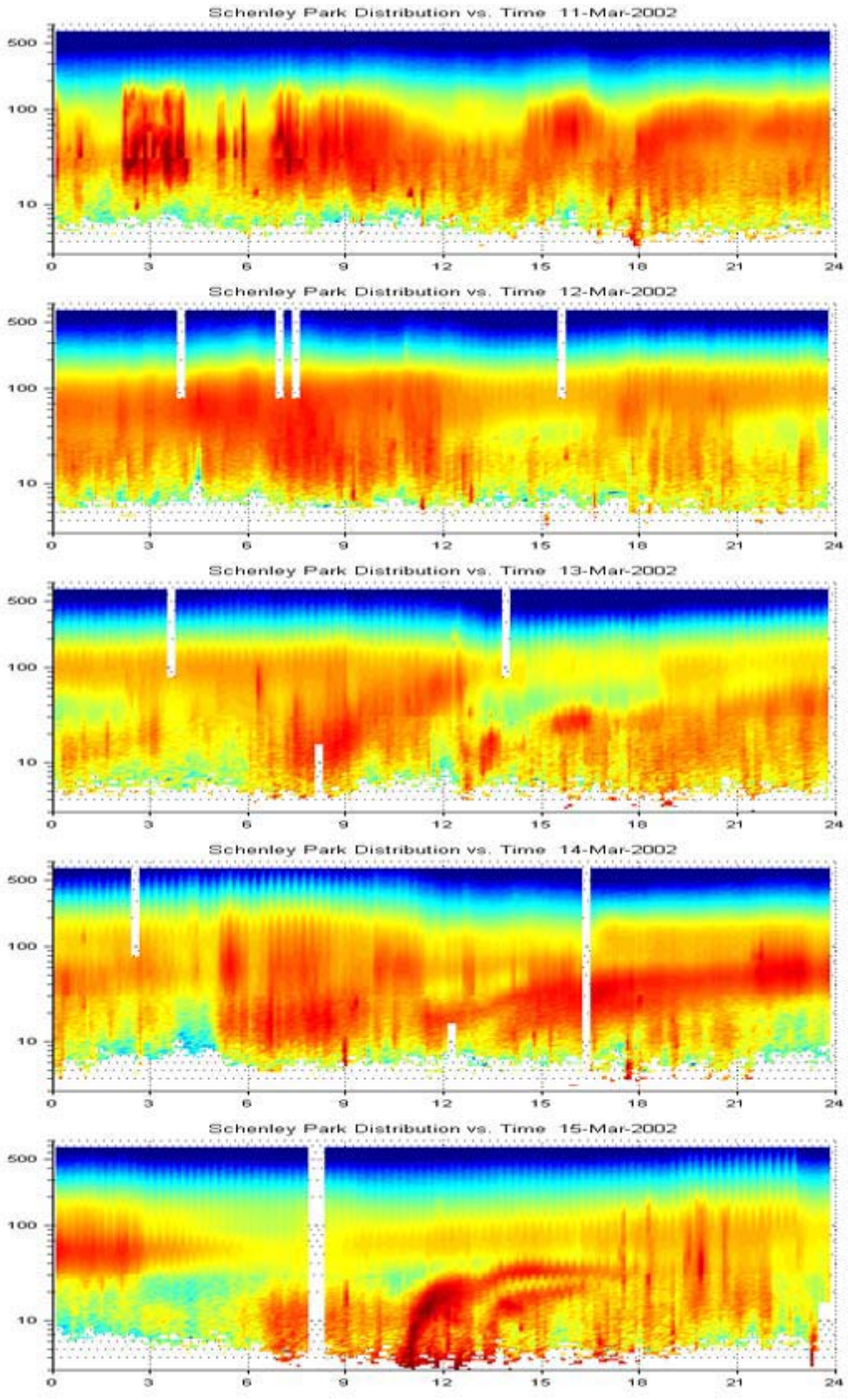
Schenley Park Distribution vs. Time 11-Mar-2002
Schenley Park Distribution vs. Time 12-Mar-2002
Schenley Park Distribution vs. Time 13-Mar-2002
Schenley Park Distribution vs. Time 14-Mar-2002
Schenley Park Distribution vs. Time 15-Mar-2002
500
100
10
0
3
6
9
12
15
18
21
24

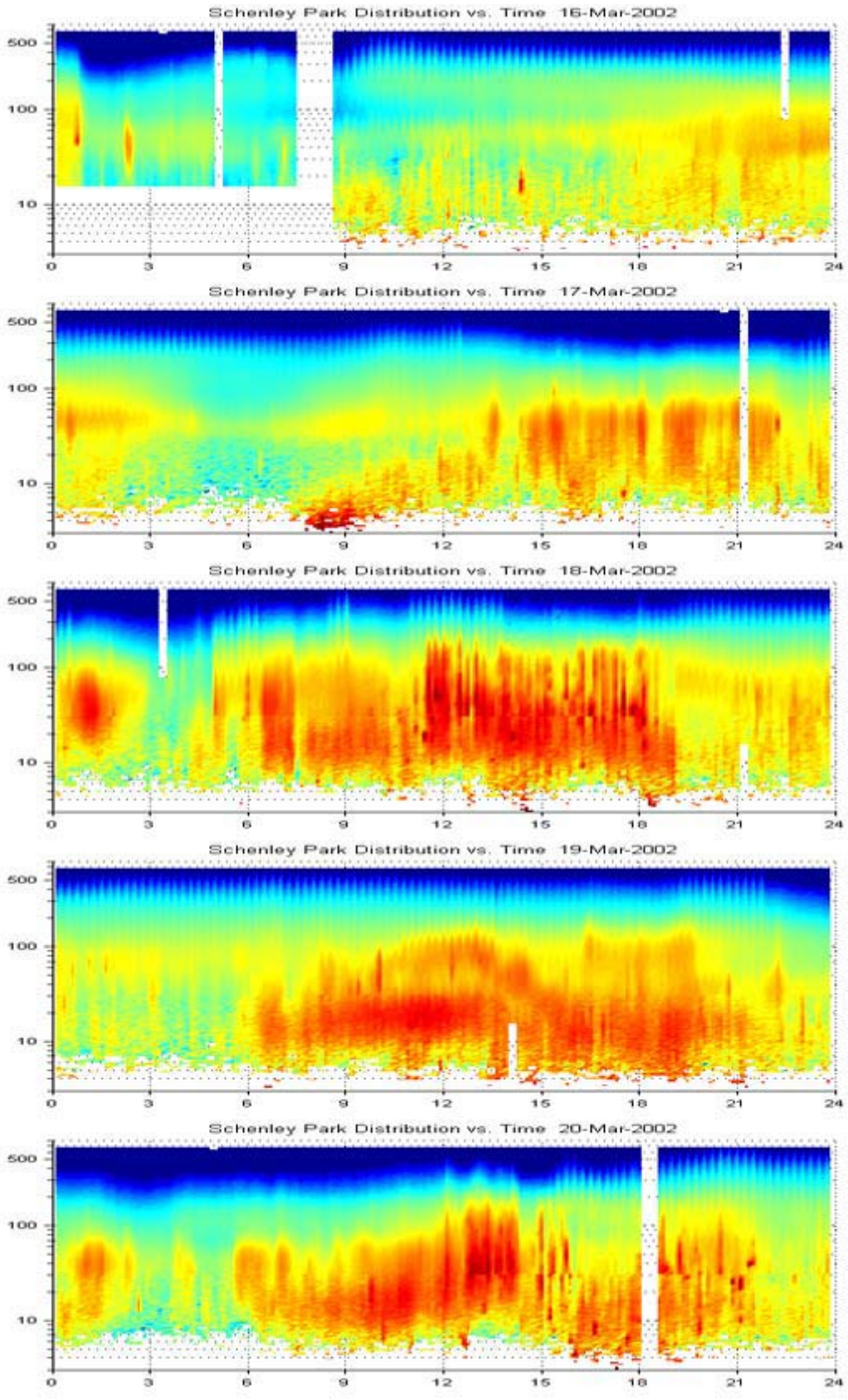
Schenley Park Distribution vs. Time 16-Mar-2002
Schenley Park Distribution vs. Time 17-Mar-2002
Schenley Park Distribution vs. Time 18-Mar-2002
Schenley Park Distribution vs. Time 19-Mar-2002
Schenley Park Distribution vs. Time 20-Mar-2002
500
100
10
0
3
6
9
12
15
18
21
24

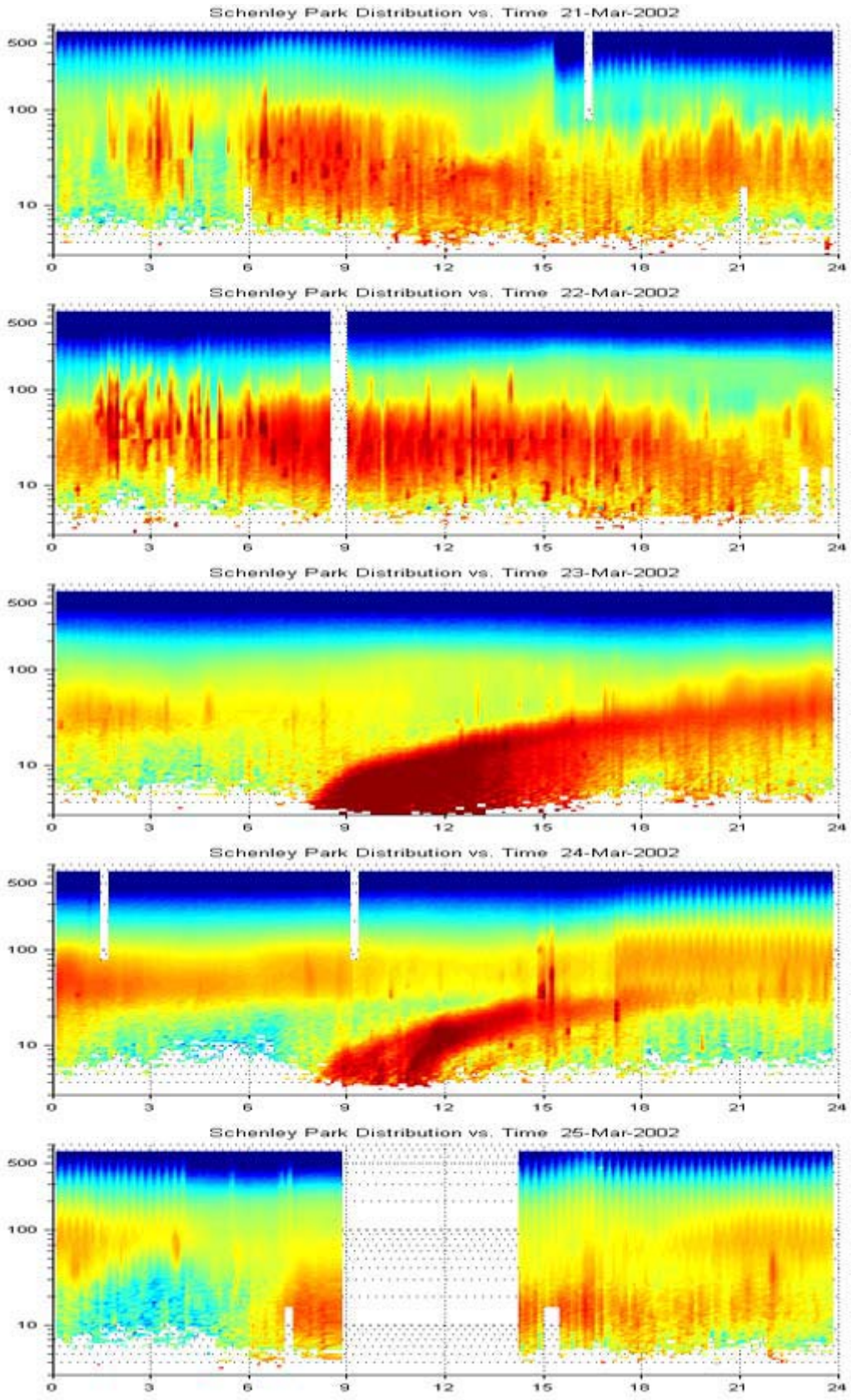
Schenley Park Distribution vs. Time 21-Mar-2002
Schenley Park Distribution vs. Time 22-Mar-2002
Schenley Park Distribution vs. Time 23-Mar-2002
Schenley Park Distribution vs. Time 24-Mar-2002
Schenley Park Distribution vs. Time 25-Mar-2002
500
100
10
0
3
6
9
12
15
18
21
24

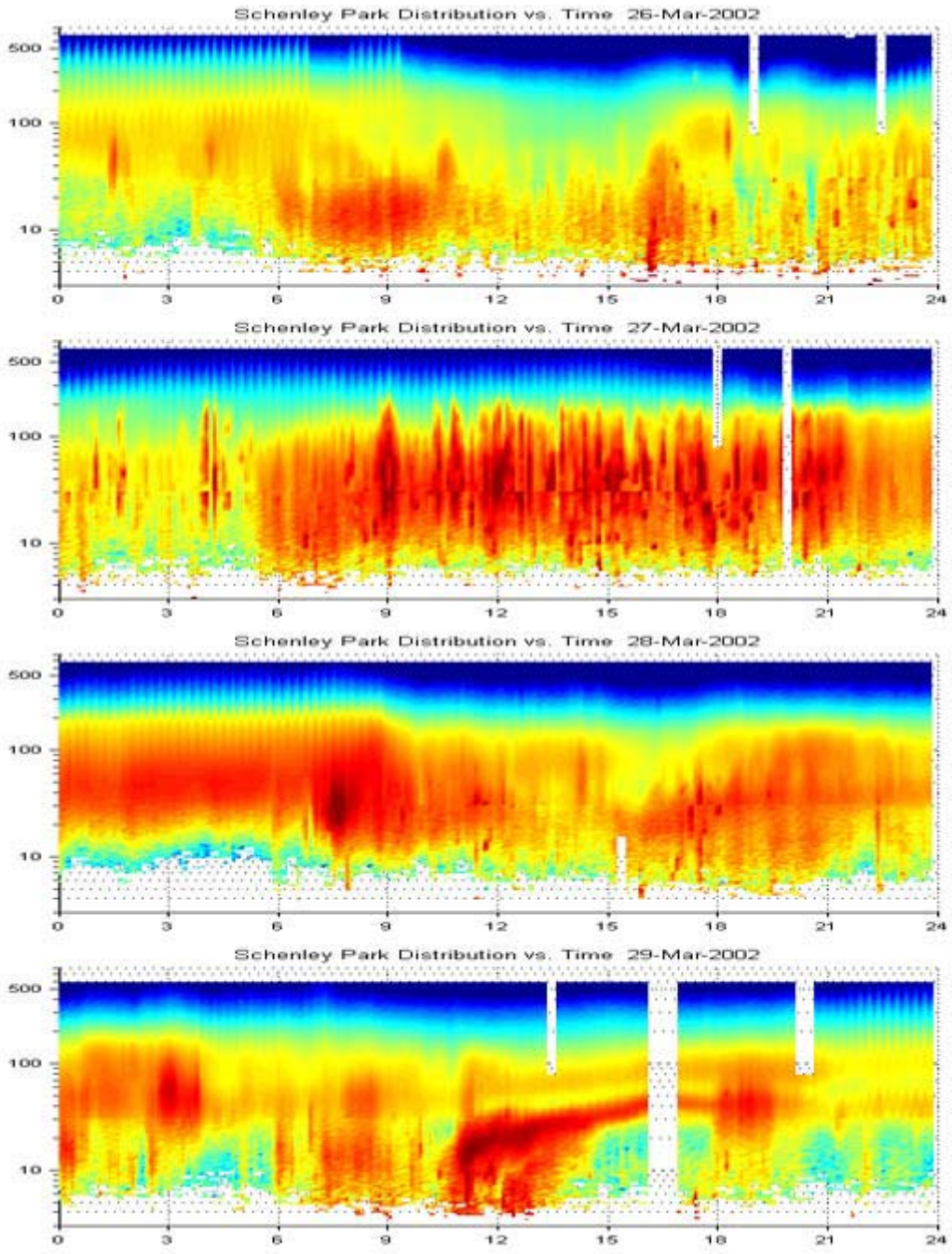
Schenley Park Distribution vs. Time 26-Mar-2002
Schenley Park Distribution vs. Time 27-Mar-2002
Schenley Park Distribution vs. Time 28-Mar-2002
Schenley Park Distribution vs. Time 29-Mar-2002
500
100
10
0
3
6
9
12
15
18
21
24

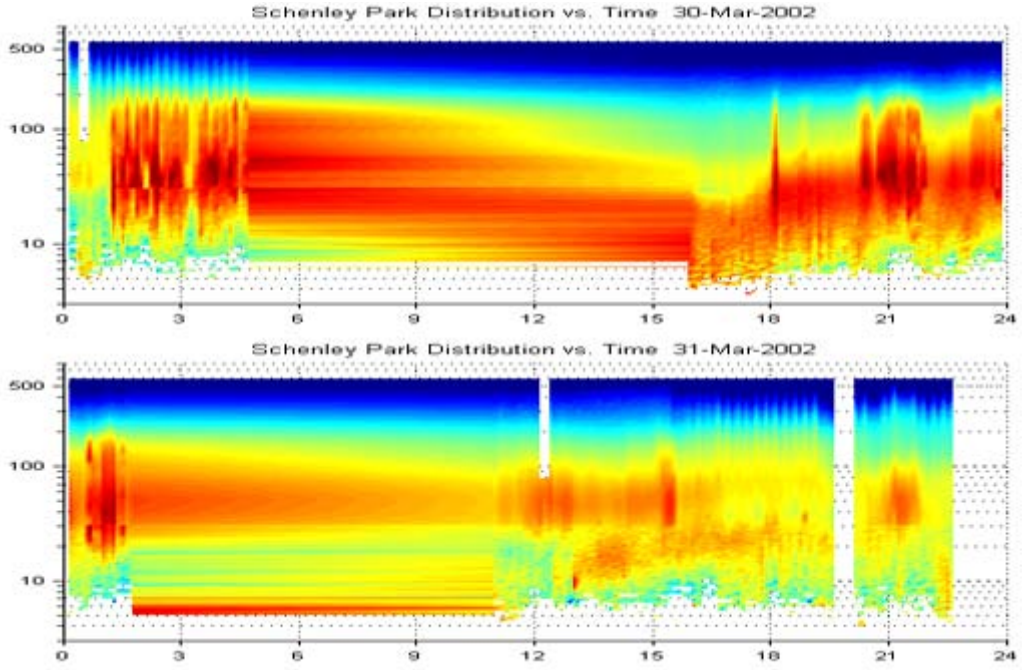
Schenley Park Distribution vs. Time 30-Mar-2002
500
100
10
0
3
6
9
12
15
18
21
24
Schenley Park Distribution vs. Time 31-Mar-2002
500
100
10
0
3
6
9
12
15
18
21
24

APRIL 2002

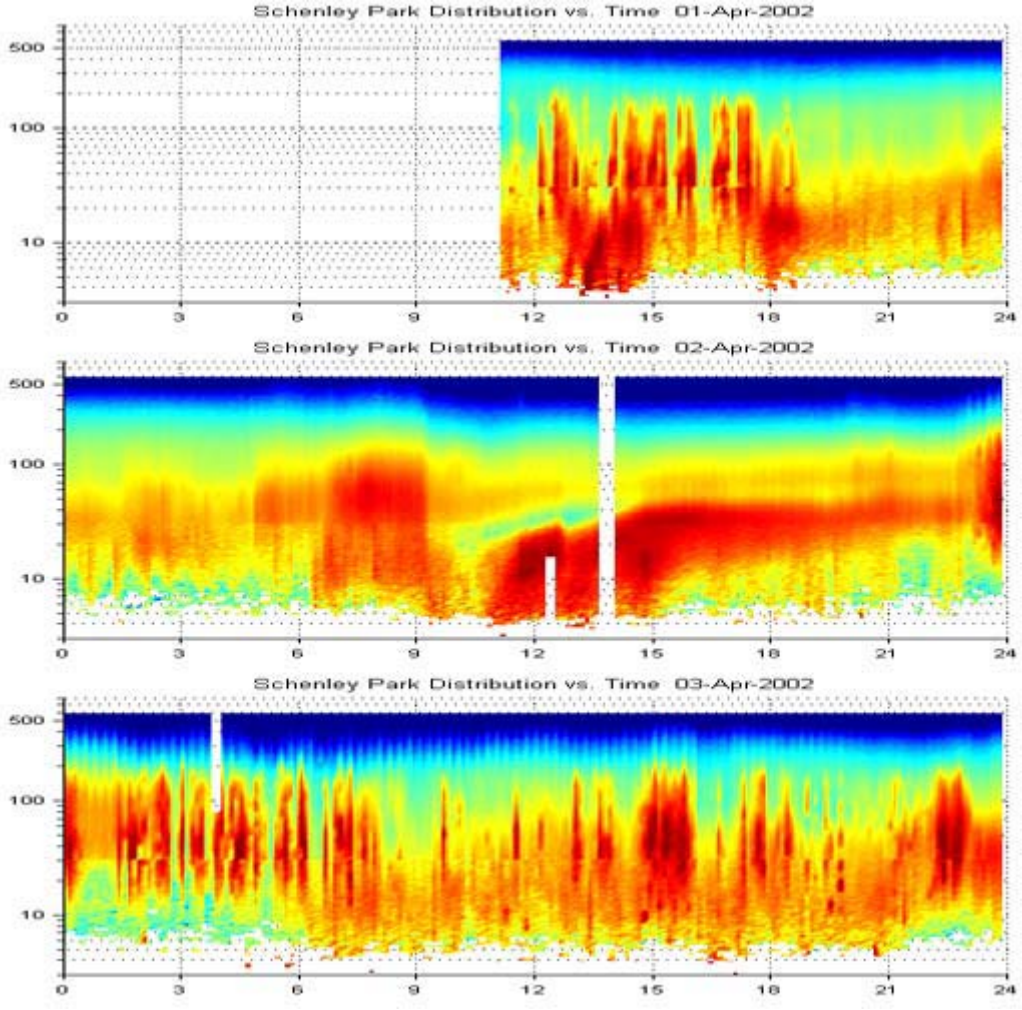
Schenley Park Distribution vs. Time 01-Apr-2002
500
100
10
0
3
6
9
12
15
18
21
24
Schenley Park Distribution vs. Time 02-Apr-2002
500
100
10
0
3
6
9
12
15
18
21
24
Schenley Park Distribution vs. Time 03-Apr-2002
500
100
10
0
3
6
9
12
15
18
21
24

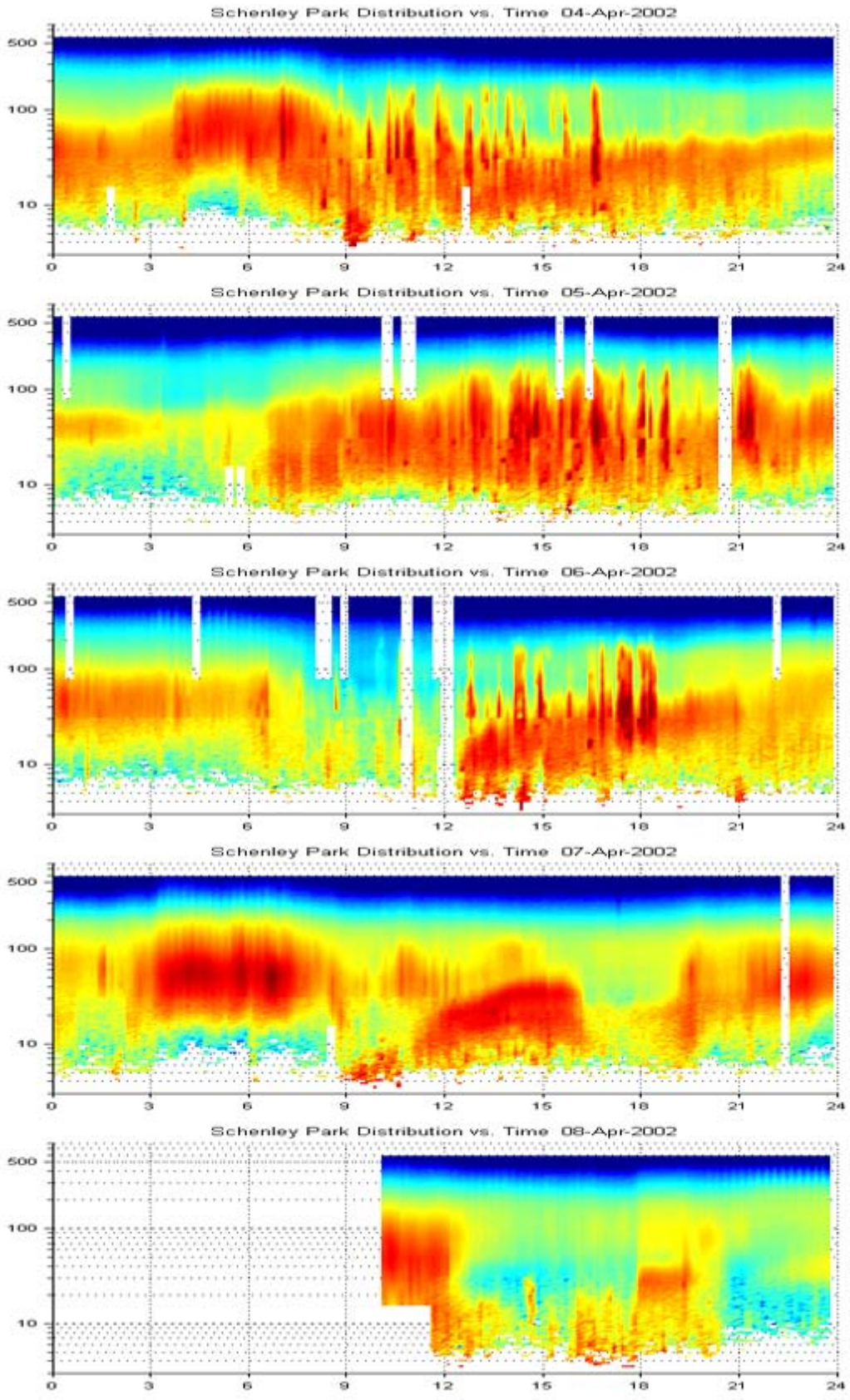
Schenley Park Distribution vs. Time 04-Apr-2002
Schenley Park Distribution vs. Time 05-Apr-2002
Schenley Park Distribution vs. Time 06-Apr-2002
Schenley Park Distribution vs. Time 07-Apr-2002
Schenley Park Distribution vs. Time 08-Apr-2002
500
100
10
0
3
6
9
12
15
18
21
24

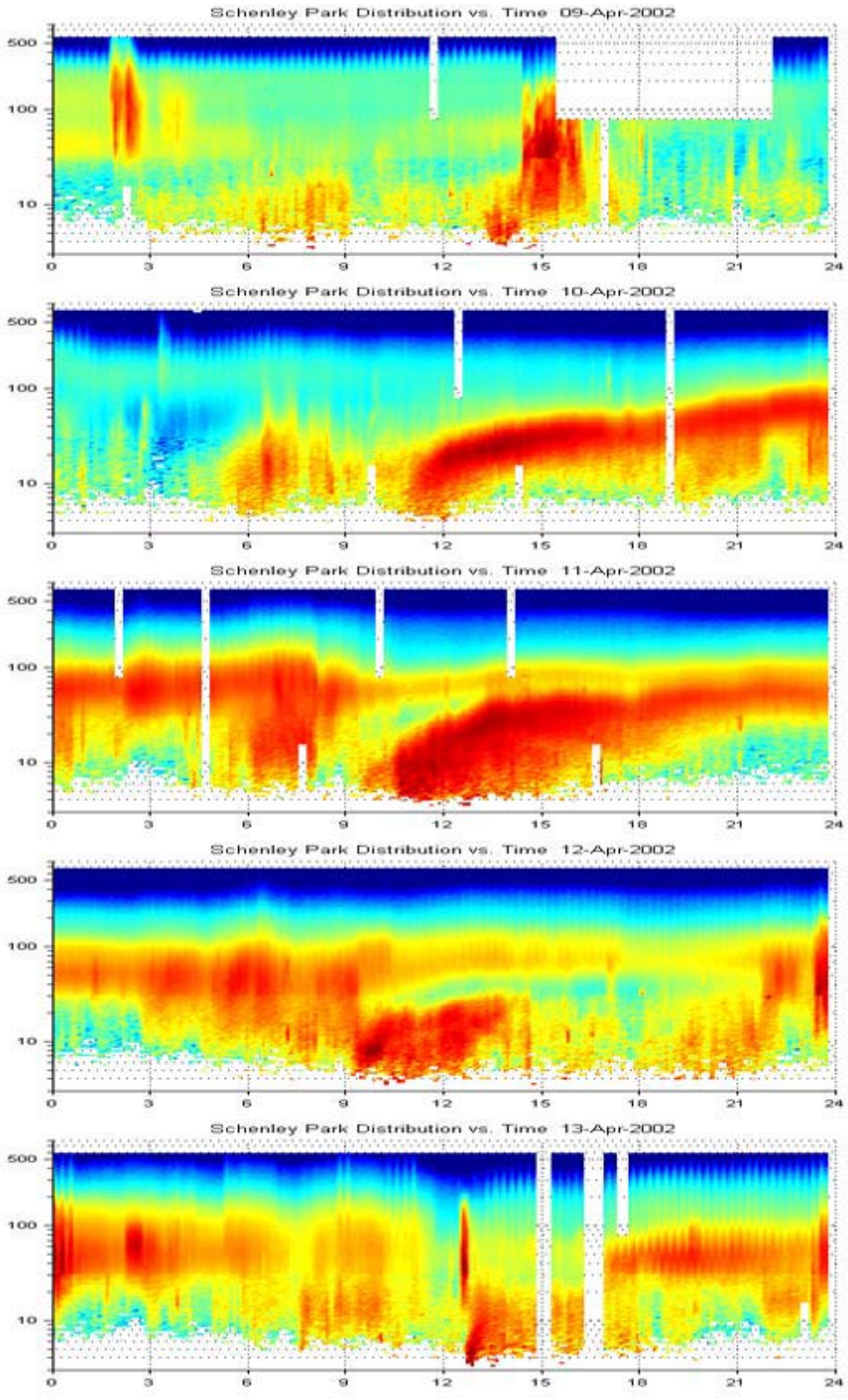
Schenley Park Distribution vs. Time 09-Apr-2002
Schenley Park Distribution vs. Time 10-Apr-2002
Schenley Park Distribution vs. Time 11-Apr-2002
Schenley Park Distribution vs. Time 12-Apr-2002
Schenley Park Distribution vs. Time 13-Apr-2002
500
100
10
0
3
6
9
12
15
18
21
24

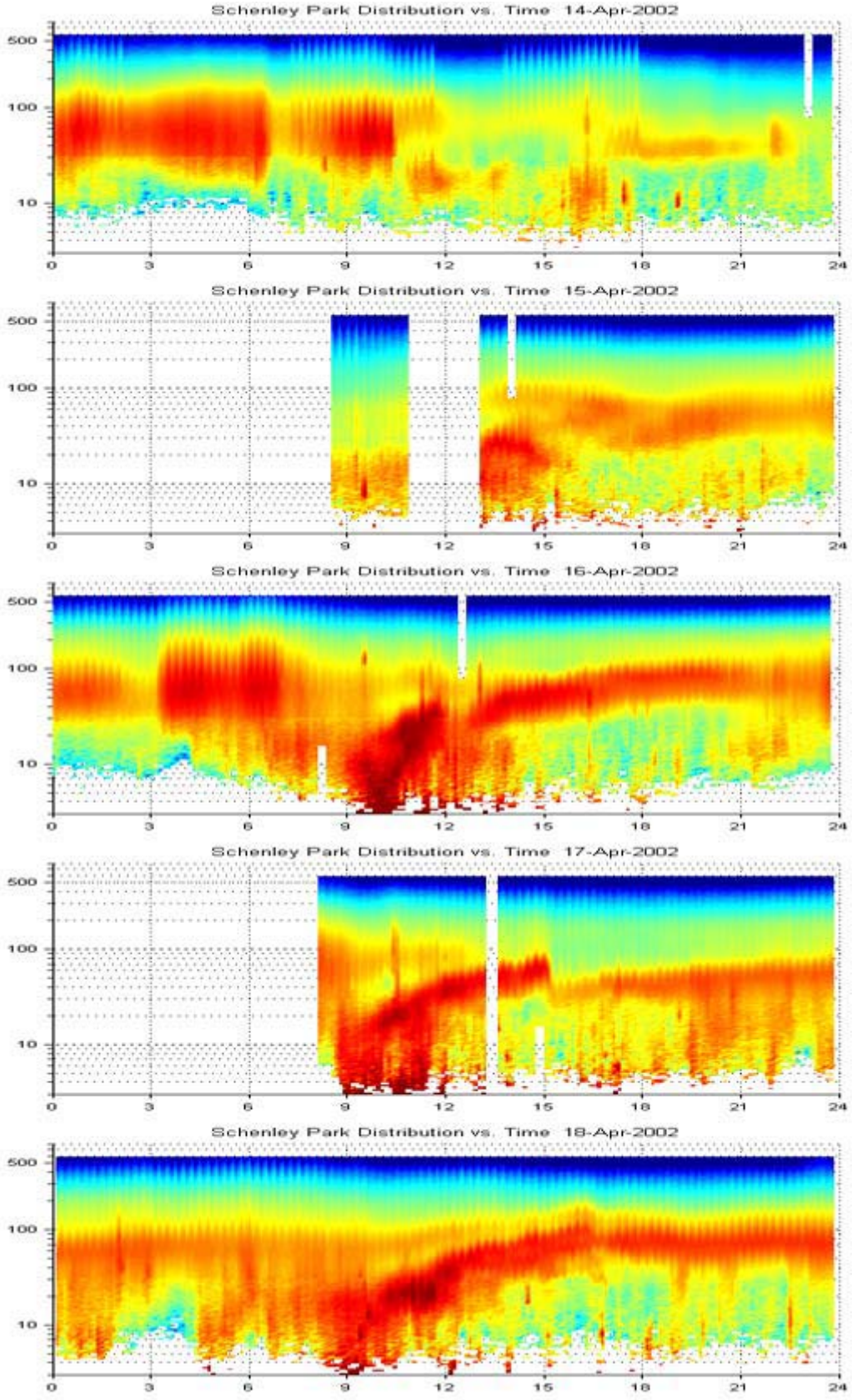
Schenley Park Distribution vs. Time 14-Apr-2002
Schenley Park Distribution vs. Time 15-Apr-2002
Schenley Park Distribution vs. Time 16-Apr-2002
Schenley Park Distribution vs. Time 17-Apr-2002
Schenley Park Distribution vs. Time 18-Apr-2002
500
100
10
0
3
6
9
12
15
18
21
24

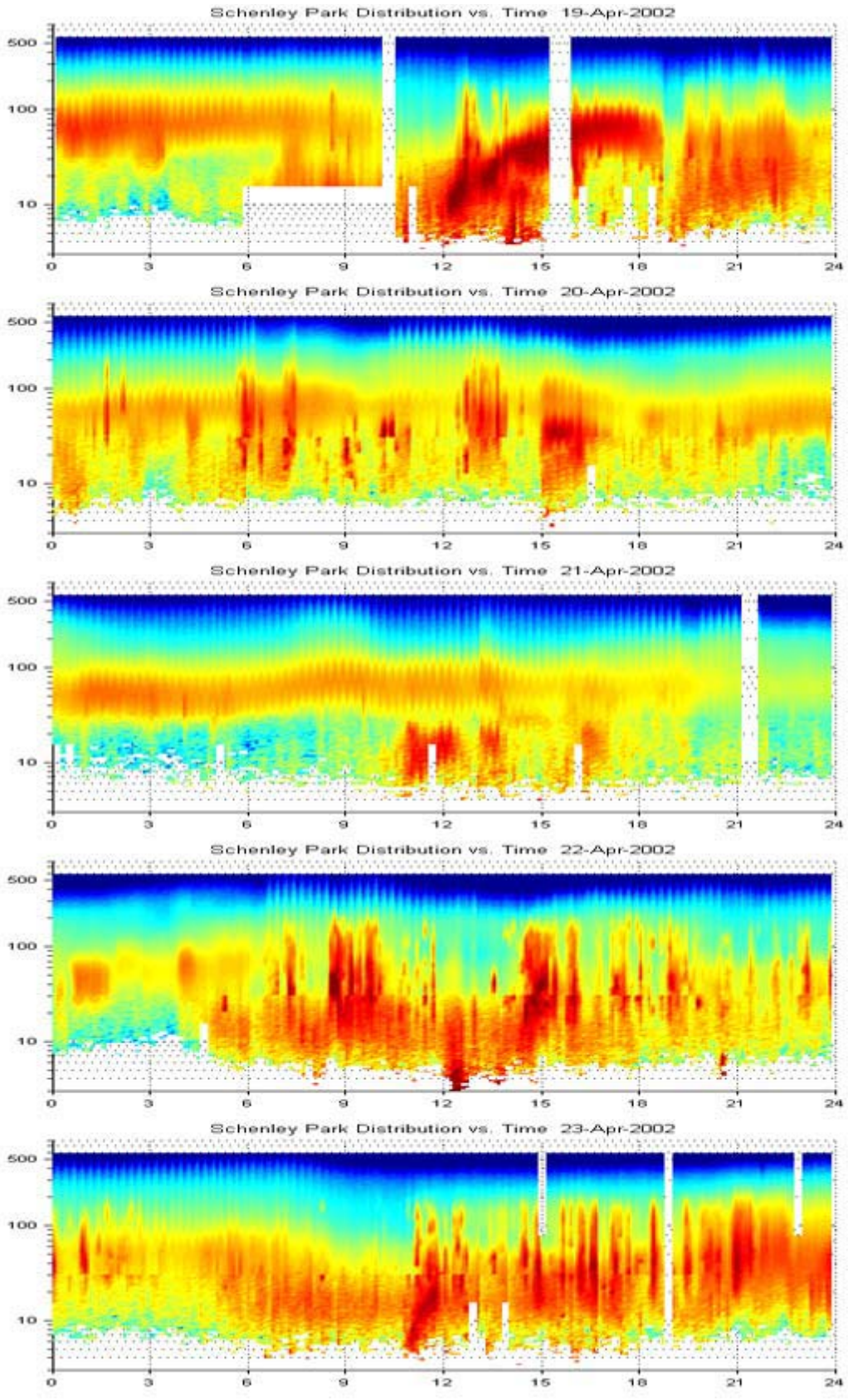
Schenley Park Distribution vs. Time 19-Apr-2002
Schenley Park Distribution vs. Time 20-Apr-2002
Schenley Park Distribution vs. Time 21-Apr-2002
Schenley Park Distribution vs. Time 22-Apr-2002
Schenley Park Distribution vs. Time 23-Apr-2002
500
100
10
0
3
6
9
12
15
18
21
24

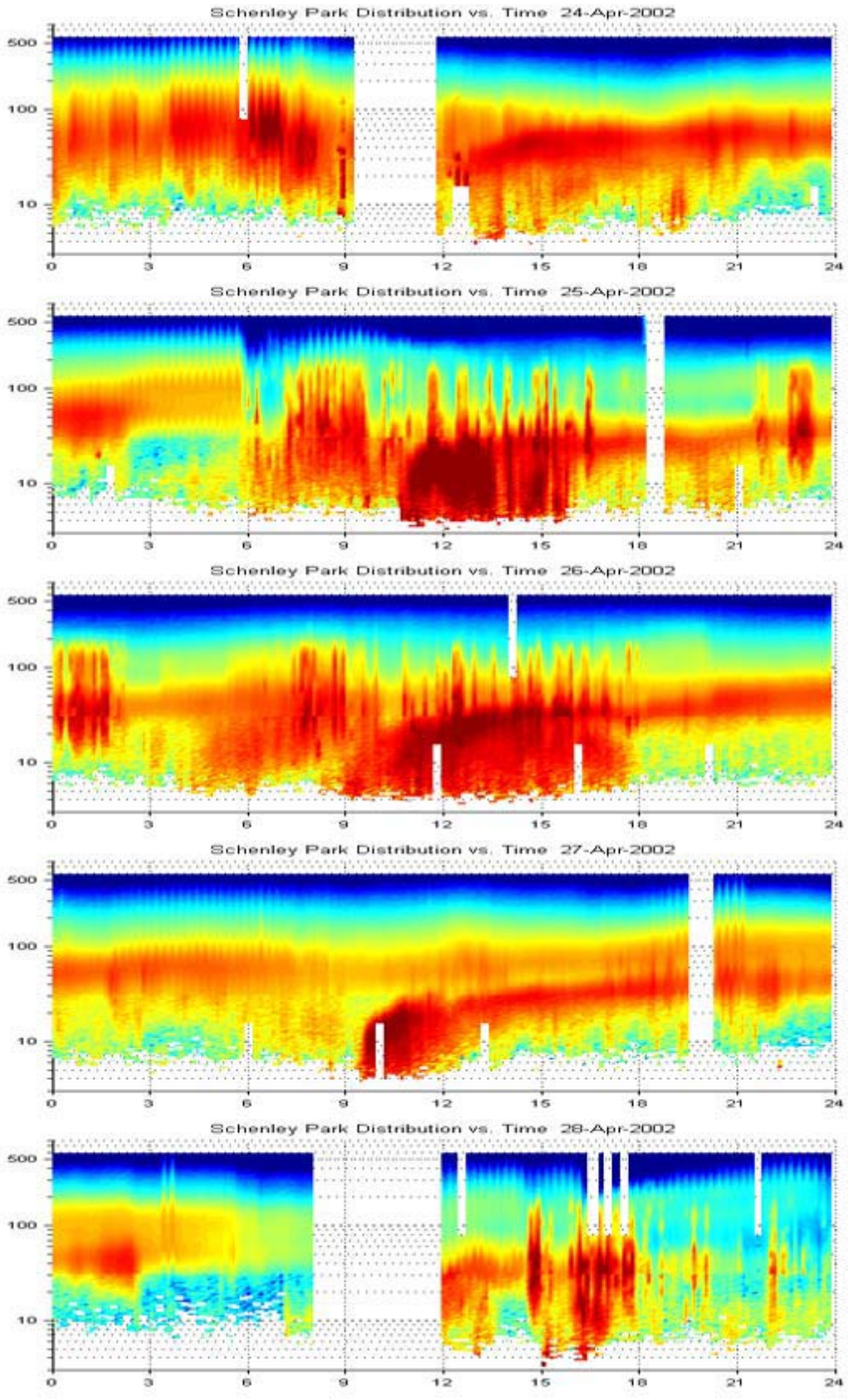
Schenley Park Distribution vs. Time 24-Apr-2002
Schenley Park Distribution vs. Time 25-Apr-2002
Schenley Park Distribution vs. Time 26-Apr-2002
Schenley Park Distribution vs. Time 27-Apr-2002
Schenley Park Distribution vs. Time 28-Apr-2002
500
100
10
0
3
6
9
12
15
18
21
24

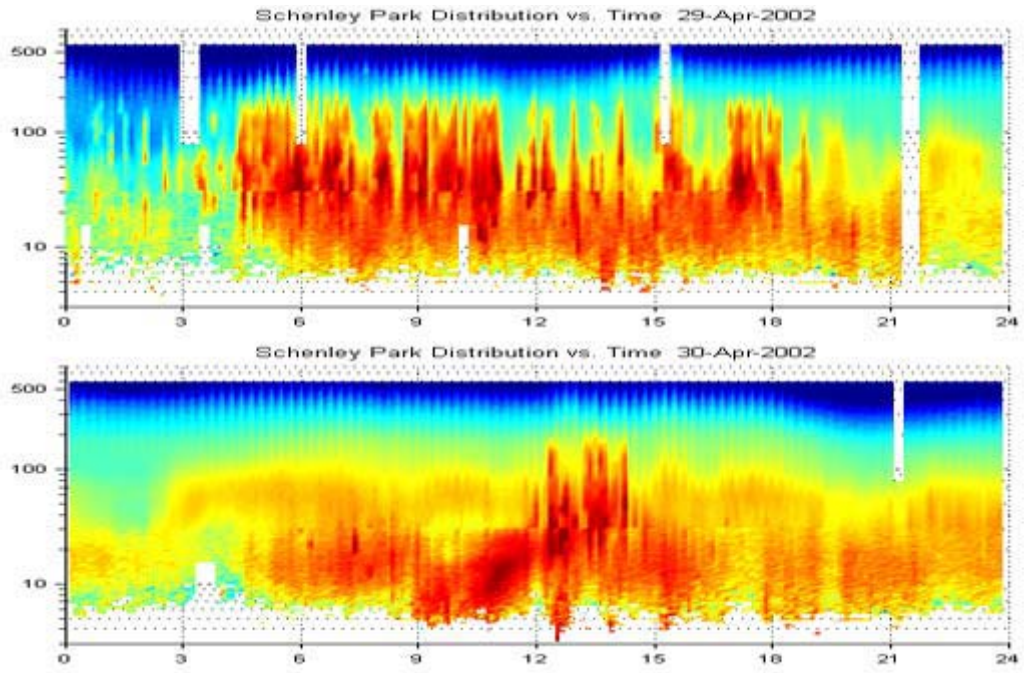
Schenley Park Distribution vs. Time 29-Apr-2002
500
100
10
0
3
6
9
12
15
18
21
24
Schenley Park Distribution vs. Time 30-Apr-2002
500
100
10
0
3
6
9
12
15
18
21
24

MAY 2002

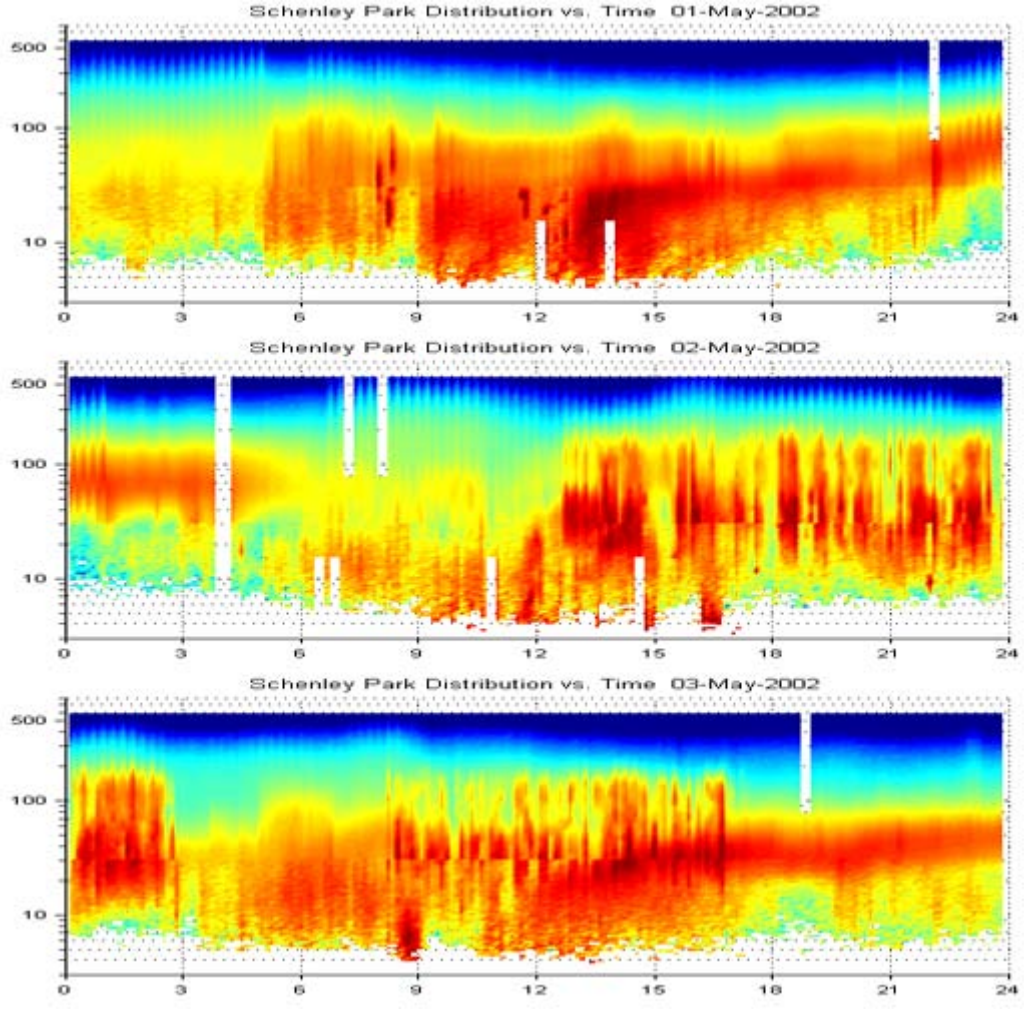
Schenley Park Distribution vs. Time 01-May-2002
500
100
10
0
3
6
9
12
15
18
21
24
Schenley Park Distribution vs. Time 02-May-2002
500
100
10
0
3
6
9
12
15
18
21
24
Schenley Park Distribution vs. Time 03-May-2002
500
100
10
0
3
6
9
12
15
18
21
24

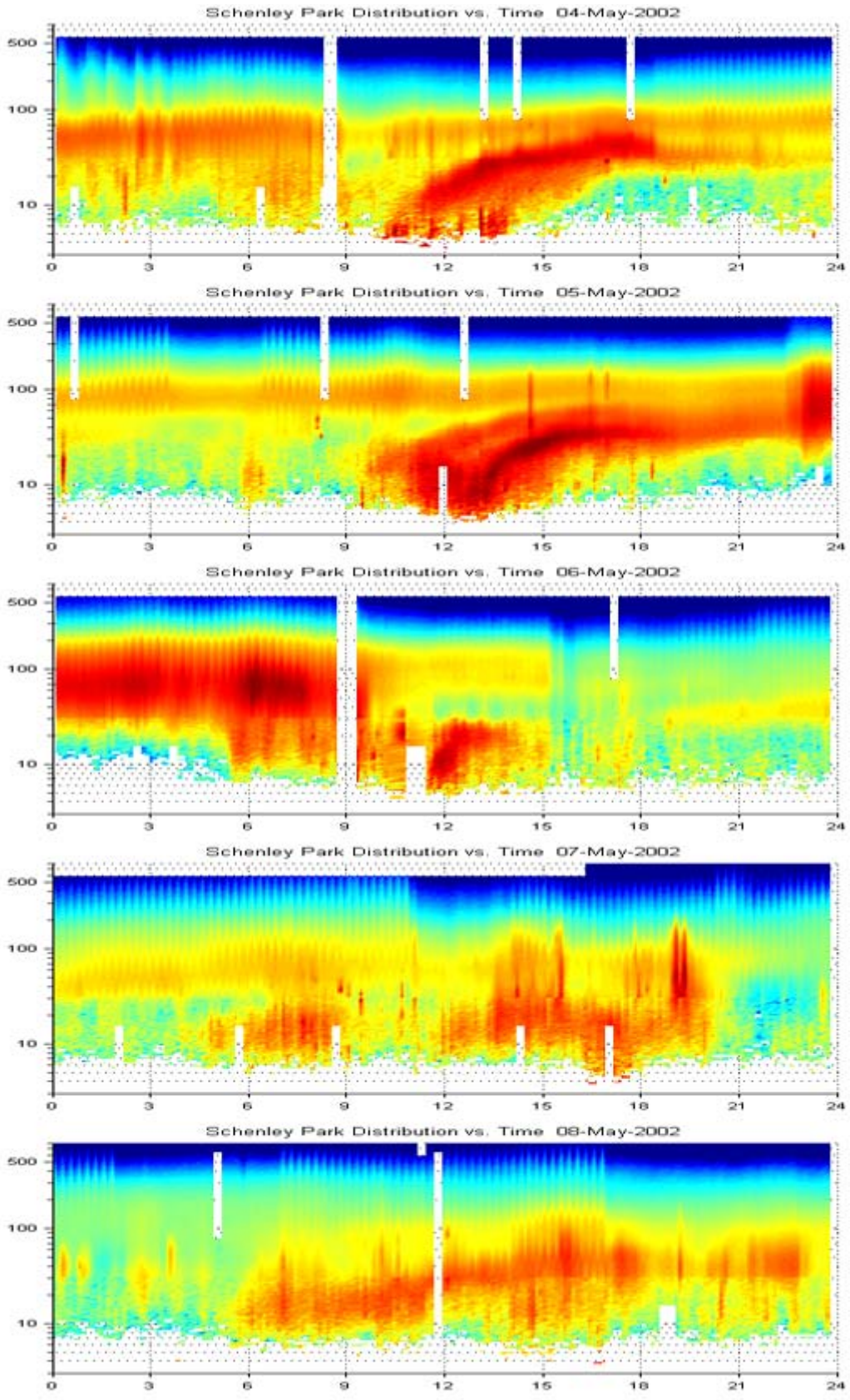
Schenley Park Distribution vs. Time 04-May-2002
Schenley Park Distribution vs. Time 05-May-2002
Schenley Park Distribution vs. Time 06-May-2002
Schenley Park Distribution vs. Time 07-May-2002
Schenley Park Distribution vs. Time 08-May-2002
500
100
10
0
3
6
9
12
15
18
21
24

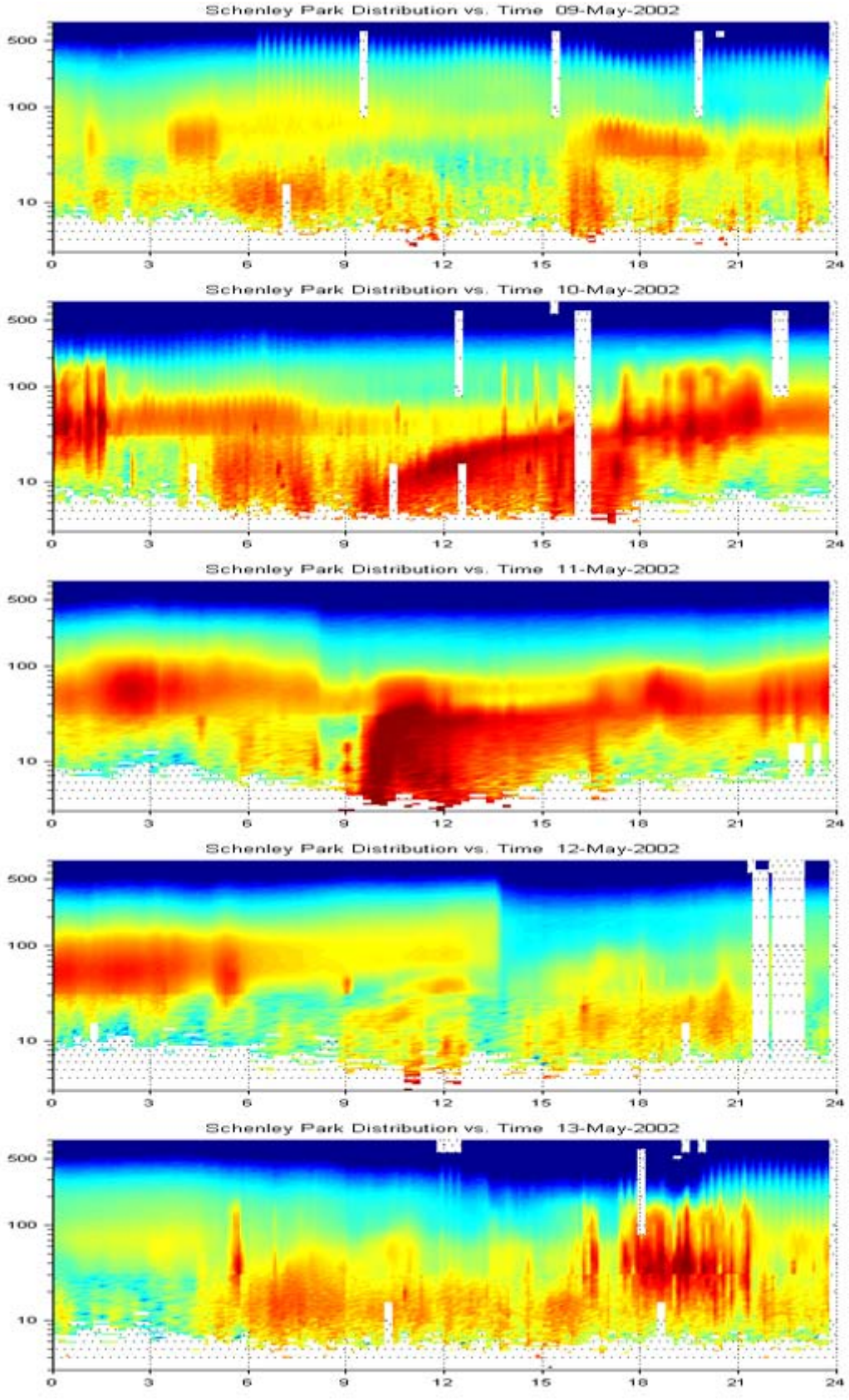
Schenley Park Distribution vs. Time 09-May-2002
Schenley Park Distribution vs. Time 10-May-2002
Schenley Park Distribution vs. Time 11-May-2002
Schenley Park Distribution vs. Time 12-May-2002
Schenley Park Distribution vs. Time 13-May-2002
500
100
10
0
3
6
9
12
15
18
21
24

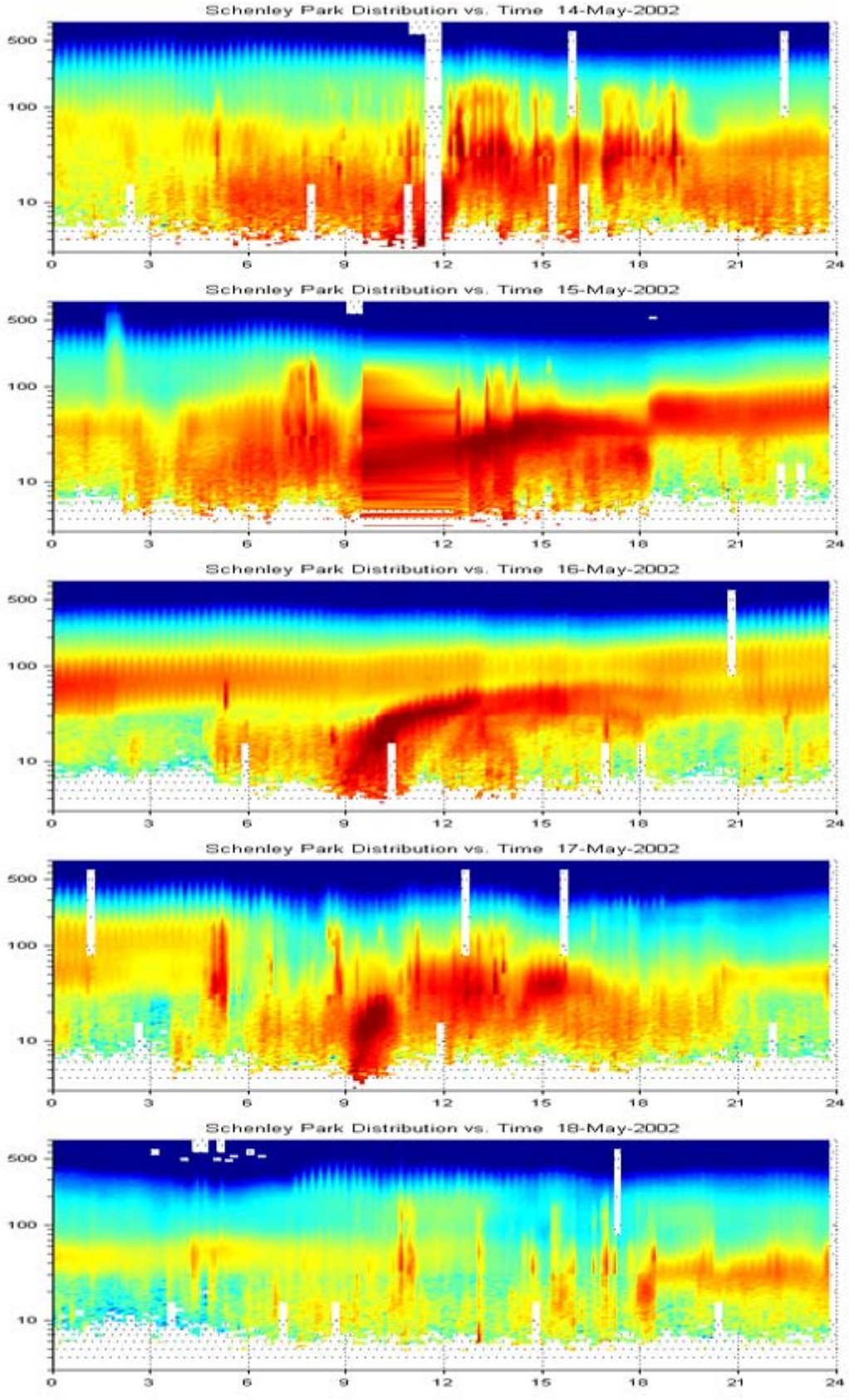
Schenley Park Distribution vs. Time 14-May-2002
Schenley Park Distribution vs. Time 15-May-2002
Schenley Park Distribution vs. Time 16-May-2002
Schenley Park Distribution vs. Time 17-May-2002
Schenley Park Distribution vs. Time 18-May-2002
500
100
10
0
3
6
9
12
15
18
21
24

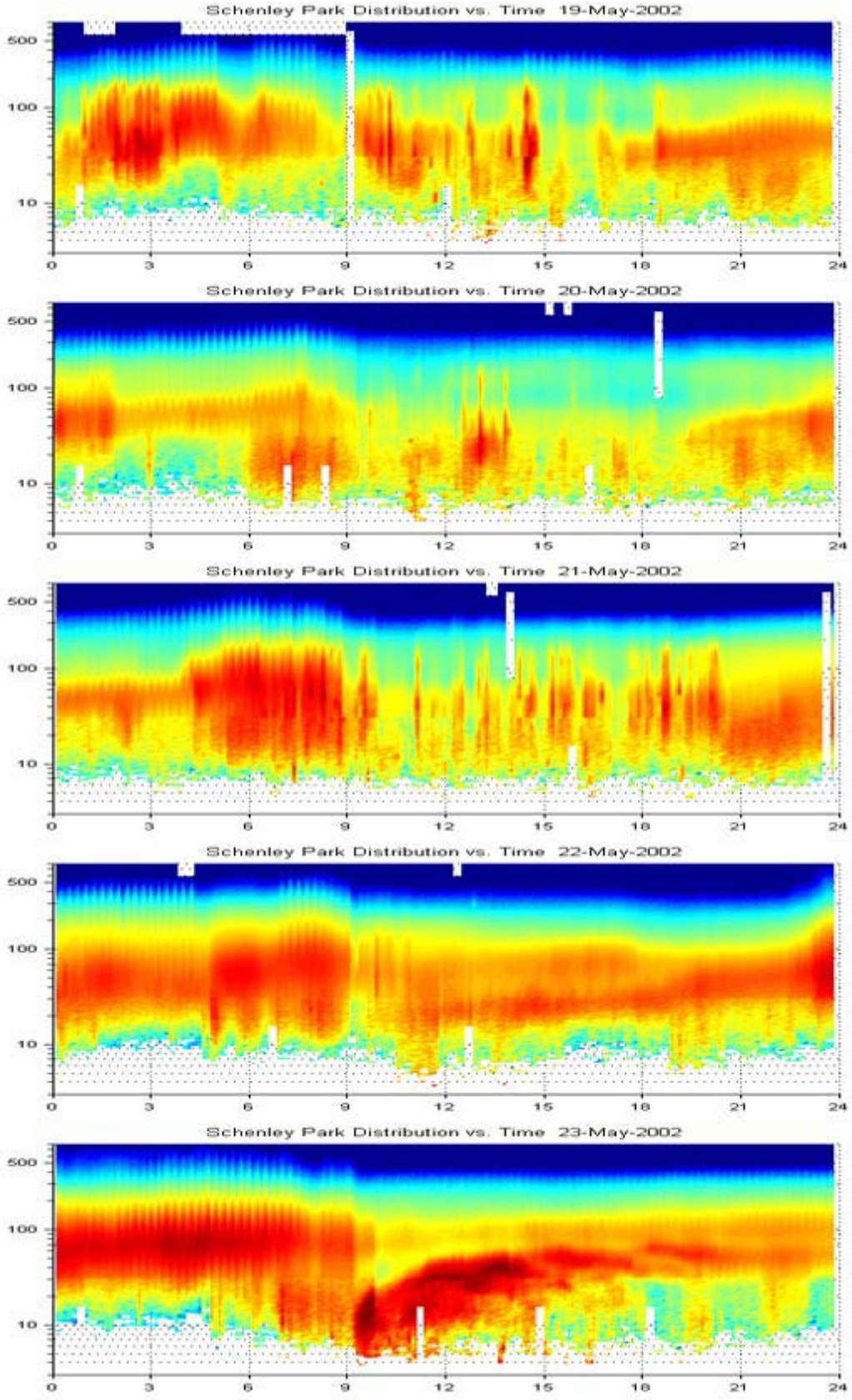
Schenley Park Distribution vs. Time 19-May-2002
Schenley Park Distribution vs. Time 20-May-2002
Schenley Park Distribution vs. Time 21-May-2002
Schenley Park Distribution vs. Time 22-May-2002
Schenley Park Distribution vs. Time 23-May-2002
500
100
10
0
3
6
9
12
15
18
21
24

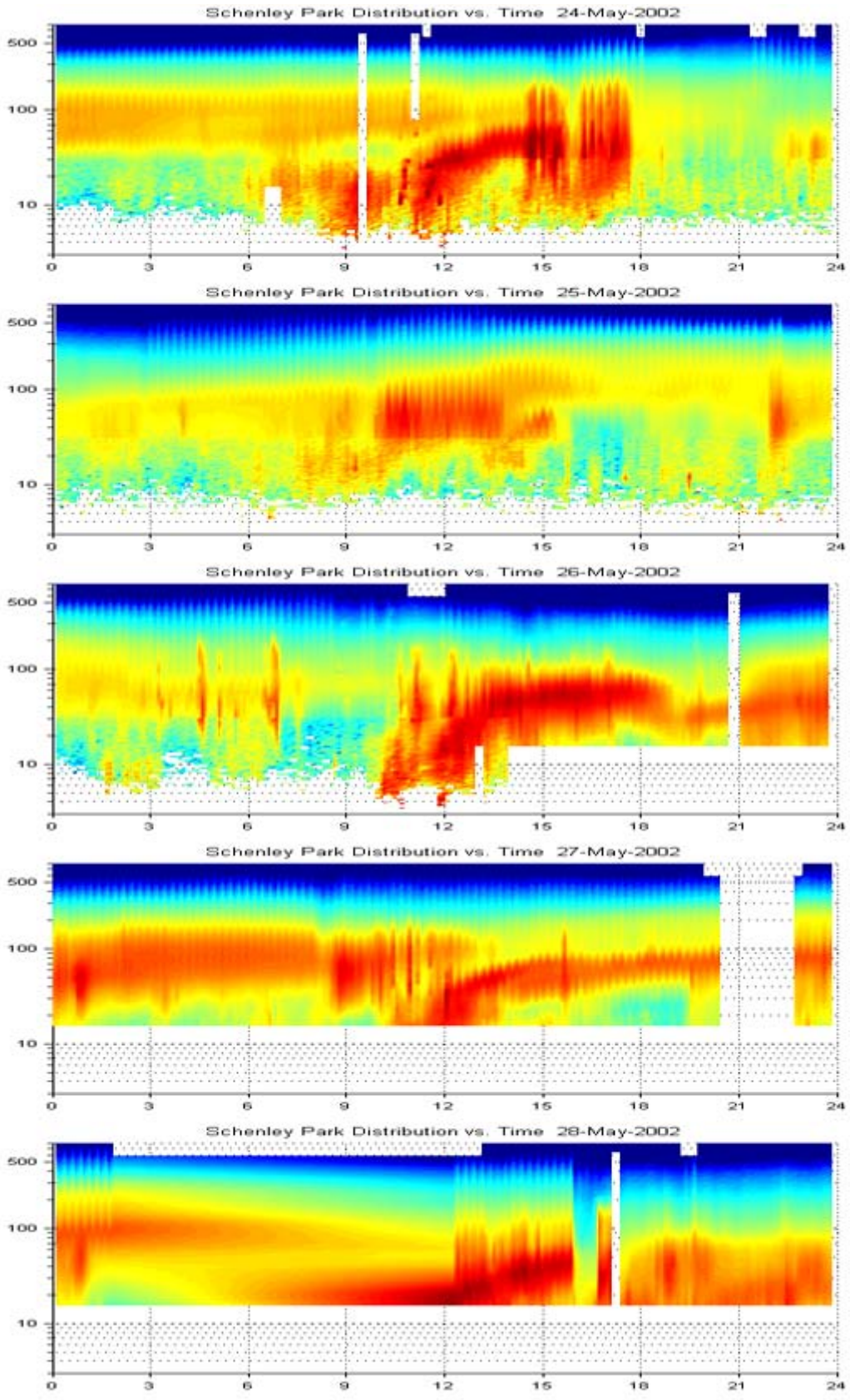
Schenley Park Distribution vs. Time 24-May-2002
Schenley Park Distribution vs. Time 25-May-2002
Schenley Park Distribution vs. Time 26-May-2002
Schenley Park Distribution vs. Time 27-May-2002
Schenley Park Distribution vs. Time 28-May-2002
500
100
10
0
3
6
9
12
15
18
21
24

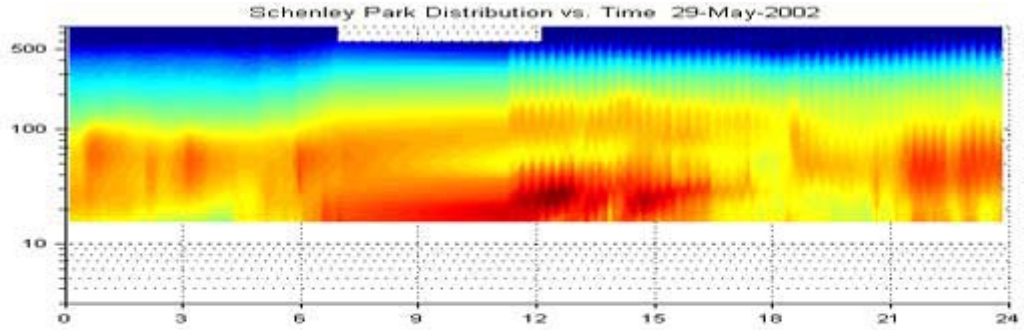
Schenley Park Distribution vs. Time 29-May-2002
500
100
10
0
3
6
9
12
15
18
21
24

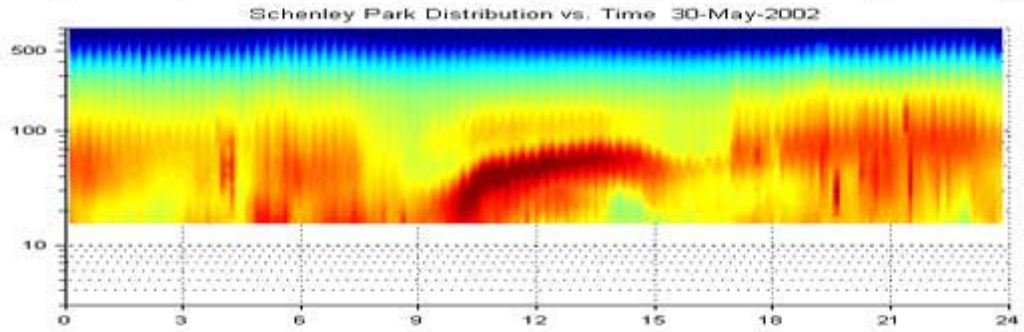
Schenley Park Distribution vs. Time 30-May-2002
500
100
10
0
3
6
9
12
15
18
21
24

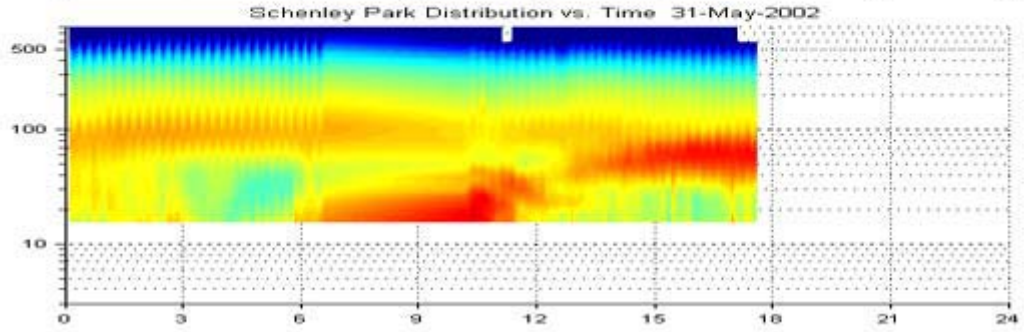
Schenley Park Distribution vs. Time 31-May-2002
500
100
10
0
3
6
9
12
15
18
21
24

JUNE 2002

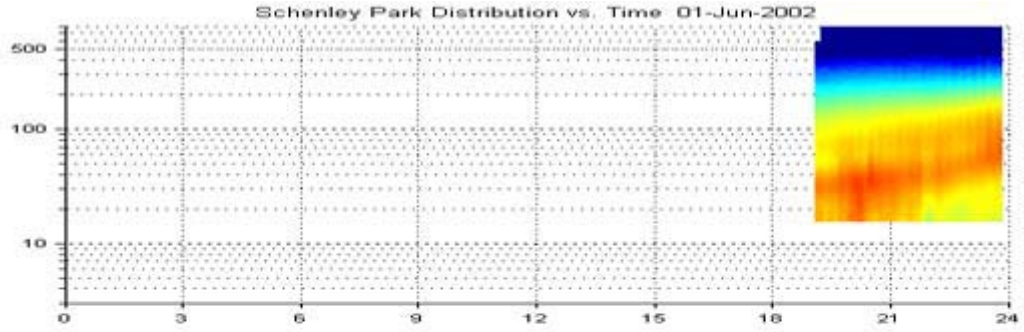
Schenley Park Distribution vs. Time 01-Jun-2002
500
100
10
0
3
6
9
12
15
18
21
24

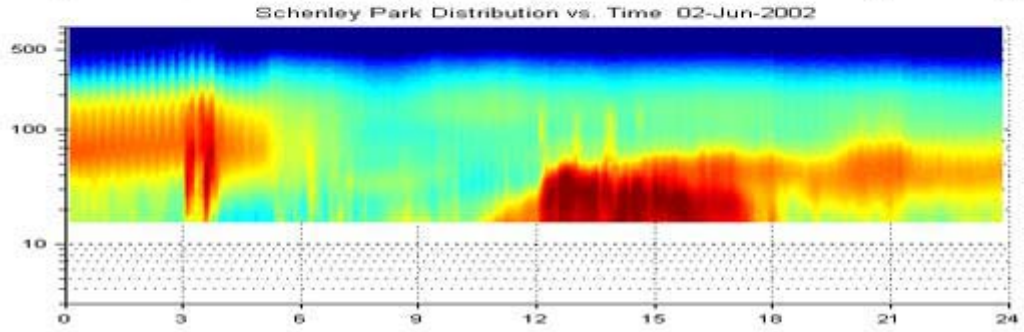
Schenley Park Distribution vs. Time 02-Jun-2002
500
100
10
0
3
6
9
12
15
18
21
24

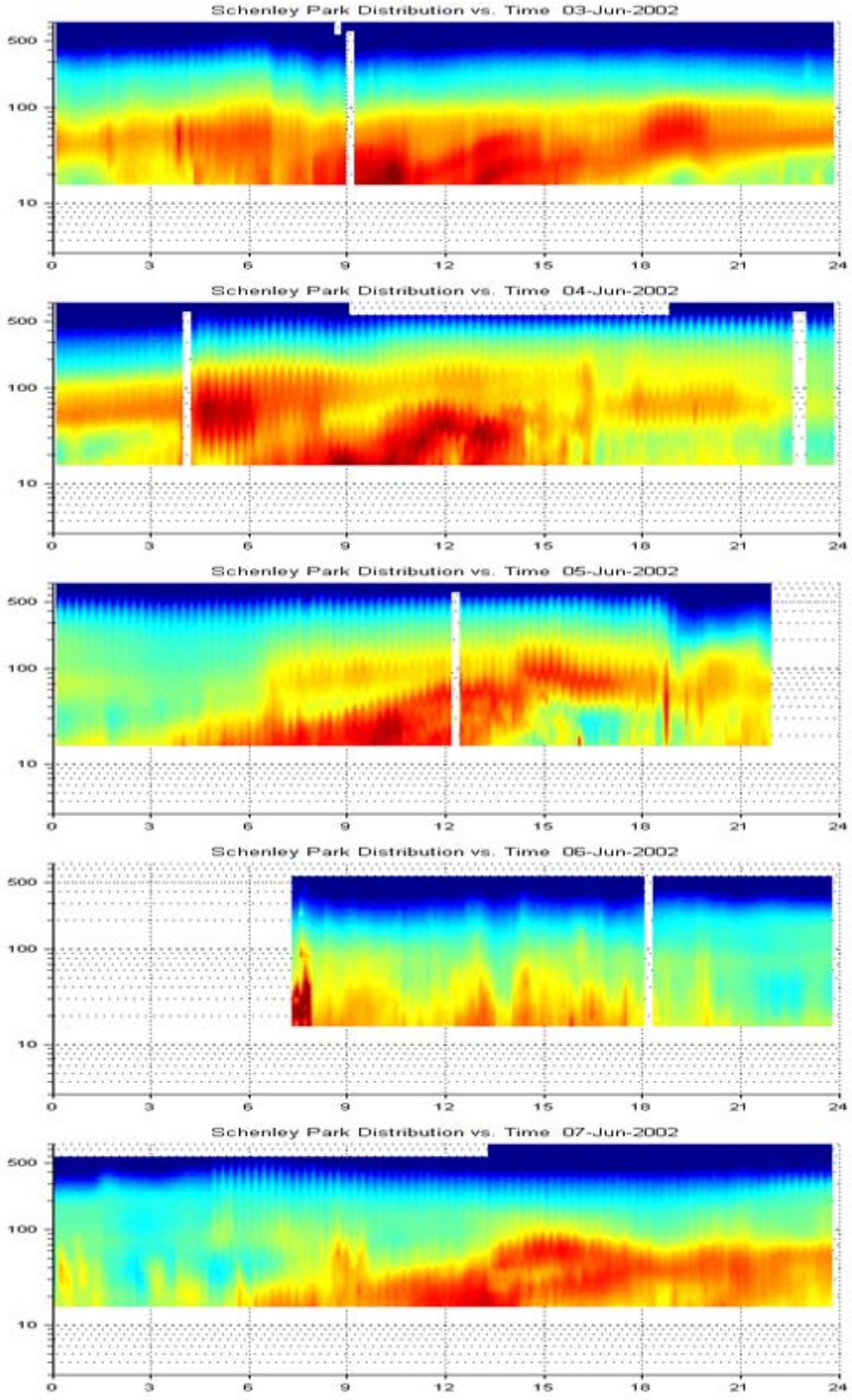
Schenley Park Distribution vs. Time 03-Jun-2002
Schenley Park Distribution vs. Time 04-Jun-2002
Schenley Park Distribution vs. Time 05-Jun-2002
Schenley Park Distribution vs. Time 06-Jun-2002
Schenley Park Distribution vs. Time 07-Jun-2002
500
100
10
0
3
6
9
12
15
18
21
24

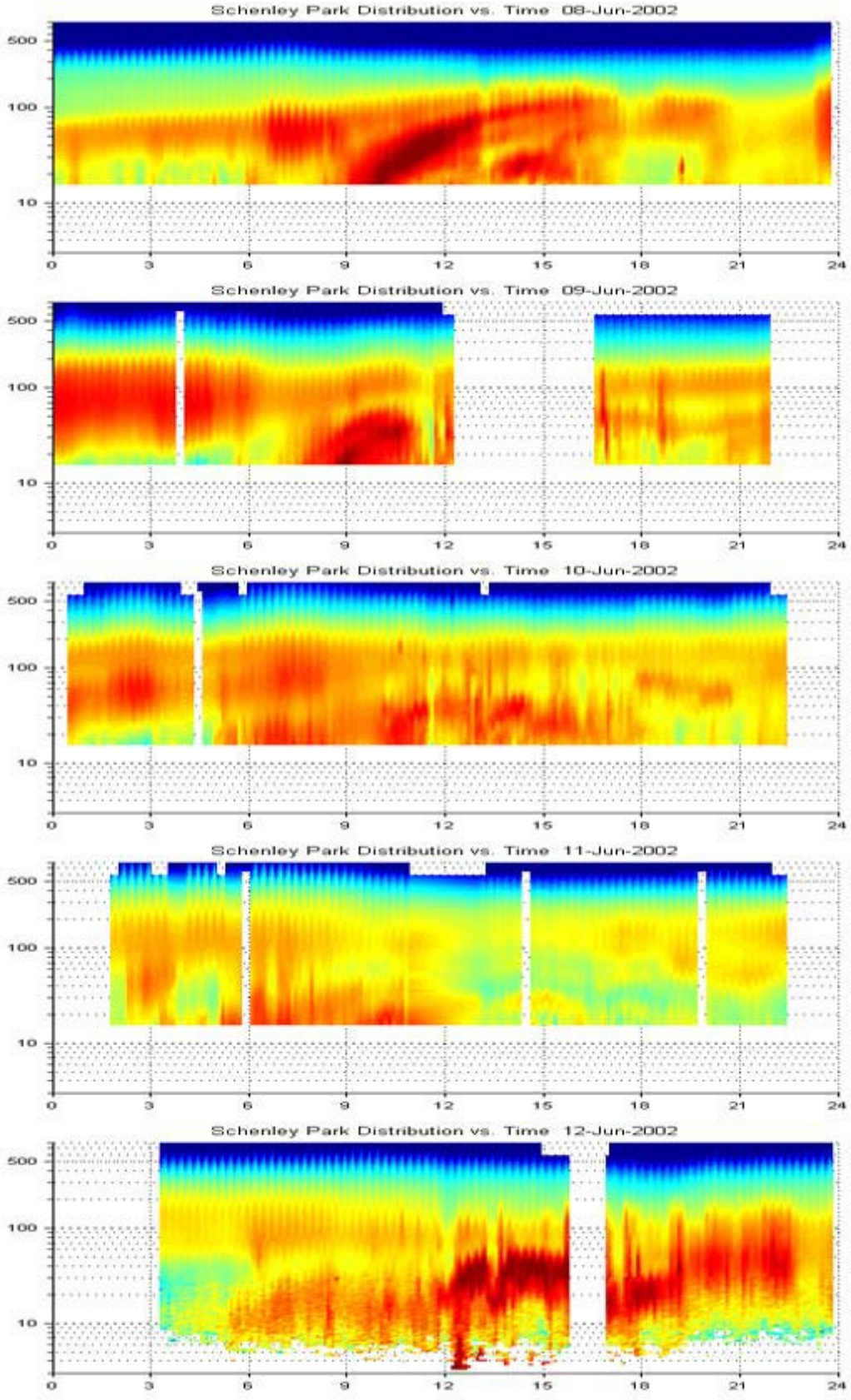
Schenley Park Distribution vs. Time 08-Jun-2002
Schenley Park Distribution vs. Time 09-Jun-2002
Schenley Park Distribution vs. Time 10-Jun-2002
Schenley Park Distribution vs. Time 11-Jun-2002
Schenley Park Distribution vs. Time 12-Jun-2002
500
100
10
0
3
6
9
12
15
18
21
24

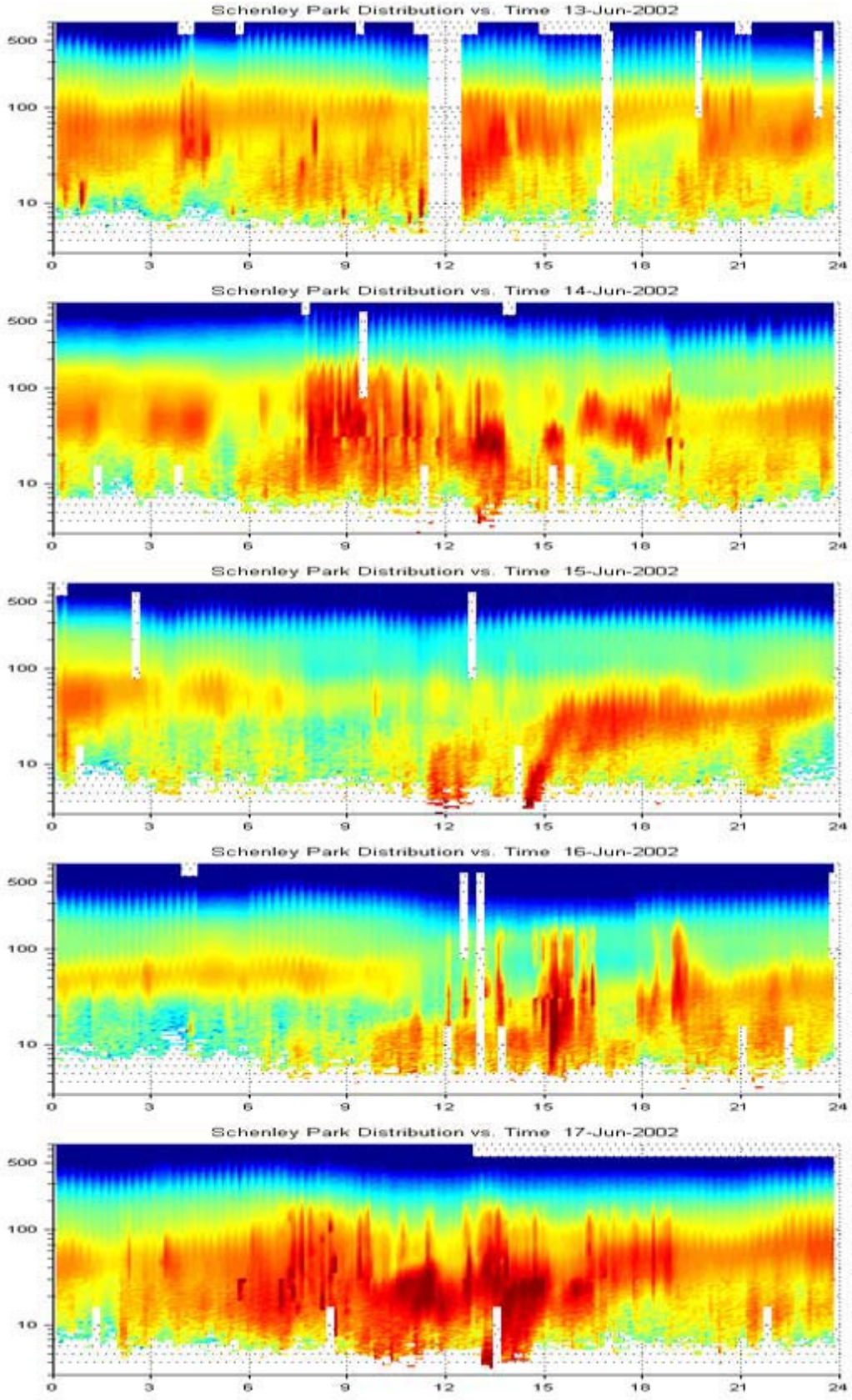
Schenley Park Distribution vs. Time 13-Jun-2002
Schenley Park Distribution vs. Time 14-Jun-2002
Schenley Park Distribution vs. Time 15-Jun-2002
Schenley Park Distribution vs. Time 16-Jun-2002
Schenley Park Distribution vs. Time 17-Jun-2002
500
100
10
0
3
6
9
12
15
18
21
24

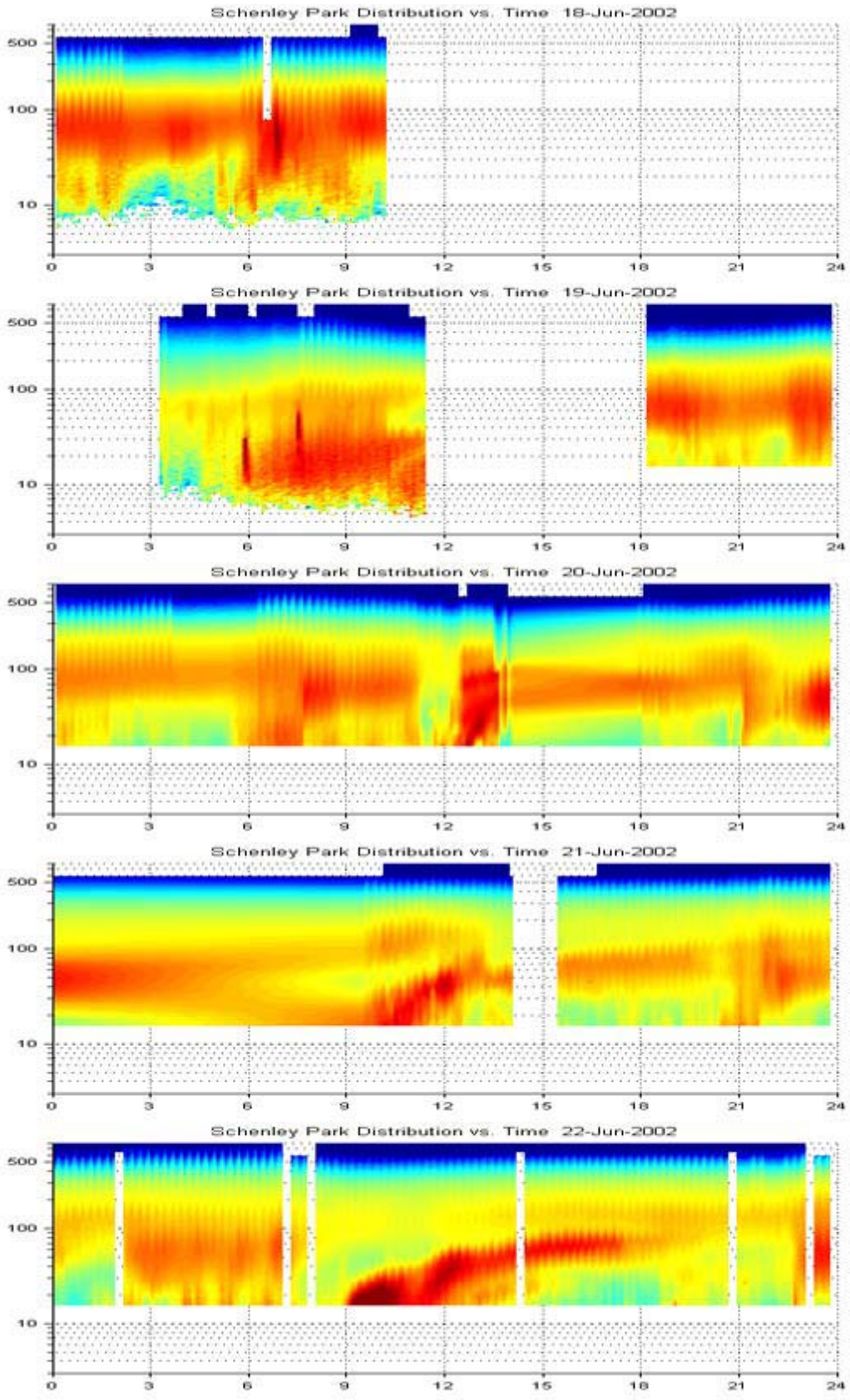
Schenley Park Distribution vs. Time 18-Jun-2002
Schenley Park Distribution vs. Time 19-Jun-2002
Schenley Park Distribution vs. Time 20-Jun-2002
Schenley Park Distribution vs. Time 21-Jun-2002
Schenley Park Distribution vs. Time 22-Jun-2002
500
100
10
0
3
6
9
12
15
18
21
24

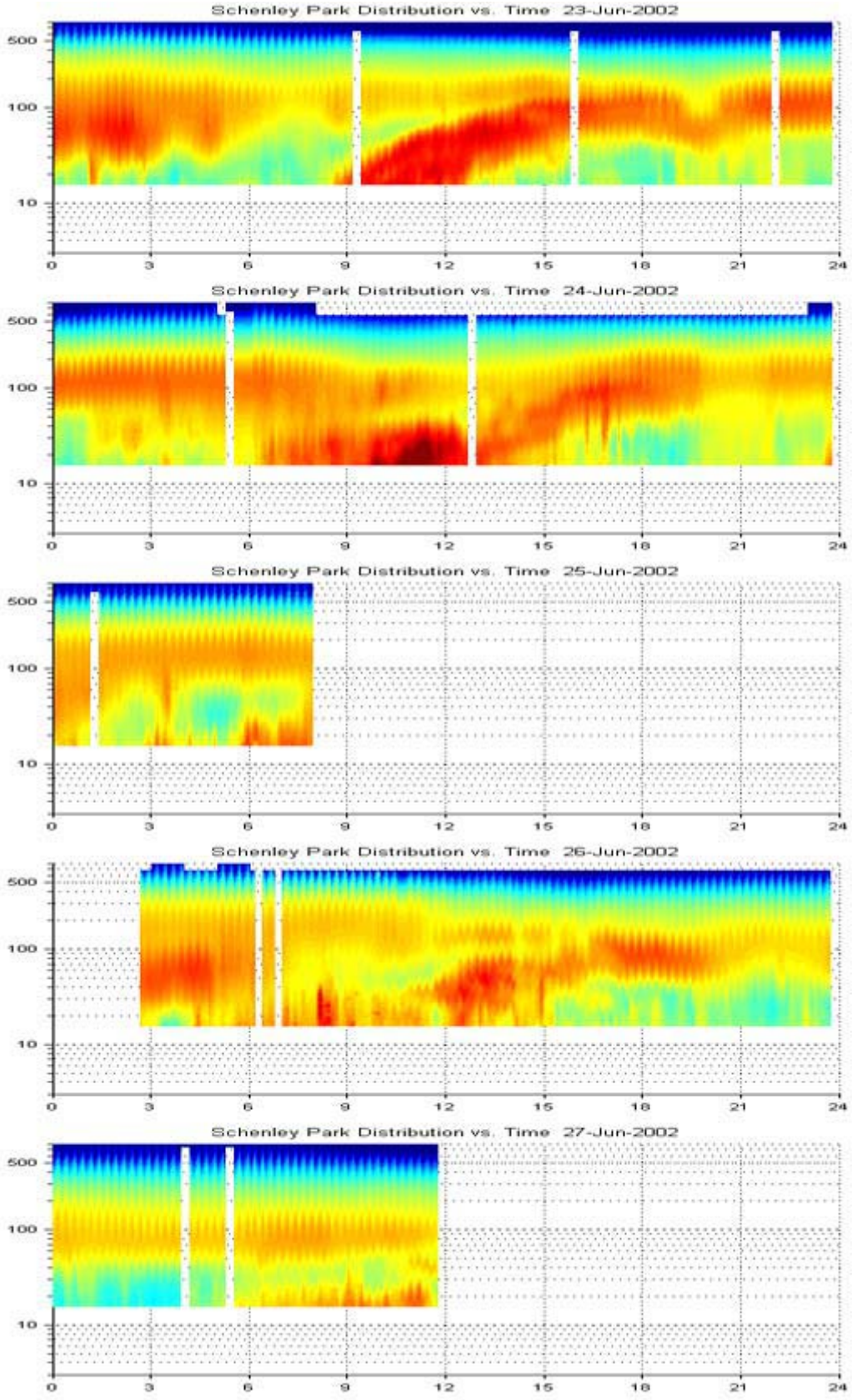
Schenley Park Distribution vs. Time 23-Jun-2002
Schenley Park Distribution vs. Time 24-Jun-2002
Schenley Park Distribution vs. Time 25-Jun-2002
Schenley Park Distribution vs. Time 26-Jun-2002
Schenley Park Distribution vs. Time 27-Jun-2002
500
100
10
0
3
6
9
12
15
18
21
24

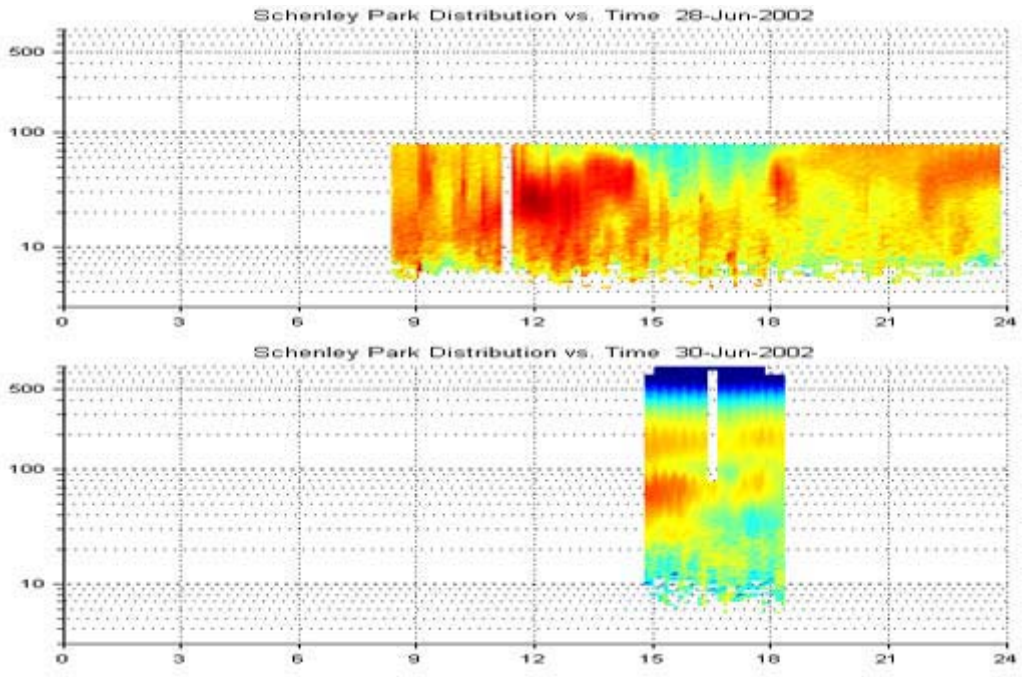
Schenley Park Distribution vs. Time 28-Jun-2002
500
100
10
0
3
6
9
12
15
18
21
24
Schenley Park Distribution vs. Time 30-Jun-2002
500
100
10
0
3
6
9
12
15
18
21
24

Appendix B
Dry-Ambient Aerosol Size Spectrometer Data Quality Statement

1. Introduction

The purpose of this data quality statement is to provide information on the quality of size distributions measured by the Dry-Ambient Aerosol Size Spectrometer (DAASS) during the Pittsburgh Air Quality Study.

The Dry-Ambient Aerosol Size Spectrometer (DAASS) includes three particle sizing instruments with associated supporting equipment as shown in Figure 1. The particle sizing instruments include two Scanning Mobility Particle Sizers (SMPS) and one Aerosol Particle Sizer (APS). The SMPS instruments size particles from 3 – 80 nm (TSI 3936N25) and 13 – 680 nm (TSI 3936L10), while the APS (TSI 3320/3321) covered 0.5 – 10 μm. These systems are referred to as the Nano-SMPS, SMPS, and APS systems. Two separate relative humidity controlled inlets served the aerosol sizing instruments. One inlet conditioned aerosols for the SMPS systems while a separate inlet conditioned aerosols for the APS. Supporting these components are a dry air supply system, and humidity conditioning systems for the sheath air flows of both SMPS systems and the APS.

The DAASS ran from June 1, 2001 – September 26, 2002. However, as of May 22, 2003 only the dried size distributions from the first 12 month period (2001/7/1 – 2002/6/30) have been submitted to NARSTO. Two papers summarize the first 12 months of results and the design and operation of the DAASS. These are:

- Charles O. Stanier, Andrey Y. Khlystov, Wanyu R. Chan, Mulia Mandiro, Spyros N. Pandis. (2003) A Method for the In-situ Measurement of Fine Aerosol Water Content of Ambient Aerosols: The Dry-Ambient Aerosol Size Spectrometer (DAASS). Aerosol Science and Technology, in press.

- Charles O. Stanier, Andrey Y. Khlystov, and Spyros N. Pandis. (2003) Ambient Aerosol Size Distributions and Number Concentrations Measured During the Pittsburgh Air Quality Study (PAQS). Submitted to Atmospheric Environment.

Also of interest to the data user may be the paper:

- Andrey Khlystov, Charles Stanier, Spyros Pandis. (2003) An Algorithm For Combining Electrical Mobility And Aerodynamic Size Distributions Data When Measuring Ambient Aerosol. Aerosol Science and Technology, in press.

For the design and operation of the DAASS, the reader is referred to the method paper listed above. The discussions of error and uncertainty in the cited papers are used in this data quality assessment with additional quantification.

2. Quality Control Information

The data presented here are Level 2 validated, i.e. NARSTO flags were applied to all data points, data between the 3 aerosol size instruments were reviewed comparatively, and data was compared to other highly time-resolved measurements and checked for qualitative (meteorology, SO_2, NO_x, CO) and quantitative (TEOM PM2.5) agreement.

3. Methods for calculating MDL, Precision, Accuracy, and Data Completeness

The following calculations are done to assess how faithfully the DAASS data represents the true aerosol size distribution. The DAASS size distributions are reported in the NARSTO data archive as 5 minute samples reported every 7.5 or 15 minutes. Ideally the reported size distribution would equal the true 5-minute average of the size distribution with perfect precision and zero bias.

3.1 MDL (Minimum Detection Limit)

Each of the instruments operated on physical principles allowing detection of individual particles. Therefore, there is no inherent “minimum detection limit” in terms of aerosol number concentration. The smallest size particle detectable by the system was governed by the ability of the TSI 3025 ultrafine CPC to detect particles. The 50% detection cutoff of this particle counter was determined by laboratory tests at the University of Minnesota Particle Technology Laboratory to be 2.9 nm (Sakurai, 2002). The sampling of very small (<20 nm) particles and

large (> 1 μm) particles was also affected by losses in the inlet. The effect of this is discussed in the accuracy and precision sections.

3.2 Precision (The coefficient of variation, CV(%))

Sampling precision by an SMPS system is dependent on particle size and the ambient particle concentration. The equations for theoretical precision of the instruments are developed in Appendix 1 and then applied to the DAASS in Table 2. The coefficient of variation (σ_N/N) for the individual size channels of the instruments when measuring a typical size distribution are below 15% for all instruments for aerosol sizes greater than 10 nm. The best precision (<2% coefficient of variation) is expected by the SMPS instrument between about 50 and 300 nm, and by the APS instrument between 0.63 and 1.0 μm. The worst precision is expected by the N-SMPS below 10 nm, with decreasing precision at smaller sizes.

The coefficient of variation is calculated in Table 2 for some representative particle sizes and values of N. It should be noted that the precision is calculated in Table 2 is for the bin sizes reported for the DAASS in the NARSTO archive (64 channels per decade for SMPS & manufacturer size bins for APS). Precision can be improved by binning data less finely. The non size-dependent parameters are listed for the various instruments in the following Table.

	N-SMPS	**SMPS**	**APS**
Δt	2.34 sec	2.34 sec	90 sec
Q	1.5 LPM	1.0 LPM	1 LPM
Q_{mono}/Q_{sh}	1.5 / 7.0	1.0 / 3.2	NA
DR_{CPC}	50	1	1

Table 1. Important parameters for instrument precision

1	2	3	4	5	6	7	8	9	10	11	12	13 perfect inlet	14	15 with inlet losses	16
Size (nm)	Concen. dN/dln(Dp)	Inst	deltat	Q	Qmono	Qsh	Qmono/Qsh	DRCPC	f+1	transinlet	effcount	c	CV	c	CV
3	7000	N-SMPS	2.34	1.5	1.5	7	0.21	50	1.1%	1.0%	100%	19.3	22.8%	0.2	227.6%
6	7000	N-SMPS	2.34	1.5	1.5	7	0.21	50	2.3%	24%	100%	40.7	15.7%	9.8	32.0%
10	7000	N-SMPS	2.34	1.5	1.5	7	0.21	50	4.1%	55%	100%	72.1	11.8%	39.7	15.9%
15	7000	N-SMPS	2.34	1.5	1.5	7	0.21	50	6.4%	70%	100%	111.6	9.5%	78.1	11.3%
15	7000	SMPS	2.34	1	1	3.2	0.31	1	6.4%	70%	100%	5,427.0	1.4%	3,798.9	1.6%
50	7000	N-SMPS	2.34	1.5	1.5	7	0.21	50	17%	93%	100%	297.7	5.8%	275.4	6.0%
50	7000	SMPS	2.34	1	1	3.2	0.31	1	17%	93%	100%	14,471.9	0.8%	13,386.5	0.9%
100	7000	SMPS	2.34	1	1	3.2	0.31	1	21%	96%	100%	18,243.5	0.7%	17,513.7	0.8%
500	57	SMPS	2.34	1	1	3.2	0.31	1	14%	95%	100%	97.5	10.1%	92.6	10.4%
630	31	SMPS	2.34	1	1	3.2	0.31	1	13%	95%	100%	47.3	14.5%	44.9	14.9%
630	31	APS	90	1	na	na	na	na	na	100%	72%	33,486.7	0.5%	33,486.7	0.5%
1000	2.2	APS	90	1	na	na	na	na	na	100%	90%	2,970.6	1.8%	2,970.6	1.8%
2500	0.26	APS	90	1	na	na	na	na	na	83%	100%	390.1	5.1%	323.8	5.6%

Table 2. Results of precision calculation for size distribution measurements at PAQS. Notice that coefficient of variation (CV), columns 14 and 16 is very size (Column 1) dependent. Concentrations (column 2) are within 50% of the grand average for the study. Column 4 is the approximate time (sec) spent sampling at a given size channel during each 5 minute scan. Q is the inlet flow in LPM. Qmono and Qsheath are flows in the DMA (LPM). f+1 is the fraction of particles charged to +1. c (columns 13 and 15) are the expected number of particles seen at the detector during the sampling period and the CV (column 14) is the coefficient of variation expected from Poisson statistics.

3.3 Accuracy

There are two types of accuracy required in the particle size distributions – sizing accuracy (i.e. reporting the correct mobility diameter of particle and correct position of modes in particle size distributions), and counting accuracy (e.g. reporting the correct concentration of particles for a given size).

3.3.1 Sizing Accuracy, SMPS

Sizing accuracy is mainly determined by performing the data inversion with correct values for sheath flow and column voltage. Sizing accuracy can be checked by sizing particles of known size (often monodisperse polystyrene latex (PSL) spheres). Sizing accuracy can also be assessed by comparing sizing results from one SMPS to another SMPS. Prior to the study, sizing accuracy of the SMPS instruments was measured at 3% or better using monodisperse aerosols in the laboratory. Sizing accuracy during the study was maintained to within about 10%, based on monthly checks of sheath flow values. After one year of operation, the SMPS was challenged with 155 nm PSL (6/11/02) and sized the PSL at 151-157 nm. Relative sizing between the SMPS and N-SMPS was checked extensively on 6/9/02 and 6/12/02 with agreement from 5-10% (on average N-SMPS was sizing 7% larger than SMPS).

3.3.2 Counting Accuracy, SMPS

Assessing counting accuracy is difficult as there is no primary standard for total or size resolved particle counts. However, estimates are made for the SMPS counting accuracy during PAQS. To summarize, the SMPS size-resolved counting accuracy is within 25% for sizes greater than 50 nm, accurate to a factor of 2 at 10 nm, accurate to a factor of 4 at 6 nm, and accurate to a factor of 10 at 4 nm.

Accurate counting by SMPS depends on accurate inversion of the raw data. The inversion requires knowledge of many parameters, including the charge distribution of particles, instrument flowrates, inlet transmission efficiency, and the DMA transfer function. The accuracy of the inversion at 5 nm is estimated by Birmili et al. (2003) as ~ ±30% including errors in CPC counting efficiency (~ 10%), DMA transfer function (~ 20%), and bipolar charge distribution (~ 20%). This accuracy improves to ~20% at larger sizes (50 nm – 500 nm). This can be thought of as a best case accuracy of SMPS in a long-term field deployment. Indeed, one spot check of counting efficiency was done during PAQS where aerosol in the 50-500 nm range was fed to the DAASS system and to a stand-alone 3010 CPC, with agreement in particle number to 20%.

This best case accuracy (± ~30% at 5 nm and ± ~20% from 20-500 nm) is modified by circumstances specific to the DAASS and the Pittsburgh Air Quality Study. These are listed in the following table:

Feature or circumstance	Affect on SMPS accuracy	Reference
Inversion only considered +1 charges and impactor not used to reduce contribution of multiple charging	Bias count of large (>~300 nm) particles high by up to 10%	Khlystov et al. (2003)
Charging may be done at different relative humidity than particle sizing due to placement of charger relative to DMA. Charging was typically done at a RH higher than the final RH of the dried samples.	Bias count of particles <200 nm high by as much at 15%. Bias count of particles >200 nm low by as much as 15%.	Stanier et al. (2003a)
Larger inlet (for drying) than typically used for N-SMPS studies had high and uncertain losses	In data inversion , 50% transmission of inlet assumed at 9 nm, but could be anywhere from 3 nm- 10 nm. Therefore, particle counts become increasingly uncertain from 10 nm to 3 nm. The following estimates may be useful in interpreting data: Size range: Transmission used In data reduction: Possible range 10 nm: 54%: 50% - 75% 8 nm: 40%: 38% - 69% 6 nm: 26%: 21% - 58% 5 nm: 14%: 13% - 50% 4 nm: 5%: 5% - 40% 3 nm: 1%: 0.6% - 25%	Experimental data on inlet loss down to 20 nm and modeling of losses using correlations in Willeke and Baron (1993)

Table 3. Known biases and uncertainties in SMPS particle counts

3.3.3 Combined Sizing and Counting Accuracy, APS

Because of the lack of a primary standard for particle number, a reasonable method for assessing sizing and counting accuracy for an APS is to first gage sizing accuracy by challenging with monodisperse aerosol, and then (with known sizing accuracy) compare the APS aerosol volume (in conjunction with other particle sizers) to continuous mass records such as TEOM2.5 or FRM filters. One can then compute an effective density required to reconcile the mass time series (TEOM) and the volume (APS-SMPS) time series. If the counting and sizing of the APS is accurate, the effective density will be a reasonable value consistent with the aerosol chemistry.

Unfortunately, during PAQS, the APS was only challenged with monodisperse aerosol prior to deployment and once in the field. As a consequence, there is not a sufficient database to independently judge sizing and counting accuracy. Therefore, counting and sizing accuracy are assessed together, rather than independently. Details of the assessment follow, but results are summarized here:

(1) July1 – October 7, 2001. Assessment for this time period (1) is that sizing and counting are the least biased of the study. Calculated densities for overlap with SMPS are reasonable, if somewhat more variable than expected. Ghost particles distorting volume distribution at sizes above 5 microns. APS PV2.5 volume good to about a factor of 1.5.

(2a) May 7, – May 31, 2002. APS response highly variable during this period. On average, either sizing is biased toward large sizes or counting is high. Accuracy of aerosol PV2.5 volume calculated from APS probably only good to a factor of 2. Ghost particle problem gone.

(2b) June 1 – June 17, 2002. APS response less variable than previous period, but biased toward small sizes by about 20% and to low counts. APS calculated PV2.5 volume during this period good to about a factor of 3.

(2c) June 18 – June 30, 2002. APS variability not too bad, although sizing and/or counting seem to be biased high. APS PV2.5 volumes during this period good to about a factor of 2.

An important note before the detailed QA considerations: The sizes reported in the NARSTO archive are the aerodynamic sizes recorded by the APS assuming a density of 1.0. The calibration curves are based on calibration with monodisperse PSL (correcting for density of 1.05) and monodisperse ammonium sulfate (correcting for density of 1.76) for sizes less than 2.5 μm and manufacturer calibration curve at sizes > 2.5 μm. In other words, a spherical particle of diameter 1.0 μm with density 1.0 gcm^{-3} is reported as a 1.0 μm particle. A 1.0 μm with density 1.5 gcm^{-3} is reported as a $1.0/\sqrt{1.5}$ = 0.82 μm particle (neglecting slip correction). The relationship between density, size, and shape is discussed at length by Khlystov et al. (2003). Also reported in the NARSTO archive is an effective density, calculated for each hour of the study according to the procedures in Khlystov et al. (2003). Using the effective density, the reported aerodynamic number distribution can be converted to a "mobility" number distribution that should line up with the SMPS in the overlap region of 530-680 nm. The following section assesses the accuracy of the aerodynamic sizes measured by the APS, but not the accuracy of the effective density estimates or

the “mobility” number distributions (for that, the data user is referred to Khlystov et al. 2003). The sizing of the APS depends on the calibration curve relating the time of flight of particles (measured by the APS) to their aerodynamic size. This calibration table is provided by the manufacturer (TSI Inc.) based on individual instrument calibrations done with monodisperse PSL. For PAQS, the manufacturer calibration curve was discarded and new calibration curves were constructed, using the procedure described in Khystov et al. (2003).

For QA purposes, the APS deployment is divided into: (1) the APS 3320 deployment (July – October, 2001) where accuracy was relatively good; and (2) the APS 3321 deployment May 7 – June 30, 2002. Period (2) was characterized by poor stability of the sizing calibration, inlet flowrate, and sheath flowrate. Period (2) can be divided into three periods: (2a) May 7 – May 31; (2b) June 1 – 17; and (2c) June 18 – June 30, 2002.

Deployment period 1: July – October 2001

The APS was run for two distinct periods during PAQS, and was serviced and upgraded during the interval between. The APS ran from July 1, 2001 – October 7, 2001 in the “3320” model number configuration. The 3320 APS model suffers from an internal recirculation problem leading to the misclassification of small particles as large (Armendariz and Leith, 2002). This “ghost particle” problem has little effect on the number distribution, but badly distorts the volume distribution at sizes above 5 μm, as can be seen from the impactor-APS comparison in Figure 2. The second problem experienced from July 1 – October 7 was an electronic problem specific to the instrument run at PAQS. During increasing frequent intervals, the APS reported unreasonably high particle counts, and reported particle counts even with a filter attached to the inlet. These periods typically lasted several hours and occurred during times of high (>80% RH) and low temperature (<18 ºC). This transient problem was determined to be an electronic problem in the photodetector sensitivity. During the problem periods, the threshold for particle detection was lowered such that particles were incorrectly counted. These periods have been identified through comparison with the LDMA and invalidated using NARSTO flag M2.

Deployment periods 2: May – June 2002

During the winter of 2001-2002, the APS was upgraded to the "3321" model configuration. The upgrade specifically includes a redesigned inlet to remove the particle recirculation causing the "ghost particle" phenomenon. The electronics are upgraded as well, improving performance in the correlated sampling mode (not used during PAQS). Through laboratory testing, it was verified that the ghost particle problem was eliminated by the upgrade. The APS 3321 was then deployed and sampled from May 7, 2002 – June 30, 2002, using an in-house calibration curve. The APS 3321 was challenged with 2.06 μm PSL on June 12, 2002 and sized it at 1.6-1.7 μm. During this time, the APS sheath and aerosol flows were not as stable as normally seen (variations of ±30% from setpoints). The APS inlet was cleaned on June 17, improving the flow stability issue, and recalibrated on 6/18/02. From June 18, 2002 – June 30, 2002, it performed well and compared reasonably to the SMPS results in the overlap range.

To quantify the performance of the APS, we rely on the fact that a "reasonable" density should reconcile the aerodynamic diameter measured by the APS with the mobility size measured by the SMPS. An effective density of 1.0 means that no adjustment to the APS distribution is required for agreement. Effective densities of greater than 1.0 mean that the APS distribution must be shifted to the smaller sizes to match SMPS data and that the raw APS particle counts at aerodynamic sizes 530-680 nm are greater than the particle counts at mobility sizes 530-680 nm by SMPS. Effective densities of less than 1.0 mean that the APS distribution must be shifted to larger sizes and that the raw APS particle counts at aerodynamic sizes 530-680 nm are less than the particle counts at mobility sizes 530-680 nm by SMPS. A time series of hourly effective densities is shown in Figure 3. Figure 3b shows that the counting (and possibly sizing) accuracy of the APS was poor after its redeployment on May 7, 2002. Figure 3b divides that data into three periods: May 7 – May 31, June 1-June 17, and June 18-June 30. As noted in section 3.3.1.2, flow control problems were noted during this period.

To make a quantitative estimate of bias, we assume a correct density, and calculate a combined sizing/error according to the following formula, adapted from Khlystov et al. 2003:

$$\frac{\rho_{eff,calc}}{\rho_{true}} = (Z)^{1/B}\sqrt{M} \quad (5)$$

Where Z is the factor by which the APS undercounts (e.g. Z=1 is perfect counting; Z=1.1 is undercounting by 10%), M is the factor by which sizing if off (M=1.1 means measured aerodynamic size is 10% larger than actual), B is the slope of the power law that describes the decay of the number distribution (assumed to be -3 Khlystov et al. 2003), and ρ_{true} and $\rho_{eff,calc}$ are the true particle density and density required for SMPS-APS reconciliation, respectively. $\rho_{eff,calc}$ is graphed in Figure 3 for Periods 1 and 2 of the APS deployment.

By plugging in reasonable values* of ρ_{true} into equation (5) we can calculate estimates of counting accuracy (assuming perfect sizing) and sizing accuracy (assuming perfect sizing). These results of this analysis are shown in the following table.

* As both the SMPS and APS are measuring dried aerosol size distributions, we expect particle densities representative of ammonium sulfate and organic compounds, the main contributors to aerosol mass (Anderson et al. 2002). In other words, we expect densities between 1.2 and 1.77 gcm^{-3} (Stanier et al. 2003a).

Table 4. Assessment of sizing/counting accuracy of APS

Period	Range ρ_{true}	Range ρ_{calc}	Worst case sizing accuracy if perfect counting*	Worst case counting accuracy if perfect sizing*	Source
(1) July1 – October 7, 2001	1.2 – 1.77	0.94 – 1.94	x 1.2, ÷ 1.4	x 1.25, ÷ 2	Figure 3a
	1.5	1.25 – 1.8	x 1.4, ÷ 1.4	x 1.7, ÷ 1.7	Figure 4
	Assessment for this time period (1) is that sizing and counting are the least biased of the study. *Calculated densities for overlap with SMPS are reasonable, if somewhat more variable than expected. Ghost particles distorting volume distribution at sizes above 5 microns. APS PV2.5 volume good to about a factor of 1.5.*				
(2a) May 7, – May 31, 2002	1.2 – 1.77	1.1 – 2.5	x 2.0, ÷ 1.15	x 2.8, ÷ 1.3	Figure 3b
	APS response highly variable during this period. On average, either sizing is biased toward large sizes or counting is high (note factory calibration was used). Accuracy of aerosol PV2.5 volume calculated from APS probably only good to a factor of 2. Ghost particle problem gone.				
(2b) June 1 – June 17, 2002	1.2 – 1.77	0.7 – 1.8	÷ 1.1 to 2.4	÷ 1.1 to 3.3	Figure 3b
				÷ 1.2	Challenge with PSL
	APS response less variable than previous period, but biased toward small sizes by about 20% and to low counts. APS calculated PV2.5 volume during this period good to about a factor of 3.				
(2c) June 18 – June 30, 2002	1.2 – 1.77	1.4 – 2.2	x 1.3 to 1.5	x 1.5 to 1.9	Figure 3b
	APS variability not too bad, although sizing and/or counting seem to be biased high. APS PV2.5 volumes during this period good to about a factor of 2.				

*x 1.2 means APS is measuring 1.2 times true aerodynamic diameter or counting 1.2 times the true number of particles.

3.4 Data Completeness

Data completeness is calculated from Table 1 of Stanier et al. (2003b). A complete day of data is defined as having valid data for at least 75% of the hours of the day. (A complete hour has at least 75% of possible scans valid during the hour). Using this metric, data completeness was 83%, 90%, and 28% for the N-SMPS, SMPS, and APS respectively, versus a data completeness objective of 70%.

4. List of key calibrations and maintenance activities

During the 12 months covered by this data quality statement, there were several major malfunctions, including the APS, the dry air supply system, a CPC 3010, and two N-SMPS sheath blowers. These are listed in Appendix 2 together with the routine checks performed for quality assurance.

5. Overall Data Quality Findings

Relative to data quality objectives stated at the beginning of the project, the quality of the data collected during the period July 1, 2001 – June 30, 2002 met objectives except as noted below:

- APS data completeness 28% versus target of 70%
- APS accuracy goals of sizing (±20% goal) & counting (±30% goal) met during all operational periods accept 5/7/02-5/31/02.
- SMPS sizing accuracy goal (±4% goal) not met for entire study. Sizing accuracy was maintained to ~10% or better (and to 4% or better for Summer 2001 intensive)
- SMPS counting accuracy (±30% goal) met except at sizes below 10 nm, where uncertain aerosol charging and inlet losses increase uncertainty

6. References

Anderson, R.R., Martello, D.V., Rohar, P.C., Stazisar, B.R., Tamilia, J.P., Waldner, K., and White, C.M. (2002). Sources and Composition of $PM_{2.5}$ at the National Energy Technology Laboratory in Pittsburgh During July and August 2000, *Energy and Fuels* 16:261-269.

Armendariz, A.J., and Leith, D. (2002). Concentration Measurement and Counting Efficiency for the Aerosol Particle Sizer 3320, *J. Aerosol Sci.* 33:133-148.

Birmili, W., Berresheim, H., Plass-Dulmer, C., Elste, T., Gilge, S., Wiedensohler, A., Uhrner, U. (2003). The Hohenpeissenberg aerosol formation experiment (HAFEX): a long-term study including size-resolved aerosol, H2SO4, OH, and monoterpenes measurements.

Khlystov, A., Stanier, C., Pandis, S. (2003) An Algorithm For Combining Electrical Mobility And Aerodynamic Size Distributions Data When Measuring Ambient Aerosol. Aerosol Science and Technology, in press.

Leinert, S. and Wiedensohler, A. (2000). APS Counting Efficiency Calibration for Submicrometer Particles. *J. Aerosol Sci*. 31:S404-S405.

Sakurai, Hiromu (2002) Personal communication.

Stanier,C., Khlystov, A., Chan, W.R., Mandiro, M., Pandis, S. (2003a) A Method for the In-situ Measurement of Fine Aerosol Water Content of Ambient Aerosols: The Dry-Ambient Aerosol Size Spectrometer (DAASS). Aerosol Science and Technology, in press.

Stanier, C., Khlystov, A., and Pandis, S. (2003b) Ambient Aerosol Size Distributions and Number Concentrations Measured During the Pittsburgh Air Quality Study (PAQS). Submitted to Atmospheric Environment.

Weis, N. (1995) *Introductory Statistics*, 4th ed. Addison-Wesley Publishing Company: New York.

Willeke, K., and Baron, P.A. (1993) *Aerosol Measurement Principles, Techniques, and Applications*. Van Nostrand Reinhold: New York.

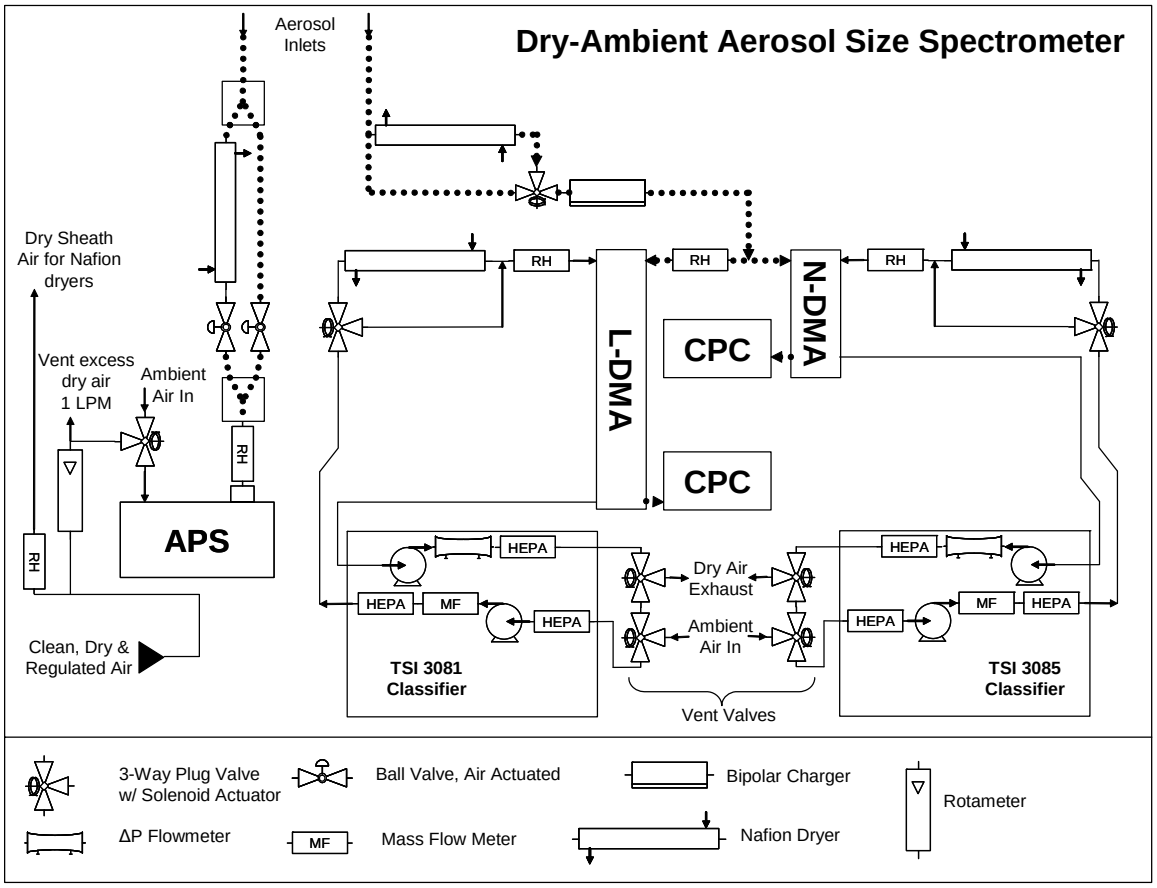

Figure 1. Flow diagram of Dry-Ambient Aerosol Size Spectrometer (DAASS). Aerosol streams are shown by dotted lines and other flows are indicated by solid lines.

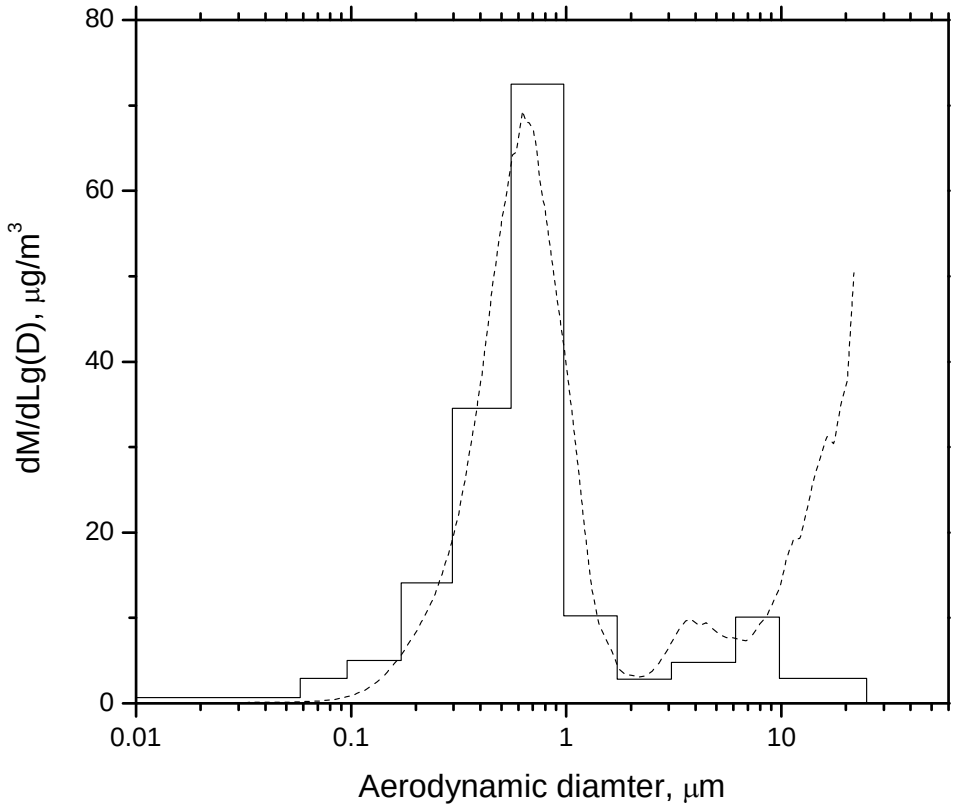

Figure 2. APS – MOUDI comparison

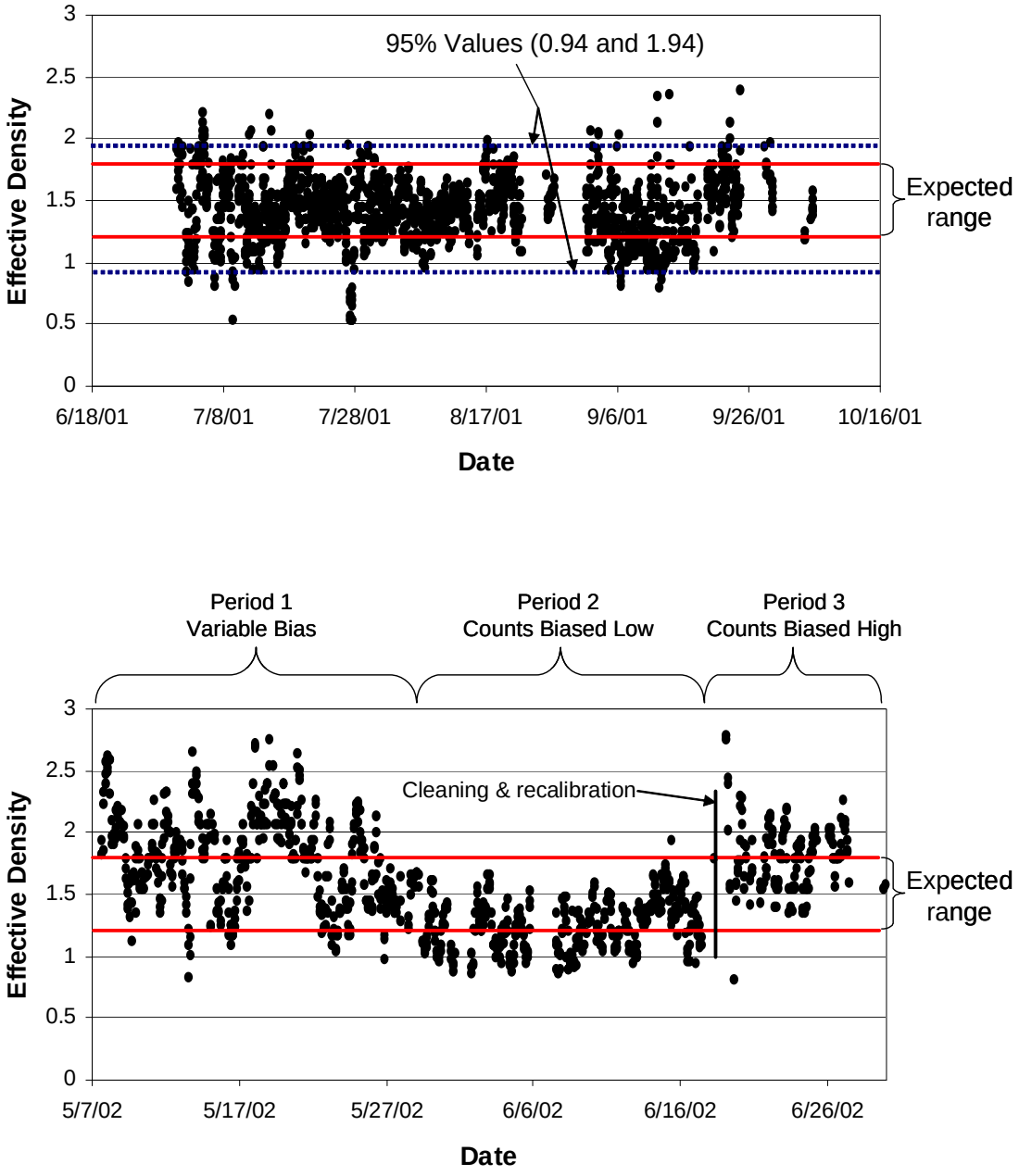

Figure 3. Time series of APS effective densities, (a) July – October 2001, and (b) May – June 2002.

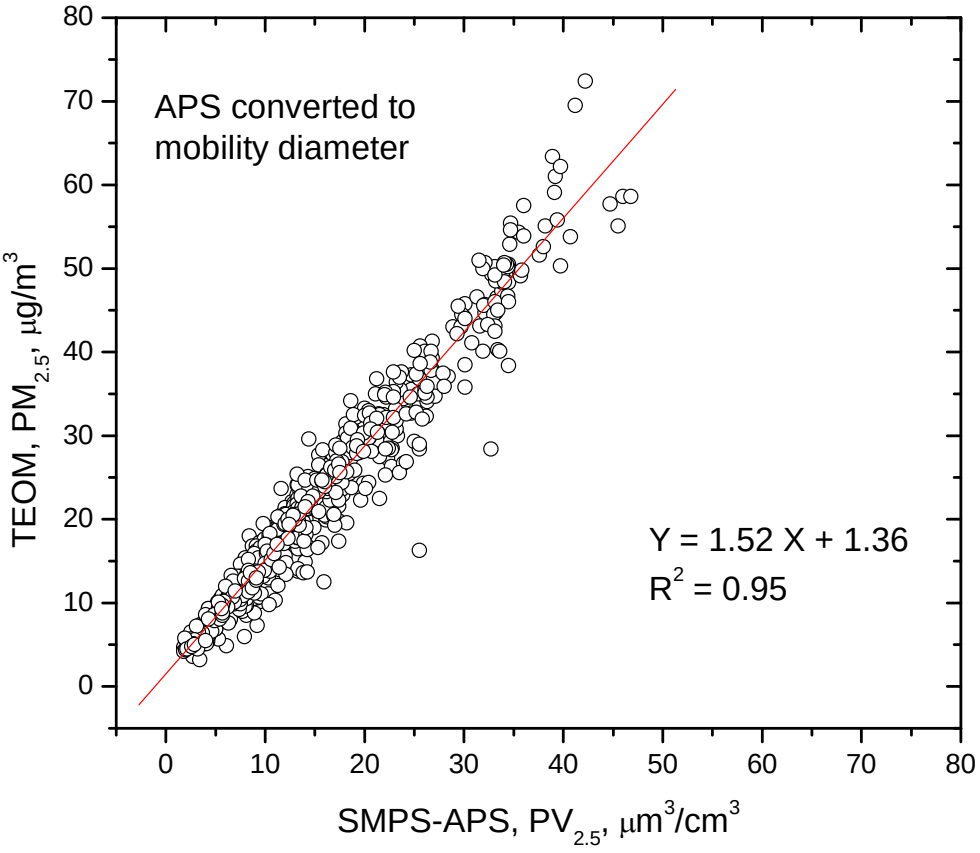

Figure 4. Comparison of SMPS-APS volume to TEOM PM2.5 for July 2001

Attachment 1 – Theoretical Precision for Particle Sizing Instruments

In SMPS sampling, if the size distribution function (dN/dlnDp) is n^e_N at the size in question, the concentration of +1 charged particles reaching the condensation particle counter, accounting for the DMA transfer function and particle charging (but not particle losses) is approximately.

$$N^{+1} = f^{+1}(D_p) n_N^e(D_p) \ln\left(1 + \frac{Q_{mono}}{Q_{sheath}}\right) \approx f^{+1}(D_p) n_N^e(D_p) \frac{Q_{mono}}{Q_{sheath}} \quad (1)$$

where f^{+1} is the fraction of +1 particles, and Q_{mono}/Q_{sheath} is the ratio of the aerosol to sheath flow in the DMA. Assuming that the SMPS system spends a time interval Δt sampling at this size channel, the number of +1 particles reaching the CPC (ignoring losses) is given by:

$$p = 16.67 N^{+1} \Delta t Q \quad (2)$$

where Q is the sample flowrate ($Lmin^{-1}$), and Δt is the time (s) spent on that size channel.

Factoring in size dependent losses, CPC counting efficiency, and any internal dilution in the CPC, the number of particles counted by the CPC is given by:

$$c = \frac{ptrans_{inlet} eff_{count}(D_p)}{DR_{CPC}} \quad (3)$$

where $trans_{inlet}$ is the transmission efficiency through the inlet and transfer tubing, eff_{count} is the detector counting efficiency, and DR_{CPC} is dilution occurring within the CPC. This type of sampling follows a Poisson distribution such that the standard deviation on c is $\sigma_c = \sqrt{c}$ (Weiss, 1995).

Precision will be calculated as the coefficient of variation (CV), the ratio of standard deviation of N to the value N (σ_N/N). This coefficient can be calculated as:

$$CV = \frac{\sigma_N}{N} = \frac{\sigma_c}{c} = \frac{\sqrt{c}}{c} = \frac{1}{\sqrt{\frac{16.67 \Delta t Q \frac{Q_{mono}}{Q_{sheath}} f^{+1}(D_p) trans_{inlet}(D_p) eff_{count}(D_p) n_N^e(D_p)}{DR_{CPC}}}} \quad (4)$$

The formula for CV makes intuitive sense. The CV can be reduced by sampling for a longer time, increasing the inlet flow Q, and increasing the total concentration. The CV is increased as the DMA resolution in improved, CPC dilution is used, and as the charging fraction, counting fraction, and transmission efficiency are reduced. Equation (4) also applies to the APS, but ignoring (replacing by unity) the Q_{mono}/Q_{sheath}, f^{+1}, and DR_{CPC} terms.

Attachment 2 – List of Major Maintenance and QA Activities

Date	Description	Value (if applicable)	Goal or Setpoint (if applicable)
7/17/01	HEPA on inlet	Acceptable	
7/28/01	HEPA on inlet	Acceptable	
8/4/01	SMPS Sheath Flow Calibration Check	3.21 / 6.94	3.20 / 7.00
8/17/01	SMPS Sheath Flow Calibration Check	3.25 / 7.05	3.20 / 7.00
	APS Sheath Flow Calibration Check	4.03	4.00
	LDMA Sheath Loop Integrity	Acceptable	
	Inlet Flow Rate	2.60 SMPS 1.02 APS dry	2.50 1.00
8/24/01	DMA Columns moved outside to reduce temperature difference between DMA's and ambient		
	HEPA on inlet	Acceptable	
8/26/01	Alternation between ambient RH and dried stopped due to compressor failure. Sampling in dried mode only, with limited drying capacity		
8/28/01	HEPA on inlet	Acceptable	
10/7/01	HEPA on inlet – APS failed due to electronic noise problem	FAILURE	
10/7/01	SMPS Sheath Flow Calibration Check	3.24 / 7.15	3.20 / 7.00
10/17/01	Inlet Flow Rate	2.51 SMPS 1.03 APS dry	2.50 1.00
10/23/01	HEPA on inlet – SMPS failed due to failure in CPC-3010 Laser	FAILURE	
10/26/01	"CPC3" is swapped in for malfunctioning "CPC2" S/N XXXX on SMPS system		
10/26/01	HEPA on inlet	Acceptable	
10/30/01	Inspection of APS inlet for buildup of aerosol	No buildup	
11/14/01	"CPC2" S/N is swapped in after repair by TSI Inc. on SMPS system		
11/14/01	HEPA on inlet	SMPS unusually high at 6 #/cm3 (still OK)	
11/26/01	HEPA on inlet	SMPS unusually high at 0.6 #/cm3	
11/26/01	SMPS Sheath Calibration Check	3.25 / 7.07	3.20 / 7.00
11/26/01	Inlet flowrate check	2.51	2.50
12/05/01	HEPA on inlet; SMPS fails badly; CPC2 returned to TSI due to incomplete repair job		
12/06/01	"CPC3" S/N put in SMPS system		
12/06/01	HEPA on inlet	Acceptable	
12/07/01	SMPS CPC Zero Check (see if particles counted with zero flow)	Zero particles counted	
12/23/01	Desiccant dryer added to SMPS Sheath Loop to reduce RH		
12/31/01	Desiccant dryer added to N-SMPS Sheath Loop to reduce RH		
12/31/01	HEPA on inlet	Acceptable	
1/1/02	N-SMPS Desiccant moved to outside enclosure; comparison of size distributions shows that data reduction (for the period 12/31/01 – 2/2/02) requires a N-SMPS sheath flow rate of 6.0 LPM rather than setpoint of 7.0 LPM. Reason for this is (1) increased pressure drop due to dryer in loop; (2) gradual failure of N-SMPS bypass blower; (3) possible positive pressure leak.		
1/8/02	HEPA on inlet	Acceptable	
1/30/02	N-SMPS Sheath Calibration Check (check showed flowrate was not as steady as usual)	7.2±0.25	7.0

Date	Description	Value (if applicable)	Goal or Setpoint (if applicable)
2/2/02	N-SMPS bypass blower replaced; still having trouble reaching and staying at 7.0 LPM setpoint		
2/2/02	HEPA on inlet	Acceptable	
2/2/02	Inlet flow check	2.56	2.50
2/11/02	HEPA on inlet	Acceptable	
2/11/02	SMPS Sheath Calibration Check – N-SMPS Flow out of range	3.27 / 7.54	3.20 / 7.00
2/13/02	N-SMPS desiccant dryer removed to reduce pressure drop		
2/15/02	Nafion dryer for N-SMPS sheath loop swapped for new unit (no change in drying performance)		
2/15/02	SMPS Sheath Calibration Check	7.01	7.00
2/15/02	Inline Sheath Flowrate Check	3.37 / 7.10	3.20 / 7.00
3/3/02	Failure of N-SMPS Sheath Blower; reconfiguration to run in "single blower mode" but with no drying of the sheath air loop. N-SMPS not dried as much as usual during the period 3/6/02 – 4/19/02		
3/6/02	HEPA on inlet	Acceptable	
3/6/02	N-SMPS Sheath Calibration Check	7.0±0.2	7.0
3/6/02	Inlet flowrate check	2.69	2.50
4/9/02	Inline sheath flowrate check	3.20±0.05	3.20
4/13/02	HEPA on inlet	Acceptable	
4/13/02	Inlet flowrate check	2.45	2.50
4/19/02	N-SMPS Sheath Calibration Check	7.0±0.1	7.0
4/19/02	N-SMPS Sheath blower replaced with new and system returned to "dual blower mode" with sheath air drying		
4/19/02	N-SMPS Sheath Calibration Check	6.96	7.00
4/19/02	N-SMPS and SMPS sizing of monodisperse ammonium sulfate compared	N-SMPS=42 nm SMPS = 41 nm	
5/6/02	APS returned to service after servicing, upgrade to 3321 model, and laboratory calibration		
5/6/02	APS inlet HEPA check	Acceptable	
5/12/02	SMPS inlet HEPA check	Acceptable	
5/27/02	U-CPC removed from service for calibration; replaced with 3010 CPC borrowed from Lynn Russell at Princeton University (N-SMPS)		
5/27/02	Inlet flowrate check (SMPS)	1.83	1.91
6/9/02	Inlet flowrate check (APS)	1.16	1.00
6/9/02	HEPA on inlet	Acceptable	
6/9/02	Inline sheath flowrate check	3.06 / 7.68	3.20 / 7.00
6/9/02	Challenge SMPS with 155 nm PSL	151-157 nm	155 nm
6/9/02	Compare sizing of monodisperse ammonium sulfate with N-SMPS and SMPS. Results listed as N-SMPS / SMPS size	60 / 56 40 / 36	
6/10/02	HEPA on inlet	Acceptable	
6/10/02	SMPS sheath calibration check	3.22	3.20
6/11/02	Inlet flow rate check (APS / SMPS)	1.10 / 2.45	1.00 / 2.50
6/11/02	Removed Princeton 3010 CPC from N-SMPS and returned the U-CPC to service.		
6/11/02	HEPA on SMPS inlet	Acceptable	
6/11/02	Challenge SMPS with 155 nm PSL	151-157 nm	155 nm
6/12/02	Challenge APS with 2.06 μm PSL	1.60-1.72 μm	2.06 μm
6/18/02	APS pulled from service for poor flow control and sizing; inlet cleaned; returned to service and recalibrated		

Date	Description	Value (if applicable)	Goal or Setpoint (if applicable)
6/18/02	HEPA on SMPS and APS inlets	Acceptable	
6/18/02	APS Sheath Calibration Check	3.87	4.00
6/21/02	HEPA on SMPS and APS inlets	Acceptable	
6/25/02	U-CPC flooded with butanol; returned to service after replacing all internal filters and butanol fill valve		
6/25/02	HEPA on SMPS and APS inlets	Acceptable	
6/27/02	HEPA on SMPS and APS inlets	Acceptable	
6/27/02	SMPS sheath loop accidentally flooded with liquid water & took several days to dry out		
6/30/02	Inlet flow rate check	2.42	2.50

These results of the checks in Appendix 2, together with analysis of time series of aerosol size data, analyses of aerosol counts and mode positions in overlapping size ranges, and comparisons of TEOM PM2.5 data with SMPS and APS data, have been used to make minor adjustments to the size distributions entered into the NARSTO database.

Appendix C
Research Protocol for Operation of the Aerosol Spectrometers for Measurement of Aerosol Size Distributions

SCOPE & APPLICABILITY.

This Research Protocol contains procedures necessary for performing measurements of dry and wet particle number size distributions (3 nm – 10 mm in diameter) in outdoor air for the Pittsburgh EPA PM supersite study using a newly designed set of aerosol instruments. The set consists of two Scanning Mobility Particle Sizers (SMPS, TSI Inc, Models 3936L10 and 3936N25) and Aerodynamic Particle Sizer (APS, TSI Inc, Model 3320).

This is an evaluation version of an anticipated standard operating procedure (SOP), which will result from experiences with this research protocol (RP). Due to this fact this RP is subject to changes. Every addition to this RP will be added as an Appendix during this study.

SUMMARY OF METHOD.

Aerosol size distributions are measured using a newly designed instrument that couples a differential mobility analyzer (DMA) with a condensation nucleus counter (CNC) and an aerodynamic particle sizer (APS). The instruments employ the principle of size classification according to electrical mobility (SMPS) and aerodynamic sizing (APS). These instruments and their operating principles are in detail described in references 1 - 5. Presently, no single technique is available for sizing particles over the entire range of interest for this study (0.01 to 10.0 μm diameter), so multiple instruments are necessary. Data are reported as number concentration per size bin. The SMPS-1 measures particle concentration as a function of size in the size range from 3 nm to 60 nm (diameter) at concentrations in that size range between 0 and 10^7 cm^{-3}. The SMPS-2 measures particles in the size range from 20 nm to 500 nm (diameter) at concentrations between 0 and 10^7 cm^{-3}. The APS measures particle concentration as a function of size in the size range from 0.5 μm to 10 μm (diameter) at concentrations in that size range between 0 and 10^4 cm^{-3}.

Measurements of the dry and wet size distributions are made using a flow system that incorporates several Nafion diffusion dryers and several solenoid valves (Fig.1). During the “wet” measurements the dryers are bypassed and the aerosol is measured at ambient conditions. During “dry” measurements the aerosol is led through a the dyers which bring it to equilibrium at 30-40% RH. Dry and wet measurements are made alternately every 6 minutes.

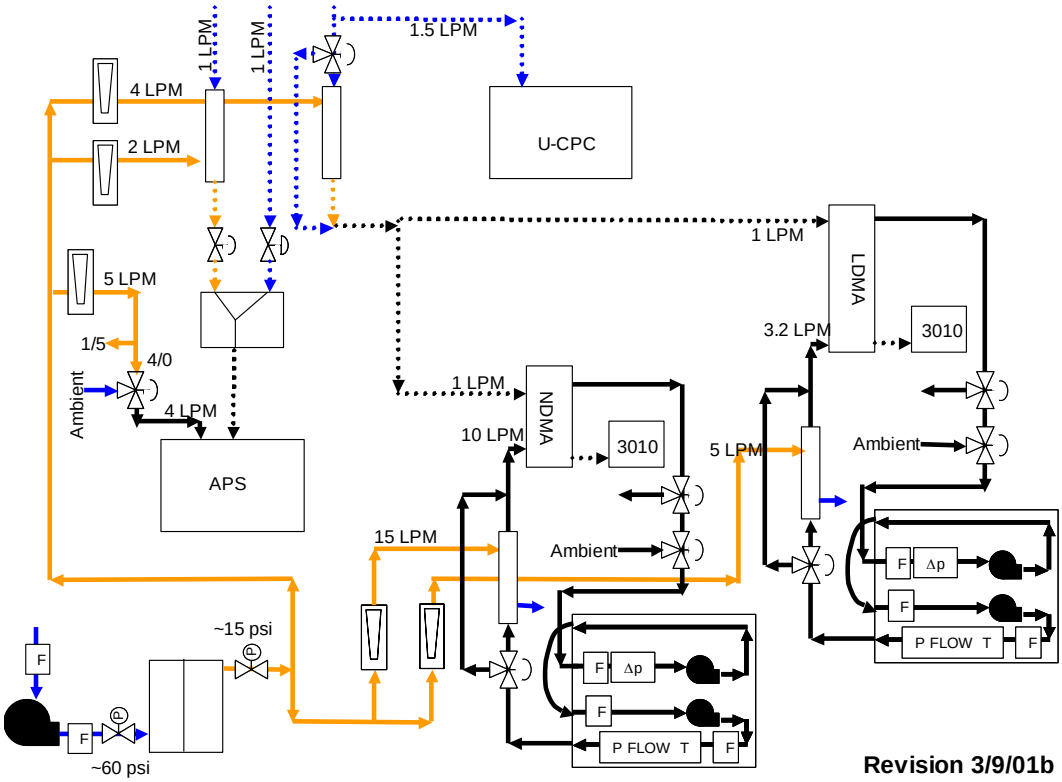

Figure 1. A flow diagram for dry and wet measurements of aerosol size distributions.

(see revised figure – Attached)

DATA QUALITY OBJECTIVES.

Data accuracy is ensured through a combination of advanced instrumentation, routine tests, and consistency checks with collocated measurements.

Aerosol size spectrometers measure both size and number concentration of particles. Thus, quality assurance procedures are required for both the sizing and counting. The accuracy and precision of sizing can be verified using available standards, like monodisperse latex (PSL) particles. There is no verifiable standard for counting accuracy.

The sizing accuracy of the SMPS and APS depend on the accuracy of each of the flow rates in the instruments and the applied voltage in the SMPS. For this reason all of these parameters will be precisely controlled. Computer-based data acquisition cards are used to fully automate the system, thereby enabling continuous monitoring of all relevant parameters, and control of flow rates and voltage to within 1% accuracy. All flow rates are monitored using mass flow meters with the pressure and temperature correction, by measuring differential pressure drop across laminar flow elements, and controlled using either

proportional solenoid valves or variable-speed pumps. The flows will be verified using certified Gilibrator.

The sizing accuracy will be verified monthly using monodisperse PSL particles. The objective for the accuracy and precision of the sizing of the SMPS is 4% and for the APS – 10% (the values correspond to the size resolution of the instruments).

Uncertainty in concentration measurements using SMPS arises from the uncertainty in charge properties of the aerosol, errors in aerosol sizing and flow rates. Aerosol charging probability has been extensively studied, but is still often poorly characterized due to variability in charging techniques, environmental conditions, and aerosol properties and concentration. Past experience has shown that variability in charging probability between seemingly identical chargers can exceed 20%. Prior calibration may only partially improve upon this due to the sensitivity of particle charging to gas-phase properties, which are likely to change in the field.

Additional uncertainties arise as a result of multiple charging. Large particles possessing more than one elementary charge will have mobility characteristics identical to smaller particles with only a single charge. This must be taken into consideration when relating the concentration of particles reaching the detector to the ambient concentration, and is especially a problem for those particles that are beyond the DMA size range when singly charged. To minimize this source of uncertainty, the APS is operated in parallel to the SMPS. The independent sizing capability of the APS facilitates the multiple charge correction due to large particles and permits verification of the multiple charge correction in the overlap size region between the SMPS and APS.

Particle loss and poor counting statistics also contribute to the uncertainty of the number concentration measurements using the SMPS and APS. The size dependent particle losses through the sampling lines and in the instruments will be carefully determined prior to the study.

The uncertainty in the counting efficiencies of both of the SMPS systems will be assessed by comparing the concentrations of each of the SMPS in the overlap size range (20-50nm) and in the overlap size range with the APS (500-800 nm). Occasional tests with a stand-alone CPC will be made to compare the total number concentration measured with the CPC and the number concentration obtained by integrating measurements of the SMPS systems and the APS. Also comparisons with other techniques (cascade impactors, single particle analyzer) will also be used to assess the accuracy of the instruments.

The objective for the precision of the counting for the SMPS and APS is 30%. It is not possible to determine the accuracy of counting, because there is no absolute standard.

The objective for the completeness of the data set is 70%.

DEFINITIONS

APS:	Aerodynamic Particle Sizer, Model …, TSI Inc.
SMPS:	Scanning Mobility Particle Sizer, Model 3936L10 and 3936N25, TSI Inc.
CPC:	Condensation Particle Counter, Model 3010 and 3025A, TSI Inc.

HEALTH & SAFETY WARNINGS.

LASER SAFETY

The Model 3936 SMPS and Model 3010, 3025A CPC are Class I laser-based instruments. During normal operation you will not be exposed to laser radiation. However, you must take this precaution: do not remove any instrument housing or parts when power is applied.

ELECTRICAL SAFETY

The Model 3981 and 3083 DMAs and Model 3010, 3025A CPC have high voltage points within their cabinets/cases. Service or maintenance should be performed only by qualified personnel.

CHEMICAL SAFETY

CPCs use n-butyl alcohol (butanol) as a working liquid. Butanol is flammable. Butanol is also toxic if inhaled. Refer to a material safety data sheet on butanol and take these precautions:

- Use butanol only in a well ventilated area
- Butanol vapor is identified by its characteristically strong odor and can easily be detected. If you smell butanol and develop a headache, faint or nauseous, leave the area at once.

RADIATION SAFETY

The Model 3081 and 3085 DMA contain model 3077 Aerosol Neutrolizer with a Krypton-85 source. Under normal circumstances, you will not come into contact with hazardous radiation. Use precautions specified in the user manual to assure safe operation of the instrument.

CAUTIONS.

The CPCs and the APS are optical instruments. Avoid sudden shocks to the instrument body and the inlet.

The CPCs contain liquid butanol. Do not tip the instrument, otherwise butanol can be drawn into the optical chamber and cause instrument malfunction.

Do not overfill CPCs with butanol to avoid flooding of the optics.

Do not leave the supply bottle with butanol connected to the CPC. The automatic valve may malfunction which will lead to flooding of the optics.

PERSONNEL QUALIFICATIONS.

All maintenance operations should be performed by personnel familiar with the instruments.

APPARATUS & MATERIALS.

SMPS-1

a) DMA (Model 3083, TSI)

b) Kr-85 neutralizer (Model 3077, TSI)

c) CPC (Model 3025, TSI)

d) Personal computer

e) Spare parts SMPS (filters, fitting, tubing, computer cables)

f) Spare parts CPC (filters, butanol)

SMPS-2

a) DMA (Model 3081, TSI)

b) Kr-85 neutralizer (Model 3077, TSI)

c) CPC (Model 3010, TSI)

d) Personal computer

e) Spare parts SMPS (filters, fitting, tubing, computer cables)

f) Spare parts CPC (filters, butanol)

APS

a) APS (Model 3320, TSI)

b) Spare parts APS (filters, fitting, tubing, computer cables)

DRYING SYSTEM

a) Nafion single and multi-channel dryers (Permapure)

b) Heatless dryer (Permapure)

c) 3-way solenoid valves

d) Air compressor

e) Temperature and RH sensors

FLOW METER

a) Gilian Gilibrator 2

b) Flow cell 2-30 lpm

c) Flow cell 20 cc – 6 lpm

d) Flow cell soap

MATERIALS

a) Filters for SMPS: TSI P/N 1602015, Gelman 12144

b) Filter for CPC: TSI P/N 1602028, TSI P/N 1602059,

c) Filter for CPC: Balston P/N DFU-9922-05-AQ

d) 1-butanol extra pure (Merck)

PAPER MATERIALS

a) Field forms to record performance parameters in the field

b) Laboratory book

INSTRUMENT CALIBRATION AND QUALITY ASSURANCE.

The sizing accuracy of the instruments will be checked once each 6 months with monodisperse PSL aerosol (see Sections 12.7 and 12.8).

Quality control of the data is achieved on daily basis by:

a) checking the critical operation parameters of the instruments (flow rates etc., see 9.3)

b) comparing number concentrations in the overlapping size ranges of different instruments (see 9.4)

c) visual checks of hourly averaged size distributions (see 9.5)

CHECK FOR CRITICAL OPERATION PARAMETERS

The following operation parameters will be checked according to the maintenance schedule:

a) sheath and excess flow rates of SMPS should be within 5% of the set points of the flow controllers

b) the standard deviation of both sheath and excess flows of SMPS during one scan is within 10%

c) sample flow rate of SMPS should be within 20% from the set point.

d) sample flow rate of APS should be within 10% from the set point.

e) sizing accuracy of SMPS as determined with PSL is within 5%

f) sizing accuracy of APS as determined with PSL is within 20%.

If one or more operating parameters are deviating from the nominal, the instrument in question should be checked and adjusted to the nominal parameters

as soon as possible. Data collected with that instrument during the period of malfunction should be corrected, if possible, for the observed deviations (see 9.6).

COMPARISON OF NUMBER CONCENTRATIONS IN THE OVERLAPPING SIZE RANGES

Hourly averaged number concentrations in the following overlap regions will be regularly checked:

a) SMPS-1 vs. SMPS-2: 20 - 50 nm

b) SMPS vs. APS: 500-600 nm

If the instruments consistently deviate by more than 30%, both instruments should be checked as soon as possible. If instrument is found to be malfunctioning, it should be adjusted to normal operation. Data collected with that instrument during the period of malfunction should be corrected, if possible, for the observed deviations from nominal operating parameters (see 9.6). If no malfunctioning is found, data from both instruments is accepted as is and is not rejected. However, it should be marked appropriately to indicate the discrepancy between the two instruments.

VISUAL CHECKS OF HOURLY AVERAGED SIZE DISTRIBUTIONS

Hourly-averaged size distributions should be checked visually by an experienced operator for persistent (for more than 3 hours in a row) “gaps”, i.e. whether the spectra appear to be “missing” particles at some sizes.

If such persistent “gaps” are found the instruments should be checked as soon as possible by an experienced operator. If instrument is found to be malfunctioning, it should be adjusted to normal operation. Data collected with that instrument during the period of malfunction should be corrected, if possible, for the observed deviations from nominal operating parameters (see 9.6). If no malfunctioning is found, data from the instruments is accepted as is and is not rejected.

CORRECTION OF DATA FOR RECOVERABLE INSTRUMENTAL MALFUNCTION

If an instrumental malfunction was found, the data can be corrected for the observed deviation, in the following cases:

a) sample flow of SMPS deviates by less than 50% from the set point.

b) sheath /excess flows of SMPS deviate by less than 50% from the set point.

c) std of sheath and excess flows in SMPS during one scan is less than 10%.

d) sample and sheath flows of APS deviate by less than 50% from the set points.

Corrected data should be marked, the reason and the procedure of correction should be described.

DATA VALIDATION

The data are considered invalid, if it is discovered that the instrument was operated outside the nominal operating conditions, for which no correction can be applied (see 9.6), or if one or more critical parts of the instrument (i.e. laser of CPC or APS, pumps, empty butanol reservoir of CPC, etc.) were not functioning or were out of order.

SAMPLE COLLECTION AND HANDLING.

Not applicable.

SAMPLE PREPARATION AND ANALYSIS.

Not applicable.

ROUTINE OPERATION / PREVENTIVE MAINTENANCE & REPAIRS.

DAILY MAINTENANCE OF SMPS

a) Check whether the voltage indicated by the program is changing synchronically with the voltage indicated on the DMA.

b) Check butanol level in CPC, fill if necessary (do not leave refill bottle connected to the CPC). Record the time of filling.

c) Check indicator LED on CPC front.

d) Check flows.

e) Check operation of the dryers (observe RH during dry measurements).

DAILY MAINTENANCE OF APS

a) Check and record indicator LEDs on the instrument

b) Check (remotely) flows and their std

WEEKLY MAINTENANCE OF SMPS

a) Stop data acquisition. Record the time.

b) Drain CPC and refill with fresh butanol (more frequent refills may be required if the weather is warm an humid).

c) Check null counts of the SMPS, while scanning, by placing an absolute filter in front of the sample inlet. Record the time.

d) Start data acquisition. Record the time.

WEEKLY MAINTENANCE OF APS

a) Check null counts by placing an absolute filter in front of the sample inlet. Record the time.

MONTHLY MAINTENANCE OF SMPS

b) Check and record sample flow rate with the Gilibrator, thorough check of the plumbing and flow meters will be needed if the flow deviates by more than 10% from the set value.

c) Once in 6 months check sizing properties with monodisperse PSL aerosol of 30 and 100 nm. Record the time and file name.

MONTHLY MAINTENANCE OF APS

a) Check sample flow with Gilibrator

b) Change label with operation parameters on front of the instrument and inform routine personal if necessary

c) Once in 6 months check sizing properties with monodisperse PSL aerosol of 0.2 μm (to be done simultaneously with the calibration of SMPS, see 7.3). Record the time and file name.

HANDLING OF PERSISTENT INSTRUMENTAL DEVIATIONS

If any adjustment of the operating parameters (see 7.1 and 7.2) yields no sufficient result (i.e. normal operating conditions can not be achieved) or number concentration differences between the instruments (see 8.3) remain unacceptable,

personal doing the routine maintenance is requested to report the problem and actions undertaken to solve it to an experienced operator as soon as possible.

TROUBLESHOOTING.

Refer to the user manual or an experienced operator for troubleshooting.

DATA ACQUISITION, CALCULATIONS & DATA REDUCTION.

Instrument operation and data acquisition will be performed using advanced computerized systems. The data will be inverted using the state of the art software packages. Size distribution data will be reported as dN/dLgD in cm^{-3}. The format of the data output will be as defined by the data management protocol of the study.

AVERAGING OF HOURLY AND DAILY MEAN SIZE DISTRIBUTIONS

For the purpose of quality assurance comparisons will be done with other instruments operated in this study. Since most of the other instruments operate on hourly or daily basis, averaging of the spectrometer data will be performed.

Hourly average concentrations are calculated if at least 66% of the valid data (see 8.5) for one hour are available. Daily average number concentrations are valid, if at least 16 hourly averages are available for one day. Daily means will be provided for time intervals corresponding to other 24-hour measurements employed in the study.

CALCULATION OF PARTICLE VOLUME AND MASS DISTRIBUTIONS

To compare the size spectrometers with the mass-based (gravimetric) measurements, size distributions in dN/dLgD will be converted into volume or mass size distributions (dV/dLgD and dM/dLgD, respectively).

The number concentration distribution data will be convoluted into particle volume distributions assuming spherical particles of the nominal particle diameter of the given size intervals.

From the daily means of the particle volume concentrations and the daily PM2.5 measurements an apparent density will be determined for each day, which will be averaged over the entire measuring period.

Based on the particle volume distribution data and the mean apparent particle density particle mass concentration will be calculated.

DATA MANAGEMENT & RECORDS MANAGEMENT.

All maintenance procedures must be recorded in the respective field forms. All data will be validated and flagged. All data will be backed up on two copes of storage media (zip-discs or CDs).

CONTACTS.

A. Khlystov
e-mail: andrey@andrew.cmu.edu
tel.: (412) 268-5778

TSI Inc.
e-mail: particle@tsi.com
tel.: 1-800-677-2708 / (651) 490-2833

REFERENCES.

1. Model 3936 SMPS (Scanning Mobility Particle Sizer). Instruction manual. (1999) TSI Incorporated, St.Paul, MN.

2. Adachi, Okuyama, Kousaka (1985) J. Chem.Eng., Japan, 16:229.

3. Knutson, Whitby (1975) J.Aerosol Sci., 6:443.

4. Wang, Flagan (1990) Aerosol Sci. Technol. 13:230-240.

5. Wiedensohler, Lutkemeier, Feldpausch, Helsper (1986) J.Aerosol Sci. 17:413.

Attachment 1

Revised diagram of DAASS as constructed and operated during the field study. Revision date 6/2/03.

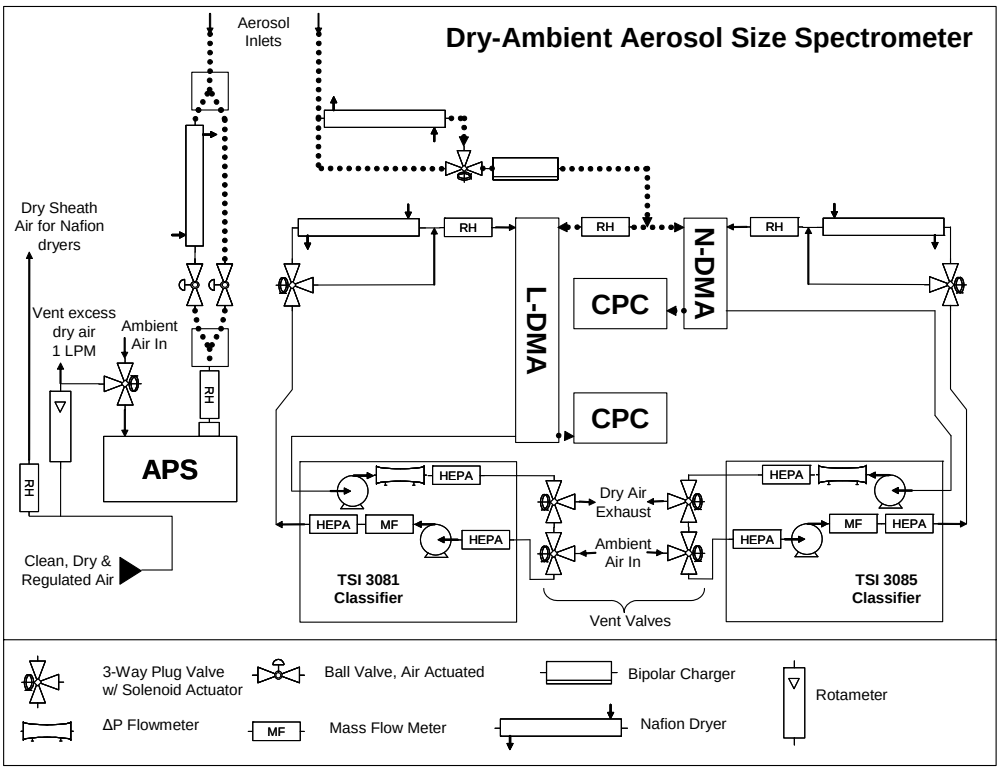

Correction to section 4. APS model number is 3320 and 3321.

Addition to section 9.1, Critical Operation Parameters

g) Computer clock shall be within 2.5 minutes of standard time, and corrected if outside this range

h) An inlet leak test performed with a HEPA filter should give less than 1% of typical ambient concentration of particles (10 particles per cm^3 for Nano-SMPS and SMPS, 0.1 particle per cm^3 for APS).

Addition to section 12.1, Daily Maintenance

f) Check that computer clock is within acceptable range of standard time.

Appendix D
Suggested Improvements for a 2nd Generation Dry-Ambient Aerosol Spectrometer

- Improved aerosol drying performance. For example, Nafion dryer performance can be improved by drawing a vacuum on the shell-side dry-air outlet to reduce the partial pressure of water vapor on the shell side. For example, see the TEOM Sample Equilibration System by Rupprecht and Pataschnick (Meyer et al., 2000).
- Improved sheath and aerosol flow control and monitoring. Include a conveniently located differential pressure flow indicator (magnehelic gage and coil of tubing for pressure drop) for each leg of the sheath flow.
- Operate ambient channel relative humidities closer to ambient relative humidity through (a) more complete purging of the DMAs, possibly using supplemental vacuum or pressure during venting; and (b) active humidification of air.
- Include ability to humidify to a standard (85%) humidity as an operating mode in addition to drying and ambient relative humidity.
- Adapt design for easy manual calibration or automated daily calibration. This is particularly important for the APS, whose calibration curve seemed to change with time.
- Automate butanol sheath air drying and butanol fill-drain cycles.
- Improve resolution of DMAs by using 10:1 sheath to aerosol flow ratios.
- Use low-pressure drop valves rather than electrical solenoid valves to reduce system pressure drop and prevent wear-and-tear on minispiral blowers.
- Improve the mechanical stiffness of the APS inlet, as the APS sizing and counting seems to be sensitive to small changes in the alignment of the inlet.

- Change the inlet plumbing for (a) lower particle losses; (b) no heating of the aerosol en route to sizing (e.g. – move entire inlet to a ventilated, shaded, outdoor area). Consider a short low-loss ambient RH inlet for sampling < 15 nm aerosols (sacrificing dry-ambient data). Dry sheath air only for the NDMA.
- Improve data acquisition system for (a) automatic time synchronization with a time server; (b) eliminate bad data points from serial data acquisition errors; (c) eliminate missed data due to software crashes.
- Improve automatic recovery after power failure.
- Avoid the use of Labview for control software. Use a "traditional" line-by-line programming language, with graphical user interface to build a control panel. Contact John Ondov regarding control software used for the SEAS metals sampler.

References

Meyer, M.B., Patashnick, H., Ambs, J.L., and Rupprecht, E., 2000. Development of a sample equilibration system for the TEOM continuous PM monitor. Journal of Air and Waste Mangement *5*0:8, 1345-1349.

Appendix E
Procedures for Data Reduction and Validation of DAASS Data

Documents have been scanned for this Appendix. Scanned documents have titles of Appendix A and Appendix B. Scanned documents refer to MATLAB code that handled processing of DAASS data. Source code is not included in this thesis and can be obtained by contacting Charles Stanier at the permanent forwarding address: cstanier@alumni.princeton.edu.

Appendix A: Level 0 Validations Procedures

Data Reduction Procedure "A": Copying SMPS data
Written by: Charles Stanier on 5/22/02
Modified by: Hanyong Lim on 12/11/02

1.0 Insert CD into "E" drive of "Stanier" (the upper drive of the two CD drives).
2.0 Open Windows Explorer to folder "ssite_data" in drive "D".
3.0 Edit the batch file "mv9.bat" by right clicking on the file and select "edit", the following will be shown in a text file:

```
mkdir .\11_22_02\raw
mkdir .\11_22_02\raw\ldma
mkdir .\11_22_02\raw\ndma
mkdir .\11_22_02\raw\aps
mkdir .\11_22_02\raw\florence
mkdir .\11_22_02\raw\ldma\dry
mkdir .\11_22_02\raw\ldma\wet
mkdir .\11_22_02\raw\ndma\dry
mkdir .\11_22_02\raw\ndma\wet
xcopy E:\dma_data\11_17_02\*WL* .\11_17_02\raw\ldma\wet\*.*
xcopy E:\dma_data\11_17_02\*DL* .\11_17_02\raw\ldma\dry\*.*
xcopy E:\dma_data\11_17_02\*WN* .\11_17_02\raw\ndma\wet\*.*
xcopy E:\dma_data\11_17_02\*DN* .\11_17_02\raw\ndma\dry\*.*
xcopy E:\dma_data\11_17_02\*dry* .\11_17_02\raw\*.*
xcopy E:\dma_data\11_17_02\*dma* .\11_17_02\raw\*.*
mkdir .\11_22_02\matlab
mkdir .\11_22_02\reports
pause
```

4.0 Search and replace ALL the dates in the above text file to the date of the data in question.
5.0 Save the modified file.
6.0 Execute the file "mv9.bat" by double-clicking on it. This should create a bunch of folders to the "D" drive, and copy a bunch of files from the CD to these folders.

Data Reduction Procedure "B": Exporting SMPS data
Written by: Charles Stanier on 5/22/02
Modified by: Hanyong Lim on 12/11/02

1.0 Open the SMPS program by double-clicking on the TSI icon (grey and blue ion) on the desktop. Or go to "Start | Programs | TSI | SMPS".
2.0 Choose "File | Export".
3.0 Select the correct working folder

3.1.1 Immediately select the "d" drive, do not change any other setting before this.
3.2 Select the "d:\ssite_data" folder (it appears as "[ssite_~1]").
3.3 Select the folder for the day in question (e.g. "05_20_02").
3.4 Select "raw" directory, where the data is.

4.0 Set preferences
4.1 Channel Resolution: 64
4.2 Weighted by: Number
4.3 Units: Conc.dW/dlogDP
4.4 Charge correction: UNCHECKED
4.5 Output to: File (DO NOT check the other two options)
4.6 Export File Delimiter: comma

5.0 Export the files
5.1 Do LDMA Dry files first.
5.1.1 Select folder "ldma | dry".
5.1.2 Select all files in the directory for exporting, this is done by moving all the files to the right hand window with the "Add All >" button.
5.1.3 Hit "Set Path".
5.1.4 Under "Folders", select "raw" by double-clicking on it.
5.1.5 Under "File name", enter "E_L_D.TXT", then hit "OK".
5.1.6 Back in the export menu, hit "Export".
5.2 Repeat for "ldma | wet" with the file name "E_L_W.TXT".
5.3 Repeat for "ndma | dry" with the file name "E_N_D.TXT".
5.4 Repeat for "ndma | wet" with the file name "E_N_W.TXT".

Data Reduction Procedure "C": Copying and exporting APS data
Written by: Charles Stanier on 5/22/02
Modified by: Hanyong Lim on 12/11/02

1.0 First we need to split up the APS files in the CD into the correct directories on the "D" drive.
1.1 Open two explorer windows.
1.1.1 One explorer windows should be opened to the CD "E:\aps_data\mm_dd_yy".
1.1.2 The other should be open to "D:\ssite_data\mm_dd_yy\raw\aps", the directory for the date in question.
1.1.2.1 Copy the data files (type A20 or A21) generated **on the day in question** from the CD to the "D" drive (e.g. for the day 05/20/02, copy the A20 or A21 file "samples05_20_02" to the folder "D:\ssite_data\05_20_02\raw\aps". Note that the file name may be slightly different, but they will definitely have the date on it).
NOTES:

1) Timestamps on the files may be slightly after midnight on the next day.
2) To see what type of file they are (i.e. A20 or A21 or P21), go to "view" on the explorer menu and select "details".
3) A20 or A21 files with a numerical extension to it are APS data for ANOTHER day, e.g "sample05_20_02.1" is the APS data for 05/21/02, "sample05_20_02.2" is for 05/22/02, etc. Therefore, copy these files to the relevant folders on the "D" drive (i.e. in another "\raw\aps" folder of the relevant date)
4) A20 or A21 files with an alphabetical extension to it are APS data for the SAME day, eg, "sample05_20_02a" is the 2nd APS data file for 05/20/02, "sample05_20_02b" is the 3rd APS data file for 05/02/02.

1.1.2.2 Also copy one parameters file, "P21" from the same sequence of samples as each of the APS data files (i.e. copy the P21 file, that exist in the same folder as the original A21 file, to the same "\raw\aps" folder the A21 file was copied to).

1.1.2.3 Ensure that there are equal number of P21 files and A21 or A20 files in the "D:\ssitc_data\mm_dd_yy\raw\aps" folder. Each P21 file has to correspond to an A20 or A21 file by having the same name (e.g, you may have the following A21 files: "sample05_19_02.2", "sample05_21_02", "sample05_21_02a", and the following P21 files: "sample05_19_02", "sample05_21_02". In this case, change the name of the P21 file "sample05_19_02" to "sample05_19_02.2", make another copy of the P21 file "sample05_21_02" and rename it as "sample05_21_02a". Now, you have one P21 file that corresponds to each A21 file with the same name)

1.1.2.4 Repeat the procedure for all the APS data in the CD, copying all the APS data from all the "E:\aps_data\mm_dd_yy" folders into the relevant "D:\ssite_data\mm_dd_yy\raw\aps" folders.

2.0 Now we have to change the file preferences in order to export them with the program.

2.1 Select an A20, or A21, or P21 file by rightclicking it.

2.2 Select "Properties".

2.3 Under the "General" tab, uncheck all the "Attributes" properties.

2.4 Repeat for all A20, A21, and P21 files.

3.0 Now that the files are copied, we can export them.

3.1 Open up the Aerosol Instrument Manager Software using the "AIM" icon on the desktop. Or go to "Start | Programs | TSI inc | Aerosol Instrument Manager".

3.2 Open the 1st APS data file for the day in question with "File | Open" (the APS files with a numerical extension are the 1st APS file for that day, those with the alphabetical extension are the later files for that day, e.g. if you have "sample05_19_02.2", "sample05_21_02", and "sample05_21_02a", the first file is "sample05_19_02.2", followed by "sample05_21_02", and then "sample05_21_02a").
3.2.1 Answer "NO" to the sequence file question that pops up.

4.0 Select all the samples by holding down "[Ctrl]+A".

5.0 Now export the files.
5.1 Select "File | Export".
5.2 Select preferences.
5.2.1 Select "Numbers" with "dW/dlogDp"
5.2.2 Delimiter: Comman
5.2.3 Orientation: Row
5.2.4 Hit "Enter".
5.2.5 Filename: "E_APS1.TXT" in path "d:ssite_data\mm_dd_yy\raw" (one level above with the other "E_X_X" files).

6.0 Repeat for the rest of the APS data for the day starting at step 3.2, naming the files "E_APS2.TXT", "E_APS3.TXT", etc.

Data Reduction Procedure "D": Running the MATLAB program
Written by: Charles Stanier on 05/22/02
Modified by: Hanyong Lim on 12/12/02

1.0 Open MATLAB (the MATLAB program written by Charles should have been installed).

2.0 Type "edit mp_header" and then hit "enter".
2.1 Make the relevant changes to the mp_header file (in bold).
2.1.1 mp_dates = [**2 digit day of the data**] (e.g. 20 for the date 05/20/02).
2.1.2 mp_months = repmat(**2 digit month of the data**, size(mp_dates)) (e.g. 05 for the date 05/20/02).
2.1.3 mp_years = repmat (**4 digit year of the data**, size(mp_dates)) (e.g 2002 for the date 05/20/02).
2.2 Select options in the "mp_header" file.
2.2.1 "process.dp = 1".
2.2.2 "process.mdp = 1".
2.2.3 "process.rep = 1".
2.2.4 All the rest = 0.

3.0 Save the amended "mp_header" file, and run the program by typing "mp" and then hit "enter".

Note: This procedure applies to data obtained from setup similar to that in Schenley Park. Extracting data for setup in Clariton, Tunnel, and Floremce requires slightly different procedure, in which Charles' consultation would be needed.

Appendix B: Level 1 Validations Procedures

Data Reduction Procedure "E": Creating "inflag" files
Written by: Hanyong Lim on 12/13/02

1.0 Open MATLAB.
2.0 In MATLAB, open the file "outflagddmmyy.txt" of the date in question (this file should be created after level 0 validations). This is a file containing data points that failed the maximum, and minimum value tests specified. Thus, these data points are the potential erroneous data. The test specifications are indicated in all the outflag files.
  2.1 There are 3 ways to open the file.
    2.1.1 In MATLAB, there are usually 3 default windows, on the bottom left window, select the tab "Current Directory".
      2.1.1.1 Hit "..." button and go to the directory "d:\ssite_data\mm_dd_yy\matlab".
      2.1.1.2 A list of the files in that directory will be displayed in the window, you should see the file "outflagddmmyy.txt". Double-click to open.
    2.1.2 Or go to "File | Open" locate the file in the specified directory to open it.
    2.1.3 Or on the tool bar, hit "..." button beside the "Current Directory", and follow step 2.1.1.1 onwards.
  2.2 Due to the specifications of the tests, ALL ldma data points will appear in this file. See Annex F for sample of the outflag file.
3.0 On the first line of the outflag file, insert the date of the file with the format **mm/dd/yy**.
4.0 After the line "For Output date = **XX**" (XX is the 2 digit day of the data), insert the comment "% flagged by **YY** on **mm/dd/yy**" (YY is your initials).
5.0 Go to "File | Save As".
6.0 Save the file in the same "matlab" folder as "inflagddmmyy.txt". See Annex G for a sample of an inflag file.

Data Reduction Procedure "F": Flagging the inflag file
Written by: Hanyong Lim on 12/13/02

1.0 A data point, or a range of data points had to be "flagged" if they are determined to be erroneous (See Procedure "G").
2.0 Flagging:
  2.1 For a single data point.
    2.1.1 If the data point is in the list, simply insert the flag ID besides the word "FLAG". For example,
      2.1.1.1 Before flagging: FLAG 03-Aug-2002 00:49:20 ldma
      2.1.1.2 After flagging: FLAG**FF** 03-Aug-2002 00:49:20 ldma
      2.1.1.3 **FF** is the flag ID.

2.1.1.4 The column of dates should be aligned after the flag is inserted.

2.1.2 If the data point is not in the list, simply copy a line from the list and change the relevant information, e.g, if the data point 080302_N002_001031 is considered to be erroneous, but it does not appear in the list, simply copy a similar row and paste it at the top of the list, then change the original time and ID number of that data point to that of 080302_N002_001031.

2.2 For a range of data point, simply add the line "**MULTFF EEEE hh:mm:ss HH:MM:SS**" to the top of the list, adding a comment to indicate the reason for flagging. Ensure that EEEE is aligned with the column of dates for the list of data.

2.2.1 EEEE refers to the data type in question (i.e. "ndma", "ldma", or "aps_").

2.2.2 hh:mm:ss refers to the start time (military time). Typically, ss = 00.

2.2.3 HH:MM:SS refers to the end time (military time). Typically, SS = 59.

2.2.4 See Annex G for a sample of the flagging of a range of data, note the alignment of EEEE.

Data Reduction Procedure "G": Level 1 validations

Written by: Charles Stanier on 06/04/02
Modified by: Hanyong Lim on 12/13/02

1.0 For date in question, view the HTML report.

1.1 Two methods of this. Go to "d:\ssite_data\mm_dd_yy\reports\rep1.html" and double-click on it to open. Or open a previous report in internet explorer: using history, the report appear in the history as "My computer => **BLANK**", i.e. there is no title shown for the report, it just appears blank. Once any of the report is open, change the date on the "Address" bar to the date in question.

2.0 Open the file "inflagddmmyy.txt" for the date in question (See Procedure "F").

3.0 Note any recorded special events or known errors. Flag these data points in the inflag file if necessary.

3.1 Check the "summary log for particle sizing equipment" and write down anything that would affect measurements on page 2 of the data reduction worksheet under "Notes" (see Annex E for a sample of the data reduction worksheet).

3.2 See if you can see these events on the HTML report, especially on the color plots. e.g. you might see a sudden increase in the particle numbers on days when there was grass-trimming near the sampling equipments.

4.0 Note other obviously suspicious scans that you see in the color plots, write down on the worksheet the instrument that is questionable, and the time that it occurred (e.g ndma ~0815h); this will help you to locate the bad data in the inflag file.

4.1.1 Need to look at all colorplots for discontinuities. See e.g. in Fig 1.

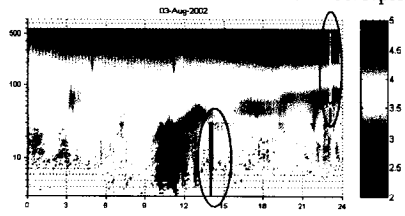

Fig 1: The discontinuities are shown clearly with a sudden change in color. They are circled in the diagram; these are typically the "bad scans" and should be discarded. There are several discontinuities noted here, for the examples circled, we can note down "ndma ~1400h" and "ldma ~ 2300h".

There are a few similar plots with slightly different variables on the axis, some may give a clearer indication of a bad scan than this plot. Note that they do not always appear as a "strip", they may appear as a "dot" in the middle of a distribution. The latter discontinuities may be easier detected in the distribution plots.

4.1.2 Need to look at distributions for discontinuities. See e.g. in Fig 2.

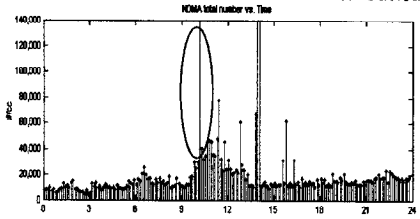

Fig 2: One of the discontinuities is circled in the diagram; these are typically the "bad scans" and should be discarded. Some of the discontinuities might not be very clear in the 1st plot, however, we can see them clearly from their individual size distribution plot. Similar plots are available for ldma and aps data.

5.0 Locate the ID of the bad data points and flag them with the appropriate flags in the inflag file. The respective flag ID for various errors can be found on page 2 of the data reduction sheet on the bottom section. Typically, only "O1" and "O2" are used. The former is used to flag data points that were collected while the instruments' CPC is being refilled with butanol, and the latter is used for most of the rest of the sampling errors.

5.1 For the ndma data, the bad points typically failed the maximum test. These are indicated with the number "100000" after the data ID, see e.g.,

```
FLAG  03-Aug-2002 13:55:31 ndma   080302_N112_135531  100000   2e+008      MAX1
```

5.2 For the ldma data, it may not be easy to identify the bad data point, since all the ldma data are listed in the inflag file. One way of identifying is to use script viewer.m written by Charles.

5.2.1 Open the Mathlab file "rep_header.m". This can be done by typing "edit rep_header" in MATLAB.

5.2.2 Find and replace the date in question at all THREE of the date positions. Save the modified file.

5.2.3 Run the script viewer.m at the command line (type "viewer"). Inspect the size distributions for the time periods noted in step 4.0.

5.2.3.1 Write information for bad size distributions on Page 2 of the Data Reduction Worksheet. E.g. L056_062315. The first letter represents the type of data (ldma "L", or ndma

"N", or aps "A"), the 3 digit number is the sequencing number, the last 6 digits are the time. Note that for different data type with the same sequencing number, the time may be different.

6.0 Once all bad scans are identified, flag them in the inflag.txt file (see procedure "F").

7.0 Save the modified "inflagmmddyy.txt".

8.0 Now rerun written MATLAB codes with the appropriate options selected.
- 8.1 "process.dp = 0".
- 8.2 "process.fdp = 1".
- 8.3 "process.mdp = 1".
- 8.4 "process.rep = 1".
- 8.5 All the rest = 0.

9.0 If the new HTML looks good, you are done. Else repeat step 3.0 onwards.

10.0 If a data point is wrongly flagged, in order to remove the flag, (1)the flag have to be removed from the inflag file, then (2) rerun the MATLAN codes with the following options selected.
- 10.1 "process.dp = 1".
- 10.2 "process.fdp = 1".
- 10.3 "process.mdp = 1".
- 10.4 "process.rep = 1".
- 10.5 All the rest = 0.
- 10.6 dp.m will read in all data points as original again while fdp will apply the flag simultaneously. It takes a longer time to run the program with dp.m option selected, so, it is advised not to have both dp and fdp on at all times, unless needed to.

Note: Some of the steps outlined by Charles in the original procedures were omitted as they were no longer needed to be executed.

Other notes on flagging:

- **There is no need to flag blank data points, i.e. if the instrument did not register any scan data at any time, the plot will just appear white.**
- **If the instrument appears to be registering a series of zeros for a distribution that is usually non-zero, these data points are suspicious and should be flagged.**
- **If there seemed to be a sudden increase of PM concentration over a short period of time, they may not be bad scans; instead, there may be some reasons for occurrence. It is recommended to leave them unflagged BUT writing down notes on the data reduction worksheet so that these points can be further looked into in level 2 validations.**

Appendix F
Smog Chamber Port Design

In 2002, ports for Teflon chambers were designed by Ken Meyer and Charles Stanier, and machined from Teflon sheet (McMaster-Carr) by Ken Meyer. The ports were designed for leak-free insertion of various tubes into the chamber, and to be supported externally to minimize stress on the weak Teflon bag.

One drawing and two photographs are attached.

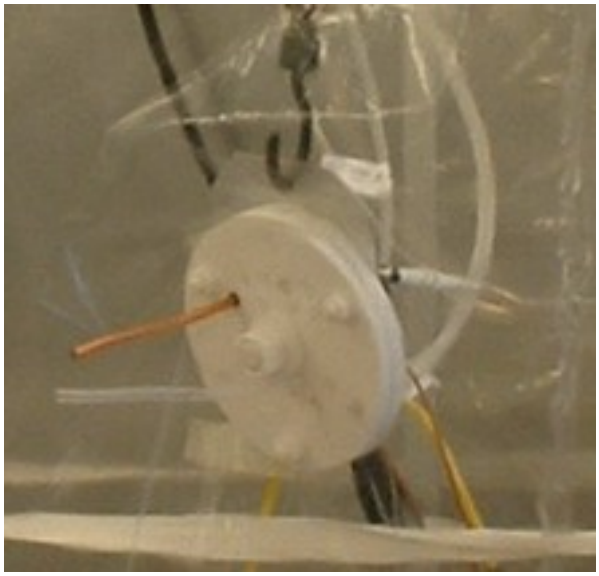

Teflon port installed on 10 m^3 teflon bag.

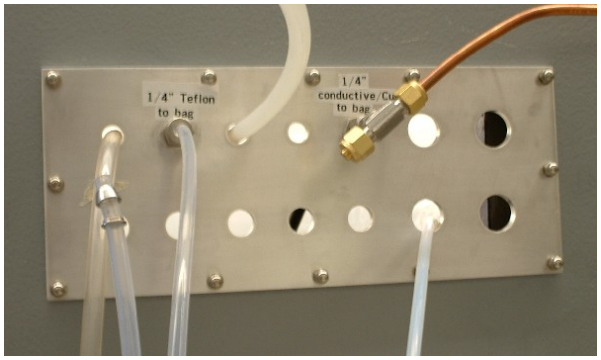

Aluminum port installed in wall of smog chamber.

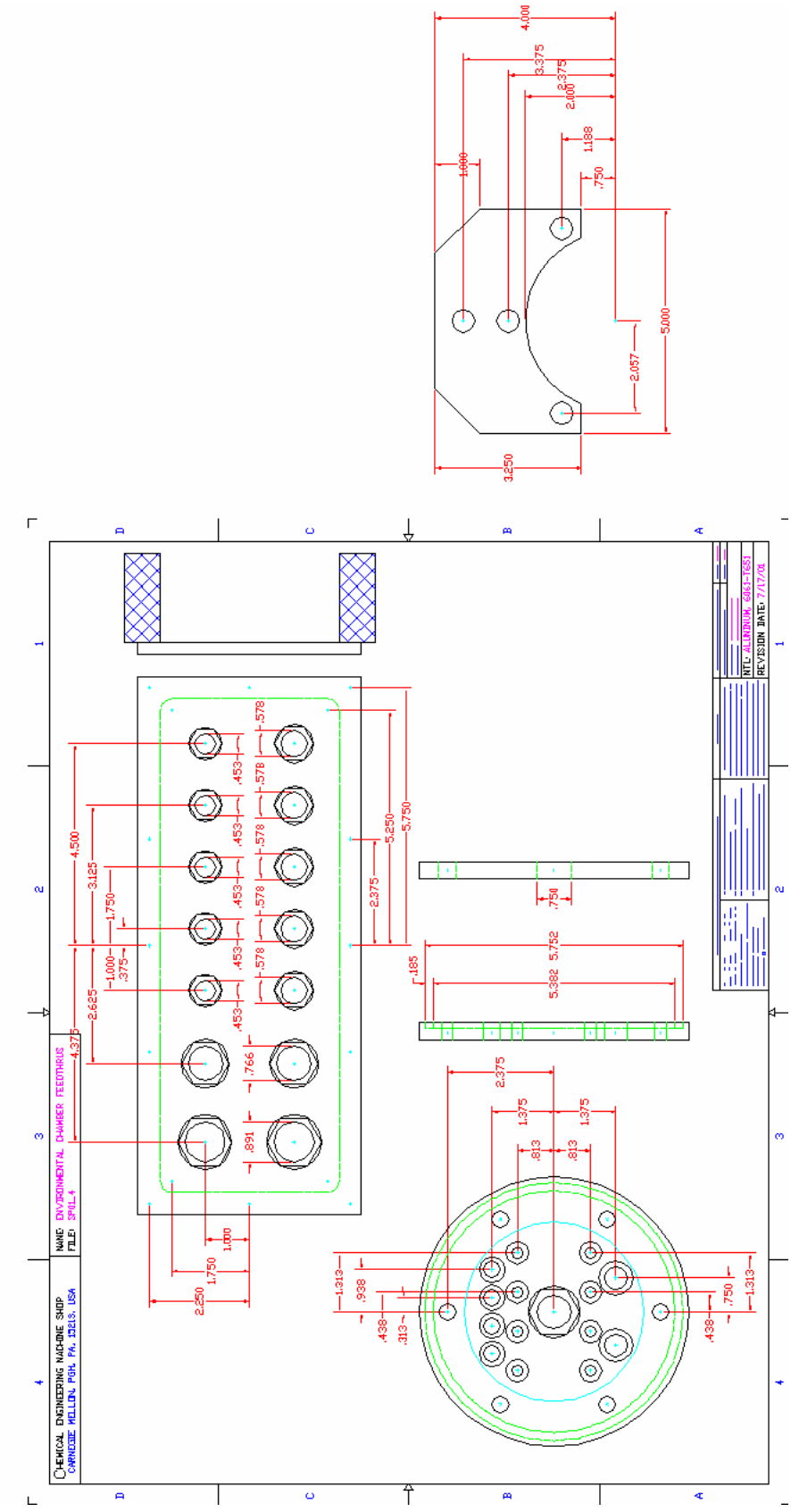
CHEMICAL ENGINEERING MACHINE SHOP
CARNEGIE MELLON PGH, PA. 15213, USA
NAME ENVIRONMENTAL CHAMBER FEEDTHRUS
FILE: SPOL4
MTL: ALUMINUM 6061-T651
REVISION DATE: 7/17/01
4.000
3.375
2.375
2.000
1.188
1.000
.750
5.000
2.057
3.250
4.500
3.125
1.750
1.000
.375
2.625
4.375
.578
.453
.766
.891
2.375
5.250
5.750
.750
.185
5.752
5.382
1.375
.813
1.313
.938
.438
.313
2.250

Appendix G
Laboratory and Field Photographs

Photos that supplement Chapter 7.

Smog Chamber (Exterior) B201 Doherty Hall

Glassware for Evaporating Volatile Organic Liquids into the Chamber

Teflon Bag Hanging inside the HVAC Controlled Enclosure

Photo through Teflon Bag to Port with Various Lines Going Into Chamber

Photos that supplement chapters 3 and 4.

Main Sampling Site at Schenley Park DAASS is in White Shed on Top

View Toward Downtown Pittsburgh (West) from Main Sampling Site on Clean (top) and Dirty (bottom) Days

Satellite Site in Florence PA

View Toward PA State Game Lands from Florence Site

Photos that supplement chapters 2-6.

LDMA Running in Small Enclosure at Florence

DAASS System Running at Schenley Park

Detail of DMA Columns of DAASS, Deployed Outside of Enclosure to Reach Ambient Temperature

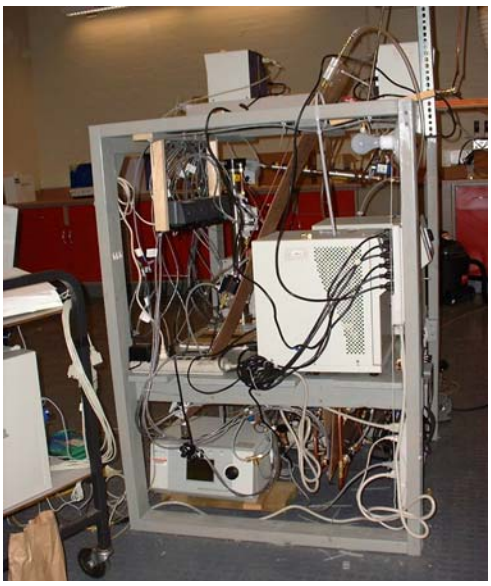

DAASS Set Up in Laboratory for Pre-PAQS Testing and Development

These photos supplement the text description and diagrams of DAASS in section 2.2.

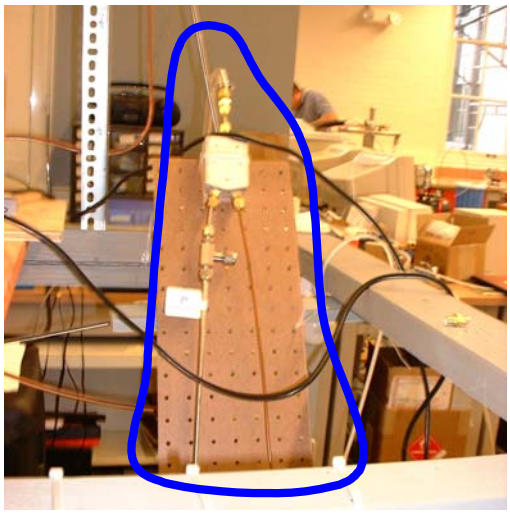

Detail of Top Portion of APS Inlet Showing Flow Splitting to Dryer (Left) and Bypass (Right)

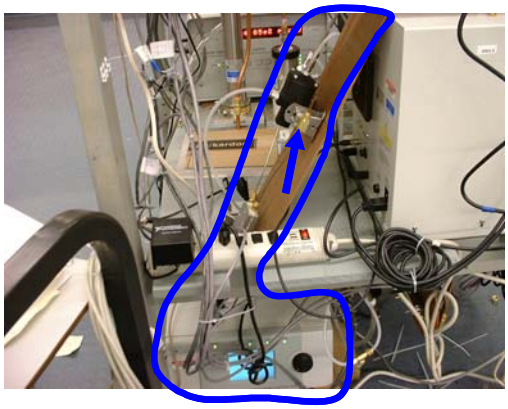

Side View of Lower Portion of APS Inlet and APS. Arrow points to Ball Valve Used to Select Flow Path.

Arrows Point to Electrically Actuated Solenoid Valves Used in Sheath Drying Loops for NDMA and LDMA. Valves are partially obsured by support for Vaisala RH Meter Electronics

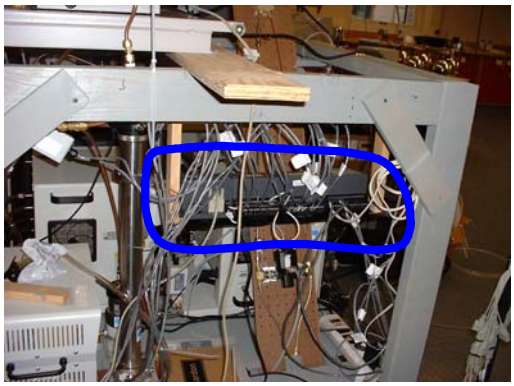

Behind many signal wires, the Analog to Digital "Fieldpoint" Unit used for Analog Signal Acquisition and Control of Relays

Appendix H Temperature and Relative Humidity Sensor Locations for DAASS

The following diagram shows locations (relative to the overall process flow) of the 7 relative humidity and temperature sensors used in the DAASS. In raw relative humidity and temperature files, the signals are recorded in the following format:

Column 1	Time	(Measured in days since 00:00:00 1/1/2001)
Column 2	RH1	NDMA Sheath RH
Column 3	RH2	Utility Flow RH
Column 4	RH3	SMPS Aerosol RH
Column 5	RH4	LDMA Sheath RH
Column 6	RH5	APS Aerosol RH
Column 7	RH6	Inside Shed RH
Column 8	RH7	Outside Shed RH
Column 9	T1	NDMA Sheath T
Column 10	T2	Utility Flow T
Column 11	T3	SMPS Aerosol T
Column 12	T4	LDMA Sheath T
Column 13	T5	APS Aerosol T
Column 14	T6	Inside Shed T
Column 15	T7	Outside Shed T

Starting on 8/23/01, an additional Omega HX93 sensor was installed. Although the signal was acquired and saved, the sensor was never plumbed into a line and can be considered an additional "inside shed" sensor, although the position of the sensor was not representative. It was usually located by the inside wall of the enclosure, above and to the right of the APS. After 8/23/01, the column assignments of the raw RH and temperature file is:

Column 1	Time	(Measured in days since 00:00:00 1/1/2001)
Column 2	RH1	NDMA Sheath RH
Column 3	RH2	Utility Flow RH
Column 4	RH3	SMPS Aerosol RH
Column 5	RH4	LDMA Sheath RH
Column 6	RH5	APS Aerosol RH
Column 7	RHnew	Inside Shed RH (see above)
Column 8	RH6	Inside Shed RH
Column 9	RH7	Outside Shed RH
Column 10	T1	NDMA Sheath T
Column 11	T2	Utility Flow T
Column 12	T3	SMPS Aerosol T
Column 13	T4	LDMA Sheath T
Column 14	T5	APS Aerosol T
Column 15	Tnew	Inside Shed T (see above)
Column 16	T6	Inside Shed T
Column 17	T7	Outside Shed T

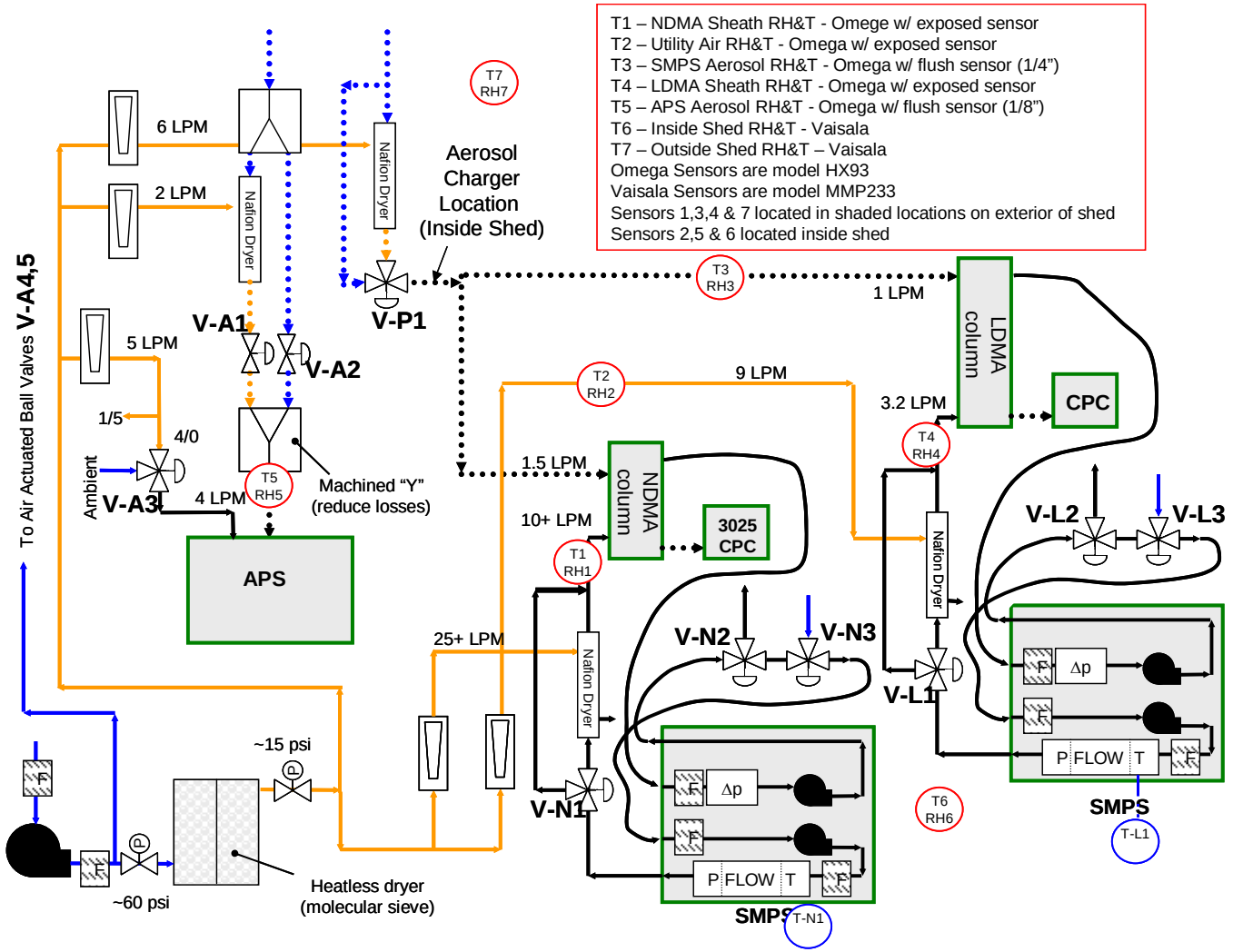
T1 – NDMA Sheath RH&T - Omege w/ exposed sensor
T2 – Utility Air RH&T - Omega w/ exposed sensor
T3 – SMPS Aerosol RH&T - Omega w/ flush sensor (1/4")
T4 – LDMA Sheath RH&T - Omega w/ exposed sensor
T5 – APS Aerosol RH&T - Omega w/ flush sensor (1/8")
T6 – Inside Shed RH&T - Vaisala
T7 – Outside Shed RH&T – Vaisala
Omega Sensors are model HX93
Vaisala Sensors are model MMP233
Sensors 1,3,4 & 7 located in shaded locations on exterior of shed
Sensors 2,5 & 6 located inside shed
T7 RH7
Aerosol Charger Location (Inside Shed)
6 LPM
2 LPM
Nafion Dryer
V-A1
V-A2
V-P1
5 LPM
1/5
4/0
Ambient
V-A3
T5 RH5
Machined "Y" (reduce losses)
4 LPM
APS
To Air Actuated Ball Valves V-A4,5
T3 RH3
1 LPM
LDMA column
T2 RH2
9 LPM
3.2 LPM
CPC
T4 RH4
1.5 LPM
NDMA column
10+ LPM
3025 CPC
T1 RH1
V-L2
V-L3
V-N2
V-N3
V-L1
25+ LPM
V-N1
~15 psi
~60 psi
Heatless dryer (molecular sieve)
Δp
P FLOW T
SMPS
T-N1
T-L1
T6 RH6